CALIBRATION ENHANCEMENT OF NON-LINEAR VNA SYSTEM

A thesis Submitted to Cardiff University

in candidature for the degree of

Doctor of Philosophy

By

Anoor Shuaib Aldoumani, BSc, MSc.

Division of Electronic Engineering

School of Engineering

Cardiff University

United Kingdom

DECLARATION

This work has not previously been accepted in substance for any degree and is not concurrently submitted in candidature for any degree.

Signed …………………………………………………… (Candidate)

Date ……………………………………………………………

STATEMENT 1

This thesis is being submitted in partial fulfilment of the requirements for the degree of PhD.

Signed …………………………………………………… (Candidate)

Date ……………………………………………………………

STATEMENT 2

This thesis is the result of my own independent work/investigation, except where otherwise stated. Other sources are acknowledged by explicit references.

Signed …………………………………………………… (Candidate)

Date ……………………………………………………………

STATEMENT 3

I hereby give consent for my thesis, if accepted, to be available for photocopying and for inter-library loan, and for the title and summary to be made available to outside organisations.

Signed …………………………………………………… (Candidate)

Date ……………………………………………………………

STATEMENT 4

I hereby give consent for my thesis, if accepted, to be available for photocopying and for inter-library loans after expiry of a bar on access approved by the Graduate Development Committee.

Signed …………………………………………………… (Candidate)

Date   ……………………………………………………

ACKNOWLEDGEMENTS

ABSTRACT

Communication systems are generally found wherever data is to be transmitted from point-to-point or from a point to many points. It is impossible to imagine modern life without communication systems such as radio, telephone, TV, Satellite and etc.

The transmission of information from one place to another requires an operation or other alteration to be sent through an electrical signal; the same principle applies for the receiving terminal.

Modern life requires that efficient wireless communication systems for long range transmission be built, therefore, base-stations must use high power transistors almost exclusively. Furthermore, modern cellular communication systems also need to transmit across long distances, hence, to achieve this aim successfully, a radio frequency (RF) power amplifier is employed. That is considered to be a key element of any wireless communication system. Efficient communication systems must have minimum spectral re-growth, interference and employ linear.

Signal amplification is one of the core circuit functions in modern microwave and RF systems. The Power Amplifier (PA) is a key element in the construction of all wireless communication systems. The PA uses the most current because it is the last stage in the transmission chain.

In modern PA design, the RFPA designer must have accurate S-parameter data for the DUT, thereby allowing the creation of an accurate system model and to reduce the re-design and rework effort. The ultimate aim of the research work presented in this thesis is to achieve improvement in the accuracy of a waveform measurement system by increasing the accuracy of the small-signal calibration used. This involved removing the phase reference from the NVNA during calibration and operation, which in turn removes the bandwidth and frequency limitations that the phase reference imposes, as well as reducing the complexity of the overall system.

Essential contributions to this research work concentrated in two areas; firstly, developments that allow for Enhanced Vector Calibration of Load-pull measurement systems, especially near the edge of the Smith Chart, and secondly, the operation and

calibration of a VNA-based large-signal RF I-V waveform measurement system without using a harmonic phase reference standard.

The first research area described in this thesis involved investigating the prospect of improving vector measurement accuracy, especially near the edge of the Smith Chart, by using load pull technology. Increased measurement error near the edge of the Smith chart was observed during calibration. To help correct this, the realisation of novel optimization that increases the accuracy of all the raw data which was collected during calibration process and therefore increases the accuracy of calibration at reflection coefficients close to unity. This research work focuses on taking advantage of the load-pull capability during calibration, this reduces the effect of measurement errors on the raw data when measuring the calibration standards before being applied in traditional LRL/TRL calibration algorithms. Leading to time proved measurement accuracy and eliminates the requirement to use complex optimisation algorithms post calibration.

The second concept developed simplifies the NVNA architecture and removes the complexities and bandwidth limitations introduced when employing a harmonic phase reference generator. A key capability of the Rohde and Schwarz ZVA-67 VNA is that it incorporates internal signal and local oscillator sources and employs direct digital synthesis was exploited to advantage allows the Vector Network Analyzer to be operated as a NVNA without the need for a harmonic phase reference generator. This is due to such a Vector Network Analyzer based NVNA configuration provided a system with both coherent receivers and sources. This feature combined with a modified calibration procedure, means that during calibration only the internal signal sources and an external phase meter are required during measurement. All the internal signal sources and receiver port are available to measure, also now since no phase reference required, bandwidth and functionality issues and avoided.

LIST OF PUBLICATION

First-author papers

1- A. Aldoumani, P. J. Tasker, R. S. Saini, J. W. Bell, T. Williams and J. Lees, "Operation and calibration of VNA-based large signal RF I-V waveform measurements system without using a harmonic phase reference standard," Microwave Measurement Conference (ARFTG), 2013 81st ARFTG, Seattle, WA, 2013, pp. 1-4.doi: 10.1109/ARFTG.2013.6579055.
URL:http://ieeexplore.ieee.org/stamp/stamp.jsp?tp=&arnumber=6579055&isnumber=6579016

2- A. Aldoumani, T. Williams, J. Lees and P. J. Tasker, "Enhanced vector calibration of load-pull measurement systems," Microwave Measurement Conference (ARFTG), 2014 83rd ARFTG, Tampa, FL, 2014, pp. 1-4.
doi: 10.1109/ARFTG.2014.6899508.
URL:http://ieeexplore.ieee.org/stamp/stamp.jsp?tp=&arnumber=6899508&isnumber=6899500

Additional papers

1- N. Aldoumani, T. Meydan, C. M. Dillingham and J. T. Erichsen, "Enhanced tracking system based on micro inertial measurements unit to track sensorimotor responses in pigeons," *SENSORS, 2015 IEEE*, Busan, 2015, pp. 1-4.doi: 10.1109/ICSENS.2015.7370309
URL: http://ieeexplore.ieee.org/stamp/stamp.jsp?tp=&arnumber=7370309&isnumber=7370096

TABLE CONTENTS

CONTENTS

ABBREVIATIONS

A	Amperes
AC	Alternate Current
ADC	Analog to Digital Converter
ADS	Advanced Design System
ALG	Algorithm
A_n	Incident voltage travelling wave, where n is the port number
ARFTG	Automatic Radio Frequency Techniques Group
B_n	Voltage travelling wave, where n is the port number
BW	Bandwidth
C	Capacitance
CAD	Computer-Aided Design
CW	Continuous Wave
dB	Decibels
dB_m	Decibels (reference to 1mW)
DC	Direct Current
DCIV	DC measurement of the device's output current/voltage plane
DSO	Digital Sampling Oscilloscope
DE	Drain Efficiency
DSP	Digital Signal Processing
DUT	Device Under Test
ESG	Electronic Signal Generator
F	Farads
FEC	Forward Error Correction

FET	Field Effect Transistor
FFT	Fast Fourier Transform
f_0	Fundamental Tone of a signal
Hz	Hertz
I	Current
I_{DC}	DC drain bias current
IF	Intermediate Frequency
IFFT	Inverse Fast Fourier Transform
I-V	Current-Voltage
L	Inductance
LSNA	Large Signal Network Analyser
m	Meter
MTA	Microwave Transition Analyser
NVNA	Non-Linear Vector Network Analyser
P	Power
PA	Power Amplifier
R	Resistance
RF	Radio Frequency
RFPA	Radio Frequency Power Amplifier
S-parameters	Scattering Parameters
t	Time
V	Voltage
V_{DC}	DC drain bias voltage
V_{DS}	Drain-Source Voltage
V_{GD}	Gate-Drain Voltage
V_{GS}	Gate-Source Voltage

VNA	Vector Network Analyser
VSA	Vector Signal Analyser
W	Watts
X	Reactance
Z	Impedance
Z_{load}	Load Impedance
Γ	Reflection Coefficient
Ω	Ohm, unit of Impedance
η	Efficiency
λ	Wavelength
π	Pi
ω	Radian Frequency, $\omega = 2\pi f$
∞	Infinity
| |	Magnitude
<	Angle
º	Degree

1. CHAPTER 1

INTRODUCTION

1.1 BACKGROUND

The reason behind the consideration of RFPA as a key element is due to the presence of a trade-off between power per cost vs. efficiency and linearity [1].

Digital communication requires more peak power for the same bit error rate, transmitters must be more linear to minimise spectral re-growth, interferences, higher power and broader bandwidth to clear modulation scheme. There are two behaviour regions for the operation of PA, linear and non-linear [1].

Devices are considered to be a linear response only if the number of harmonics in input equals the numbers of harmonics in output, whereas non-linear devices generate more harmonics in the output. Many components that exhibit linear behaviour in normal cases, if driven with large enough input signal, will exhibit non-linear behaviour [2].

RFPA designers require information in order to make correct decisions throughout all stages of the design process, They need to be informed on stability analysis, DC network analysis, harmonic balanced analysis, convolution analysis, transient analysis, 3D EM analysis, modulation envelop analysis, smith tool utility and load pull analysis. Normally, PA designers start designing in the linear region depending on S-parameter. This provides insight into the characteristics of behaviour of the linear two-port device, S_{21} =forward transmission coefficient (gain or loss), S_{12} =reverse transmission coefficient (isolation), S21=forward reflection coefficient (input match), S22=reverse reflection coefficient (output match) [2].

$$\begin{bmatrix} b_1 \\ b_2 \end{bmatrix} = \begin{bmatrix} S_{11} & S_{12} \\ S_{21} & S_{22} \end{bmatrix} \cdot \begin{bmatrix} a_1 \\ a_2 \end{bmatrix} \qquad \text{EQUATION 1-1}$$

Measurement: Within the context of this thesis, measurement involves applying a sequence of stimuli to the DUT and measuring its response to these stimuli. During this process, the order of the various tests must be considered, along with other testing conditions and other aspects of the stimulus [3]. RF measurement can be considered in two general groups, with sometimes overlapping categories:-

1. Signal Measurements:-"observation and determination of the absolute characteristics of waves and waveforms. This includes frequency and time characteristics that are intentionally imparted into or onto a signal such as modulation by information or unintentional signal perturbations including phase and amplitude noise"[4].

2. Network Measurements: "determines the relative terminal and signal transfer characteristics of devices and systems with any number of ports. Networks such as modulators and communication paths are sometimes characterized as linear time variant paths requiring both signal and network measurements for characterization"[4].

In RFPA design, a first-pass methodology and elimination of the need for post-production tuning requirements and rework is desirable. If there is an absence of reliable non-linear models, this goal can only be fully accomplished by undertaking all relevant measurements of the device to be used in the RFPA design. As a result, continuous waveform measurements are considered a very important step in the RFPA design procedure, especially for nonlinear devices and circuits [5].

All new systems are built based on these aforementioned measurement requirements. To further expand the boundaries future systems are pushing towards multi-tone excitation. The driving factors are a demand for faster CW device characterisation and the ability to build measurement systems that can perform ultra-rapid CW characterisation. These enhanced measurement systems allow the users to more rapidly generate models and in turn provide faster time-to-market for products [6].

AS the nonlinear measurements are used to generate a model for DUT, the precision of these models is clearly dependent on the density of measured information. This density

can be dramatically increased by using a modulated impedance environment and modulated stimuli. The second demand comes from the dramatic growth in the complexity of modulation schemes, predominantly operating over wide bandwidths [7].

The relationship between traditional CW measurements and the eventual simulation the device or circuit encounters in the final application is a concern. To address these problems, further measurements need to be performed under more simulation stimuli, allowing the performance of the device in the measurement system to be directly linked to the final application [6-8].
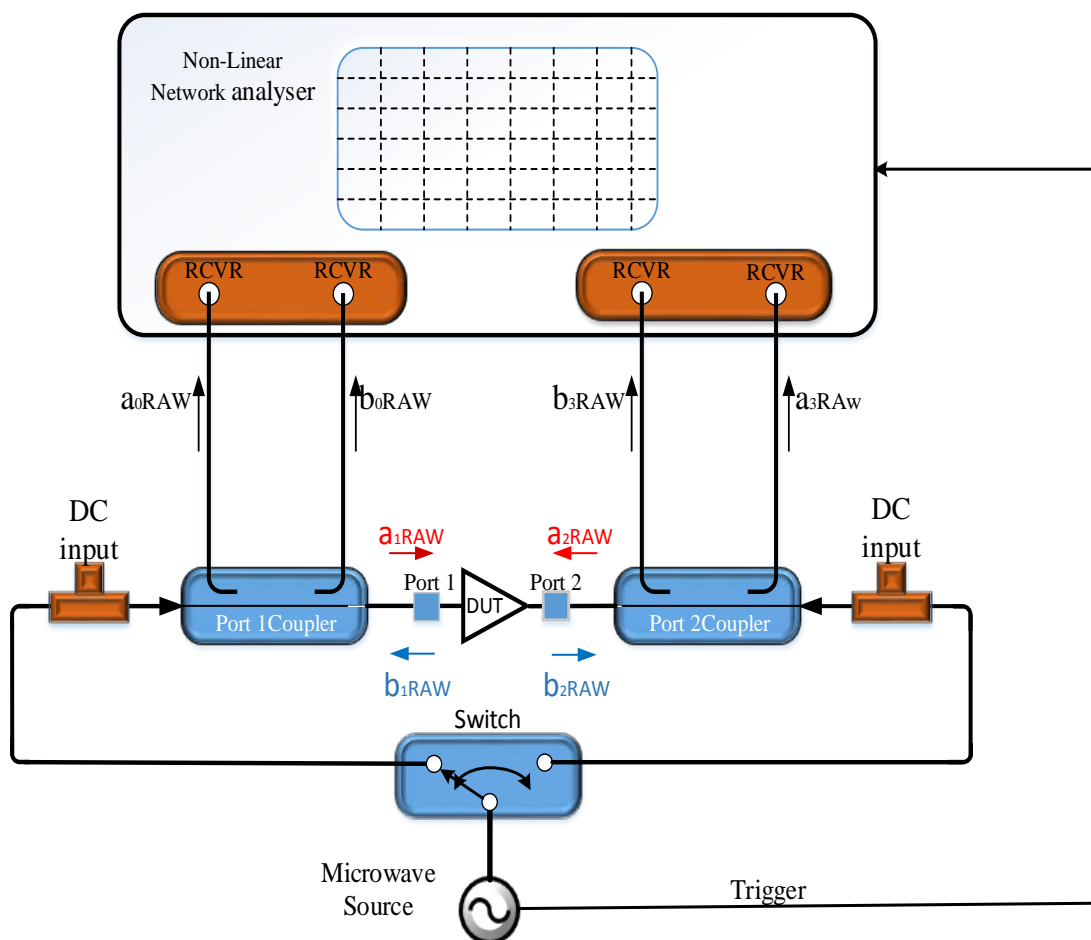
FIGURE 1-1 NON LINEAR NETWORK ANALYSER.

1.2 MOTIVATION

According to recent market research [5], firm insight research Corp, the total revenue for telecommunications industry for 2015 is set to reach $2.1 trillion and expected industry revenue will grow up at an average annual rate of 5.3% to $2.7 trillion in 2017. Growing revenue combined with a requirement for new end products that not only provide added functionality, but also offer continually improving performance, poses major challenges, pushing the industry to evolve and change. The demand for high spectral efficiency and high data rates inevitably results in new modulation schemes and increased design complexity. In order to meet these growing requirements for performance a more flexible, faster and accurate design and realisation approach for RF devices, circuits and systems is required [7]. Generating, testing and validation of robust computer aided design (CAD) models opens the door to design, test and optimisation of devices and circuits being linked within simulation environments [8].

Appropriate measurement data should be used to generate CAD models. The use of CAD tools is becoming fundamental in PA design to obtaining 1st pass design success, but this depends heavily on the accuracy of the models for the DUT. A non-accurate measurement system, leads to a poor model which means at the simulation stage the design is not optimised correctly. This will give unsatisfactory results increased design costs and fabrication processes, moreover leading to increased time expenditure. This in turn means the accurate extraction and validation for DUT models is an important factor that determines the success of the design [9- 11].

For linear design, the desired measurement data are S-parameters. S-parameter measurements are carried out under small signal conditions by using vector network analysis (VNA) as shown below in Figure 1-2.
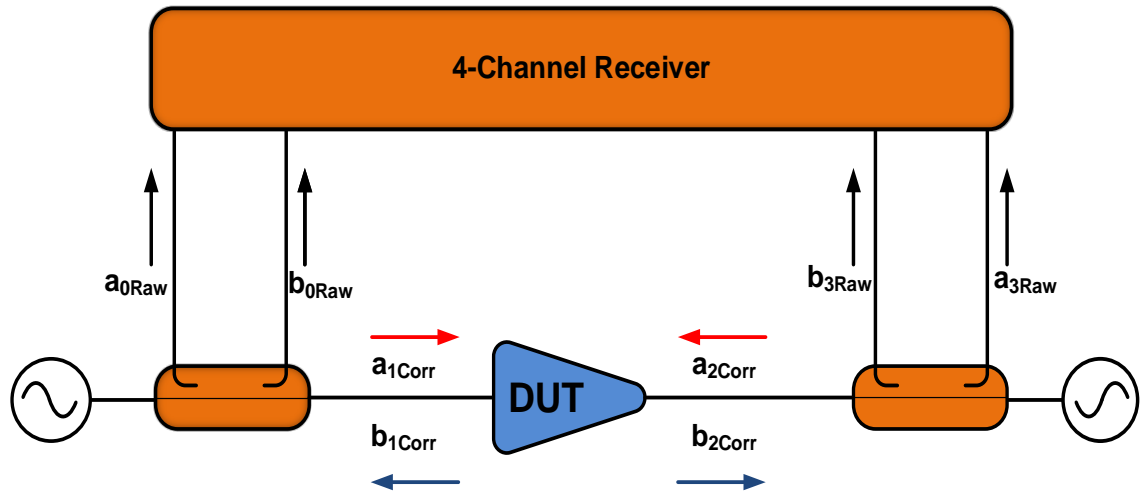
FIGURE 1-2 A GENERIC TWO PORT LSNA RF ARCHITECTURE WITH INTEGRATED ACTIVE LOAD-PULL.

Only the perfect instrument would not need correction, however measurement instruments have imperfections and thereby do not provide the ideal measurement required by PA designers. Therefore all measurement results include some measurement uncertainty. The sources of uncertainty (error in VNA measurements) are essentially the result of systematic, random, and drift errors. Systematic error can be removed by using the equation 1-2 which is representing the general calibration formula. Random and drift measurement errors vary randomly as a function of time, this type of error, cannot be completely removed but random errors could be reduced by averaging, and drift errors limited by controlling the environment [11, 12].

$$
\begin{bmatrix} b_1 \\ a_1 \\ b_2 \\ a_2 \end{bmatrix} =
\begin{bmatrix}
\dfrac{1}{e_{01}e_{10}} & \dfrac{-e_{00}}{e_{01}e_{10}} & 0 & 0 \\[2mm]
\dfrac{e_{11}}{e_{01}e_{10}} & \dfrac{(e_{01}e_{10}-e_{00}e_{11})}{e_{10}e_{01}} & 0 & 0 \\[2mm]
0 & 0 & \dfrac{1}{e_{32}e_{10}} & -\dfrac{e_{33}}{e_{32}e_{10}} \\[2mm]
0 & 0 & \dfrac{e_{22}}{e_{32}e_{10}} & \dfrac{(e_{32}e_{23}-e_{33}e_{22})}{e_{32}e_{10}}
\end{bmatrix}
\cdot
\begin{bmatrix} b_0 \\ a_0 \\ b_3 \\ a_3 \end{bmatrix}
\qquad \text{EQUATION 1-2}
$$

Spectrum analysers, power meters, oscilloscopes and vector network analyzer (VNA) are used to acquire and analyse RF signals. Operating the transistor nearer to its compression region is due to increased demand for enhanced performance from the transistor devices [13].

Nonlinear vector network analyzer (NVNA) is an instrument that depends on VNA measurements with extended capabilities. It must be used with large signal RF measurements to truly characterise the nonlinear devices. A historical overview of the development of the LSNA, by M. Sipila was published in 1988 a first prototype of a LSNA, The aim was to build a measurement system that could perform accurate measurement of the voltage and current waveforms at the gate and drain of a HF transistor. The measurements are performed in the time domain using a broadband sampling oscilloscope and Fourier transforms into the frequency domain. After error correction, the results are transformed back into the time domain [14].

All previous measurement systems have the ability to observe and quantify the time varying voltage $V_n(t)$and current $I_n(t)$ present at all terminals of the Device Under Test (DUT): thus involves all frequencies including DC, IF and RF because this type of measurement system has fixed impedance which is lead for a limited insight into the non-linear behaviour of semiconductor devices [15].

The PA designers require more information about the DUT to improve power amplifier efficiency. It is worth mentioning that significant design effort is devoted to developing microwave transistors and high-performance RF thereby an accurate and repeatable characterisation tool is required to estimate the performance of the transistor for this *"Waveform-Engineering"* necessary to obtain these aims [16].

Waveform-engineering is defined as: The ability to modify in a quantified manner the time varying voltage $V_n(t)$and current $I_n(t)$present at the terminals of the Device under Test (DUT): thus involves all frequencies including DC, IF and RF [16, 17].

The waveform engineering technique is suitable for use in the investigation, design and evaluation loop of RF power amplifiers. Use of the waveform engineering technique in RF power amplifier design facilitates an intelligent new design process and eliminates the black box design process [18].

Theoretical waveform analysis supports power amplifier design by improving computer-aided design (CAD) accessible behavioural or the accuracy of nonlinear transistor models or behavioural model parameter datasets [18].

1.3 OBJECTIVES AND STRUCTURE OF THE THESIS

The research work present in this thesis focuses on improving the calibration of a non-linear RF measurements system and so increases the capability and accuracy of such measurements systems.

The main objective of this thesis is to advance the operation and calibration of VNA-based large signal RF I-V waveform measurements systems. Targeting the elimination of the harmonic phase reference standard and improving the vector measurement accuracy, especially near the edge of the smith chart, is very important in load-pull measurement systems. The ultimate aim for improving the operation and calibration of emerging VNA based NVNA measurement systems is to reduce restrictions on the frequency grid and bandwidth. Importantly, as no dedicated channel is required for triggering during waveform measurements, all four VNA ports are available for DUT characterisation, eliminating the need for multiplexing measurement signals, and allowing a simple and rapid measurement approach.

1.4 CHAPTER SYNOPSIS

Chapter 2: presents a literature review of the waveform measurement techniques that have been employed starting from DC to RF. Specifically mentioned and discussed are: S-parameters, error models, small signal calibration and large signal calibration. Two-port calibration techniques are also discussed in detail.

Chapter 3: shows the enhancement calibration that can be achieved by varying the output reflection coefficient around a Smith chart by using a Load-pull system in combination with a TRL calibration technique. Also described is the use of the load pull system with TRL calibration algorithm to achieve more accurate calibration results. The quality of raw data collected during calibration process and its effect on calibration accuracy is discussed, as well as changes to the reflection coefficient and its impact on the quality of raw data.

Chapter 4: contains a review of the various Nonlinear Measurement systems in use today, including sample-based and mixer based approaches. Also presented is an overview of the different architectures of several Non-linear measurement systems and calibration techniques that are used to make these measurements is acceptable.

Chapter 5: investigates a new approach that allows a Vector Network Analyzer to be operated as a Large Signal Network Analyzer without the need for a harmonic phase reference generator. Extensive verification shows how certain VNAs have coherent sources. Investigations of calibration and operation of VNAs based on LSNAs are now possible through the use of a phase meter to calibrate the measured phase of the VNA during the calibration process and allow to alignment and to improve bandwidth and thus improve measurement system utilisation efficiency.

Chapter 6: is a conclusion to the thesis that presents a discussions on future developments of the measurement system that can benefit from this work.

1.5 REFERENCE

1- White, J.F., High Frequency Techniques: An Introduction to RF and Microwave Engineering. 2003: Wiley.

2- González, G., Microwave transistor amplifiers: analysis and design. 1984: Prentice-Hall.

3- Dunsmore, J.P., Handbook of Microwave Component Measurements: with Advanced VNA Techniques. 2012: Wiley.

4- Golio, M. and J. Golio, RF and Microwave Circuits, Measurements, and Modeling. 2007: Taylor & Francis.

5- Cripps, S.C., RF Power Amplifiers for Wireless Communications. 2006: Artech House.

6- McGenn, W., RF IV Waveform Engineering Applied to VSWR Sweeps and RF Stress Testing. 2013.

7- Epstein, Z. Global telecommunications industry revenue to reach $2.1 trillion in 2012. 2012 [cited 2014 1/12]; Available from: http://bgr.com/2012/01/05/global-telecommunications-industry-revenue-to-reach-2-1-trillion-in-2012/.

8- Collin, R.E., Foundations for Microwave Engineering. 2001: Wiley.

9- Golio, M. and J. Golio, RF and Microwave Passive and Active Technologies. 2007: Taylor & Francis.

10- Agilent, Network Analyzer Basics. 2010, Agilent Technologies.

11- Agilent. S-Parameter Design Application Note Agilent AN 154. USA.

12- Sasaoka, H., Mobile Communications. 2000: Ohmsha Limited.

13- Agilent, AN 1287-3 Applying Error Correction to Network Analyzer Measurements. 2002.

14-   Sipila, M., K. Lehtinen, and V. Porra, High-frequency periodic time-domain waveform measurement system. Microwave Theory and Techniques, IEEE Transactions on, 1988. 36(10): p. 1397-1405.

15-   Tasker, P.J., Practical waveform engineering. Microwave Magazine, IEEE, 2009. 10(7): p. 65-76.

16-   Tasker, P.J. RF Waveform Measurement and Engineering. in Compound Semiconductor Integrated Circuit Symposium, 2009. CISC 2009. Annual IEEE. 2009.

17-   Tasker, P.J., et al. Wideband PA Design: The "Continuous" Mode of Operation. in Compound Semiconductor Integrated Circuit Symposium (CSICS), 2012 IEEE. 2012.

18-   El-deeb, W.S., et al., Small-signal, complex distortion and waveform measurement system for multiport microwave devices. Instrumentation & Measurement Magazine, IEEE, 2011. 14(3): p. 28-33.

2. CHAPTER 2

CALIBRATION AND OPERATION OF A NON-LINEAR MEASUREMENT SYSTEM: LINEAR CALIBRATION

1.6 INTRODUCTION

The literature review of existing linear RF measurement systems, architectures and calibration methods used to calibrate the measurements systems. The different measurement architectures will be discussed along with the advantages and the high-lighting the problems of each of the measurement techniques.

1.7 RF WAVEFORM MEASUREMENT

Waveform measurement can be defined as "the ability to observe and quantify the time varying voltage $V_n(t)$ and current $I_n(t)$ present at all terminals of a device under test (DUT): this involves all frequencies including DC, IF and RF"[1]. In general the frequency domain is normal for standard microwave measurement tools. For more than 30 years, the vector network analyzer (VNA) has been a key-tool in any RF and microwave laboratory, specifically for measuring the S-parameters of a system [2].
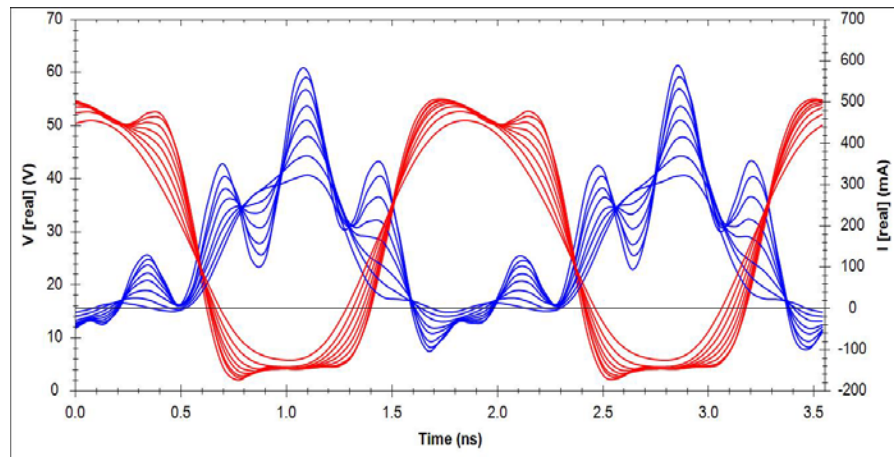
FIGURE 2-1WAVEFORM ENGINEERING.

The technique that is used to measure current and voltage (I-V) waveforms depends largely upon the relation between the length of the conductor and the wavelength of the signal. For example, a normal wire is used as a probe at low frequencies (when the length of the cables in the system are much smaller than the wavelength of the signals). At high frequencies (in practice, all frequencies higher than 10MHz are considered to be a high frequency) a different technique needs to be implemented to measure I-V waveforms. This technique is implemented because the length of conductors involved in the system is much larger than the wavelength of signals and the impossibility to control low or high impedances across the entire bandwidth, ruling out the use of simple current and voltage probes [3].

This will lead to connection mismatch problems among the DUT, signal source, and data acquisition samplers, therefore a transmission line is necessary for efficient power transmission. There are many obstacles in measuring high-frequency I-V waveforms. The main issue arises from common technological limitations that are generic at high frequencies. From the above problem, we can understand the inability of standard oscilloscopes to measure all the harmonic components, because of the restriction in bandwidth of the scopes. Obtaining I-V waveforms at high frequencies, can be achieved by measuring the incident, reflected and transmitted travelling waves travelling along the transmission line [2, 3]. The incident (a_n^h) and reflected (b_n^h) components at the terminals of the DUT consist of fundamental and harmonic waves. These can then be used to calculate the periodic current and voltage waveforms at the terminals of the device, where *h* refers to the harmonic number and *n* the DUT port number [4].

1.7.1 DC MEASUREMENT

DC measurement is considered to be an important initial step used by both RFPA designers and device manufacturers. There are many different methods to characterise the DC electrical properties of an RF transistor, but all typically involve varying input and output bias voltages, and observing the resultant drain current. This data is then plotted as output current vs. input voltage, and output current vs. output voltage, output characteristics [5].
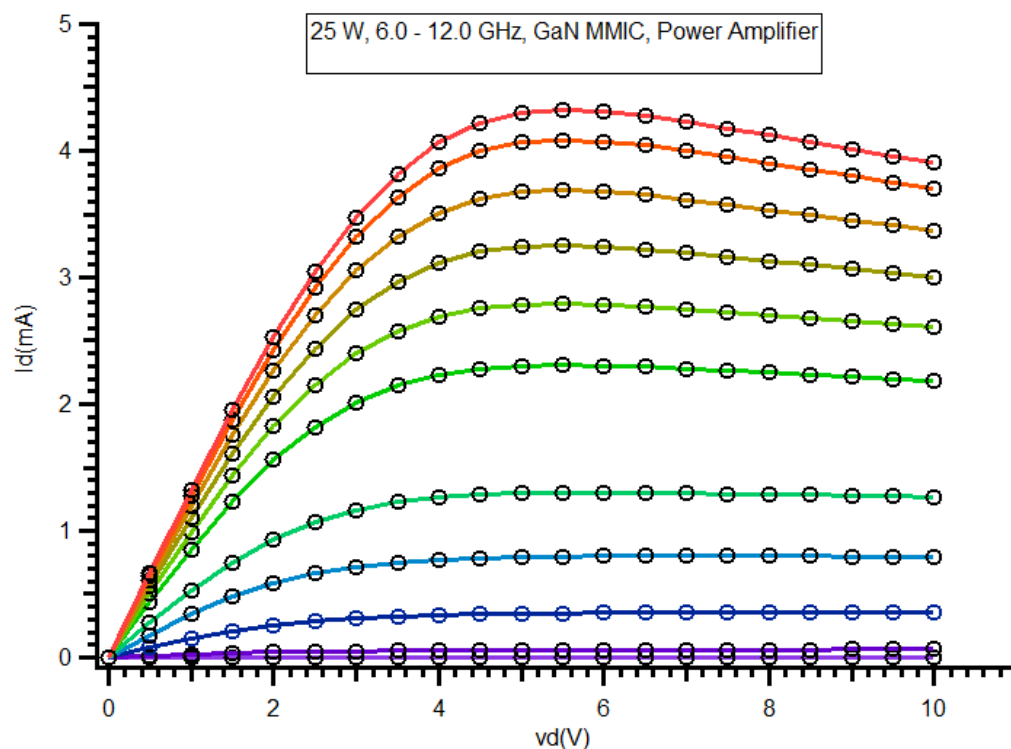
FIGURE 2-2 DCIV MEASUREMENT OF AN FET DEVICE.

1.7.2 RF MEASUREMENTS(S-PARAMETER)

Scattering- (or S-) parameters are important in microwave design, and are considered as the mathematical regime for representing linear networks at higher frequencies, being considered the optimal tool for simulation and design since the 1960s. S-parameters describe the magnitude and phase relationships between incident and reflected travelling waves, and as result are able to accurately characterise and analyse the electrical behaviour of linear time invariant systems. S-parameters are based on the super position principle, and therefore, can be used only with linear systems. S-parameters have many

advantages over other parameters which is related to familiar measurements (gain, loss, reflection coefficient etc) [5].

S-parameters represent the ratios between incident ($a(f)_n$) and reflect ($b(f)_n$) travelling waves for each port(n) as a function of frequency(f), which are related to a constant measurement impedance environment of 50Ω, as shown in equation 2-1. Where (j) refers to the receiver port and (i) refers to sender port [5].

$$S(f)_{ji} = \frac{b(f)_j}{a(f)_i}$$ EQUATION 2-1
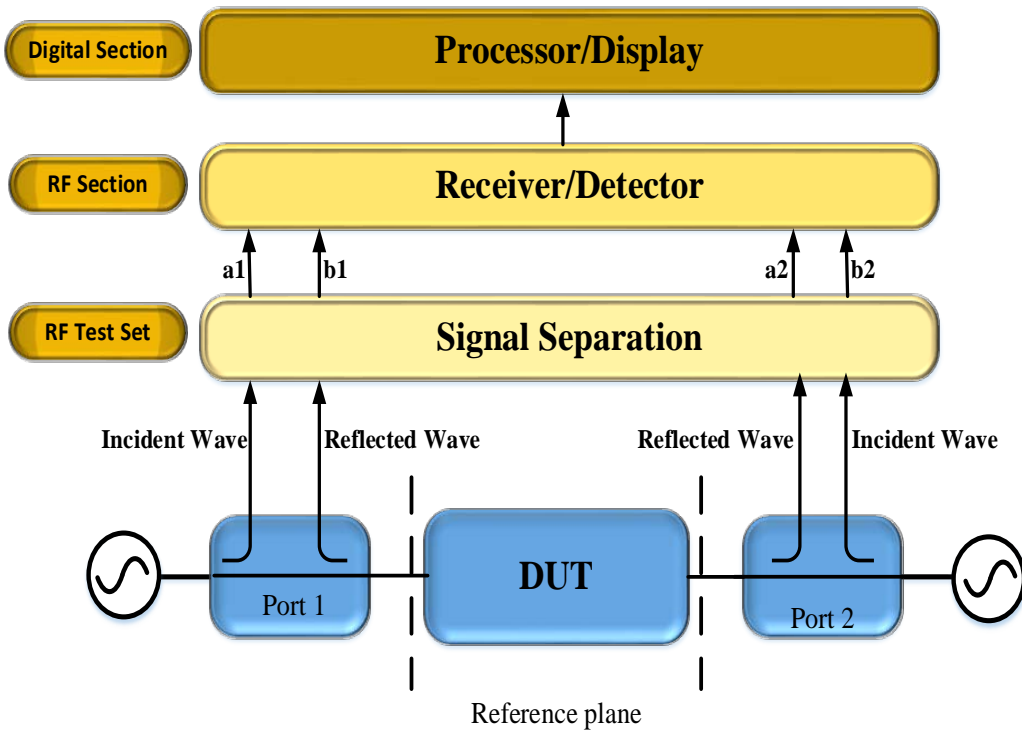
FIGURE 2-3 SIMPLIFIED BLOCK SCHEMATIC OF TWO-PORT VNA.

N^2 An N-port device is defined by N^2 S-parameters represent. By using equation 2-1, can lead to obtain equation 2-2 to represent the network which consists of N-ports in an S-parameter matrix.

$$\begin{bmatrix} b_1 \\ \vdots \\ b_n \end{bmatrix} = \begin{bmatrix} S_{11} & \cdots & S_{1m} \\ \vdots & \ddots & \vdots \\ S_{n1} & \cdots & S_{nm} \end{bmatrix} \cdot \begin{bmatrix} a_1 \\ \vdots \\ a_m \end{bmatrix}$$ EQUATION 2-2

The periodic voltage and current waveforms at higher frequencies can be calculated at the terminal of device under test from the measured travelling waves as shown in equation 2-3 and 2-4. The periodic voltage and current waveforms consist of fundamental and harmonic waves (a_n^i) and (b_n^i), where (n) represent the number of ports and (i) represent harmonic number.

$$V_n^{(i)} = \sqrt{Z_o}\left(a_n^{(i)} + b_n^{(i)}\right) \qquad \text{EQUATION 2-3}$$

$$I_n^{(i)} = \sqrt{1/Z_o}\left(a_n^{(i)} - b_n^{(i)}\right) \qquad \text{EQUATION 2-4}$$

Where Z_o is 50 Ω for all harmonics, $V_n^{(i)}$ and $I_n^{(i)}$ are the (i)th Fourier coefficients [3,6].

S-parameter data describes the behaviour of a device under test when undergoing various situations. This is achieved by measuring the incident and reflected travelling waves at the input and output of DUT. Determination of S-parameters is the principle measurement capability of vector network analyzers (VNA). Characterisation of most types of microwave components is carried out using a classic vector network analyzer (VNA) to measure the S-parameters. S-parameter data obtained from the measurement stage can be imported directly into the designers CAD environment, where the simulated device behaviour precisely copies the measured device behaviour. Highly efficient design can be achieved, by using VNA to provide a consistency check between the mathematical abstraction that resides inside the simulator and the actual physical device [7, 8].

Vector network analyzers (VNA) are an essential tool in measuring and characterising power amplifiers (PAs), components and circuits. A VNA is usually applied to measure small signal or linear characteristics of multi-port networks, at frequencies ranging from RF to beyond 100 GHz, it compares the incident wave to reflected wave. The S-parameter for represent the relationship between scattered waves (a, b) and the S-parameter values will be complex liner power quantities. The definitions of the S-parameter for two port device are shown in Equation 2-5 [8].

$$\underbrace{\begin{bmatrix} b_1 \\ b_2 \end{bmatrix}}_{\text{Reflection Waves}} = \begin{bmatrix} S_{11} & S_{12} \\ S_{21} & S_{22} \end{bmatrix} \cdot \underbrace{\begin{bmatrix} a_1 \\ a_2 \end{bmatrix}}_{\text{Incident Waves}}$$

Port where measurement in made

Port where Stimulus in made
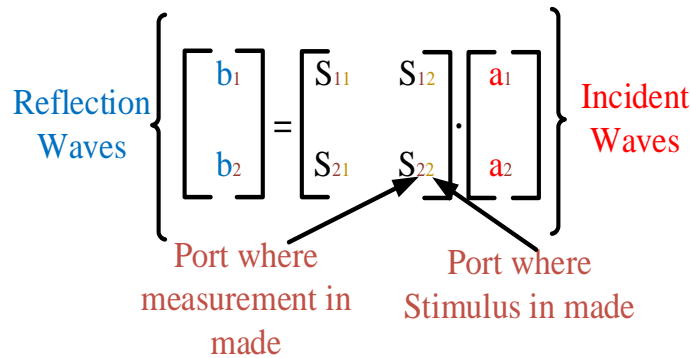
EQUATION 2-5

ABOVE DIAGRAM STIMULS IS MADE NOT IN MADE

The S-parameter terms for the two-port device will be:-

S_{11}= Forward reflection coefficient (input match),

S_{22}= Reverse reflection coefficient (output match).

S_{21}= Forward transmission coefficient (gain or loss).

S_{12}= Reverse transmission coefficient (isolation).

The VNA can perform many types of measurements such as reflection coefficients (S_{11}, S_{22}), Impedance (r+jx), Return loss (dB),Reflection coefficients vs. Distance (Fourier Transform), VSWR, gain (dB), insertion phase (degrees) and insertion loss (dB) usually used to measure small signal or linear characteristics of multi-port networks. The VNA architecture is limited for waveform engineering because the VNA is capable of measuring only a single frequency at a time. As result the VNA is not able to measure relative phase between different frequency components. Additionally, typical VNA measurements ignore non-linear effects due to memory effects and distortions generated by mixing. This means the systems are able to capture S-parameter with linear analysis because S-parameter uses the superposition principle therefore this type of system has no ability to measure, for example, energy transfer from the stimulus to other harmonic frequencies. This leads to the conclusion that the data obtained from this system has limitations for use in large signal device models [9].

A VNA made to precisely characterize the behaviour of a DUT by measuring the magnitude and phase of reflected (b) and incident (a) waves. By measuring the waves, VNA is able to give the characteristics of a DUT. The increased accuracy has lead to improvements in the design of RFPA. The cost involved prohibits the development of perfect VNA hardware that is perfect, in the sense that the need for error correction is totally eliminated.

Vector error correction is an effective method for obtaining improved in performance of system measurement. The relation between VNA hardware performance, system performance and cost, should be balanced across these elements. Vector error correction cannot amend errors due to poor VNA performance, on other hand good VNA that will not make up for inherent calibration in accuracies. Calibrating the VNA will lead to the eliminate the largest contributor to measurement uncertainty systematic errors [2, 9].

2.2.2.1 SOURCES AND TYPES OF ERRORS

It is useful for the designer to have accurate S-parameters of the DUT, thereby allowing creation of accurate system models for reduce design effort and rework. Only the perfect instrument would not need correction. Measurement instruments have imperfections, thereby leading to less than ideal measurements that are required by PA designers. Therefore, all measurement results obtained are liable to measurement uncertainty, and we can generally distinguish the source of uncertainty (error in VNA measurements) as being essentially the result of systematic, random, and drift errors [10].

Random and drift measurement errors vary randomly as a function of time. These types of errors cause measurement uncertainties that cannot easily be removed since they are unpredictable. Systematic measurement errors that cause measurement uncertainties due to imperfections in the VNA and test setup. During the measurement process, systematic errors can be removed through calibration and computational techniques, provided these errors are invariant with time. Signal leakage, signal reflections, and frequency response, are considered the source of systematic errors [11].

It is difficult to make the full correction of results because of superimposed random fluctuations in the measurement results. Both the measured (raw data) and the errors quantity (error terms) must be known to be able to correct systematic measurement errors as fully as possible; otherwise you will be unable to do this type of analysis. Calibration of VNA is therefore necessary in order to determine the error terms before starting measurement is required for the designer to obtain accurate S-parameter [11].

However, the calibration of a VNA (Small Signal) is not able to calculate all of the error terms. The calibration of one port will be able to find 3 from 4 terms, and 2 ports will be able to find 7 from 8 terms. In both cases one element is missing (e_{10}). This missing element can be found by adding more steps for calibration, but this will call large signal calibration procedure on one hand, but on the other hand, the complexity for system will be increased [2,3,12].

2.2.2.2 SMALL SIGNAL CALIBRATION

The need for reliable RF and microwave measurements appeared during the late 1950s and throughout the 1960s. Significant work was undertaken to develop coaxial connectors to achieve repeatable and reproducible measurements at microwave frequencies. Committees were established to organise and focus efforts for producing standards for these precision connectors [13].

For all network analysis measurement systems, errors can be separated into three categories, *drift errors*, *random errors* and *systematic errors*. The main factors that causes the random errors are instrument noise (the IF noise floor and sampler noise), connector repeatability and switch repeatability [11, 13].

When using network analysers, noise errors can usually be decreased by increasing source power, by using trace averaging over multiple sweeps, or narrowing the IF bandwidth. The thermal drift which is the main cause for drift error should be monitored even if the instrument has good thermal stability; these are basically caused by deviation in temperature and can be removed by controlling the environment. Any errors not invariant with time are considered to be *systematic errors* and can be removed through a calibration process. *Systematic errors* consists of six types, *Source* and *load* impedance mismatches relating to *reflections*, *crosstalk* and *directivity errors* relating to signal

leakage and frequency response errors caused by reflection and transmission tracking within the test receivers[13].

Error correction is used to correct the raw data collected during the measurement process. The error correction methods can be categorised into two groups: *response calibration,* and *vector error correction*. In general, response calibration is used widely used in calibration measurement system because of its limited ability to correct all error terms and this is due to response calibration allows correction of limited number of terms (*reflection* and *transmission tracking*). Open/short averaging is a term used to indicate the most advanced type of response calibration for reflection measurements. All systematic errors can be addressed by *vector error correction* which is a more thorough method of removing *systematic errors*. This method for correction requires a network analyzer that is capable of measuring *phase* and *magnitude* and an appropriate calibration kit with known standards [2, 13].

Calibration a procedure of steps to determine the errors terms (error models) of the VNA, which represent systematic errors under specified conditions. To obtain the error terms the relationship between the incident and reflected waves of measurement system needs to be calculated for set calibration measurements [2, 3, 14].

To recap, the measurement errors for two groups were classified as either *no error correction (random and adrift)* and *corrected (systematic)* by calibration. The first group of errors are unpredictable, but it is possible to improve them by signal to noise distance, compression of the receiver and stability of test setup and instrument. Systematic errors occur as a result of the internal and external test set, which can be corrected by system error correction and drift corrected by re-calibration. Systematic errors can be measured and removed mathematically. VNA calibration can be classified in to two different categories. The first type is a VNA hardware calibration. VNA hardware calibration is done by sending the VNA to the manufacturer which typically depends on time schedule obtained from factory, examples of this type of calibration are receiver accuracy and source power [10].

The 2nd type is the "local type". The aim of this form of calibration is to remove *systematic errors* from the measurement system as well as remove the effect of the connecting cables and probes with front panel of VNA. This type of calibration is used

every time a measurement set up is built to remove the systematic errors and effect of cables and probes. This is performed by connecting a device of known characteristics (Cal kits) to the end of cable, which is able to measure the cable effect on the signal [14].

Assuming measuring the impedance of an open circuit, the cal kit (open) is connected to the VNA through a cable. The impedance for the open circuit will be infinite and reflection (Γ=1) because the open circuit has the same magnitude and phase as the incident wave and reflect wave as shown below in Figure 2-4.
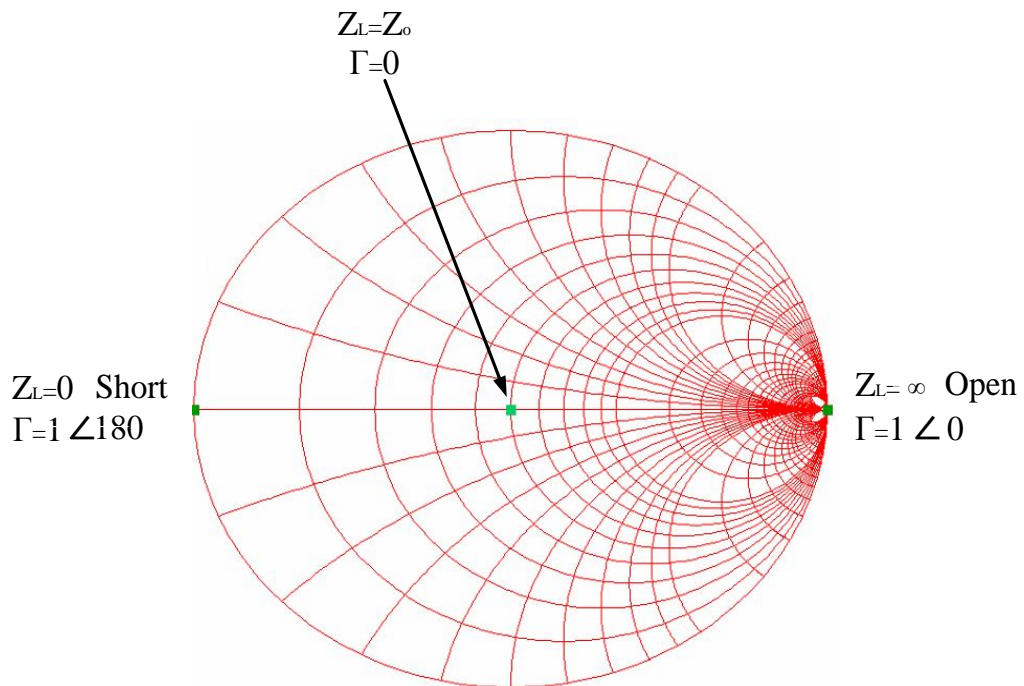
FIGURE 2-4 SMITH CHART.

The VNA measures the reflection of the open circuit which is affected by the length of cable between the open circuit and VNA port. The length of cable will affect the phase of the reflected waves. Assuming the port of the VNA is lossless, the delay due to the length of cable will obtain ($a^\sim$) as a result for the incident wave of (a). The reflection will be calculated from ,equations 2-6, 2-7 and 2-8 as shown below:-

$$a^\sim = e^{-j2\pi f\tau}.a \qquad \qquad \text{EQUATION 2-6}$$

$$b = e^{-j2\pi f\tau}.b^\sim \qquad \qquad \text{EQUATION 2-7}$$

The incident and reflected waves affected by the test port cable as shown in equations 2-8.

$$\Gamma = b\big/a = e^{-j4\pi f\tau}.\frac{b^{\sim}}{a^{\sim}} = e^{-j4\pi\tau}.\Gamma_{DUT}$$

EQUATION 2-8

The measured mismatch as result of effect the test port cable on waves, and it is this type of calibration that will be discussed in this thesis .These facts lead to the conclusion that VNA requires calibration to obtain accurate measurements. Can defined calibration as a technical procedure for removing the systematic errors from VNA, the essential requirement for removing systematic errors in VNA involves creating a model for the VNA systematic errors [2, 7, 12, 13].
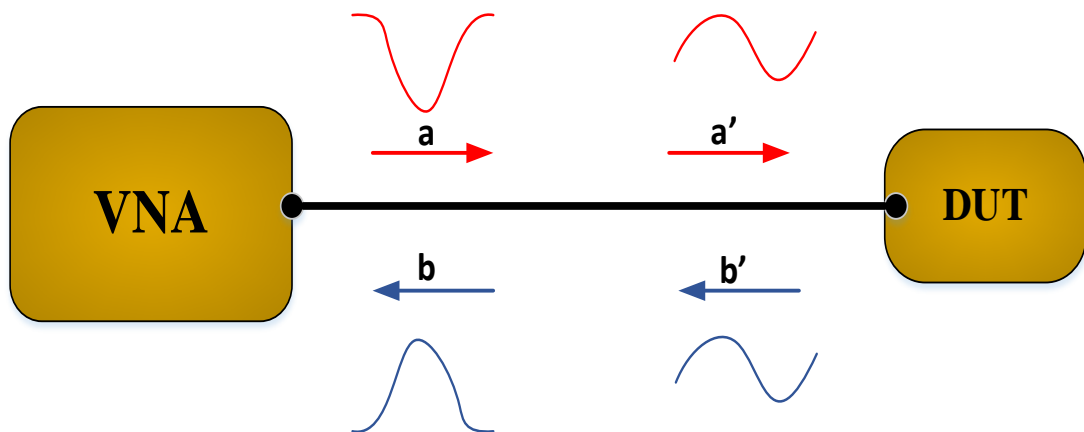
FIGURE 2-5 EFFECT OF TEST PORT CABLE ON DUT.

2.2.2.3 ERROR MODEL FOR VNA

An error model is a mathematical description of the relationship between measured data and physically present quantities. The error-model represent the systematic errors of the VNA system up to the reference plane. All error coefficients are determined at the end of the calibration process [2, 12].

At the end of the 1960s the first error models which is 12 term errors model were introduced for use in S-parameter error correction, followed by 16 and 8 term models.

The system error model, we developed provided insight into all possible signal paths including the main desired signals and match errors, losses, and leakage errors of the network analyzer along with the connectors, probes and cables that connect to DUT [12].

The error model was created to explain accurately how the calibration process is used to remove systematic error in the VNA. Figure 2-6 below shows the application in one port for VNA [15-18].
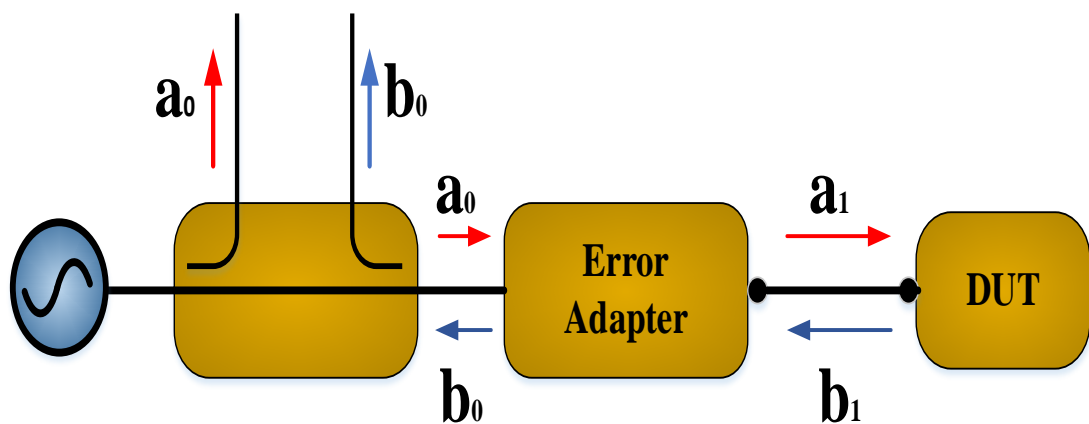
FIGURE 2-6 BASIC ERROR MODEL OF VNA.

A signal flow chart outlining a common error model (error adapter model) for one-port VNA is shown in Figure 2-7.
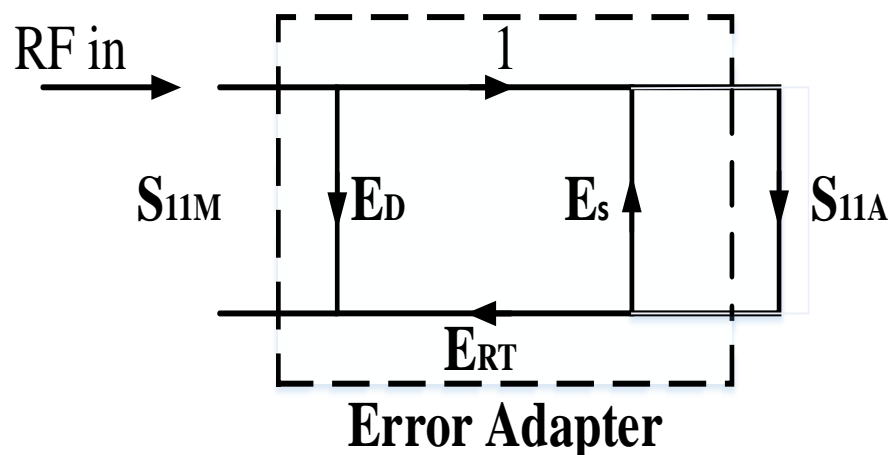
FIGURE 2-7 ONE PORT ERROR MODEL.

The error model is described using S-parameters, included in the power signal flow paths. The flow graph for the VNA one port error adapter consists of three types of errors. *Directivity* errors (E_D or e_{00}) can be defined as errors caused by directivity in the measured reflected signal, because the signal leakage paths bring about other signal components and the in directivity of the coupler. Source error E_S or e_{11} is a result of source matching which is obtained during measurement of the impedance in the reference plane and reflection of the tracking. Error E_{RT} or $e_{10}e_{10}$ is used for showing frequency tracking imperfections by comparing the reference and test channels and S measured S_{11M} and S actual S_{11A} [15].

In case of two port measurements the 12 term model represents the ability of a measurement system to measure a DUT which has two ports. This model is developed from the one-port error model. Error adapter of each port could be represented by the S-parameter model, which consists of the terms $S_{11}, S_{12}, S_{21}, S_{22}$ for each port (error adapter). This model is used mathematically to describe the relationship between corrected data and raw data (measured at the reference plane) which in turn is very useful for the calibration process and affect the accuracy of calibration results.

The 16-term error model is the ideal model for old version VNA (not used at present) to represent the measurement system using an error adapter between the actual measurements and the DUT. This error adapter represented all imaginable linear and stationary errors that are generated by the measurement system as shown in Figure 2-8 and Figure 2-9.
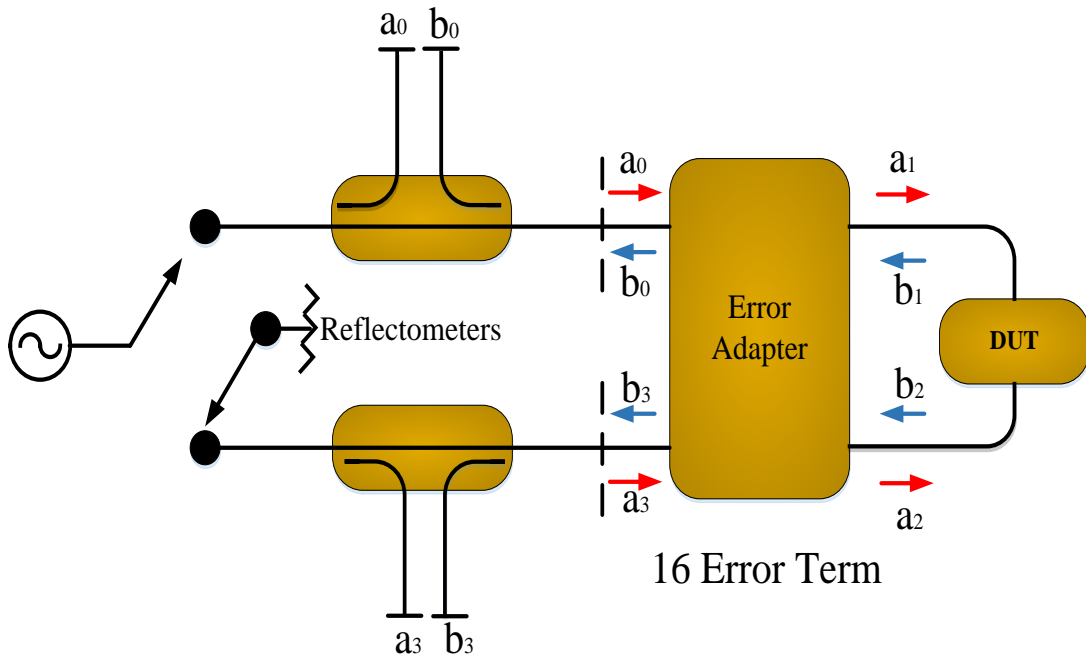
FIGURE 2-8 TERM ERROR MODEL.

e_{00}, e_{33} Directivity
e_{11}, e_{22} Port Match
$e_{10}, e_{01}, e_{32}, e_{23}$ Tracking
e_{30}, e_{03} Primary Leakage
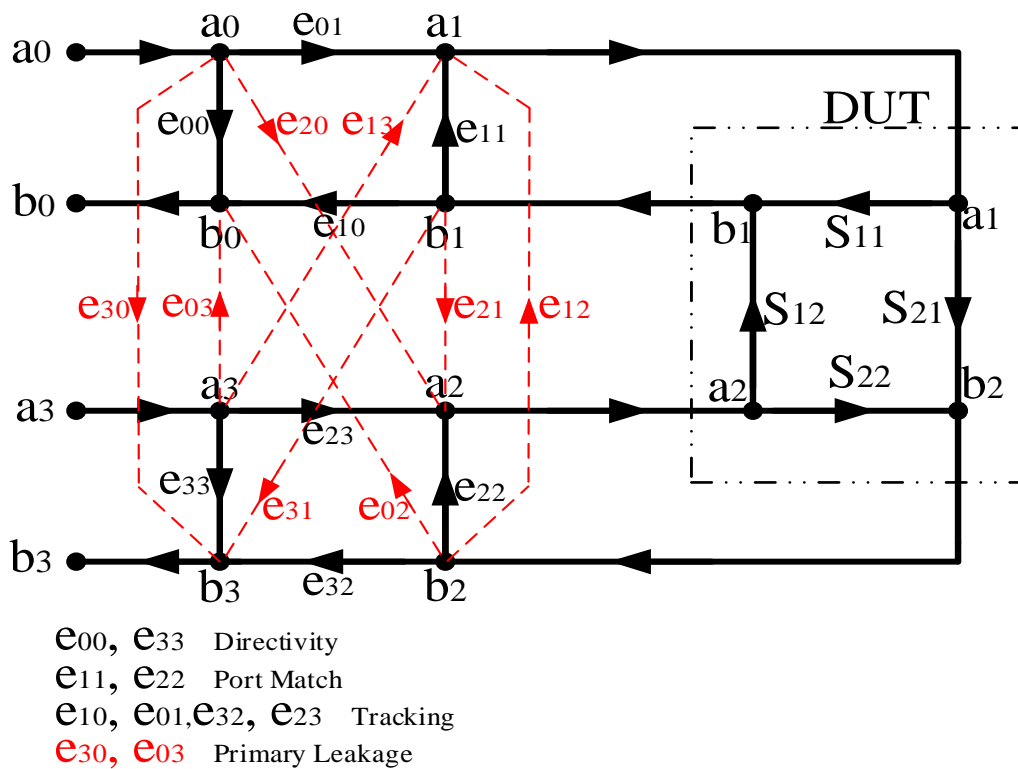
FIGURE 2-9 SMPLIFIED 16-TERM ERROR MODEL.

This model consists of 16 terms, of which 8 are critical. These 8 cover the tracking errors, port match and directivity, and the second 8 represent the leakage terms. The 8

terms model is obtained from the 16-term model by assuming that the leakage terms are all zero.

The two port error model consists of two modes a forward mode, which is a RF signal applied to Port 1 and, a reverse mode, which is a RF signal applied to Port 2 to find the 12 error term values for the two-port error model. The flow graph in Figure 2-10 shows the 12 term two port error model, which is often simplified, as shown in Figure 2-11.The flow graph in Figure 2-11 is made up of individual error adapters for Port1 and Port2.
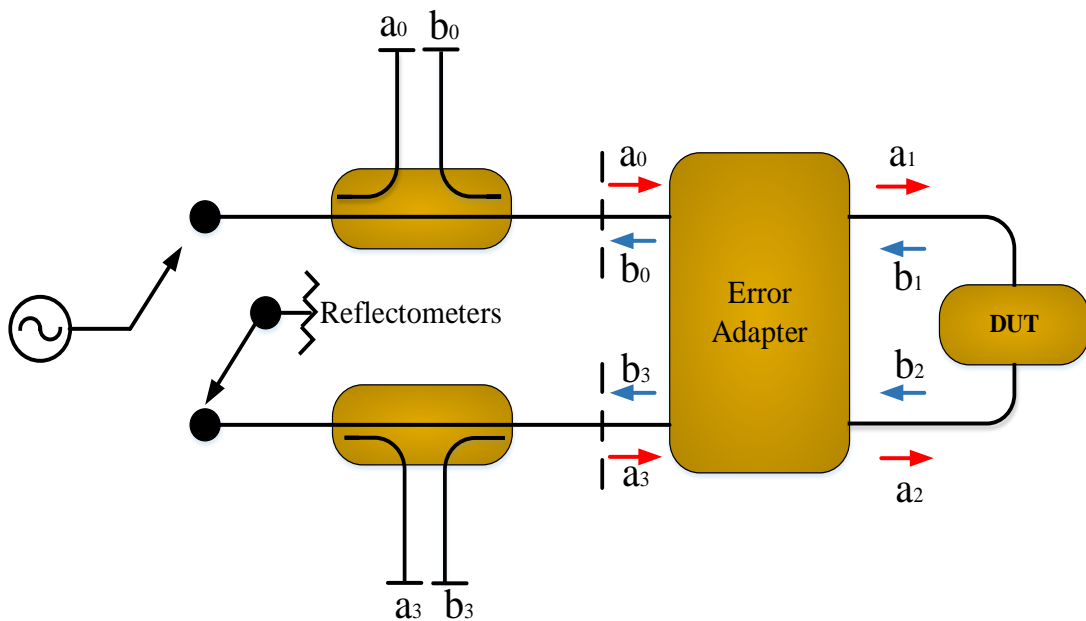
FIGURE 2-10 TWO-PORT ERROR MODEL FORMULATION.
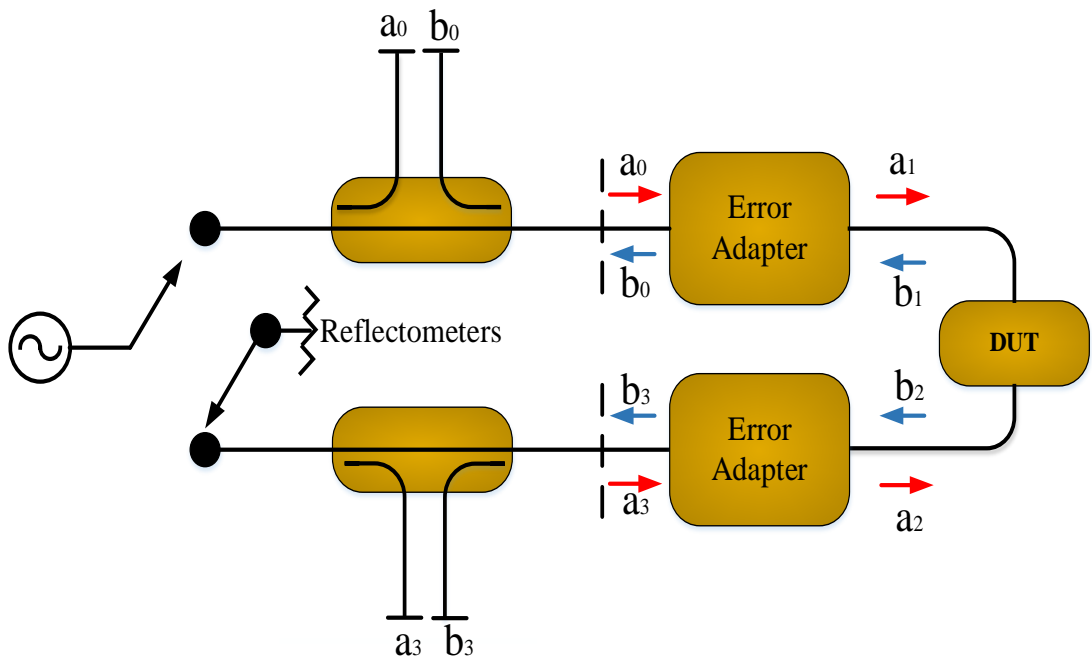
FIGURE 2-11 SIMPLIFIED TWO-PORT ERROR MODEL.

The error-adapter for the two port measurement system is simplified to one error adapter for each port, as shown in Figure 2-11. Neglect Leakage Terms: reduce to two one-port error adapter model as shown in Figure 2-12.
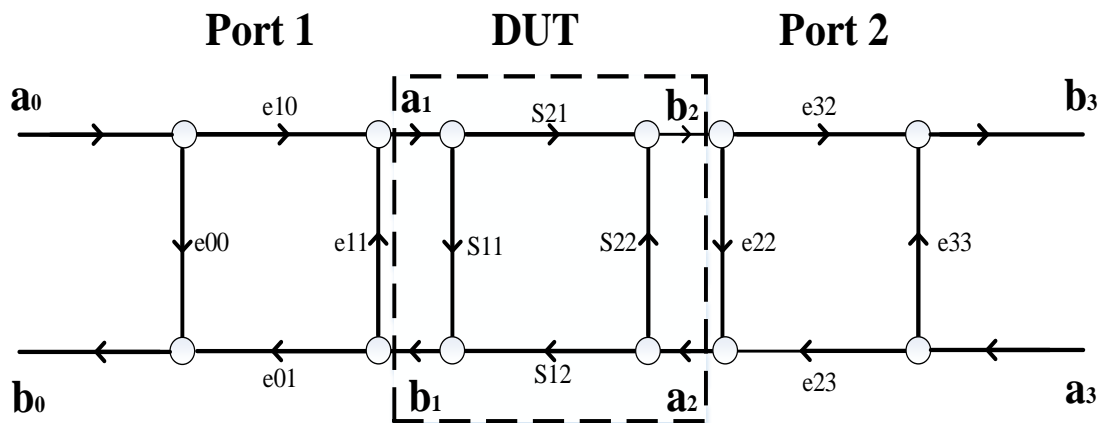
FIGURE 2-12 SIMPLIFIED TWO-PORT ERROR MODEL.

The error model for two ports consist of two directions modes: forward and reverse, to find the error terms value for two port error model. As a result, for the ability of the

VNA to measure only three waves at a time, five terms can be found in forward mode and the sixth term added to represent the leakage e_{30} , directivity e_{00} ,reflection $e_{10}e_{01}$, Port 1 forward mismatch error e_{11},transmission $e_{10}e_{32}'$ and Port 2 forward mismatch error e_{22}'. The forward flow graph for two port error model assumes $a_3 = 0$ as shown in Figure 2-13 and simplified in Figure 2-14 or Figure 2-15.

Forward (a₃ ≠ 0)
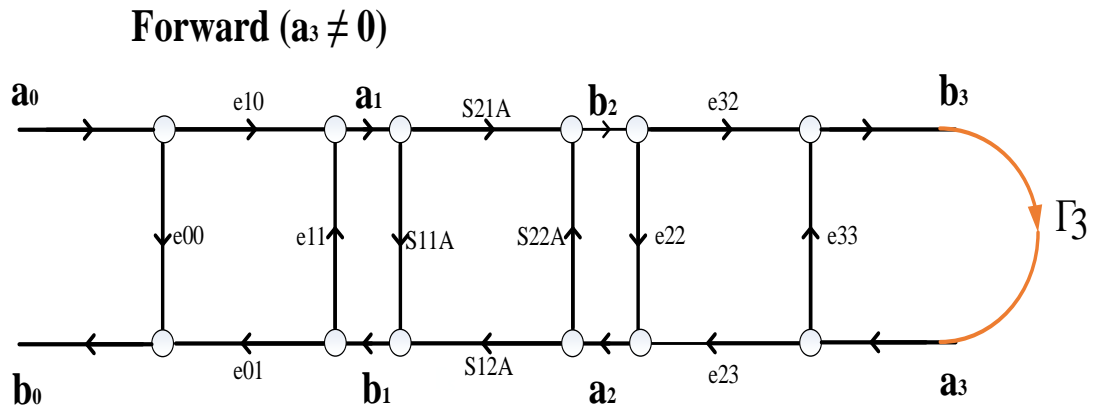
FIGURE 2-13 FORWARD TWO-PORT ERROR MODEL.

Forward Error Model
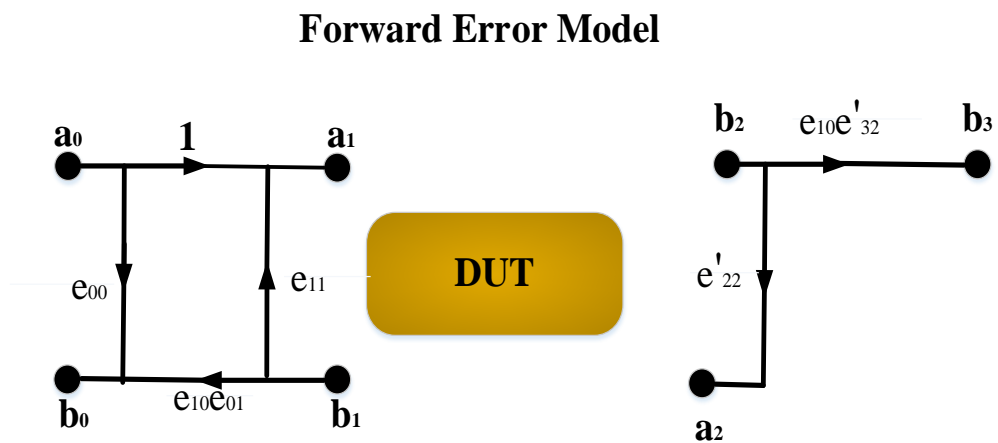
FIGURE 2-14 SIMPLIFY FLOW GRAPH.
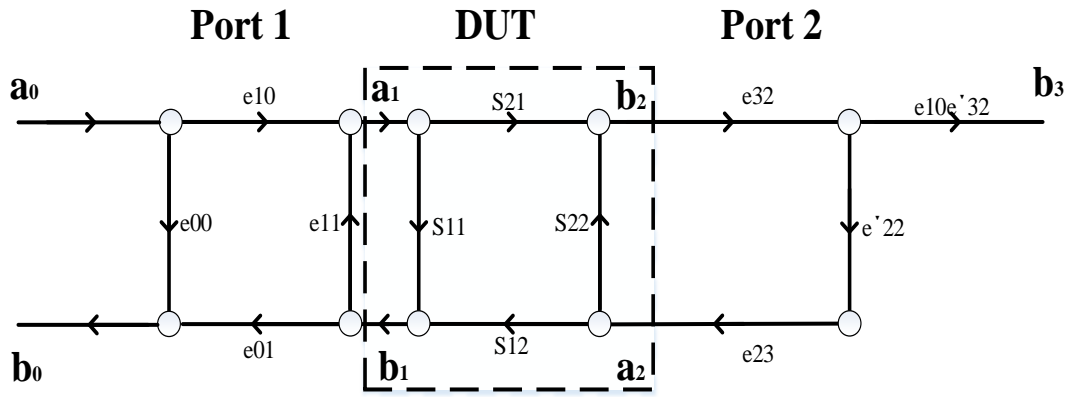
FIGURE 2-15 SIMPLIFY FLOW GRAPH.

Where

$$e'_{22} = e_{22} + \frac{e_{32}e_{23}\Gamma_3}{1-e_{33}\Gamma_3} \qquad \text{EQUATION 2-9}$$

$$e'_{32} = \frac{e_{32}}{1-e_{33}\Gamma_3} \qquad \text{EQUATION 2-10}$$

And other six error terms obtained from reverse error direction directivity e_{33}, reflection $e_{23}e_{32}$, Port 2 forward mismatch error e_{22}, transmission $e_{23}e'_{01}$ and Port 1 forward mismatch error e'_{11}. The reverse flow graph for the two-port error model assume $a_0 = 0$ as shown in Figure 2-16 and simplified in Figure 2-17.
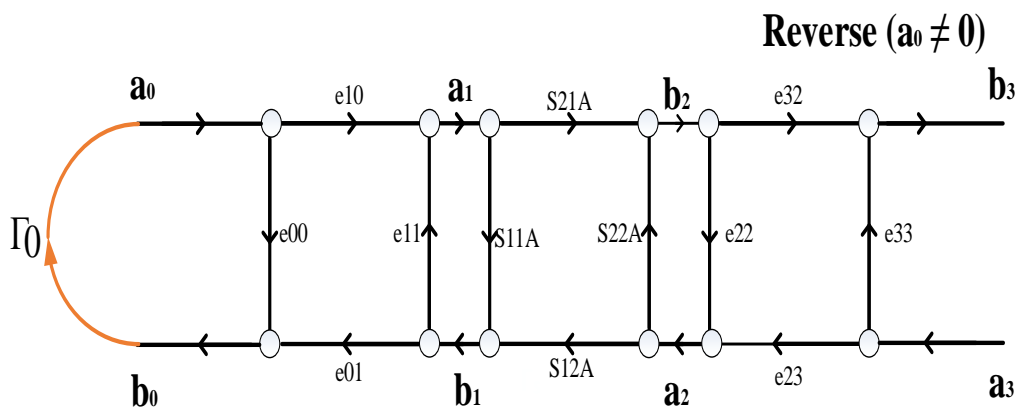
FIGURE 2-16 REVERSE TWO-PORT ERROR MODEL.

Reverse Error Model
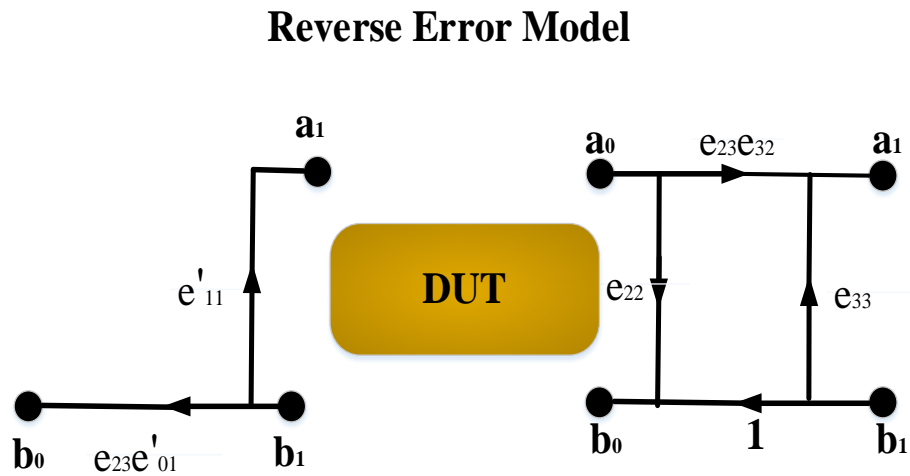
FIGURE 2-17 SIMPLIFY FLOW GRAPH.

The correction flow graph of the two-port (8 term model) is shown in Figure 2-18, and displays four error-terms for each port. The error model for the two-port model consists of 8 error-terms, as could be seen the neglected leakage terms (or crosstalk terms) for 8 term model but later will be added to the 16-term model, one for forward mode and one for reverse mode as result the number of error terms will be increased to ten terms. This model consists of 8 terms the directivity errors (e_{00}, e_{33}), reflection tracking $(e_{10}e_{01})$, transmission tracking $e_{10}e_{32}$, port mismatch errors (e_{11}, e_{22}) , tracking error $(e_{23}e_{32})$ and tracking errors $(e_{23}e_{01})$.

Error Model Port 1   DUT   Error Model Port 2

a_0 $\quad$ a_1 $\quad$ b_2 $\quad$ b_3

e_{10} $\qquad$ S_{21} $\qquad$ e_{32}

e_{00} $\quad$ e_{11} $\quad$ S_{11} $\quad$ S_{22} $\quad$ e_{22} $\quad$ e_{33}

e_{01} $\qquad$ S_{12} $\qquad$ e_{23}

b_0 $\quad$ b_1 $\quad$ a_2 $\quad$ a_3

e_{00} e_{33} =Directivity Errors

$e_{10}e_{01}$ =Reflection

$e_{23}e_{32}$ =Tracking Errors

e_{11} e_{22} =Port Mismatch Errors

$e_{10}e_{32}$ =Transmission

$e_{23}e_{01}$ =Tracking Errors
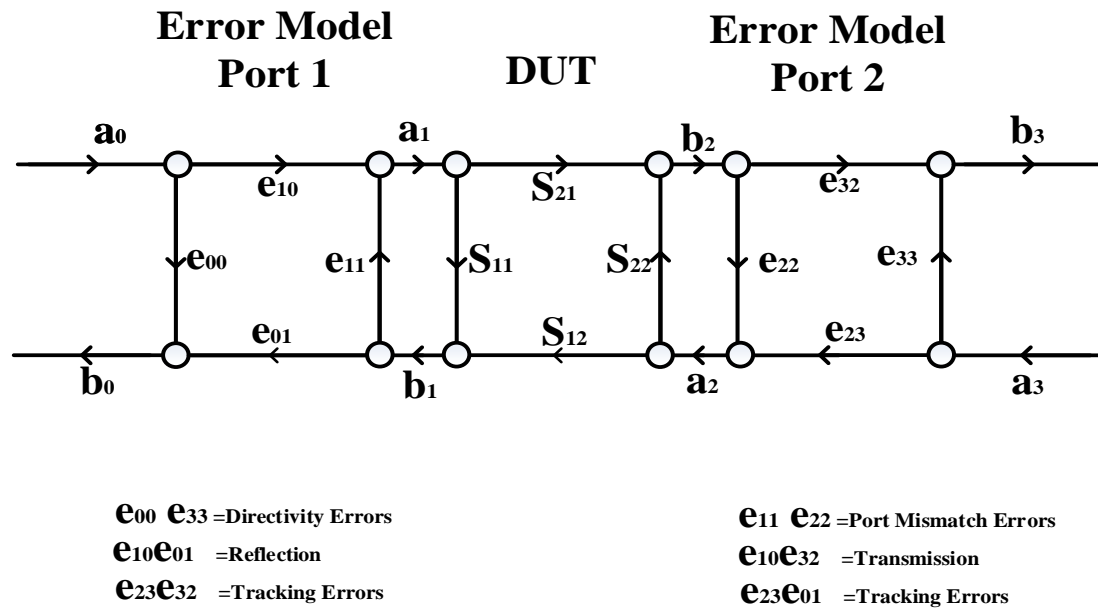
FIGURE 2-18 TERM ERROR MODEL.

The 12 error terms and 8 error terms both of them represent the error model for two port error model, there are ability to convert from 12 terms to 8 terms   or vice versa.

The vector error correction method involves a process of characterising systematic error terms which is achieved by measuring known standards to remove effects from subsequent measurements. Calibration requires several standards to determine error coefficients. The type of algorithm used in calibration determines the choose of the calibration standards. There are many type of calibration algorithms such as *SLOT, TRL, TRM, LRL, LRM, TXYZ, LXYZ, TOSL, LRRM*, and *UXYZ* [2, 15-18].

2.3 CALIBRATION METHODS

The calibration process requires connecting a set of known calibration standards (collectively known as the calibration cal kit) to a suitable reference plane. "Reference plane" often refers to the following three locations as shown in Figure 2-19:-

1- Reference for calibration plane,

2-Reference for package plane.

3-Reference of generator plane.

In this thesis the term "reference plane" refer to reference for calibration plane. The reference plane is the location at which the calibration standard is connected during the calibration process to measure the magnitude and phase relationship of incident and reflected waves by VNA. The data obtained from incident and reflected waves is then used to find impedance attached to the reference plane [19].
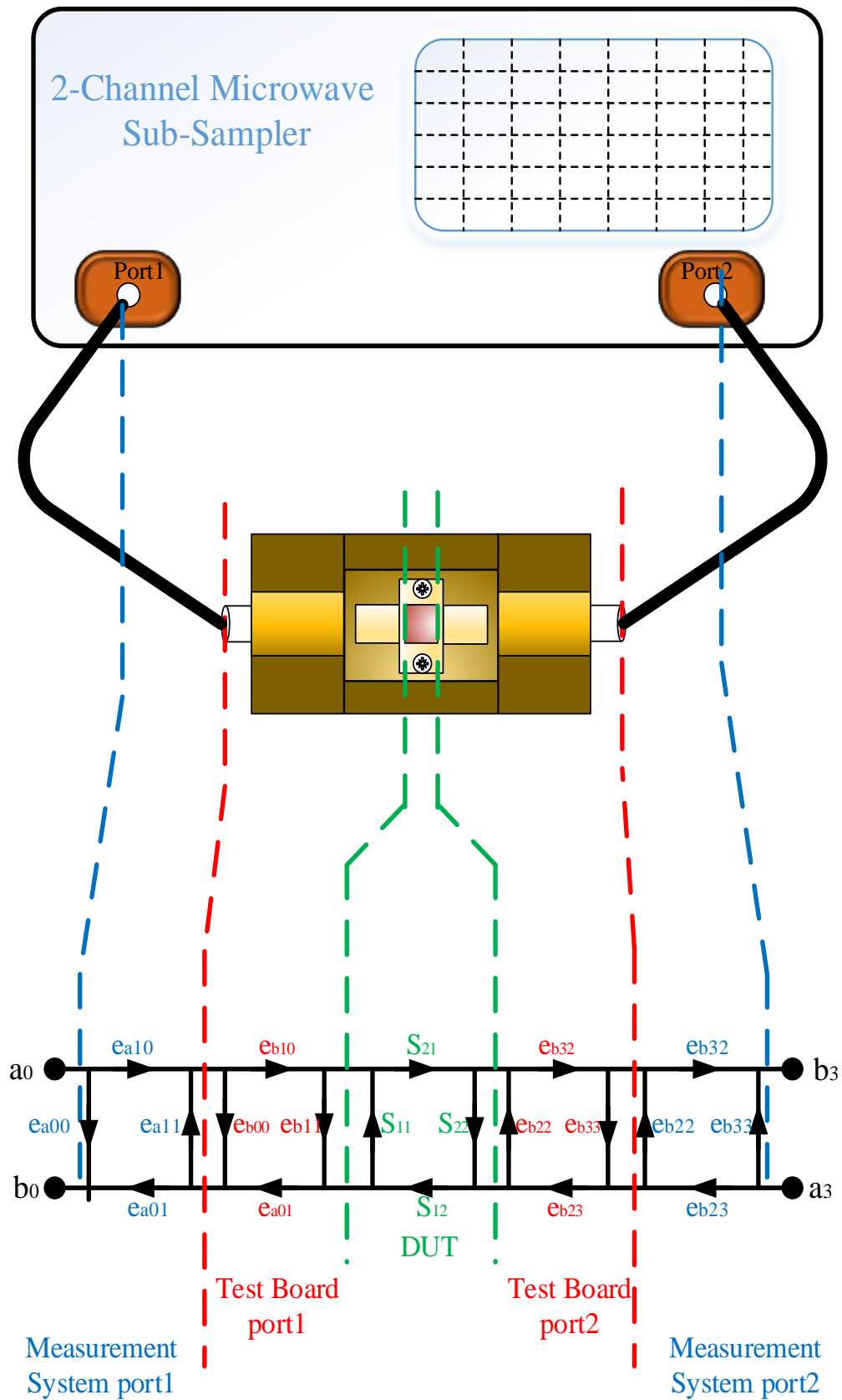
FIGURE 2-19 EMBEDDED MEASUREMENT SYSTEMS.

Actually, there are many Vector network analyzer calibration methods, each of which have unique mathematical concepts and different implementation processes. There are many types for VNA calibration methods, used in this thesis the most popular methods will be discussed [20]:-

2.3.1 SHORT-OPEN-LOAD-THRU (SOLT)

As mentioned previously TOSM (Through-Open-Short-Match) or SOLT (Short-Open-Load-Through) term use to refer to calibration algorithms and initially implemented in coaxial systems .This type of calibration was the first developed for use in a modern VNA. Definition of calibration standards significantly affected the accuracy of this calibration and also in the calibration uncertainty; in other words calibration standards accuracy has strong effect in the uncertainty of calibration accuracy. The coaxial calibration standard supplier characterises every standard and creates a model which is transformed into polynomial coefficients that are ordinarily entered into the VNA. SLOT (Short-Open-Load-Through) calibration is not the most suitable for on-wafer calibration because of this requirement.

Generally, Short, Load and Open (*SLOT*) measures have been applied in calibration. Particularly, calibrating VNA in a coaxial medium is more accurate and repeatable compared with on wafer. The characteristic for cal kits should be known, the refection coefficient for standard *short* (cal kit short) *negative one*, the reflection for standard *open plus one* and zero in load case, these values represent S_{11A} (reflection coefficient of standard cal kits) at reference plane.

As previously mentioned several standards must be used in determination of the error coefficients, and the selection of which standards to use is not necessarily unique. It is obvious that any three reflections can be applied for one port calibration. Commonly, Open, Short, Load and Thru (SOLT) are preferred as they give back pretty separation of unique S-parameter matrix, particularly in a coaxial medium that smoothens their accurate and repeatable fabrication [13, 15, 20].

$$S = \begin{vmatrix} -1 & 0 \\ 0 & -1 \end{vmatrix}$$

Short

$$S = \begin{vmatrix} 1 & 0 \\ 0 & 1 \end{vmatrix}$$

Open

$$S = \begin{vmatrix} 0 & 0 \\ 0 & 0 \end{vmatrix}$$

Z_0 Z_0 Load

$$S = \begin{vmatrix} 0 & 1 \\ 1 & 0 \end{vmatrix}$$

Thru

Port1
Reference
plane

Port 2
Reference
plane
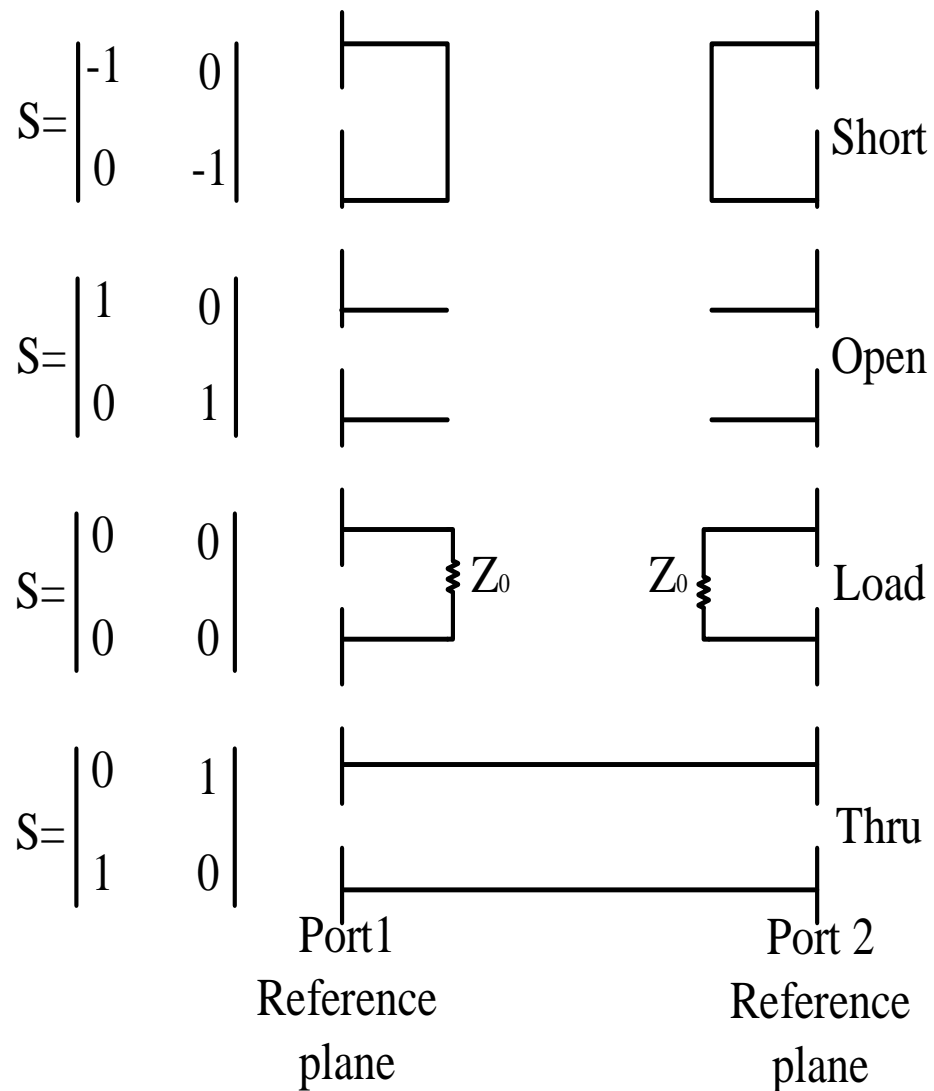
FIGURE 2-20 IDEAL SOLT STANDARDS ELECTRICAL DEFINITIONS.

Figure 2-20 shows the SOLT (Short-Open-Load-Through) standards electrical definitions for ideal and lossless (with respect to Port 1 and 2 reference planes). Clearly, it is impossible to fabricate cal kits such that they are lossless and exhibit the defined transmission and reflection coefficients at these reference planes for Port 1 and Port 2, particularly for the Load and Open ones. Moreover, the behaviour of these standards is not constant and changes with frequency. Figure 2-21 shows that physical constants and fabrications that dictate non-zero length of transmission line should be related. To complement the characteristics of the transmission line should be known, and the parameters of each standard must be defined. To overcome this problem there are

number of electrical models were developed and included in the VNA firmware to characterise the response vs. frequency of the cal kits [2, 13].
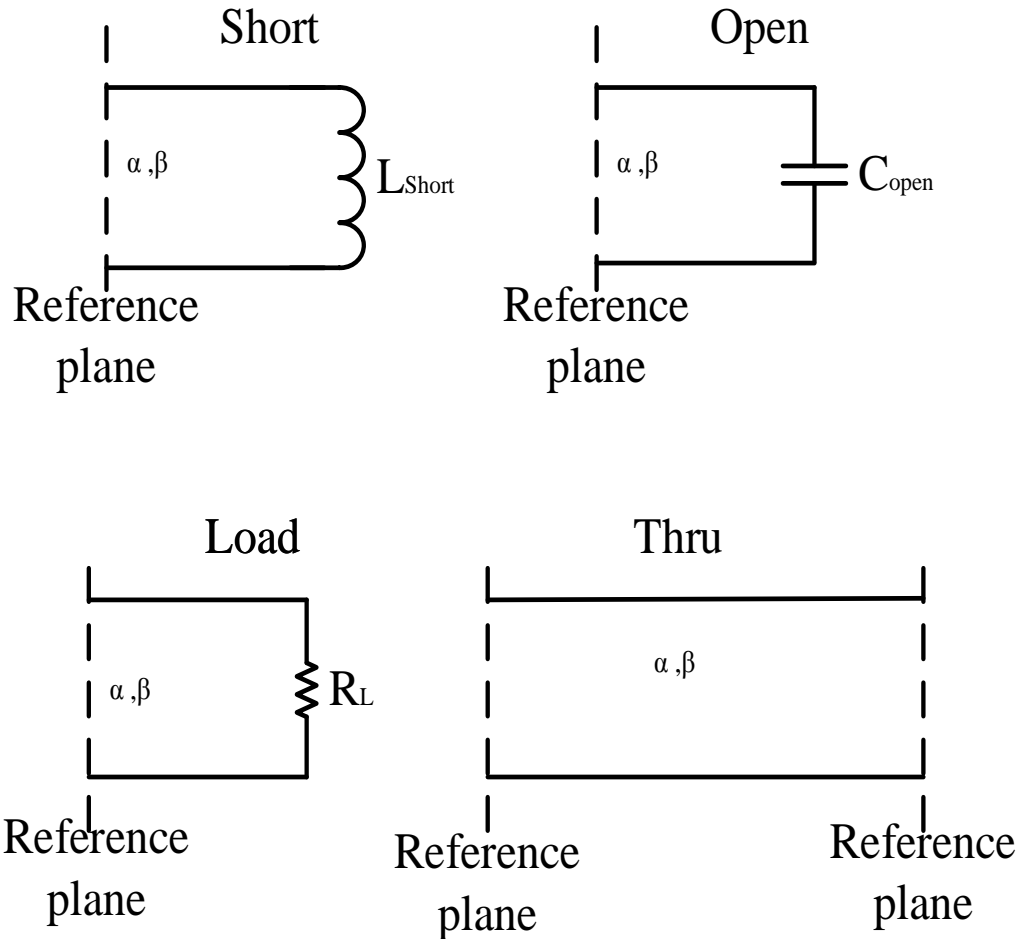
FIGURE 2-21 NON IDEAL SOLT STANDARDS ELECTRICAL DEFINITIONS.

Can described waveform propagation in free space by this equation:

$$V(z) = Ae^{-\gamma z} + Be^{\gamma z}$$ EQUATION 2-11

Where γ is the propagation constant, defined as $\gamma = \alpha + j\beta$. The polynomial fitting is a good solution to represent standards calibration, as the network consists of a parameter which is acquired as a polynomial fitting of the frequency response. These behaviours models for a calibration standard are supplied by all manufacturers [2, 16, 20, 21].

2.3.1.1 OPEN STANDARDS

There is now as an ideal open standard, all opens contain fringing capacitance and practically all opens having several offset lengths as shown below in Figure 2-22 [2, 4,30 ,33].
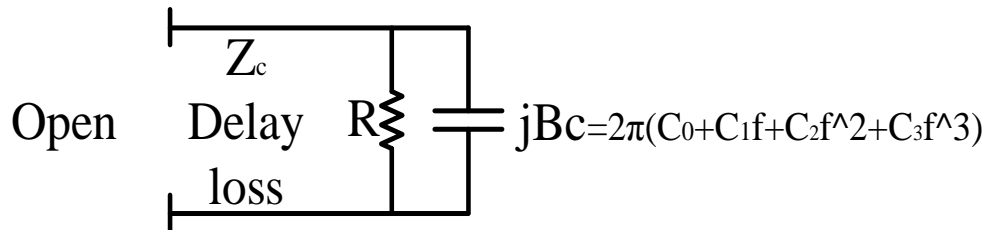
FIGURE 2-22 NON IDEAL OPEN STANDARD.

2.3.1.2 SHORT STANDARDS

Short standards follow the same principle, but are more ideal than Open standards. A short circuit has an inductance model which contains inductance versus frequency as shown in Figure 2-23. All inductance terms are considered as zero in the old RF model. With the newer model, they remain small, but are essential for accurate calibration indeed but still small what we have in open standard [2, 4, 30, 33].
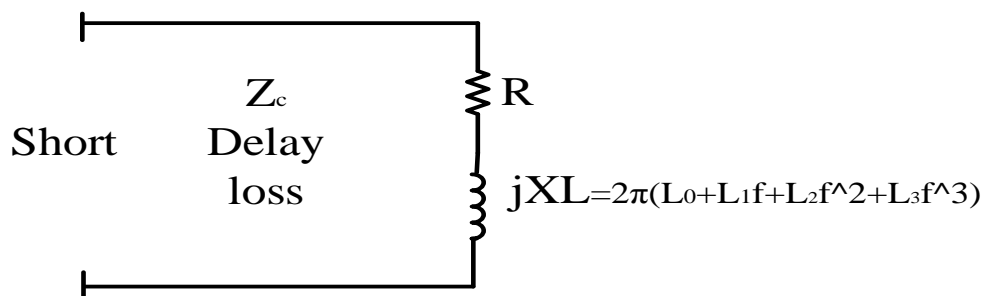
FIGURE 2-23 NON IDEAL SHORT STANDARD.

2.3.1.3 LOAD STANDARD

In general, Load standard is more difficult to manufacture, and the rate of error increases with frequency. The ideal model for load standard consists of a resistance and delay line. The practical model for load standard is series with R-L as shown in Figure 2-24 [2, 4,30 ,33].

FIGURE 2-24 NON IDEAL LOAD STANDARD.

2.3.1.4 CALIBRATION PROCEDURE

Figure 2-25 shows the difference between S_{11M} and S_{11A} ,whereas S_{11M} represents the data measure by VNA, and S_{11A} represent the actual measurement. The circuit is simplified to a flow graph with load in Figure 2-26. From the flow graph we can calculate the relationship between S_{11M} and S_{11A} [2-19].
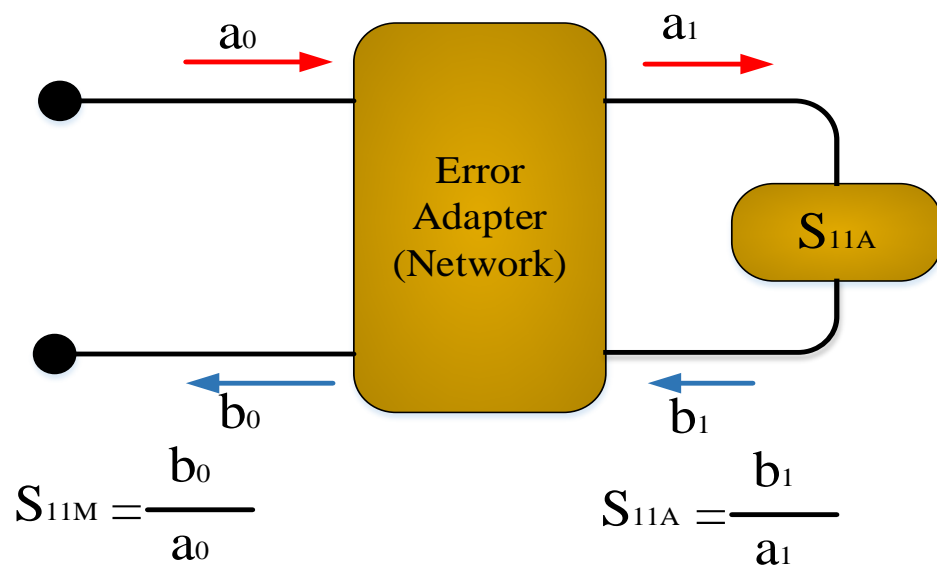
$$S_{11M} = \frac{b_0}{a_0} \qquad S_{11A} = \frac{b_1}{a_1}$$

Figure 2-25 ONE-PORT ERROR ADAPTER.
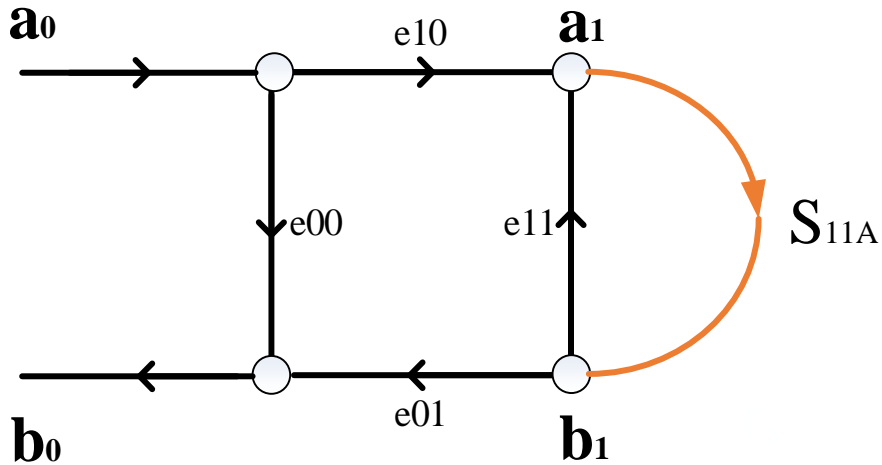
FIGURE 2-26 CORRECTION FLOW GRAPH.

$$S_{11M} = \frac{b_0}{a_0} = e_{00} + \frac{S_{11A} - e_{00}}{e_{11}(S_{11A} - e_{00}) + e_{10}e_{01}} \qquad \text{MEASURED} \qquad \text{EQUATION 2-12}$$

$$S_{11A} = \frac{b_1}{a_1} = \frac{S_{11M} - e_{00}}{e_{11}(S_{11M} - e_{00}) + (e_{10}e_{01})} \qquad \text{ACTUAL} \qquad \text{EQUATION 2-13}$$

$$a_1 = e_{10}a_0 + e_{11}b_1 \qquad\qquad\qquad \text{EQUATION 2-14}$$

$$b_0 = e_{00}a_0 + e_{01}b_1 \qquad\qquad\qquad \text{EQUATION 2-15}$$

$$b_1 = \frac{-e_{00}}{e_{01}} a_0 + \frac{1}{e_{01}} b_0 \qquad\qquad\qquad \text{EQUATION 2-16}$$

$$a_1 = e_{10}a_0 + \frac{-e_{00}e_{11}}{e_{01}} a_0 + \frac{e_{11}}{e_{01}} b_0 = \frac{e_{01}e_{10} - e_{00}e_{11}}{e_{01}} a_0 + \frac{e_{11}}{e_{01}} b_0 \qquad \text{EQUATION 2-17}$$

These equations are used to remove systematic error terms by measuring reflection coefficient for three standard (Open, Short and Load) at the reference plane. These

measurements provide three simultaneous equations with three unknowns, as shown in below in equations 2-18, 1-19 and 2-20 [2-19].

$$e_{00} + \Gamma_1 \Gamma_{MO} e_{11} - \Gamma_{z1} \Delta_e = \Gamma_{MO}$$ EQUATION 2-18

$$e_{00} + \Gamma_2 \Gamma_{MS} e_{11} - \Gamma_2 \Delta_e = \Gamma_{MS}$$ EQUATION 2-19

$$e_{00} + \Gamma_3 \Gamma_{MM} e_{11} - \Gamma_3 \Delta_e = \Gamma_{MM}$$ EQUATION 2-20

Where:

$$\Delta_e = e_{00} e_{11} - (e_{10} e_{01})$$ EQUATION 2-21

$$\Gamma_1 = Open = 1$$ EQUATION 2-22

$$\Gamma_2 = Short = -1$$ EQUATION 2-23

$$\Gamma_3 = Match = 0$$ EQUATION 2-24

At the end of this process we obtain three errors e_{00}, e_{11} and $e_{01}e_{10}$ which are used to correct measurement data. This process is called *One Port Small Signal calibration*.

$$\begin{bmatrix} b_1 \\ a_1 \end{bmatrix} = \frac{1}{e_{10}} \cdot \begin{bmatrix} 1 & -e_{00} \\ e_{11} & (e_{01}e_{10} - e_{00}e_{11}) \end{bmatrix} \cdot \begin{bmatrix} b_0 \\ a_0 \end{bmatrix}$$ EQUATION 2-25

Assume $e_{10} = 1$

Calibration of a two-port system is similar to calibration of a one port system, but in this case an extra standard know as Thru is utilised to find the delay between the two ports, as required. Calibration of a two-port system begins by calibrating Port1 with standards (Open, Short and Load) to obtain the error terms for port1 e_{00}, e_{11} and $e_{01}e_{10}$ and calibrating Port2 using (Open, Short and Load) to obtain error terms for Port2 e_{33}, e_{22} and $e_{32}e_{23}$, connect Port1 directly with Port 2 through the Thru standard to calculated the delay between two port and two error terms $e_{10}e_{32}$ and $e_{01}e_{23}$,Thru has zero electrical length[2-19].

There are two calibration modes using Thru forward and reverse, for forward mode $a_3 = 0$ as shown in Figure 2-27, by using signal-flow graph transformations in Figure 2-27, can derive the equations for S_{11m}^F and S_{21M}^F as shown equations (2-26 and 2-27) below:-
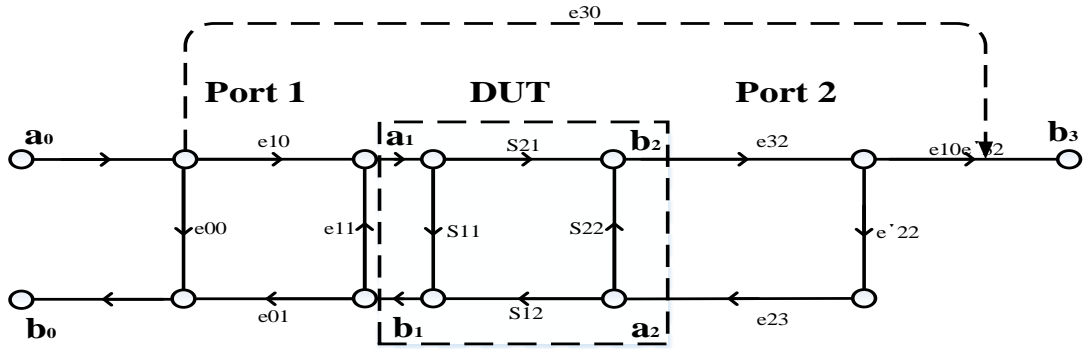
FIGURE 2-27 SIMPLIFY FLOW GRAPH (LEAKAGE TERM ADDED FOR COMPLETENESS).

$$e_{22} = \frac{b_1^F}{a_1^F} = \frac{S_{11M}^F - e_{00}}{e_{11}(S_{11M}^F - e_{00}) + (e_{10}e_{01})} \qquad \text{EQUATION 2-26}$$

$$e_{10}e_{32} = \frac{b_3^F(1 - e_{11}e_{22})}{a_0^F} \qquad \text{EQUATION 2-27}$$

For reverse mode $a_0 = 0$ as shown in Figure 2-28, using signal-flow graph transformations, as shown in Figure 2-28, can derive the equations for S_{22m}^R and S_{12M}^R in equation 2-28 and 2-29as shown below:-
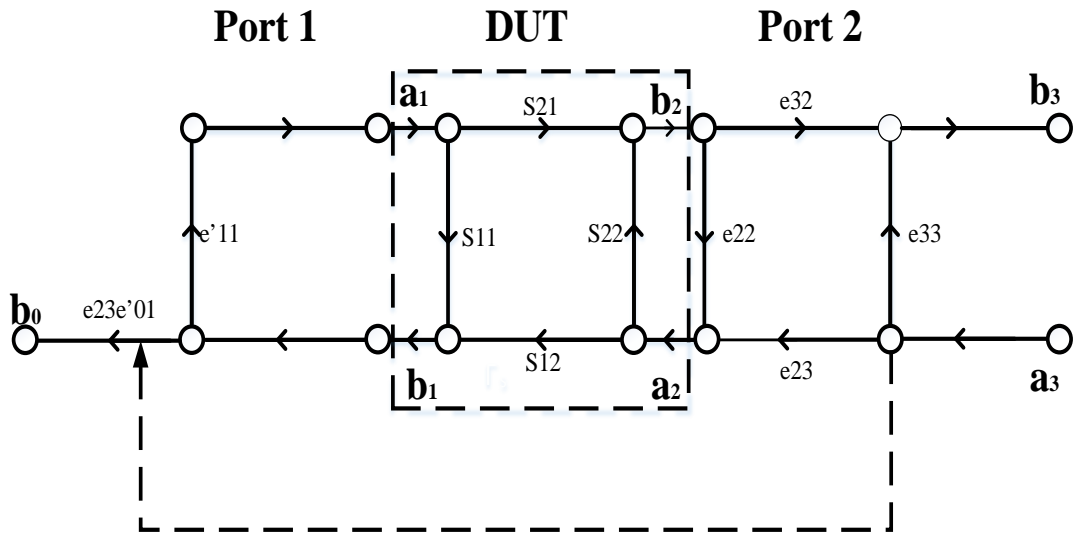
FIGURE 2-28 SIMPLIFY FLOW GRAPH (LEAKAGE TERM ADDED FOR COMPLETENESS).

$$e_{11} = \frac{b_1^R}{a_1^R} = \frac{S_{22M}^R - e_{33}}{e_{22}(S_{22M}^R - e_{33}) + (e_{32}e_{23})}$$

EQUATION 2-28

$$e_{01}e_{23} = \frac{b_0^R(1 - e_{11}e_{22})}{a_{03}^R}$$

EQUATION 2-29

This process we will term Small Signal calibration and results in the determination of 7 error terms. Small signal calibration does not include the power and phase correction term e_{10}. Small Signal calibration case will assume e_{10} or $K(f)$ is unity and the corrected data can be calculated using Equation 2-30, which is considered as the correction algorithm due to its ability to link raw data and correct data by using error models and shown in Figure 2-29 [2-19].

$$\begin{bmatrix} b_1 \\ a_1 \\ b_2 \\ a_2 \end{bmatrix} = \begin{bmatrix} \frac{1}{e_{01}e_{10}} & \frac{-e_{00}}{e_{01}e_{10}} & 0 & 0 \\ \frac{e_{11}}{e_{01}e_{10}} & \frac{(e_{01}e_{10} - e_{00}e_{11})}{e_{10}e_{01}} & 0 & 0 \\ 0 & 0 & \frac{1}{e_{32}e_{10}} & -\frac{e_{33}}{e_{32}e_{10}} \\ 0 & 0 & \frac{e_{22}}{e_{32}e_{10}} & \frac{(e_{32}e_{23} - e_{33}e_{22})}{e_{32}e_{10}} \end{bmatrix} \cdot \begin{bmatrix} b_0 \\ a_0 \\ b_3 \\ a_3 \end{bmatrix}$$

EQUATION 2-30

Where $e_{10} = 1$

Port 1

Port 2
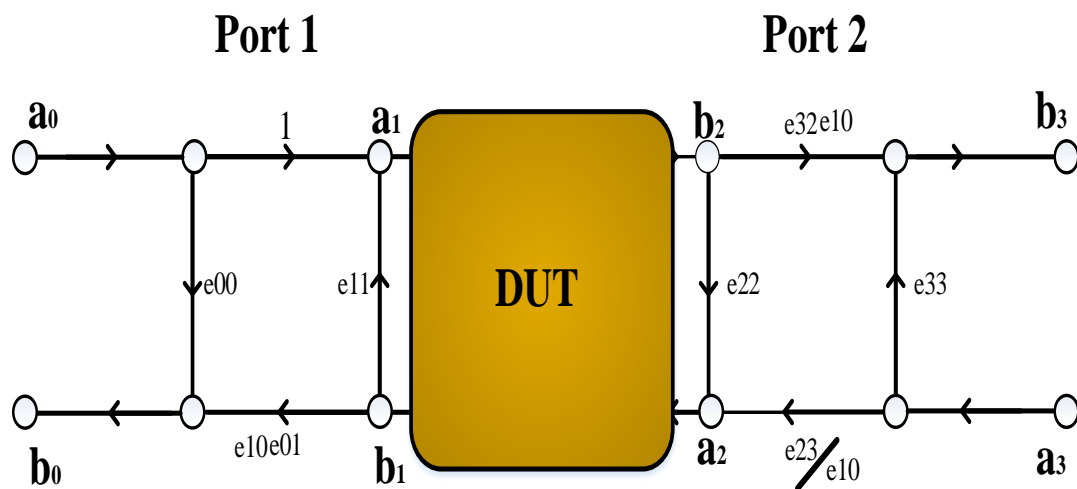
FIGURE 2-29 FLOW GRAPH OF THE EIGHT-TERM ERROR CORRECTION.

At this point the measurement system is calibrated under 7 error terms using the SLOT calibration method and four calibration standards (Short, Load, Open and Thru), as shown in Equation (2-30). This type of calibration is classified as small signal calibration [1-19].

.

2.3.2 LINE-REFLECT-LINE (LRL), (TRL) AND (TRM)

The TRL/TRM calibration method has a major advantage over the SLOT/LOST calibration method in that it does not depend on known standard loads. Hence the performed calibration method is often used for on wafer measurements are in-fixture measurements. TRL calibration is considered the second most popular calibration technique.

As it is impractical or impossible to obtain highly accurate calibration standards especially on wafer level, TRL/TRM calibration has been used to calibrate on wafer in order to obtain more accurate results. The TRL calibration method depends on mathematical process to characterise the error box, which is not on model created by default from manufacturer that can be affected by many factors.

The TRL calibration method requires the user to create their own in-circuit calibration standards. The measurement fixture and calibration standards should be compatible with each other. The operation of the TRL calibration technique uses three types of connections to allow the error boxes to be characterised completely. LRL consists of three standards Line1, Reflect (Open, Offset Open, Short, Offset Short) and Line2. The TRL consists of Line1, with an electrical length zero called Thru, Reflect (Open, Offset Open, Short, Offset Short), and a normal Line. TRM is derived from TRL, which is part of the LRL family. TRM calibration consists of three standards Line, Reflection (Open, Offset Open, Short, and Offset Short) and Match, This type of calibration is easiest to carry out than to the TRL calibration. The precision of this calibration procedure depends on Match standard quality and Thru standard impedance [19-24].

2.3.2.1 THRU- LINE- REFLECT (TRL)

In 1979 Engen and Hoer developed the TRL Calibration. The TRL (Thru-Reflect-Line) calibration, regarded as the most accurate form of calibration for on-wafer devices, is used to obtain a full two port calibration using three standards: a Thru, a Reflect (open circuit or short circuit), and a defined Line. Connecting these standards to the two ports of a VNA yields the 7 error terms for forward and reverse [22].

The LRL (Line, Reflect, Line) series of standards, The TRL (Thru, Reflect, Line) is case from LRL calibration standard which has become very poplar and LRM (Line, Reflect, Match) case from LRL. In fact, LRL became TRL when Thru was replaced with Line and TRL became TRM when Line was replaced with Match. The full electrical characterisation of each reflect is not necessary for these calibration methods [19].

TRL calibration is usually utilised for on wafer and in-fixture measurements. With the TRL technique it is necessary to create in-circuit calibration standards that suitably match a microstrip measurement fixture on wafer probes. Every calibration standard is presupposed to exhibit certain electrical criteria, depending on this, the Thru is essentially a zero-length microstrip which is means fabricating a physical dimensions close to zero length at the frequencies required. The reflect standard in general short or open circuit, in general the phase for Reflection standard is not defined. The Line

standard is similar to the Thru standard, but the Line standard has a non-zero length and must pay attention to defining the reference impedance of the measurement determined by the characteristic impedance of the Line standard. Its length is important. Lengths should be proportional to the length of the Thru, in other words the length should approach 0° or multiples of 180° . There should be no difference between the delay Line and the zero reference Thru should be seen. The three-calibration standard is shown in Figure 2-30.
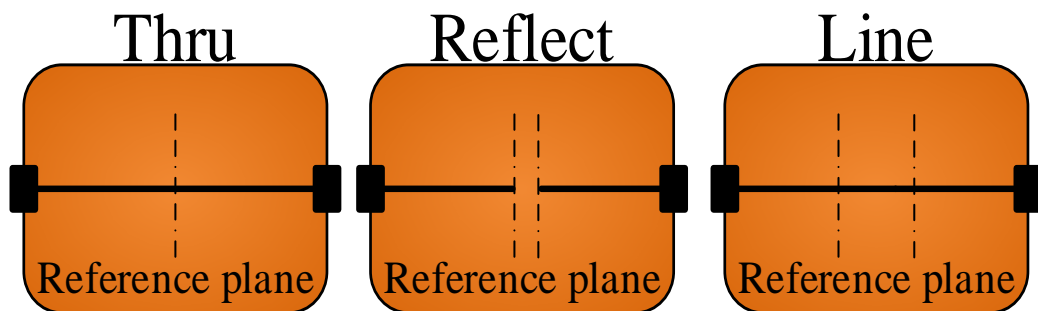
FIGURE 2-30 TRL CALIBRATION STANDARDS.

The TRL calibration process for the two ports measurement system consists of connecting Thru and the Line standards between Port1 and Port2 to measure forward and reverse raw data for each frequency at the defined frequency grid, and terminating Port 1 and Port 2 using a reflect standard (Open or Short) at the same reference plane. to modelling the calibration standards and used this raw data after converting from S-parameter to ABCD matrix in produces two error boxes, one for Port 1 and another for Port 2, as shown in Figure 3-31 [2, 14, 22].
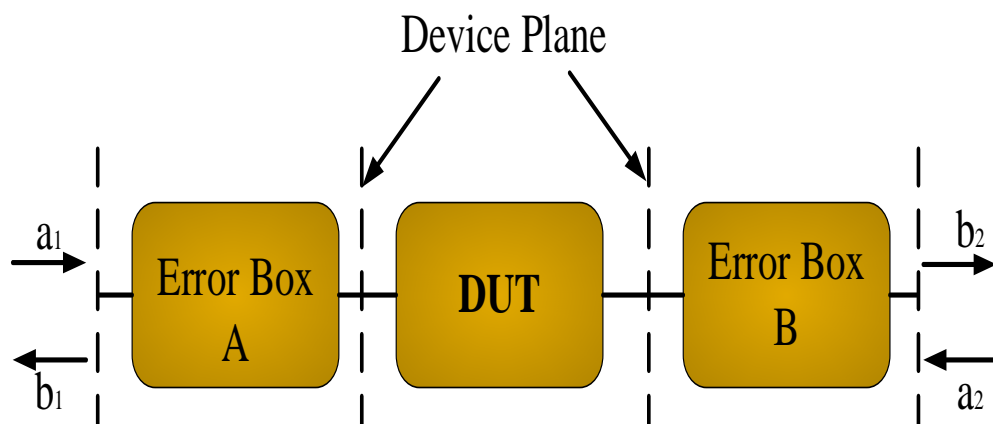
FIGURE 2-31 BLOCK DIAGRAM OF A NETWORK ANALYZER MEASUREMENT OF A TWO-PORT DEVICE.

The calibration technique requires four measurements for calibration standard:-

1-   Thru standard (4 S-parameter).

2-   Line standard (4 S-parameter).

3-   Refection connects with port 1(1 S-parameter).

4-   Refection connects with port 2(1 S-parameter).

2.3.2.2 THRU STANDARD

The calibration procedure begins by connecting the Thru standard between Port 1 and Port 2 to modelling Thru standard or obtained for raw S-parameter for the system. The ideal response for Thru during measurement $S_{11} and S_{22}$ should be equal to zero, and $S_{21} = S_{12}$ should be equal to 1, as shown in Figure 2-32.
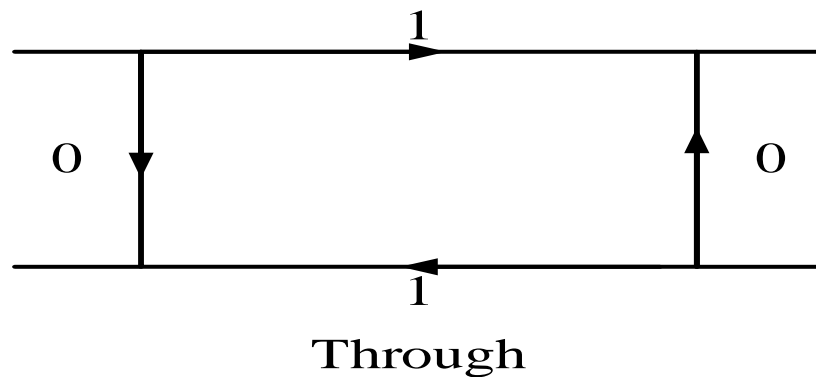
FIGURE 2-32 FLOW GRAPHS OF TRL (THROUGH) STANDARDS.

The four raw S-parameter for Thru standard were obtained from forward and reverse measurement, $S_{21 Forword}$ and $S_{11 Forword}$ were obtained during forward measurement and $S_{12\ Reverse}$ and $S_{22\ Reverse}$ obtained during reverse measurement, this process sometime called switch terms. The VNA measure the $b_1^T, b_2^T\ and\ a_1^T$ when a_2 equal zero as shown in equations 2-31, 2-32 and Figure 2-33.

$$S_{21Forword}^T = \frac{b_2^T}{a_1^T}\bigg|_{a_2^T=0} \qquad \text{EQUATION 2-31}$$

$$S_{11Forword}^T = \frac{b_1^T}{a_1^T}\bigg|_{a_2^T=0} \qquad \text{EQUATION 2-32}$$

VNA measure the b_1^T, b_2^T and a_2^T when a_1^T equal zero as shown in Equations 2-33, 2-34 and Figure 2-33.

$$S_{12Reverse}^T = \frac{b_1^T}{a_2^T}\bigg|_{a_1^T=0}$$
<div align="right">EQUATION 2-33</div>

$$S_{22\ Reverse}^T = \frac{b_2^T}{a_2^T}\bigg|_{a_1^T=0}$$
<div align="right">EQUATION 2-34</div>
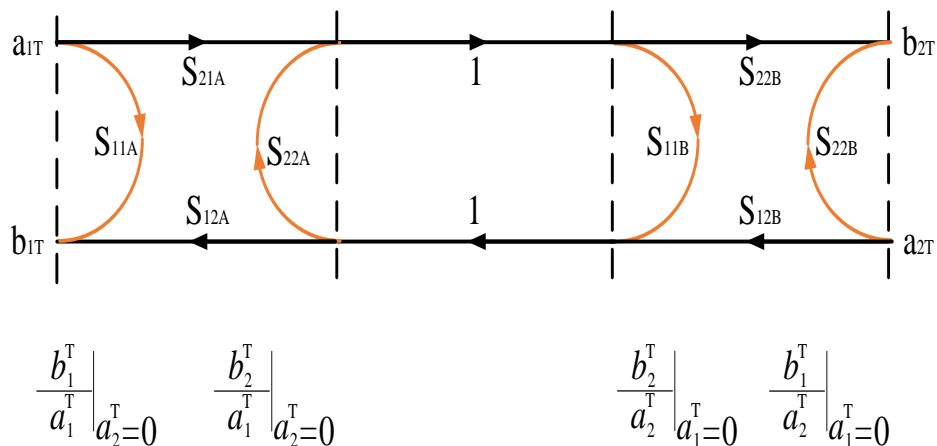
FIGURE 2-33 SIGNAL FLOW GRAPH FOR THE THRU CONNECTION.

The four raw S-parameter for Thru standard, as shown in Equation 2-35:-

$$S_{Thru} = \begin{bmatrix} S_{11} & S_{12} \\ S_{21} & S_{22} \end{bmatrix}$$
<div align="right">EQUATION 2-35</div>

Several common matrices are used by microwave engineers, of which matrices the most suitable for our aims is the T-parameter. In order to facilitate mathematical calculations, the S-parameter must be converted to T-parameter. This is due to the T-parameter being more useful when cascading a series of two port networks. This method provides a simple way for matrix multiplication to be applied with the characteristic blocks of two-port networks [2, 25-31].

The general mathematical relationship between S-parameters and T-parameters is shown in equation 2-36.

.

$$\begin{bmatrix} T_{11} & T_{12} \\ T_{21} & T_{22} \end{bmatrix} = \begin{bmatrix} -\dfrac{S_{11}S_{22}-S_{12}S_{21}}{S_{21}} & \dfrac{S_{11}}{S_{21}} \\ -\dfrac{S_{22}}{S_{21}} & \dfrac{1}{S_{21}} \end{bmatrix}$$ EQUATION 2-36

T_{MThru} represents the value obtained during measurement Thru calibration standard.

.

$$\boldsymbol{T_{MThru11}} = -\frac{S_{11}^T S_{22}^T - S_{12}^T S_{21}^T}{S_{21}^T}$$ EQUATION 2-37

$$\boldsymbol{T_{MThru12}} = \frac{S_{11}^T}{S_{21}^T}$$ EQUATION 2-38

$$\boldsymbol{T_{MThru21}} = -\frac{S_{22}^T}{S_{21}^T}$$ EQUATION 2-39

$$\boldsymbol{T_{MThru21}} = \frac{1}{S_{21}^T}$$ EQUATION 2-40

The $T_{IdealThru}$ shows in matrix below:-

$$\boldsymbol{T_{IdealThru}} = \begin{bmatrix} 1 & 0 \\ 0 & 1 \end{bmatrix}$$ EQUATION 2-41

2.3.2.3 LINE STANDARD

The Line standard is a key element of accurate calibration. The quality of calibration depends on the quality of the impedance of the Line standard. The Line standard length must different from the length of the Thru. The length of the Line standard is the critical factor not should provide phase different between Thru and Line of at least $20\ ^o$ and not more than 160° ,with the best result obtained between 60° and 120°. It is difficult to obtain unambiguous raw S-parameters to represent result obtained from measures of each standard during the calibration process, which is necessary in obtaining good calibration. If the Line standard were to be exactly 180° , the raw data obtained during

both calibration processes will be same, therefore Inability to determine the error terms This is due the raw data obtained considered insufficient independent measurements[31].

In most cases, it is assumed that the Line impedance is the same as the system impedance, hence the errors in the Line standard will become residual errors in directivity, source match and tracking. The main advantage of the TRL calibration algorithm is that it is designed to use the Line's actual impedance instead of the system impedance in determining the error terms [31].

The Line standard measurements start by connecting Line standard between Port 1 and Part 2 to modelling Line standard or to obtain for raw S-parameter for represent Line standard. The ideal response for Line during measurement $S_{11} and S_{22}$ should be equal zero and $S_{21} = S_{12}$ should be equal to $e^{-j\gamma l}$, as shown in Figure 2-34 [31].
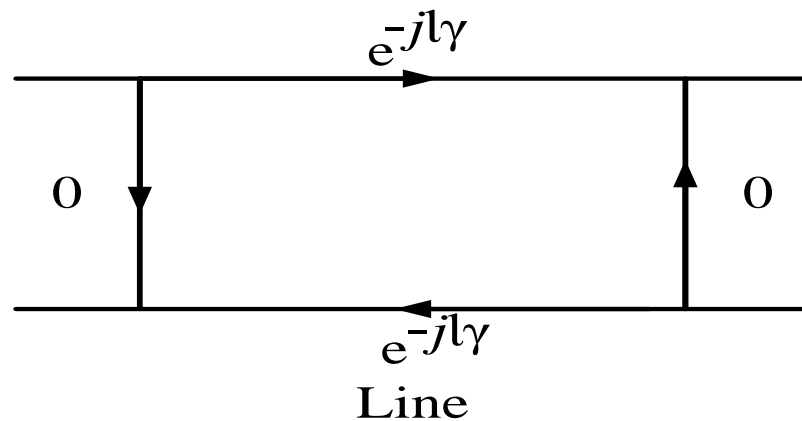
FIGURE 2-34 FLOW GRAPHS OF TRL (LINE) STANDARDS.

The four raw S-parameters for the Line standard obtained through switch terms were, $S_{21Forword}^{L}$ and $S_{11Forword}^{L}$ obtained during forward measurement and $S_{12Reverse}^{L}$ and $S_{22\ Reverse}^{L}$ obtained during reverse measurement. The VNA measure the $b_1^L, b_2^L\ and\ a_1^L$ when a_2^L equal zero as shown equation 2-42, 2-43 and Figure 2-35.

$$\boldsymbol{S_{21Forword}^{L}} = \frac{b_2^L}{a_1^L}\bigg|_{a_2^L=0} \hspace{4cm} \text{EQUATION 2-42}$$

$$\boldsymbol{S_{11Forword}^{L}} = \frac{b_1^L}{a_1^L}\bigg|_{a_2^L=0} \hspace{4cm} \text{EQUATION 2-43}$$

VNA measure the b_1^L, b_2^L and a_2^L when a_1^L equal zero as shown in equation 2-44, 2-45 and Figure 2-35.

$$S_{12Reverse}^L = \frac{b_1^L}{a_2^L}\Bigg|_{a_1^L=0}$$ EQUATION 2-44

$$S_{22\ Reverse}^L = \frac{b_2^L}{a_2^L}\Bigg|_{a_1^L=0}$$ EQUATION 2-45

$$\frac{b_1^L}{a_1^L}\Bigg|_{a_2^L=0} \qquad \frac{b_2^L}{a_1^L}\Bigg|_{a_2^L=0} \qquad \qquad \frac{b_2^L}{a_2^L}\Bigg|_{a_1^L=0} \qquad \frac{b_1^L}{a_2^L}\Bigg|_{a_1^L=0}$$
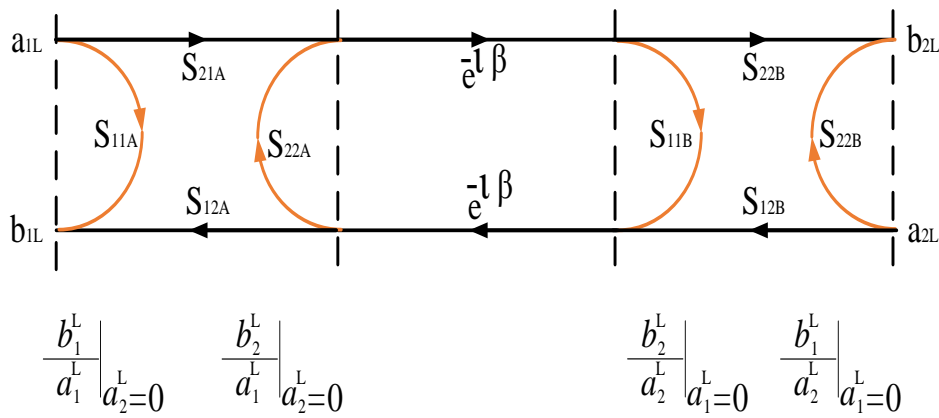
FIGURE 2-35 SIGNAL FLOW GRAPH FOR THE LINE CONNECTION.

T_{MLine} represent the value obtained during Line calibration standard measurement [2, 25-31].

$$T_{MLine11} = -\frac{S_{11}^L S_{22}^L - S_{12}^L S_{21}^L}{S_{21}^L}$$ EQUATION 2-46

$$T_{MLine12} = \frac{S_{11}^L}{S_{21}^L}$$ EQUATION 2-47

$$T_{MLine21} = -\frac{S_{22}^L}{S_{21}^L}$$ EQUATION 2-48

$$T_{MLine21} = \frac{1}{S_{21}^L}$$ EQUATION 2-49

The $T_{Idealline}$ is shown in the matrix below

$$T_{IdealThru} = \begin{bmatrix} e^{-j\theta} & 0 \\ 0 & e^{j\theta} \end{bmatrix}$$

EQUATION 2-50

2.3.2.4 REFLECTION STANDARD

The final and most simple standards used in TRL calibration is the Reflect standard. This standard considered is the simplest standard. There is only one condition for this standard, non-zero reflection should be provided equally at Port 1 and Port 2 or the same reflection given at each of the ports. The point being that this reflection should be same at both ports, of whether regardless the reflect standards are known or not. The reference plane of the ports is set using the reflector standard. VNA is calibration commonly equip for choice of using the centre of the Reflect standard to adjust reference plane [29].

The measurements of Reflect standard measurements begin by connecting the Reflect standard on Port 1 and Port 2 to model the Reflect standard or to obtain a raw S-parameter for represent the Reflect standard. The ideal response for Reflect during measurement $S_{11} and S_{22}$ should be same and equal Γ, $S_{21} = S_{12}$ should equal $zero$ as shown in Figure 2-36 [29].
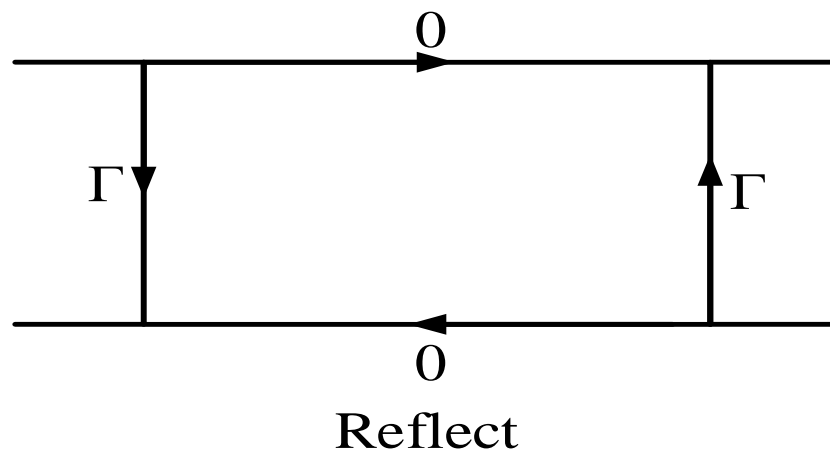
FIGURE 2-36 FLOW GRAPHS OF TRL (REFLECT) STANDARDS.

The two raw S-parameter for the Reflect standard obtained from measurement. The S_{11}^R and S_{22}^R obtained during forward measurement The VNA measure the b_1^R, a_1^R and b_2^R, a_2^R as shown in equation (2-51, 2-52) and Figure 2-37[29].

$$S_{11}^R = \left.\frac{b_1^R}{a_1^R}\right|_{a_2^R=0} \qquad \text{EQUATION 2-51}$$

$$S_{22}^R = \left.\frac{b_2^R}{a_2^R}\right|_{a_1^R=0} \qquad \text{EQUATION 2-52}$$
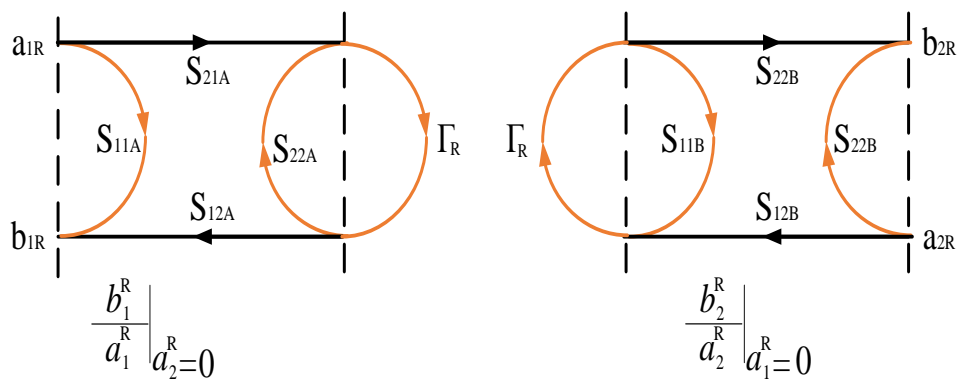
FIGURE 2-37 SIGNAL FLOW GRAPH FOR THE REFLECT CONNECTION.

After this point we are going to determine the parameters for the port 1 and port 2 error boxes.

The measurement matrix(T_{MDUT}) is the product of the unknown DUT and the matrix of the error boxes as shown in Equation 2-53 or in Equation 2-54.

$$T_{MDUT} = T_A T_{DUT} T_B \qquad \text{EQUATION 2-53}$$

OR

$$T_{DUT} = T_A^{-1} T_{MDUT} T_B^{-1} \qquad \text{EQUATION 2-54}$$

Where

$$T_A = \begin{bmatrix} T_{11}^A & T_{12}^A \\ T_{21}^A & T_{22}^A \end{bmatrix} = \begin{bmatrix} 1/F & B \\ A/F & 1 \end{bmatrix} \qquad \text{EQUATION 2-55}$$

And

$$T_B = \begin{bmatrix} T_{11}^B & T_{12}^B \\ T_{21}^B & T_{22}^B \end{bmatrix} = E \begin{bmatrix} 1/G & C \\ D/G & 1 \end{bmatrix}$$

EQUATION 2-56

To determine the performance of device (T_{DUT}), it is necessary to find the values of A,B,C,F,D,G and E to substituted in A and B boxes as shown in equation 2-54.

T_{MLine} for the measured Line standard and T_{MThru} for the measured Thru standard.

Therefore

$$T_{MThru} = T_A T_{Thru} T_B = T_A T_B$$

EQUATION 2-57

The Thru T-matrix is an identity matrix and the Line standard equation can be represented as:

$$T_{MLine} = T_A T_{Line} T_B$$

EQUATION 2-58

The aim determines the elements of box A and box B

$$T_A = \begin{bmatrix} T_{11}^A & T_{12}^A \\ T_{21}^A & T_{22}^A \end{bmatrix}$$

EQUATION 2-59

And

$$T_B = \begin{bmatrix} T_{11}^B & T_{12}^B \\ T_{21}^B & T_{22}^B \end{bmatrix}$$

EQUATION 2-60

Stage One

Equation 2-57 can be written as shown in Equation 2-61:

$$T_B = T_{Thru}^{-1} T_A^{-1} T_{MThru}$$

<div align="right">EQUATION 2-61</div>

And for Line can write it

$$T_B = T_{Line}^{-1} T_A^{-1} T_{MLine}$$

<div align="right">EQUATION 2-62</div>

$$T_{MLine} = T_A T_{Line} T_{Thru}^{-1} T_A^{-1} T_{Mthru}$$

<div align="right">EQUATION 2-63</div>

$$\because T_{Thru} = 1$$

$$T_{MLine} T_{MThru}^{-1} = T_A T_{Line} T_A^{-1}$$

<div align="right">EQUATION 2-64</div>

Where $X = T_{MLine} T_{MThru}^{-1}$

$$X T_A = T_A T_{Line}$$

<div align="right">EQUATION 2-65</div>

By solving Equation 2-65 can obtain Equations 2-66, 2-67, 2-68 and 2-69

$$X_{11} + X_{12} A = L$$

<div align="right">EQUATION 2-66</div>

$$X_{21} + X_{22} A = AL$$

<div align="right">EQUATION 2-67</div>

$$X_{11} B + X_{12} = B/L$$

<div align="right">EQUATION 2-68</div>

$$X_{21} B + X_{22} = 1/L$$

<div align="right">EQUATION 2-69</div>

Where $A = T_{21}^A / T_{11}^A$ and $B = T_{12}^A / T_{22}^A$

Stage Two

$$T_{MThru} = T_A \, T_B \qquad \text{EQUATION 2-70}$$

$$T_{B=} T_A^{-1} T_{Thru} \qquad \text{EQUATION 2-71}$$

By solving equation 2-72:

$$C = T_{12}^B / T_{11}^B \qquad \text{EQUATION 2-72}$$

And

$$C = \frac{T_{12MThru} - B \, T_{22MThru}}{T_{11MThru} - B \, T_{21MThrhu}} \qquad \text{EQUATION 2-73}$$

And

$$D = \frac{T_{21}^B}{T_{11}^B} = \frac{T_{21MThru} - A \, T_{11MThru}}{T_{22MThru} - A \, T_{21MThru}} \qquad \text{EQUATION 2-74}$$

To find other parameters it is necessary need to use reflection coefficient $S_{11MReflect}$ and $S_{22MReflect}$. Using reflection coefficient for two ports can determine the value of R through two equations:-

$$R = \frac{T_{22}^A}{T_{11}^A} \left\{ \frac{S_{11MRefelct} - B}{1 - A \, S_{11MReflect}} \right\} \qquad \text{EQUATION 2-75}$$

Where $F = \frac{T_{22}^A}{T_{11}^A}$

$$R = F \left\{ \frac{S_{11MRefelct} - B}{1 - A \, S_{11MReflect}} \right\} \qquad \text{EQUATION 2-76}$$

And   R can determinate it by Equation 2-78

$$R = \frac{T_{22}^B}{T_{11}^B} \left\{ \frac{D + S_{22MReflect}}{1 + C \, S_{22MReflect}} \right\} \qquad \text{EQUATION 2-77}$$

Where $= \dfrac{T_{22}^B}{T_{11}^B}$:

$$R = G \left\{ \dfrac{D + S_{22MReflect}}{1 + C\, S_{22MReflect}} \right\}$$

<div align="right">EQUATION 2-78</div>

Equation (2-76) and (2-78) can obtain (2-79)

$$\dfrac{F}{G} = \left\{ \dfrac{D + S_{22MReflect}}{1 + C\, S_{22MReflect}} \right\} \cdot \left\{ \dfrac{1 - A\, S_{11MReflect}}{S_{11MRefelct} - B} \right\}$$

<div align="right">EQUATION 2-79</div>

To determine the values of F and G, it is necessary to use equation 2-80

$$T_{MThru} = T^A T^B$$

<div align="right">EQUATION 2-80</div>

By solving Equation (2-80) will obtain

$$FG = \dfrac{T_{22MThru} - A\, T_{12MThru}}{T_{11MThru} - B\, T_{21MThru}}$$

<div align="right">EQUATION 2-81</div>

Multiplying   F/G by F.G will obtain F^2, Substituting F in Equation 2-76 or in Equation 2-77 can determine the G value.

AND $$\left(T_{22}^A T_{22}^B \right) = E = T_{21MThru} \left(\dfrac{F}{F + AC} \right)$$

<div align="right">EQUATION 2-82</div>

All elements for Box A founded as shown in Equation 2-83

$$T_A = \begin{bmatrix} 1/F & B \\ A/F & 1 \end{bmatrix}$$

<div align="right">EQUATION 2-83</div>

All elements for Box A founded as shown in Equation 2-84:

$$T_B = E \begin{bmatrix} 1/G & C \\ D/G & 1 \end{bmatrix}$$

EQUATION 2-84

At this point, the measurement system has calibrated the 7 error terms determined by the TRL calibration method using three calibration standards (Thru, Reflect and Line), as shown in equation 2-83 and 2-84. This type of calibration is classified as small signal calibration.

$$T_{MDUT} = T_A T_{DUT} T_B$$

EQUATION 2-85

With the input and output ports in T-parameters form, Box A and Box B can be converted to S-parameter for Port 1 and Port 2, the S-parameter for the input port representing the error box for the input port and same for Port 2. This data will use real time measurements to remove error effects [28-31].

Calibration was carried out using the TRL method, which offers 7 error terms. Full calibration(large signal) , will require for power and phase calibration [28-31].

TRL calibration is that it can only be used over a relatively frequency band, which is considered one of the essential limitations of TRL calibration , in addition to is the determination of the calibration Line lengths which was regard as the other serious issue associated with TRL calibration. Many publications have dealt with the determination of the calibration Line lengths for TRL, a recap of is given below [28-31].

Electrical length for Line standard is causing a phase shift in signal therefore the length should only be known for phase information, as mentioned before this lead for limitations of frequency ranges, frequency band depend on length of the LINE and calibration just in frequency bands. The frequency grid used in calibration or frequencies that can used in calibration process is defined by the length of the Line according to equation 2-86 [28-31].

$$l_{length} \neq n.\frac{\lambda}{2} \; WITH \; \lambda = \frac{v_p}{f_0} \; AND \; v_p = \frac{c}{\sqrt{\varepsilon_r}} \qquad \text{EQUATION 2-86}$$

Assuming the linear relation between transmission media and phase equation (2-86) can determine Line with 1/4 wavelength length at the required centre frequency. In order to cover the whole frequency range, Equation 2-87 and 2-88 should be used to determine the Line standard for each band, as shown in Figure 2-38 [28-31].

$$f_{start} = \frac{1}{360} * \frac{c}{l_{Line}} (20^o + n*180^o) \qquad \text{EQUATION 2-87}$$

$$f_{stop} = \frac{1}{360} * \frac{c}{l_{Line}} (160^o + n*180^o) \qquad \text{EQUATION 2-88}$$
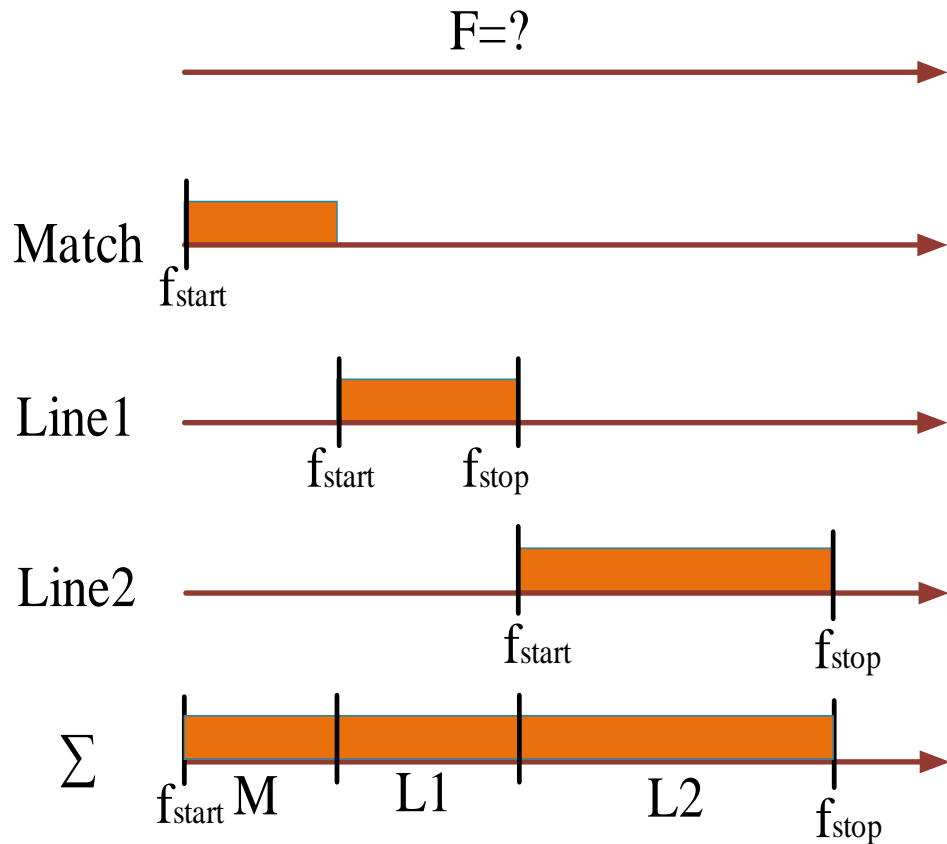
FIGURE 2-38 TRL CAL KITS (MULTILINES).

Practical at certain frequencies, the Line standard behaves in a similar way to Thru standard behaves, raw data obtained at these frequencies should not be used in the calibration process because error coefficients which are obtained would not be meaningful. As a mentioned before, the frequency range is framed by a 20° to 160° region and the Line must meeting the conditions of the acceptable insertion phase which is a 8:1 frequency span, harmonic frequencies bandwidth as shown in Equation 2-89.

$$\boldsymbol{Phase = 360^o * f * \sqrt{\frac{\varepsilon_r}{c}}}$$

<div align="right">EQUATION 2-89</div>

The grid frequency for calibration system cover over than an 8:1 frequency span, multiple Lines should used [2,25-31].

2.4 UNCERTAINTY CALIBRATION

It is crucial when making RF measurements to recognise the precision of the measurements that are being made. First of all, can any uncertainty in measurements be determined? It is necessary to understand that these errors include all RF measurements, and where they are on a VNA, source, power meter or spectrum analyser. Error correction is not able to remove the effect of load match and source match in the measurement. Therefore, raw match term will control the uncertainty value of the obtained measurement. The phase and magnitude as result of the interaction for the signals to be measured and the errors will affect on errors obtained from load match and source match and the VNA measure the result phase [8,31].

2.4.1 UNCERTAINTY IN REFLECTION

Reflection uncertainty is defined as the difference between the true value and the reading value. An upper limit for measurement can be obtained by adding measurement

to the reflection uncertainty, and a lower limit can be obtained by subtracting measurement from reflection uncertainty. Compare the s11 correct with the actual error terms driving to that correct with the estimated error terms to determine the uncertainty of reflection measure, as shown in Equation 2-90 [8, 31].

$$S_{11A} - S_{11\_PortCal} = S_{11A} - \frac{(S_{11M} - e_{00})}{[e_{10}e_{01} + (S_{11M} - e_{00}) \cdot (e_{11})]} \qquad \text{EQUATION 2-90}$$

2.4.2 Uncertainty in Source Power

Uncertainty of source power can found in any source, such as a receiver from a vector signal generator or driving a power amplifier from a VNA. Three errors are considered sources for uncertainty of source power: the source match, source tracking error, and the efficiency input match [8,31].

$$\Delta SourcePower = \left| 20 \log_{10} \left(\frac{a_{1A}}{a_{1S}} \right) \right| \qquad \text{EQUATION 2-91}$$

Where a_{1S} is the source power setting and a_{1A} the actual source power.

2.4.3 Uncertainty in Power Meter

Similar to source uncertainty, receiver uncertainty account applies just as to all kinds of receivers comprehensive VNA receiver, power meter and spectrum analyser. The uncertainty in power reading depends upon the raw input match of the measuring receivers, the raw output match of the DUT,Γ_2 receiver tracking, forward load match and BTF. It should be noted that this is relevant to all types of receivers except VNA receivers [8,31-32].

$$\Delta RcvrPower = \left| 20 \log_{10} \left(\frac{b_{2A}}{b_{2M}} \right) \right| \qquad \text{EQUATION 2-92}$$

Where b_{2A} is the actual power at the receiver and b_{2M} measure power.

2.4.4 UNCERTAINTY IN TRANSMISSION

There are many sources for transmission uncertainty: the load and source, residual, raw of the measurement system. The uncertainty value for S_{21} can be obtained through Equation 2-93.

$$\Delta s_{21} = \left| 20 \log_{10} \left(\frac{S_{21M}}{S_{21A}} \right) \cdot \left[\frac{b_{2Cal}}{b_{2M}} \cdot R_{DA} \right] \right| \qquad \text{EQUATION 2-93}$$

Where b_{2Cal} is the power level at the test receiver during calibration, b_{2M} the power level at the test receiver during measurement and R_{DA} the dynamic receiver [8, 31-32].

2.5 CONCLUSION

In modern days, the characterisation of linear and non-linear devices has become crucial, residual uncertainty in calibration has strongly affected the measurement accuracy, especially in devices having high output and input reflection coefficients[33,34].

 Normally, uncertainty consists of:- VNA measurement repeatability, connection repeatability, power level uncertainty, and residual uncertainty due to the calibration, which involves uncertainty in the standard definition and measurement repeatability. In order to reduce such error in measurements, further research is required to improve vector error correction to procedure more accurate error terms to improve and increase the accuracy of measurement systems which reflects on the overall communication systems a This will, in turn, lead to the design of effective and high performance components for future wireless systems.

The importance of major uncertainty components applicable LSNA measurements with source/load impedances near the edge of the Smith Chart have been studied [35, 36, 37,38, 39]. The LSNA must be vector error corrected using an error model to achieve accurate measurements[40].

2.6 REFERENCE

1- Tasker, P.J., Practical waveform engineering. Microwave Magazine, IEEE, 2009. 10(7): p. 65-76.

2- Golio, M. and J. Golio, RF and Microwave Circuits, Measurements, and Modeling. 2007: Taylor & Francis.

3- Agilent, Network Analyzer Basics. 2010, Agilent Technologies.

4- Rohde & Schwarz USA, I., Fundamentals of Vector Network Analysis Primer. Version 1.1.

5- Comany, A.T., DC Electrical Characterizationof RF Power Amplifiers. 2013(Application NoteSeries).

6- Ghannouchi, F.M. and M.S. Hashmi, Load-Pull Techniques with Applications to Power Amplifier Design. 2012: Springer.

7- Instirment, N., Introduction to Network Analyzer Measurements Fundamentals and Background. 2013, National Insturments

8- Dunsmore, J.P., Handbook of Microwave Component Measurements: with Advanced VNA Techniques. 2012: Wiley.

9- Anritsu, Understanding Vector Network Analysis 2009.

10- HP, S-Parameter Techniques. 1997.

11- Agilent, Network Analyzer Basics. 2010.

12- Agilent, Specifying Calibration Standards and Kits for Agilent Vector Network Analyzers Application Note 1287-11. 2011.

13- Agilent, AN 1287-3 Applying Error Correction to Network Analyzer Measurements. 2002.

14- Rumiantsev, A. and N. Ridler, VNA calibration. Microwave Magazine, IEEE, 2008. 9(3): p. 86-99.

15- Pozar, D.M., Microwave Engineering, 4th Edition. 2011: Wiley Global Education.

16- Henze, A., et al. Incomplete 2-port vector network analyzer calibration methods. in Biennial Congress of Argentina (ARGENCON), 2014 IEEE. 2014.

17- Williams, D., Traveling Waves and Power Waves: Building a Solid Foundation for Microwave Circuit Theory. Microwave Magazine, IEEE, 2013. 14(7): p. 38-45.

18- Rytting, D., Network Analyzer Error Models and Calibration Methods.

19- Rytting, D. ARFTG 50 year network analyzer history. in Microwave Symposium Digest, 2008 IEEE MTT-S International. 2008.

20- Williams, D.F., C.M. Wang, and U. Arz. An optimal multiline TRL calibration algorithm. in Microwave Symposium Digest, 2003 IEEE MTT-S International. 2003.

21- Dottorato, T.d., Measurement Techniques for Radio Frequency and Microwave Applications. 2009.

22- Marks, R.B. and D.F. Williams, Characteristic impedance determination using propagation constant measurement. Microwave and Guided Wave Letters, IEEE, 1991. 1(6): p. 141-143.

23- Engen, G.F. and C.A. Hoer, Thru-Reflect-Line: An Improved Technique for Calibrating the Dual Six-Port Automatic Network Analyzer. Microwave Theory and Techniques, IEEE Transactions on, 1979. 27(12): p. 987-993.

24- Williams, D.F. and R.B. Marks, Transmission line capacitance measurement. Microwave and Guided Wave Letters, IEEE, 1991. 1(9): p. 243-245.

25- Hoer, C.A., Choosing Line Lengths for Calibrating Network Analyzers. Microwave Theory and Techniques, IEEE Transactions on, 1983. 31(1): p. 76-78.

26- Huebschman, B.D., Calibration and Verification Procedures at ARL for the Focus Microwaves Load Pull System. ARL-TR-3985, 2006. ARL-TR-3985(Army Reserch Laboratory).

27- Schutt-Aine, J.E., ECE 451 Automated Microwave Measurements TRL Calibration. (Electrical & Computer Engineering University of Illinois).

28- Agilent, Network Analysis Applying the 8510 TRL Calibration for Non-Coaxial Measurements Product Note 8510-8A. 2001.

29- Laboratories, C.E., AN1041 Designing And Characterizing TRL fixture calibration standards for device modeling. 2003.

30- Wang Shuai, L.K., Jiang Yibo, Cong Mifang,Du Huan, and Han Zhengsheng, A thru-reflect-line calibration for measuring the characteristics of high power LDMOS transistors.

31- Ferrero, A., Multiport Vector Network Analyzers.

32- Sandia, R.D.M., Determination of the Uncertainties of Reflection Coefficient Measurements of a Microwave Network Analyzer.

33- Rytting, D.K., An analysis of vector measurement accuracy enhancement techniques 1982.

34- Rehnmark, S., On the Calibration Process of Automatic Network Analyzer Systems (Short Papers). Microwave Theory and Techniques, IEEE Transactions on, 1974. 22(4): p. 457-458.

35- Matthee, C.F. The determination of the uncertainty associated with measurements performed using a vector network analyser. in Africon, 1999 IEEE. 1999.

36- Nazoa, N., calibration and measurement uncertainty (National Physical Laboratory Teddington, UK).

37- Bednorz, T., Measurement Uncertainties for Vector Network Analysis. 1996.

38- Application note 11410-00464. Calculating VNA measurement accuracy. 2008(Anritsu).

39- Teppati, V., et al., Accuracy Improvement of Real-Time Load-Pull Measurements. IEEE Transactions on Instrumentation and Measurement, 2007. 56(2): p. 610-613.

40- Bonino, S., V. Teppati, and A. Ferrero, Further Improvements in Real-Time Load-Pull Measurement Accuracy. IEEE Microwave and Wireless Components Letters, 2010. 20(2): p. 121-123.

3. CHAPTER 3

ENHANCED TRL CALIBRATION

2.1 CALIBRATION TRL

NVNA calibration has significantly enhanced the measurement accuracy of microwave instruments. Various algorithms have been proposed throughout the last 60 years [1].

In this thesis, real time measurement systems are addressed. This chapter presents an alternative approach to improving vector measurement accuracy, especially near the edge of the Smith Chart. This is very important in load-pull measurement systems. The first task of the presented work was to improve system measurement accuracy by increasing the accuracy of the 7-term error model [1].

To improve the calibration accuracy of RF engineering waveform measurement systems, the new procedure is based on varying the load around the Smith Chart using a load pull system. The calibration accuracy strongly affects the RF engineering waveform measurement accuracy especially near the edge of the Smith Chart. Improved measurement accuracy, after vector calibration, is achieved by utilisation of the load-pull capability during calibration to minimise the impact of measurement errors on the raw data of the calibration standards before it is utilised in the traditionally implemented LRL/TRL calibration algorithm [1, 2].

2.2 INTRODUCTION TO ENHANCED CALIBRATION

Since the appearance of TRL calibration, many research publications have explored the quality of TRL/LRL calibration techniques. These publications have dealt with the problem of increasing the calibration precision using orthogonal distance regression

algorithms to improve the calibration quality or by use multiple redundant Line standards to reduce random errors. As mentioned before, this chapter presents an alternative approach to improve the vector measurement accuracy, especially near the edge of the Smith Chart, of load-pull measurement systems. Improved measurement accuracy, after vector calibration, is achieved by exploiting the load-pull capability during calibration to minimise the impact of measurement errors on the raw data of the calibration standards before it is utilised in the traditionally implemented LRL/TRL calibration algorithm. This approach eliminates the need to utilize complex optimisation algorithms post calibration.

To demonstrate the improved accuracy, NVNA is first calibrated by traditional means, and calibrated again using the new method. The results are compared [2, 3].

2.2.1 TRADITIONAL CALIBRATION

Waveform engineering measurement systems used in this thesis   consist of a vector measurement component, a Nonlinear Vector Network analyser (NVNA), integrated with source/load-pull capability, as conceptually shown in Figure 3-1.
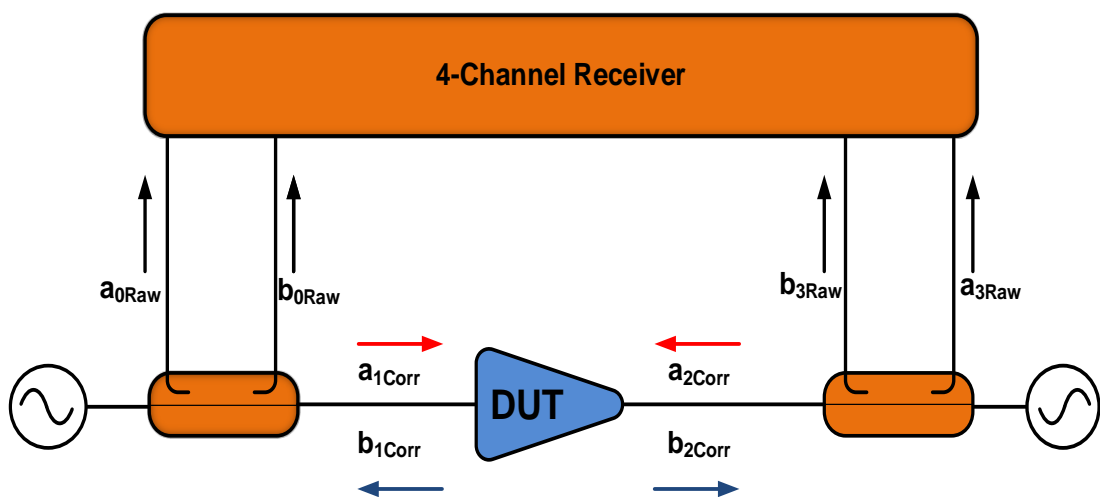
FIGURE 3-1 A GENERIC TWO PORT LSNA RF ARCHITECTURE WITH INTEGRATED ACTIVE LOAD-PULL.

The NVNA measurement component is typically either sampler based or Vector Network Analyzed (VNA) based, having a minimum of four channels. The source/load-

pull component can be either passive, mechanical tuners, or active, employing phase locked RF sources. Its main purpose is to vary, or engineer, the source and load impedance environment presented to the device during large signal operation [2, 3].

To achieve accurate measurements, the NVNA must be vector error corrected using an error model. Vector calibration and determination of the error model coefficients, involves the measurement of a set of calibration standards [3].

The LSNA error model has two elements: (linear $e(f)$, and non-liner $K(f)$), as shown in Equation 3-1.

$$\begin{vmatrix} a_1(f) \\ b_1(f) \\ a_2(f) \\ b_2(f) \end{vmatrix} = K(f) \begin{vmatrix} 1 & \beta_1(f) & 0 & 0 \\ \gamma_1(f) & \delta_1(f) & 0 & 0 \\ 0 & 0 & \alpha_2(f) & \beta_2(f) \\ 0 & 0 & \gamma_2(f) & \delta_2(f) \end{vmatrix} \cdot \begin{vmatrix} a_{0Raw} \\ b_{0Raw} \\ a_{3Raw} \\ b_{3Raw} \end{vmatrix} \quad \text{EQUATION 3-1}$$

One is identical to that used to vector correct VNA systems already discussed in the 7-term error model $\left(\alpha_1(f), \beta_{1,2}(f), \gamma_{1,2}(f) \, and \, \delta_{1,2}(f)\right)$, and it ensures that the system can perform vector corrected ratio, S-parameter, measurements. The other component, $k(f)$, scales all the measurements to allow for the measurement of power flow and phase aligns the harmonics to allow for the measurement of waveforms at the DUT terminal. The coefficients of the 7-term error model are determined from a set of un-corrected S-parameters measured on a set of calibration standards. In this case, we will use the Line Reflect-Line (LRL)/Thru-Reflect-Line (TRL) calibration procedure. It is the determination of these error coefficients that is the focus of this chapter [2-6].

In general, the new calibration flow consists of three stages, as shown in Figure 3-2.
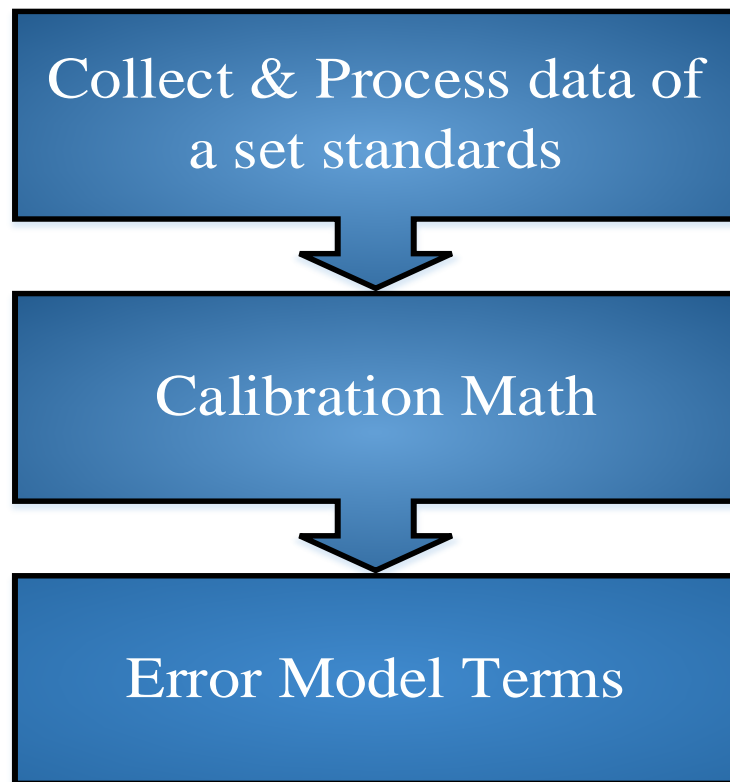
FIGURE 3-2 STAGES OF THE CALIBRATION MEASURMENT SYSTEM.

The first stage collects and processes a set of data by connecting the standards to the measurement system.

Thru standard, un-corrected measurement system is used to compute the S-parameters, hence T-parameters, of Thru by performing a forward and reverse measurement for each frequency on the defined frequency and grid points when a Thru is connected between Port 1 and Port 2 as shown in Figure 3-3 and Figure 3-4[6-8].
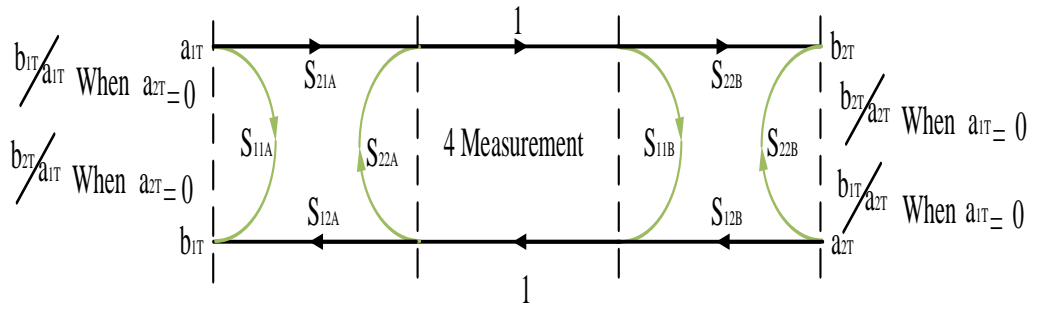
FIGURE 3-3 SIGNAL FLOW GRAPH FOR THE THRU CONNECTION.
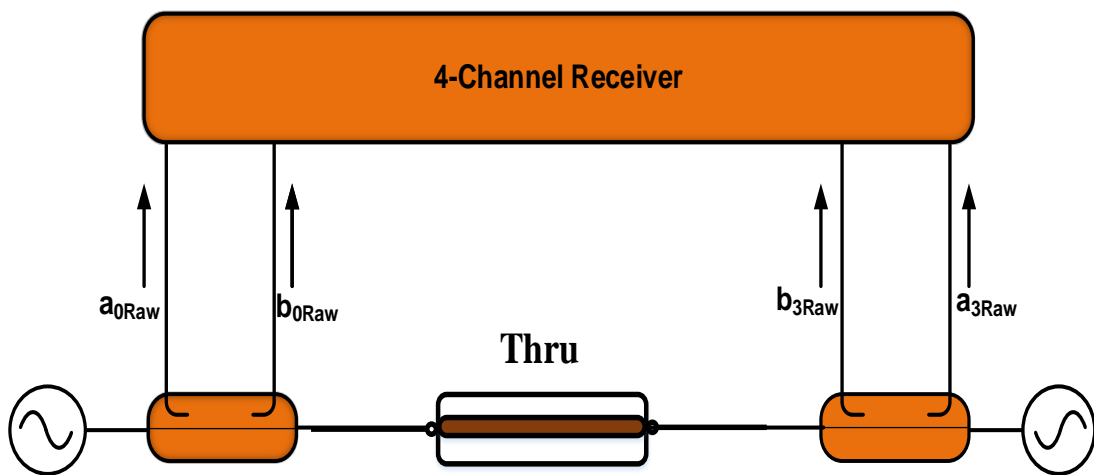
FIGURE 3-4 BLOCK DIAGRAM FOR THE THRU CONNECTION.

Line standard, the 2nd standard, un-corrected measurement system, is used to compute S-parameters, hence T-parameters, of Line by performing a forward and reverse measurement for each frequency at the defined frequency and grid points when a Line is connected between Port 1 and Port 2 as shown in Figure 3-5and Figure 3-6.
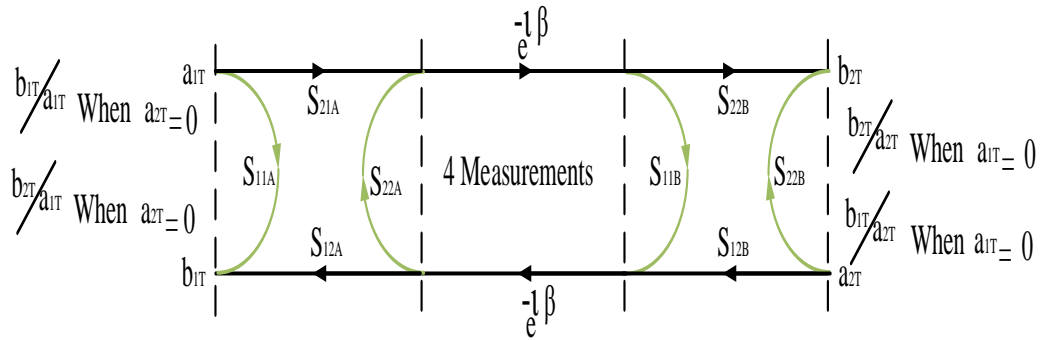
FIGURE 3-5 SIGNAL FLOW GRAPH FOR THE LINE CONNECTION.
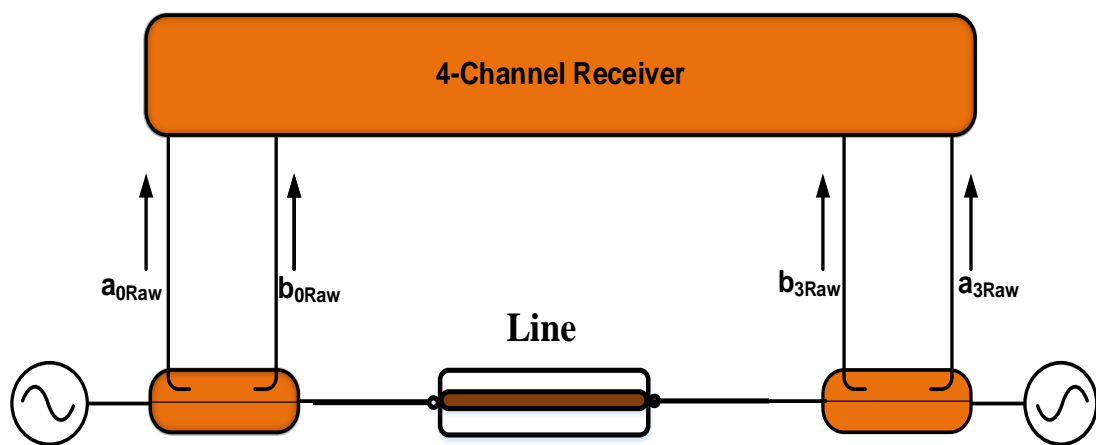
FIGURE 3-6 BLOCK DIAGRAM FOR THE LINE CONNECTION.

The last step in the measurement system calibration consists of terminated Port 1 and Port 2 by reflection (Short) and using the un-corrected measurement system to compute S-parameters and reflection coefficient as shown in Figure 3-7,Figure 3-8 and Figure 3-9.

$$\dfrac{b_{1R}}{a_{1R}} \text{ When } a_{2R}=0$$

$$\dfrac{b_{2R}}{a_{2R}} \text{ When } a_{1R}=0$$
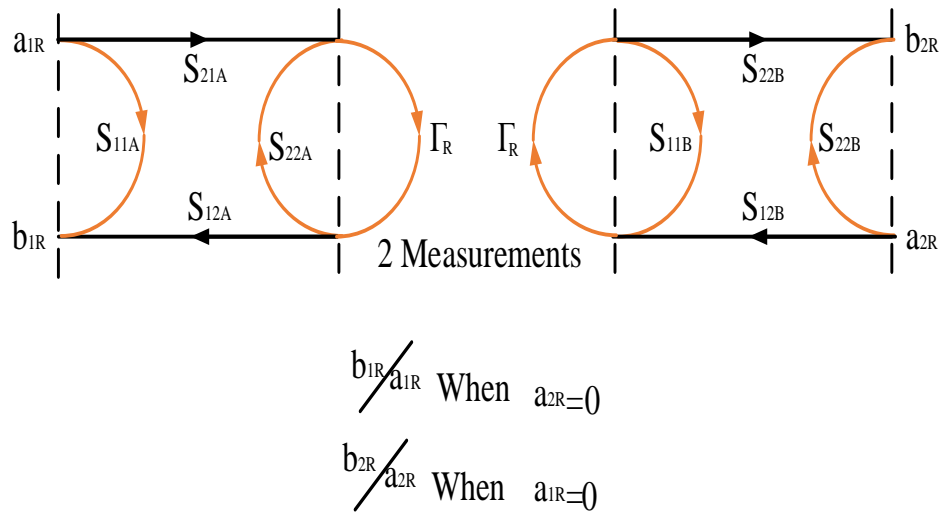
FIGURE 3-7 SIGNAL FLOW GRAPH FOR THE REFLECT CONNECTION.
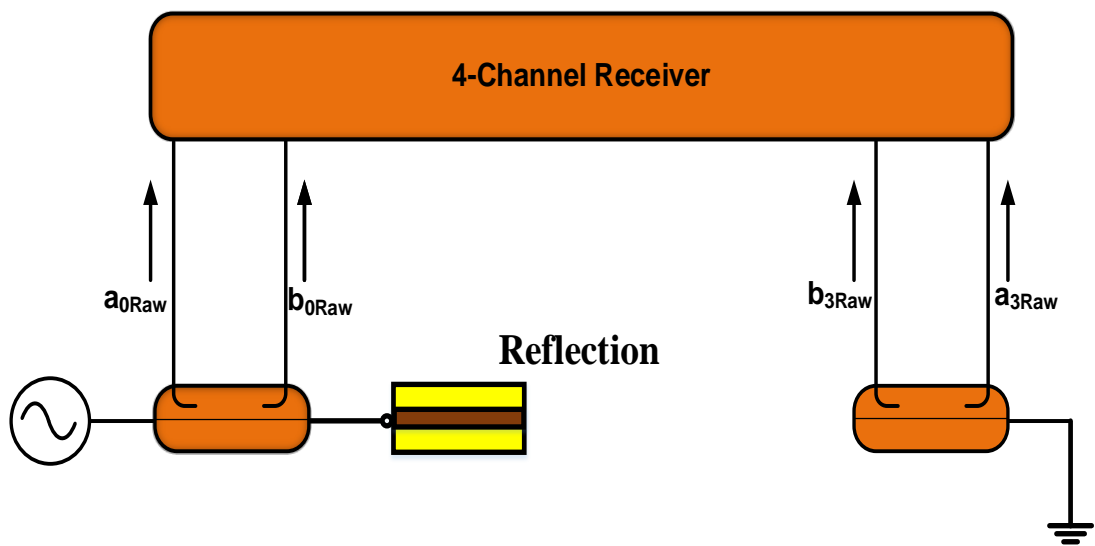
FIGURE 3-8 BLOCK DIAGRAM FOR THE REFLECT CONNECTION.
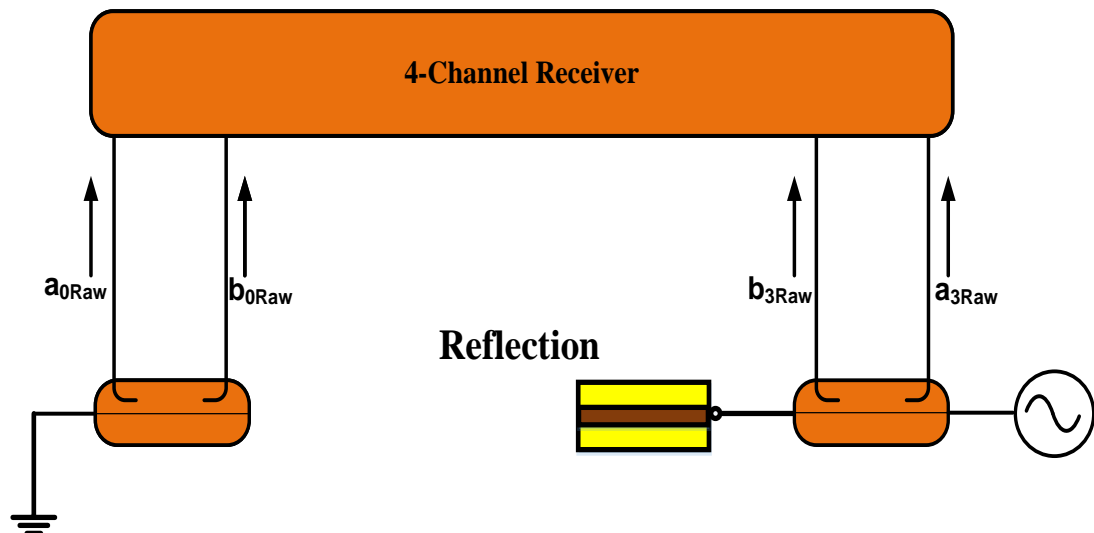
FIGURE 3-9 BLOCK DIAGRAM FOR THE REFLECT CONNECTION.

Raw data collected from these 3 calibration standard measurements, is now processed by the calibration algorithm which was presented in Chapter 2. This information is sufficient to determine the 7-term error model coefficients, the reflection coefficient of the unknown reflect standard and the transmission coefficient of the Line standard and line Thru standard [6-9].

To recap the collected raw data from measuring calibration standard, is 4 terms from Thru standard at each frequency in frequency grid, 4 terms from Line standard at each frequency in frequency grid, and 2 terms from Reflection standard for each step in frequency grid. These 10 terms passing TRL algorithm to determine the 7-terms, β and ι for each step in frequency grid, whereby β represent the propagation constant of delay Line and ι physical length [6-9].

The source/load pull measurement system used in this look consists of a VNA, which is a ZVA 67 GHz R&S with M150 load pull system from Mesuro. The measurement system was calibrated on a frequency grid starting at 2 GHz and ending at 8 GHz, with 2 GHz steps, as shown in Figure 3-10.

ZVA 67GHz
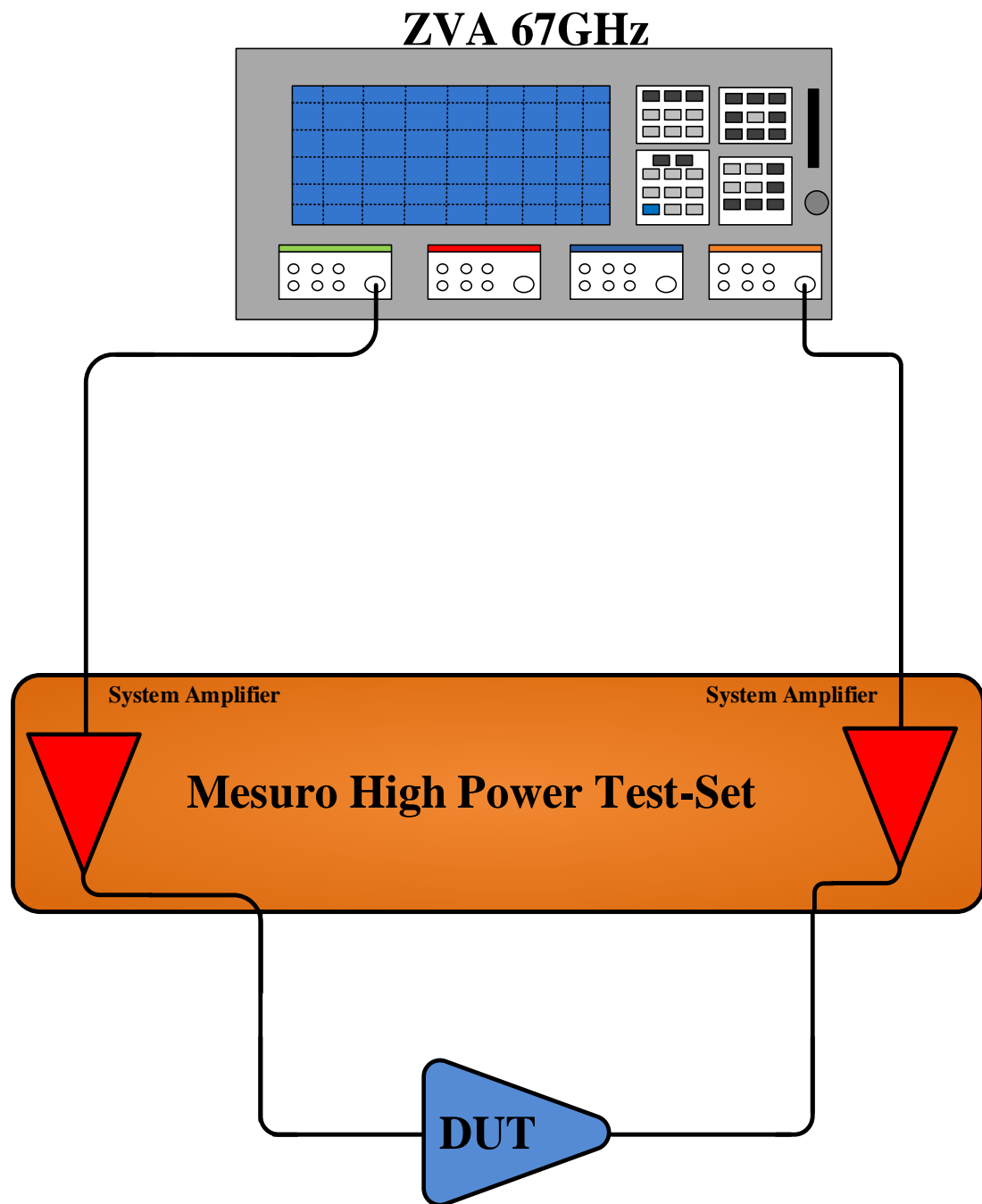
FIGURE 3-10 MESURO SYSTEM (LOAD PULL SYSTEM).

After calibration is accomplished, it is required to regularly check and validate the quality of the calibrated measurements. Checking the data quality can be achieved by computing the consistency of the measured raw, un-corrected S-parameter data of the Thru and Line standards for use in the LRL/TRL calibration algorithm. This can be quantified by introduction the following figure of matrix X, computed from the un-corrected S-parameter data of the Thru and Line standards.

$$X = \left(T_{MLine} *\quad T_{MThru}^{-1} \right)$$

<div align="right">EQUATION 3-2</div>

T_{MLine} for the measured Line standard, and T_{MThru} for the measured Thru standard.

Therefore:

$$T_{MThru} = T_A T_{Thru} T_B = T_A T_B$$

<div align="right">EQUATION 3-3</div>

The Thru T-matrix is identity matrix and Line standard equation can be represented as:

$$T_{MLine} = T_A T_{Line} T_B$$

<div align="right">EQUATION 3-4</div>

Stage One

Equation 3-3 can write it as shown in Equation 3-5:-

$$T_B = T_{Thru}^{-1} T_A^{-1} T_{MThru}$$

<div align="right">EQUATION 3-5</div>

And Line can write it

$$T_B = T_{Line}^{-1} T_A^{-1} T_{MLine}$$

<div align="right">EQUATION 3-6</div>

$$T_{MLine} = T_A T_{Line} T_{Thru}^{-1} T_A^{-1} T_{Mthru}$$

<div align="right">EQUATION 3-7</div>

Equation 2-41can obtain $T_{Thru} = 1$.

$$\therefore T_{Thru} = 1$$

$$T_{MLine} T_{MThru}^{-1} = T_A T_{Line} T_A^{-1}$$

<div align="right">EQUATION 3-8</div>

Where $X = T_{MLine} T_{MThru}^{-1}$

$$X T_A = T_A T_{Line}$$

<div align="right">EQUATION 3-9</div>

Solving Eequation 3-9 can obtain equations 3-10, 3-11, 3-12 and 3-13

$$X_{11} + X_{12}A = L \qquad \text{EQUATION 3-10}$$

$$X_{21} + X_{22}A = AL \qquad \text{EQUATION 3-11}$$

$$X_{11}B + X_{12} = B/L \qquad \text{EQUATION 3-12}$$

$$X_{21}B + X_{22} = 1/L \qquad \text{EQUATION 3-13}$$

Where $A = T_{21}^A/T_{11}^A$ and $B = T_{12}^A/T_{22}^A$

$$(X_{11} + X_{12}A)(X_{22} + X_{21}B) = 1 \qquad \text{EQUATION 3-14}$$

$$(X_{21} + X_{22}A)(X_{12} + X_{11}B) = 1 \qquad \text{EQUATION 3-15}$$

By solving equations 3-14 and 3-15

$$(X_{11}X_{22} - X_{21}X_{12})(1 - AB) = 1 - AB \qquad \text{EQUATION 3-16}$$

By dividing both part $(1 - AB)$ and$AB \neq 1$.

It can be shown that the determinate of the figure of the next matrix $\Delta(X)$ should be equal to one.

$$X_{11}X_{22} - X_{12}X_{21} = 1 \qquad \text{EQUATION 3-17}$$

It should be noted that the accuracy of the determined error model coefficients is directly related to the accuracy of the measured uncorrected S-parameters. The error terms obtained from the calibration process are not necessarily perfect (analysis shows that Thru /Line data is not consistent) as shown in Table (3-1) so inaccuracy in the acquisition of the error terms will cause errors in the measurements [10,11].

Data Extracted at 2 GHz			
S-parameter of Reflection			
S11	-0.52367-j0.50861	0+j0	S21
S12	0+j0	0.061814+j0.645351	S22
S-parameter of Thru			
S11	0.054986+j0.037029	0.629729-j0.24699	S21
S12	0.627202-j0.33811	-0.01758+j0.07304	S22
S-parameter of Line			
S11	0.052842+j0.025703	0.507919-j0.44618	S21
S12	0.461344-j0.54202	0.014314+j0.0674	S22
Analysis show Thru/Line data not consistent			

TABLE 3-1 ANALYSIS SHOWS THRU/LINE DATA IS NOT CONSISTENT.

For the *un-corrected S-parameter data* obtained from the forward/reverse measured $\Delta(X) = 1.00227+0.02143i$.

Traditional measurement system calibration as shown in Figure 3-11.
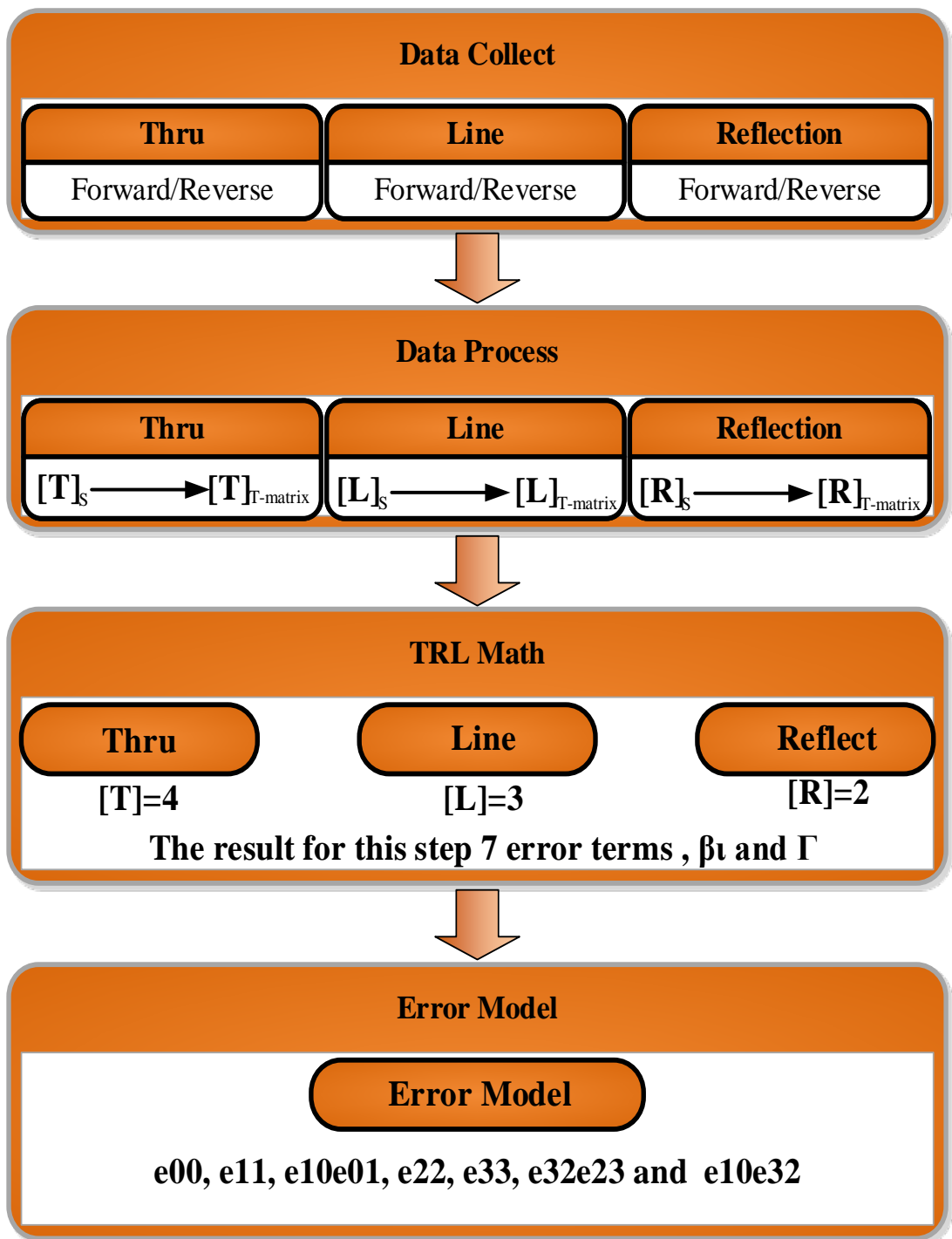
FIGURE 3-11 MATH REPORT ON THE TRL CALIBRATION PROCESS BY ENHANCED VECTOR CALIBRATION.

2.2.2 VALIDITY OF TRADITIONAL CALIBRATION

Re-measuring the Calibration-Standards is a simple way to check the calibration quality. Re-measuring the Calibration-Standards will provide information regarding the repeatability and noise in the measurement system to the operator. Usually, uncertainty contributions include VNA measurement repeatability, connection repeatability, power level uncertainty and residual uncertainty due to calibration, which involves uncertainty in the standard definition and measurement repeatability [10-13].

In this case the active load-pull system was used to perform this investigation. Typically, a verification process is used to investigate the quality of the **corrected S-parameters** determined after vector correcting raw measurement data. The **corrected S-parameters** of the Thru and Line standards were measured into different load impedance for one of the frequencies in the measurement grid (Note that during calibration the load is set to the nominal reference value of 50 ohms). A typical set of load impedances is shown in Figure 3-12 [10-13]. NO LOAD IMPEDANCES ARE SHOWN BELOW IN FIGURE 3.12
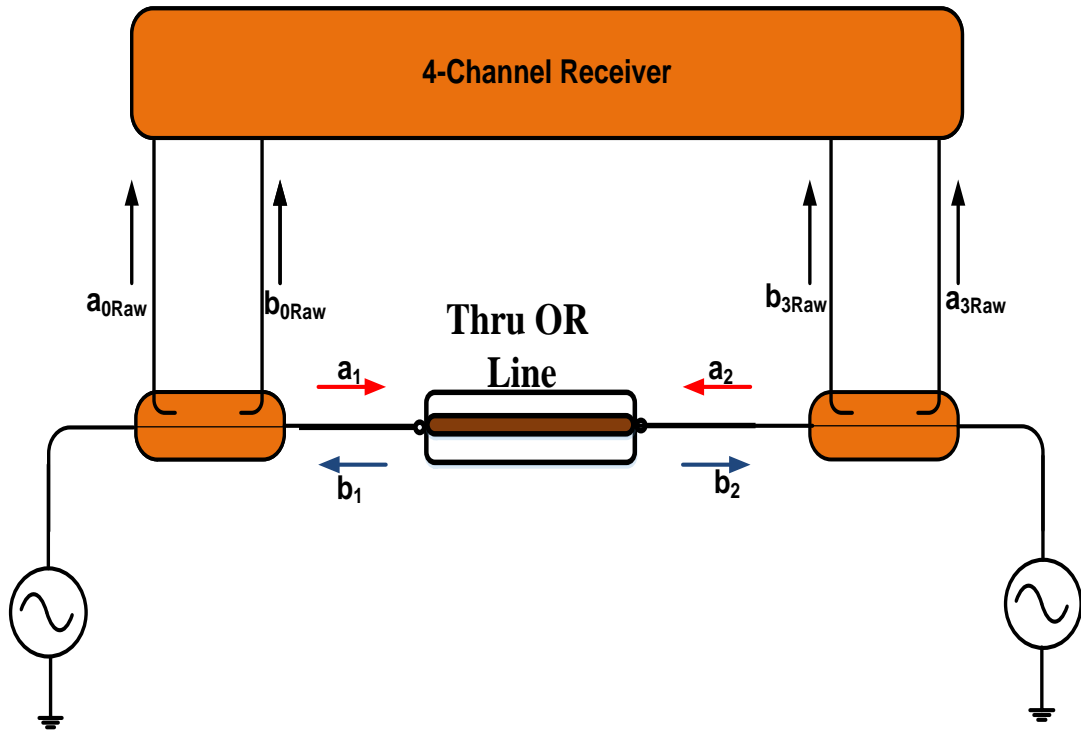
FIGURE 3-12 CALIBRATION ACCURACY IS VERIFIED BY MEASURING THE THRU AND LINE CALIBRATION STANDARDS UNDER DIFFERENT LOAD CONDITIONS.

The calibration accuracy of the system in Figure 3-12 is verified by measuring (output power P_{out}, input power P_{in}, Gain G and PAE) . The behaviour under different load conditions is shown below in equations 3-18, 3-19 and 3-20 and Figure 3-13 [10].

.

$$P_{in} = |a_1|^2 - |b_1|^2 \qquad \text{EQUATION 3-18}$$

$$P_{out} = |b_2|^2 - |a_2|^2 \qquad \text{EQUATION 3-19}$$

$$Gian = \frac{P_{out}}{P_{in}} = \frac{|b_2|^2(1-|\Gamma_L|^2)}{|a_2|^2(1-|\Gamma_L|^2)} \qquad \text{EQUATION 3-20}$$
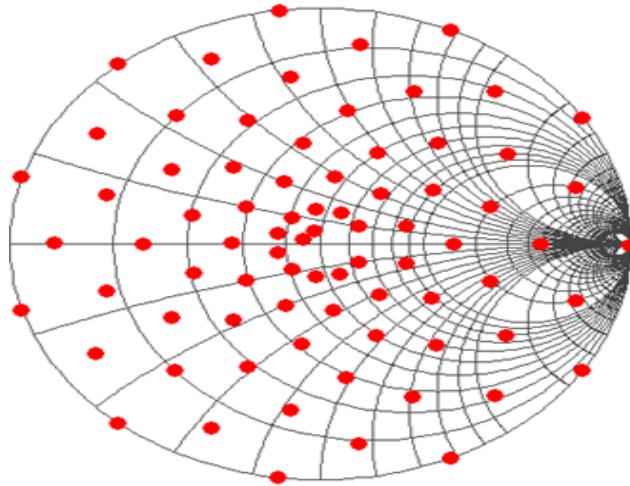
FIGURE 3-13 SMITH CHART WITH DIFFERENT LOAD CONDITIONS.

The zero-gain obtained from measuring Thru standard in ideal case only (by definition), since it has no loss or delay, where $a_1 = b_2, b_1 = a_2$ and $P_{in} = P_{out}$. Gain must be equals to 0 dB in an ideal case. Similarly for a Line the gain obtained should also be zero since it has no loss. If gain is calculated by the Equation 3-214, for If $\Gamma_L = \Gamma_{in} = 1$, Then gain is undefined. Alternatively gain can be defined as in Equation 3-21.

$$\boldsymbol{Gain = 20 \log\frac{b_2}{a_1}} \, OR \, \boldsymbol{20 \log\frac{b_1}{a_2}}$$ EQUATION 3-21
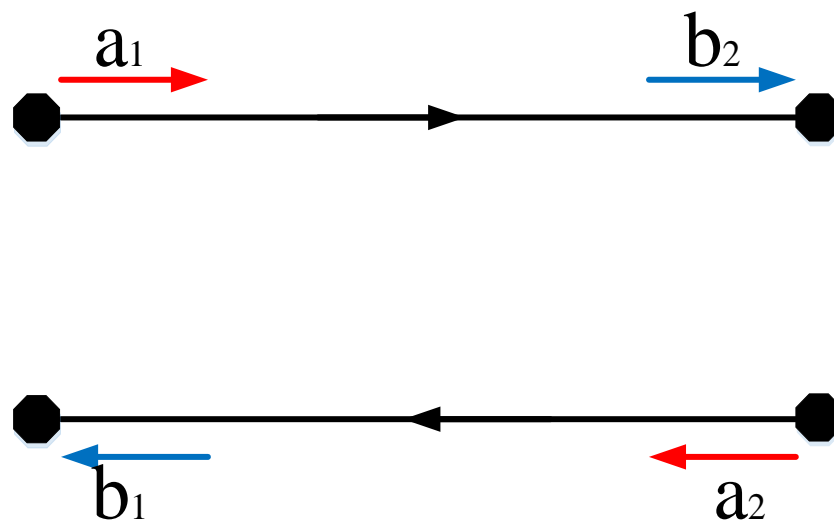
FIGURE 3-14 IDEAL CASE FOR THRU AND LINE STANDARDS.

Figure 3-14 is showing an ideal case for Thru and Line standards. The error for forward and revered should be zero as shown in equations 3-22 and 3-23.

$$Error_{For} = |b_2|^2 - |a_1|^2$$ EQUATION 3-22

$$Error_{Rev} = |b_1|^2 - |a_2|^2$$ EQUATION 3-23

Also the error factor should be one in an ideal case, as shown below in Equation 3-24.

$$Error\ Factor = \frac{a_2/b_2}{b_1/a_1} = \frac{a_2 a_1}{b_1 b_2} = 1$$ EQUATION 3-24

Setup the measurement system by connecting the Thru standard between Port 1 and Port 2 to verify the calibration accuracy, as shown in Figure 3-15. Note that during calibration the load is set to the nominal reference value (50 ohms).
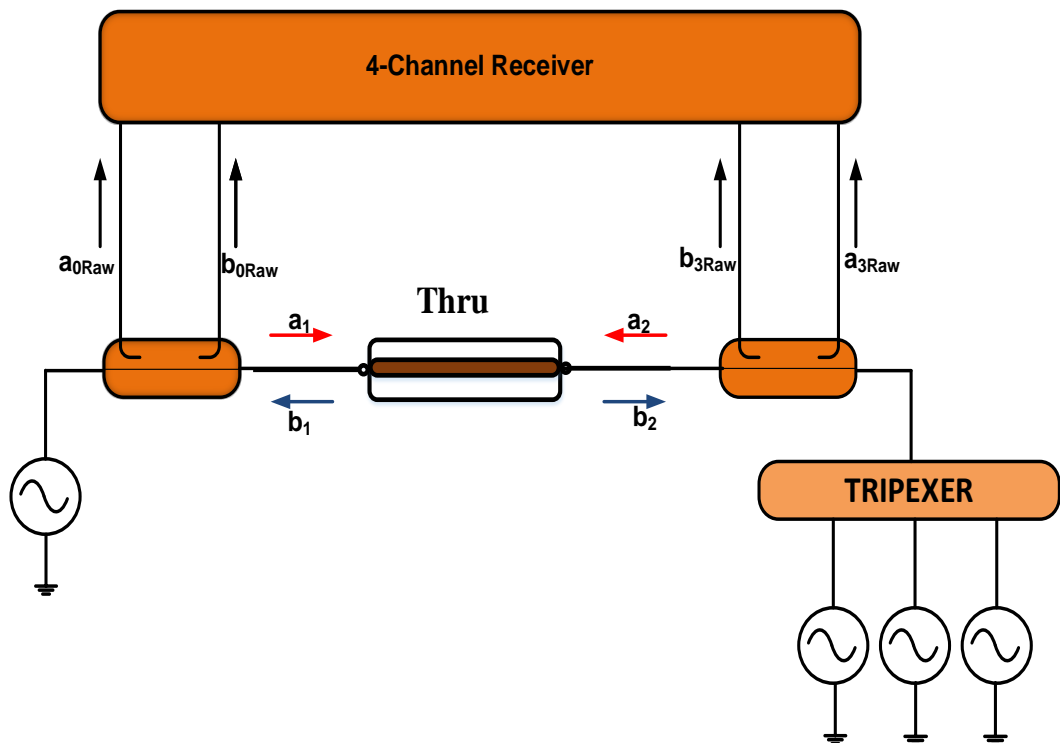
FIGURE 3-15 THE CALIBRATION ACCURACY IS VERIFIED BY MEASURING THE THRU CALIBRATION STANDARDS UNDER DIFFERENT LOAD CONDITIONS.
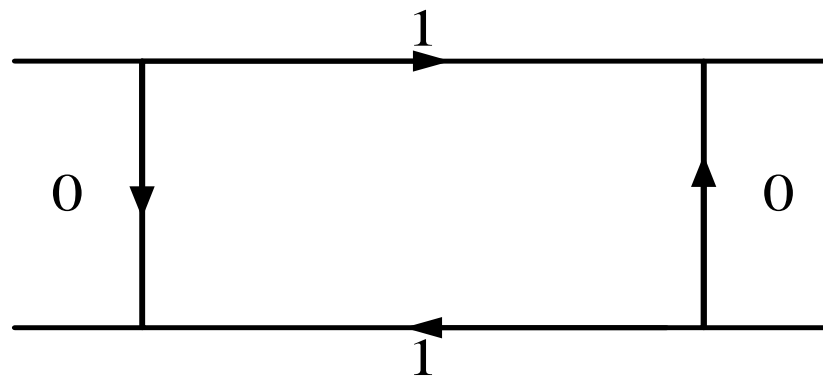
FIGURE 3-16 FLOW GRAPHS OF TRL(THRU) STANDARDS.

Figure 3-17 is showing the results obtained from the measurement of the gain when connecting Thru standards between Port 1 and Port 2.
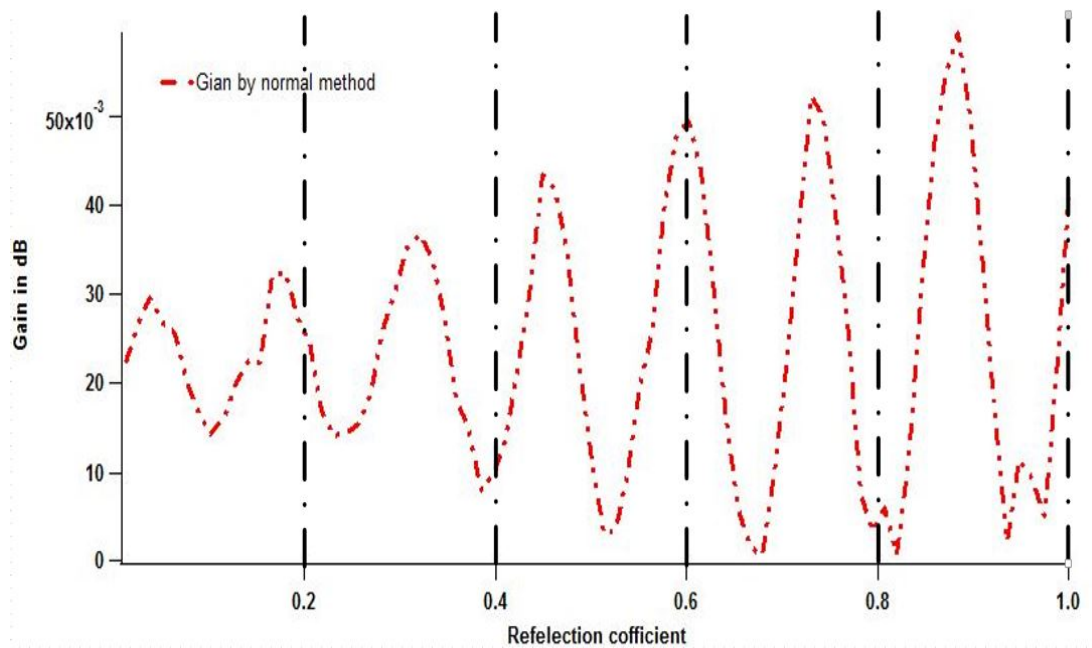
FIGURE 3-17 GAIN (B2/A1) OBTAINED FROM MEASURING THRU USING LOAD PULL SYSTEM WITH TRADITIONAL CALIBRATION METHOD.

The same result can be represented as contours in a Smith Chart, as shown in Figure 3-18.
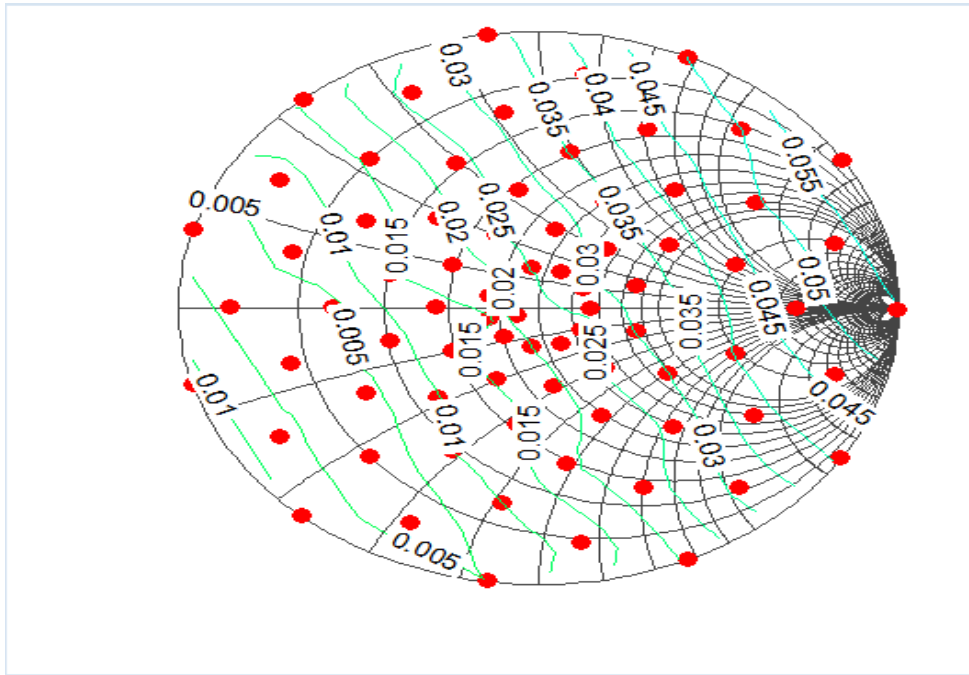
FIGURE 3-18 GAIN (B2/A1) OBTAINED FROM MEASURING THRU USING A LOAD PULL SYSTEM WITH TRADITIONAL CALIBRATION METHOD REPERSENTED IN A SMITH CHART.

In the case Line standard, setup the measurement system by connecting the Line standard between Port 1 and Port 2 to verify the calibration accuracy as shown in Figure 3-19. Note that during calibration the load is set to the nominal reference value (50 ohms).
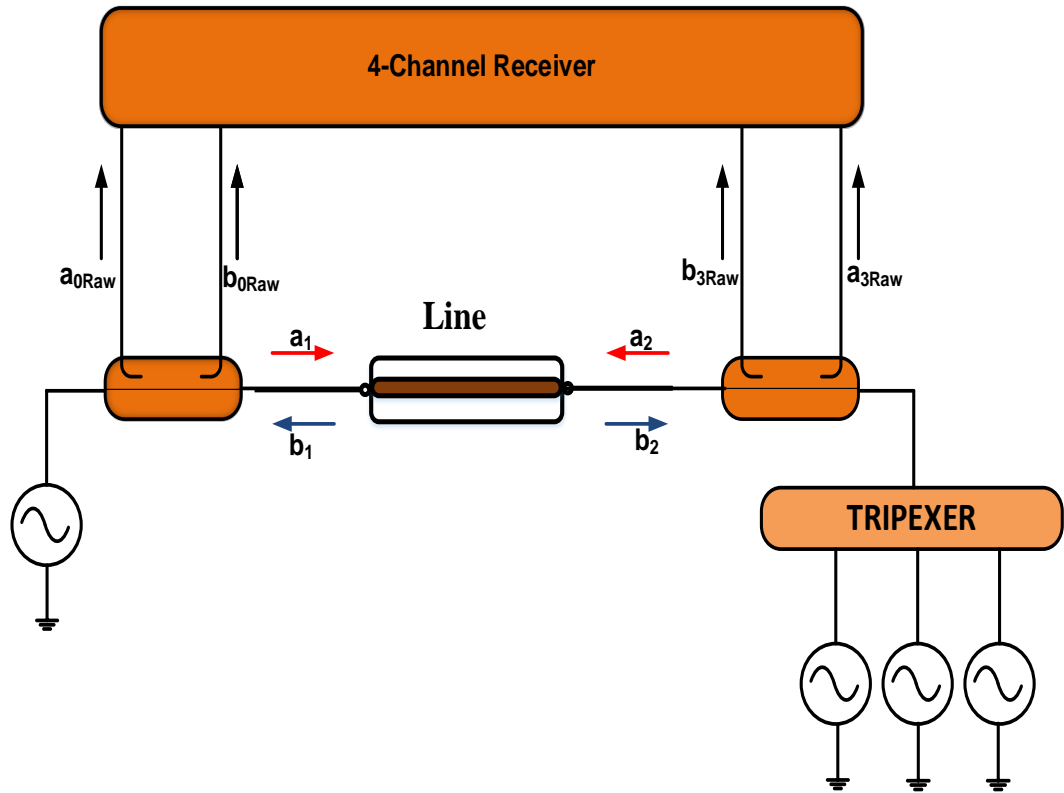
FIGURE 3-19 THE CALIBRATION ACCURACY IS VERIFIED BY MEASURING THE LINE CALIBRATION STANDARDS UNDER DIFFERENT LOAD CONDITIONS.

Figure 3-20 shows the results obtained from the measurement of the gain when connecting Line standard between Port 1 and Port 2.
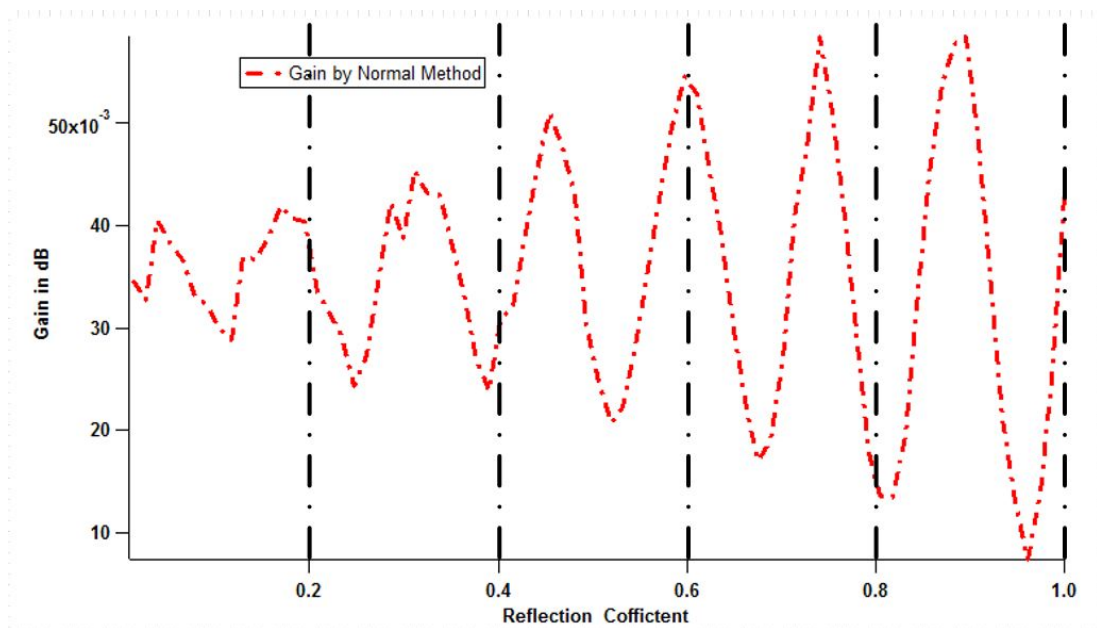
FIGURE 3-20 GAIN (B2/A1) OBTAINED FROM MEASURING LINE USING LOAD PULL SYSTEM WITH THE TRADITIONAL CALIBRATION METHOD.

The same result can be represented as contours in a Smith Chart, as shown in Figure 3-21.
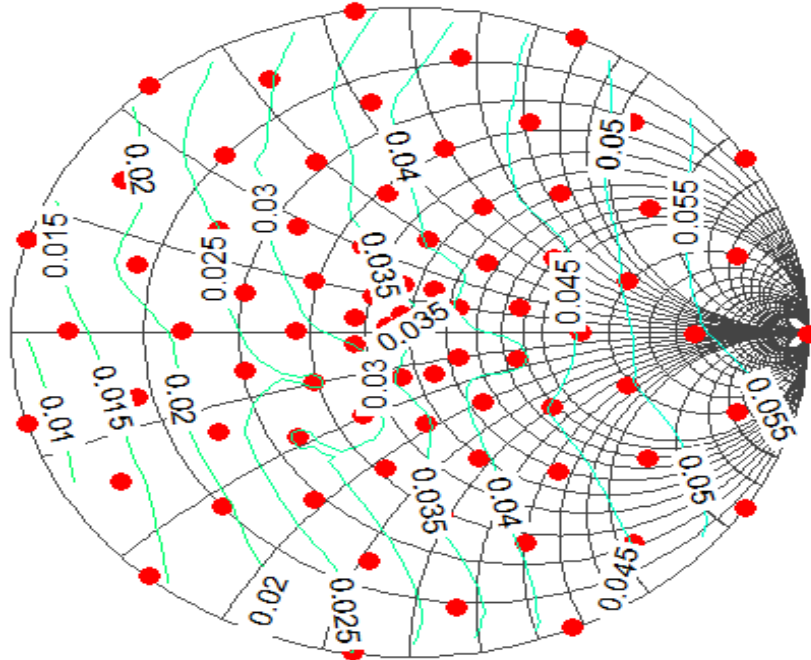
FIGURE 3-21 GAIN (B2/A1) OBTAINED FROM MEASURING LINE USING LOAD PULL SYSTEM WITH THE TRADITIONAL CALIBRATION METHOD.

Irrespective of the load impedance the measured corrected S-parameters of Thru or Line should be invariant. For example, the ratio $20 \log \frac{b_2}{a_1}$ should be invariant and equals to zero. Figure 3-17 and Figure 3-20 show, as contours, the results achieved on the Thru and Line standards, respectively. They indicate a variation of around 0.06 dB, which results from inaccuracies in the determined error model coefficients. This error, increases for load impedances near the edge of the Smith Chart.

The above can be summarised as follows:

- The measurement systems accuracy during this process will, unfortunately, limit the quality of the determined error coefficients; hence the accuracy of all subsequent error corrected S-parameter measurements. This investigation, consistent with previous research has shown that this effect is most noticeable

when performing measurements with source/load impedances near the edge of the Smith Chart.

- To improve the accuracy of the measurement system, Thru /Line measurements need to be taken at impedance other than the normal (50 Ohm) during calibration.

- Increased numbers of measurements will multiple standards cause random errors to increase due to connector repeatability.

- The load pull system allows us to avoid this type of error, providing for an increased number of measurements allowing TRL calibration without the need for multiple standards.

2.2.3 ENHANCED CALIBRATION (NEW METHOD)

In this part of the chapter, an alternative, more systematic, approach is used to improve the accuracy of the determined error coefficients and so yield an improved measurement system accuracy. To achieve this aim, load-pull measurements are used during the calibration process (new approach). The goal is to use the increased number of measurements performed on the Thru and Line standards to pre-process the data, hence minimise the impact of measurement uncertainties and random error, during determination of un-correct S-parameters before executing the standard LRM/TRM calibration algorithm.

The traditional method for TRL calibration requires 4 measurements to compute the raw Thru standard S-parameter, 4 measurements to compute the raw Line standard S-parameter, and 2 measurements to compute the raw Reflection standard S-parameter at Port 1 and Port 2. All these raw S-parameters will be processed by the TRL calibration to produce the 7 error coefficients. The enhancement calibration method requires N set of 4 measurements to compute the raw Thru standard S-parameter, N sets of 4 measurements to compute the raw Line standard S-parameter, and 2 of the same measurements to compute the raw Reflection standard S-parameter at Port 1 and Port 2. These improved raw standard S-parameters will now pass to same TRL calibration to again produce the 7 error coefficients. Figure 3-22 shows the proposed calibration procedure.
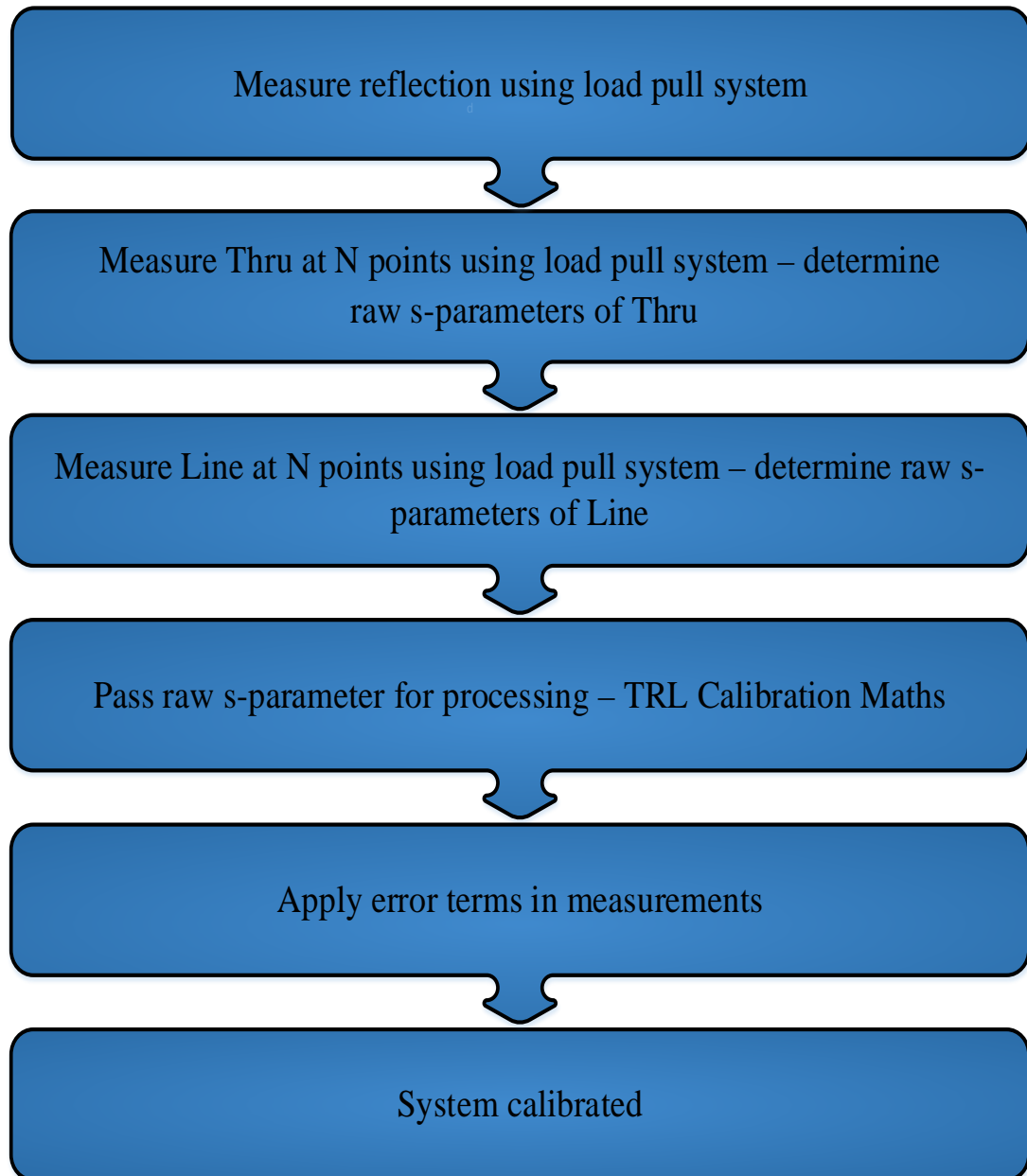
FIGURE 3-22 PROCEDURE FOR THE NEW CALIBRATION METHOD.

The new procedure key steps can be summarised as follows:-

1. Replace the two measurements (forward and reverse) to determine the un-correct S-parameters of Thru and Line with multiple measurements at different load impedances (target the complete coverage of the Smith Chart)

2. Utilise a least squares minimisation technique to process the Thru and Line multiple measurements (raw data without any correction) to determine a more accurate measure of their, raw, un-corrected S-parameters respectively.

3. These Thru and Line un-corrected S-parameters along with the Reflection standard measurements, can be used directly, without modification, by the standard LRM/TRM calibration algorithm to obtain 7-term error model coefficients.

This process should be repeated for each frequency in the frequency grid or just at selected frequencies where the need for improved accuracy is essential. At other frequencies, the un-corrected S-parameters determined from the forward and reverse measurements can be used as normal.

The enhancement calibration process is as follows:-

The first step in the measurement system (Load pull system) calibration consists of terminated Port 1 and Port 2 by reflection (Short) to measure the raw S-parameters of reflection as shown in Figure 3-23 and Figure 3-24, for each required frequency or for each frequency in the frequency step.
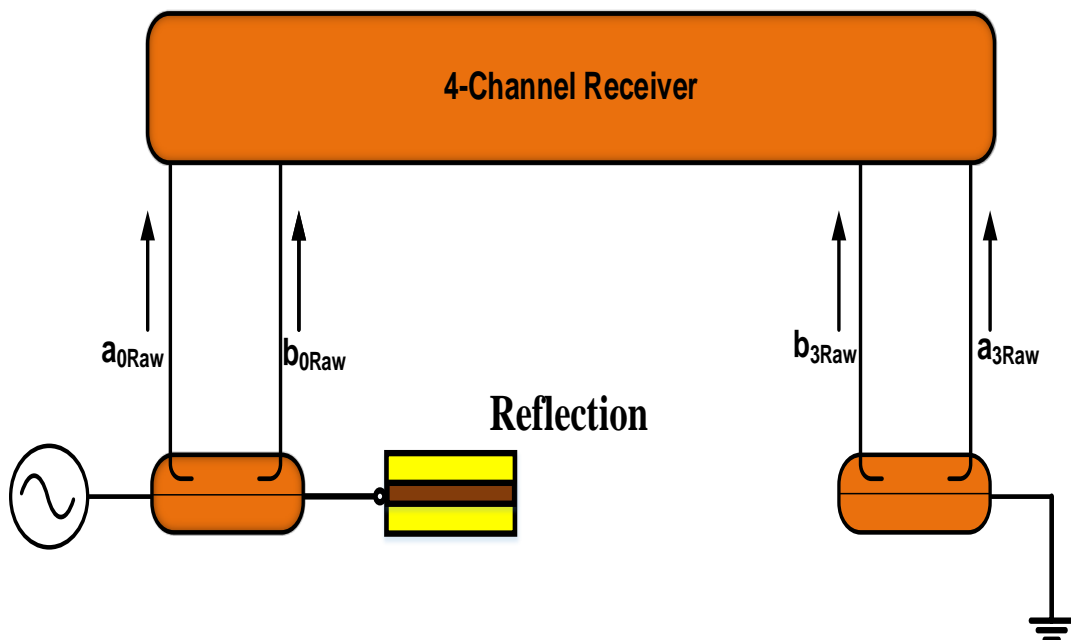
FIGURE 3-23 BLOCK DIAGRAM FOR THE REFLECT CONNECTION.
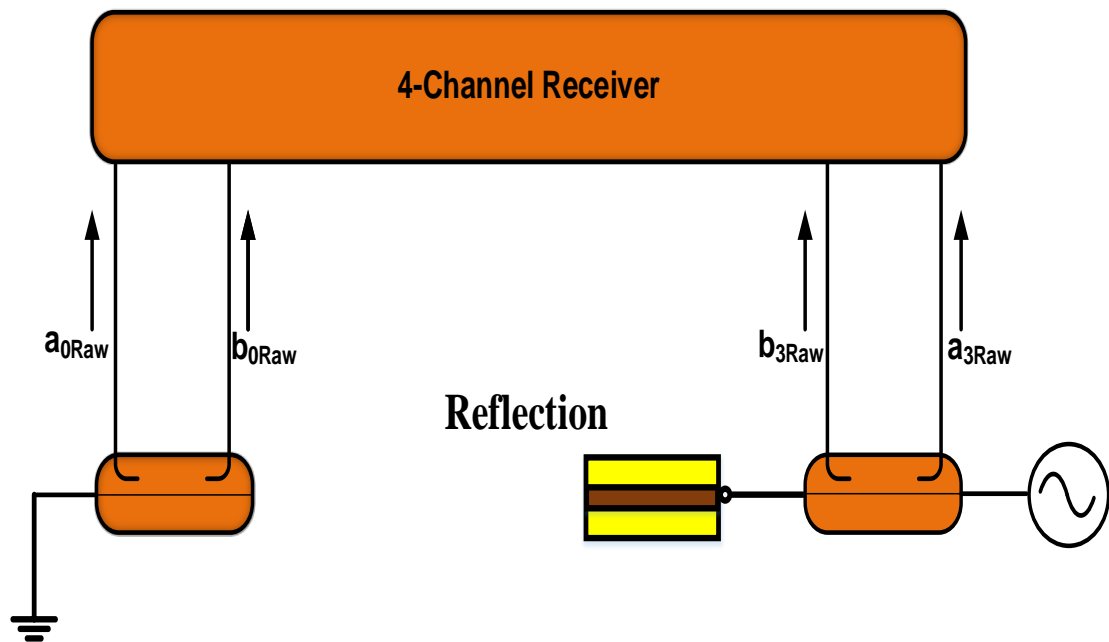
FIGURE 3-24 BLOCK DIAGRAM FOR THE REFLECT CONNECTION.

The 2nd step starts by setting up the measurement system as shown in Figure 3-25 to compute raw S-parameters, hence T -parameters of Thru by N forward measurement use a load pull system when a Thru is connected between Port 1 and Port 2, after the system is connected, measure (a_{0Raw}, b_{0Raw}, a_{3Raw} and b_{3Raw}) for each load then calculate the raw S-parameter of the Thru. Calculate NMSE of the system to check the maximum accuracy that can be achieved.

.
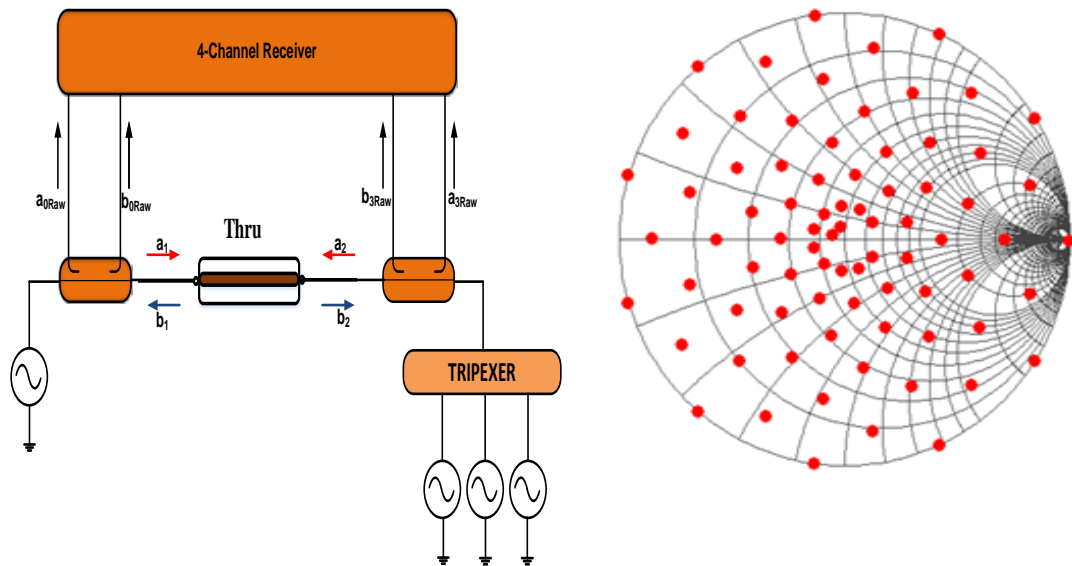
FIGURE 3-25 CALIBRATION BY MEASURING THE THRU STANDARDS UNDER DIFFERENT LOAD CONDITIONS. NOTE THAT DURING STANDARD CALIBRATION THE LOAD IS SET TO THE NOMINAL REFERENCE VALUE (50 OHMS).

The 3rd step consists of setting up the measurement system as shown in Figure 3-26 to compute raw S-parameters, hence T-parameters of Line by measuring N points using the load pull system when a Line is connected between Port 1 and Port 2. After connecting the system, start measuring (a_{0Raw}, b_{0Raw}, a_{3Raw} and b_{3Raw}) for each load then compute the raw S-parameter for followed by calculating the NMSE of the system to check for the maximum accuracy that can be achieved.
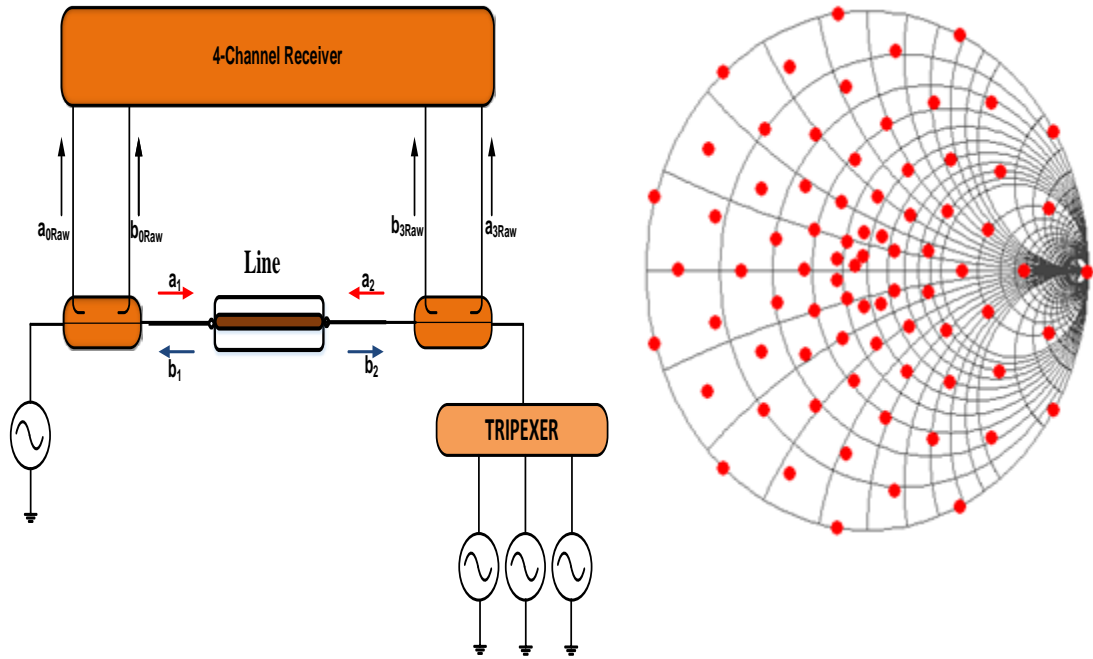
FIGURE 3-26 CALIBRATION BY MEASURING THE LINE STANDARDS UNDER DIFFERENT LOAD CONDITIONS. NOTE THAT DURING STANDARD CALIBRATION THE LOAD IS SET TO THE NOMINAL REFERENCE VALUE (50 OHMS).

The traditional method uses a single forward and reverse measurements to determine the raw S-parameter of the calibration standard for use in TRL math (the minimum necessary to measure 4 S-parameters). The enhanced calibration method uses multiple N-forward measurements, to compute each standard raw S-parameter (Line and Thru standards). Before using the result to determine the error coefficients the validity of the raw data, collected by the load pull system, should be first investigated. This is achieved determining to the validity and accuracy of determining of the un-corrected S-parameters of the Thru and Line standards using multiple measurements at different load impedances.

Since the device under test is invariant during these measurements they can all be described by Equation 3-25:-

$$\begin{bmatrix} b_1^1 & \cdots & b_1^n \\ \vdots & & \vdots \\ b_2^1 & \cdots & b_2^n \end{bmatrix} = [S_{Raw}].\begin{bmatrix} a_1^1 & \cdots & a_n^1 \\ \vdots & & \vdots \\ a_2^1 & \cdots & a_2^n \end{bmatrix} \qquad \text{EQUATION 3-25}$$

The Load pull system provides a number of independent measurements which can be used to compute the S_{Raw} required by the calibration process. The S_{Raw} can be determined by substituting the measured b values and a values in Equation 3-25.

S-parameters can be computed directly using raw data results of measurements using Equation 3-26.

$$[B_{Meas}] = [S_{Raw}].[A_{Meas}]$$
<div align="right">EQUATION 3-26</div>

$$[S_{Raw}] = [B_{Meas}].[A^T_{Meas}][A_{Meas} \quad A^{-1}_{Meas}]$$
<div align="right">EQUATION 3-27</div>

The validity and accuracy can be investigated by re-computing the b-waves using equation 3-28.

$$\begin{bmatrix} B_1(f)_{Cal(Model)} \\ \vdots \\ B_N(f)_{Cal(Model)} \end{bmatrix} = \begin{bmatrix} S_{11}(f)_{Raw} & S_{12}(f)_{Raw} \\ S_{21}(f)_{Raw} & S_{22}(f)_{Raw} \end{bmatrix}.\begin{bmatrix} A_1(f)_{Meas} \\ \vdots \\ A_N(f)_{Meas} \end{bmatrix}$$
<div align="right">EQUATION 3-28</div>

This is successfully demonstrated in Figure 3-27 and Figure 3-28.
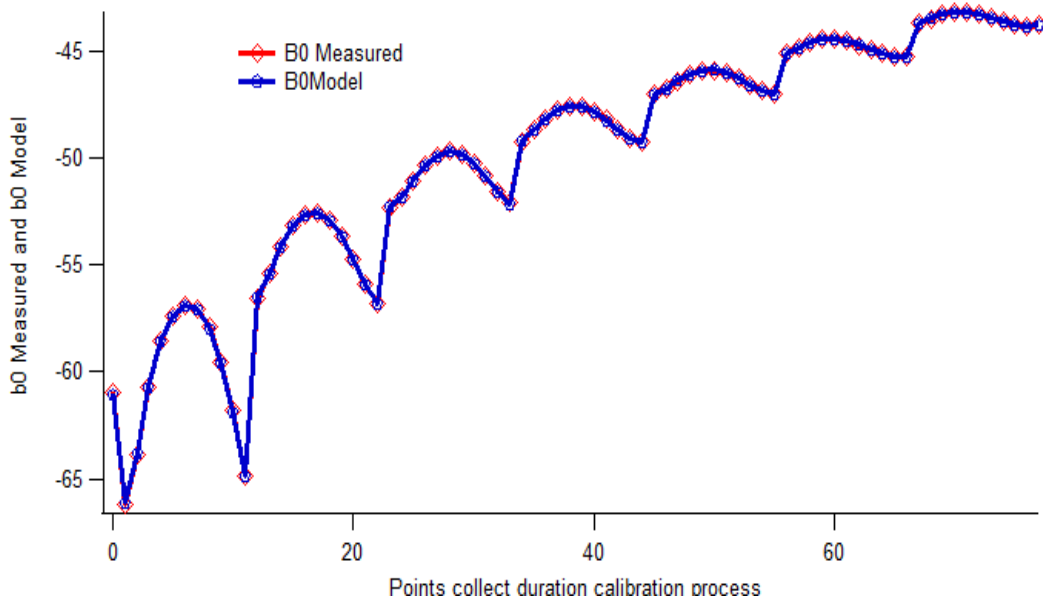
FIGURE 3-27 COMPARISON BETWEEN MEASURED AND MODELLED, USING THE DETERMINED RAW S-PARAMETERS, OF THE VALUES OF B₀^I IN THIS CASE THE DUT IS THE THRU.
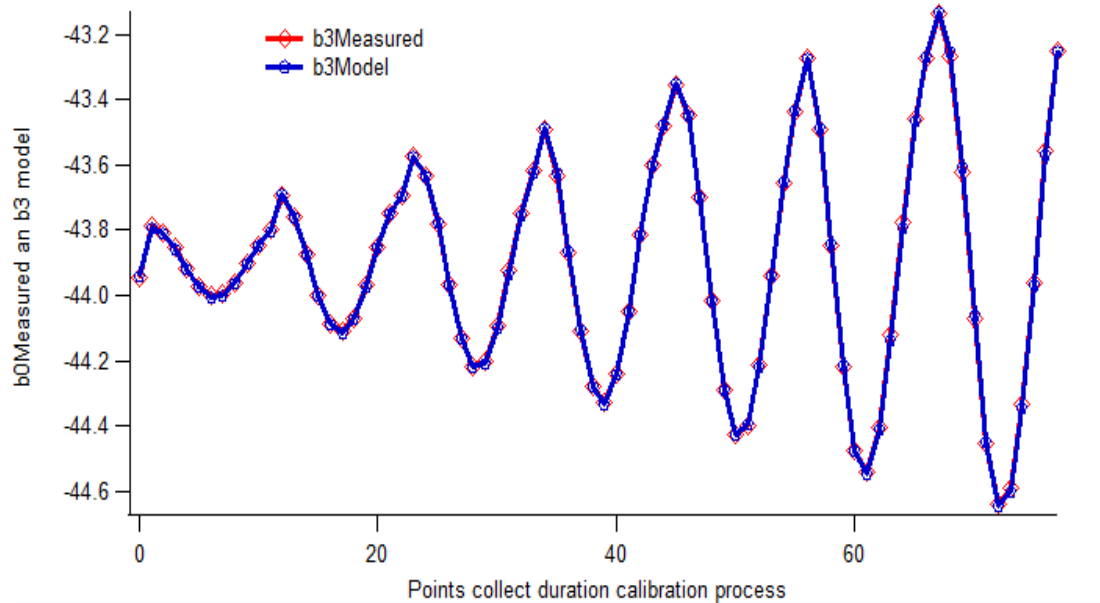
FIGURE 3-28 COMPARISON BETWEEN MEASURED AND MODELLED, USING THE DETERMINED RAW S-PARAMETERS, OF THE VALUES OF B3^I IN THIS CASE THE DUT IS THE THRU.

It is important to evaluate the quality of this fitting process in order to understand the level of accuracy that can be achieved. This can be quantified by computing the normalized mean square error ($NMSE$) for both $b_{0,3}$ waves [14].

$$NMSE_{0,3} = \frac{\sum \left| b_{0,3}^{meas} - b_{0,3}^{mod} \right|^2}{\sum \left| b_{0,3}^{meas} \right|^2}$$ EQUATION 3-29

This was investigated as a function of the number of load impedance points used and the area of the Smith Chart covered. It was observed, see Figure 3-29 that the accuracy improved if higher reflection coefficient load impedances were used, In fact values greater than unity can be used in the case of an active load-pull system. Also, as shown in Figure 2-29, greater than 40 points were required to minimise the impact of measurement uncertainties and random error, on the computed, raw un-corrected S-parameters.

.
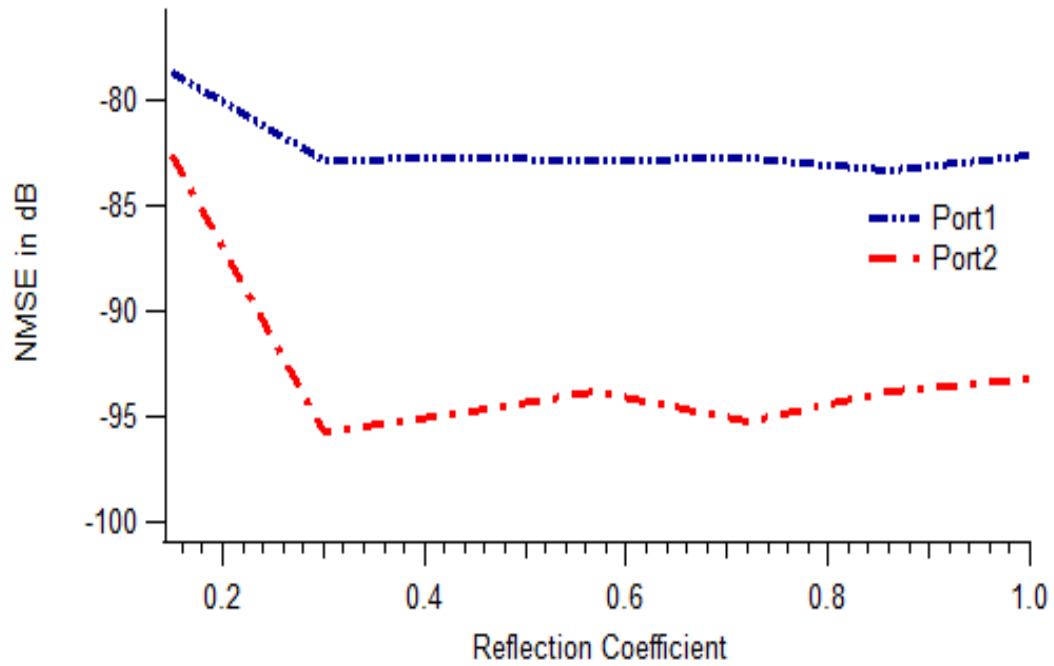
FIGURE 3-29 SENSITIVITY OF THE CALCULATED NMSE TO THE MAXIMUM REFLECTION COEFFICIENT OF LOAD-PULL POINTS.

Alternatively the error obtained from subtracted the b_{model} from the b_{measured} and distribution on the Smith Chart is shown Figure 3-30 and Figure 3-31. The random nature of the error in the raw data which was collected from the load-pull system can be observed in these plots.

$$error = \left| b_3^{meas} - b_3^{mod} \right|$$

<div align="right">EQUATION 3-30</div>
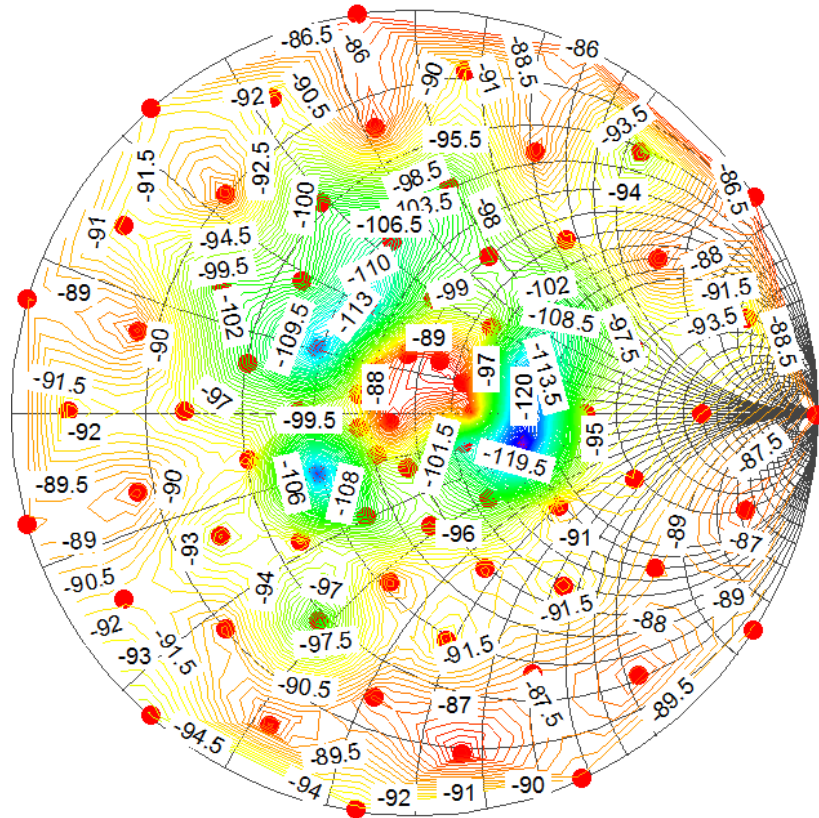
FIGURE 3-30 A SMITH CHART SHOWS THE DIFFERENCE BETWEEN B3 MEASURED AND B3 MODELLED FOR THRU. SOME RANDOM ERROR CAN STILL BE SEEN IN THE RAW DATA WHICH WAS COLLECTED FROM THE LOAD-PULL SYSTEM.

The above Smith Chart shows the difference between b3 measured and b3 modelled in Thru.

FIGURE 3-31 A SMITH CHART SHOWS THE DIFFERENCE BETWEEN B3 MEASURED AND B3 MODELLED FOR LINE. SOME RANDOM ERROR CAN STILL BE SEEN IN THE RAW DATA WHICH WAS COLLECTED FROM THE LOAD-PULL SYSTEM.

Figure 3-30 and Figure 3-31 show difference between b3 measured and b3 modelled, for Thru and Line respectively, at each measurement point. These measurement are used to check the capability of the new method to remove all errors from raw data which is collect by the from measurement system. The nature of this random error can still be seen in Figure 3-30 and Figure 3-31.

The ability of the 7-term error model coefficients computed using the more accurate raw, un-corrected S-parameters, of the Thru and the Line to provide more accurate measurements is demonstrated using the previously discussed verification approach.

Set the measurement system as shown in Figure 3-32 to evaluate the calibration quality by measuring the calibration standards (Line and Thru) again. Note the measured value of ratio b_2/a_1 (in dB) as a function of load which should ideally be 0 dB.

FIGURE 3-32 CALIBRATION OF THE SYSTEM BY CONNECTED LINE OR THRU STANDARDS BETWEEN PORT1 AND PORT 2 UNDER DIFFERENT LOAD CONDITIONS BY USING THE LOADPULL SYSTEM.

The results obtained in this Line case are shown in Figure 3-33 as, contours of gain variation computed as a function of load impedance from the corrected S-parameters.
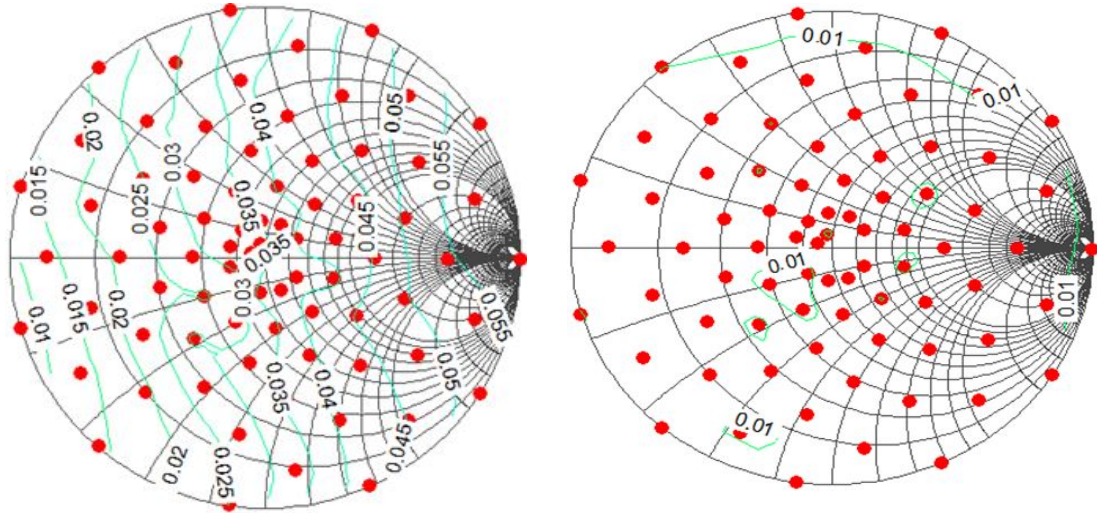
a) Gain $20\log(b_2/a_1)$ variations observed on the corrected S-parameters obtained from measuring the Line while varying the load impedance after performing a standard TRL calibration procedure.

b) Gain $20\log(b_2/a_1)$ variations observed on the corrected S-parameters obtained from measuring) the Line while varying the load impedance after performing a enhanced TRL calibration procedure.

FIGURE 3-33 COMPARISON BETWEEN THE TRADITIONAL METHOD AND THE ENHANCEMENT METHOD FOR CALIBRATION MEASUREMENT SYSTEM (LINE).

The results obtained in this Thru case are shown in Figure 3-34 as, contours of gain variation computed as a function of load impedance from the corrected S-parameters.
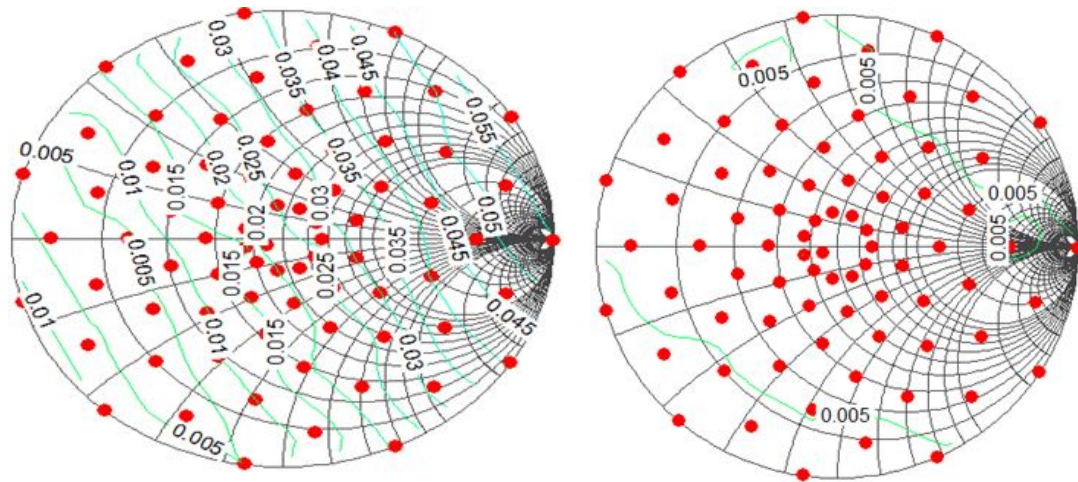
b) Gain $20\log(b_2/a_1)$ variations observed on the corrected S-parameters obtained from measuring the Thru while varying the load impedance after performing a standard TRL calibration procedure.

b) Gain $20\log(b_2/a_1)$ variations observed on the corrected S-parameters obtained from measuring) the Thru while varying the load impedance after performing an enhanced TRL calibration procedure.

FIGURE 3-34 COMPARISON BETWEEN TRADITIONAL METHOD AND ENHANCEMENT METHOD FOR CALIBRATION MEASUREMENT SYSTEM.

In this calibration a variation of around 0.006 dB, an order of magnitude improvement, is observed. This accuracy is maintained up to the edge of the Smith Chart, as shown in Figure 3-34. This is also highlighted in Figure 3-35 and Figure 3-36. The higher point numbers correspond to higher reflection coefficient magnitudes.
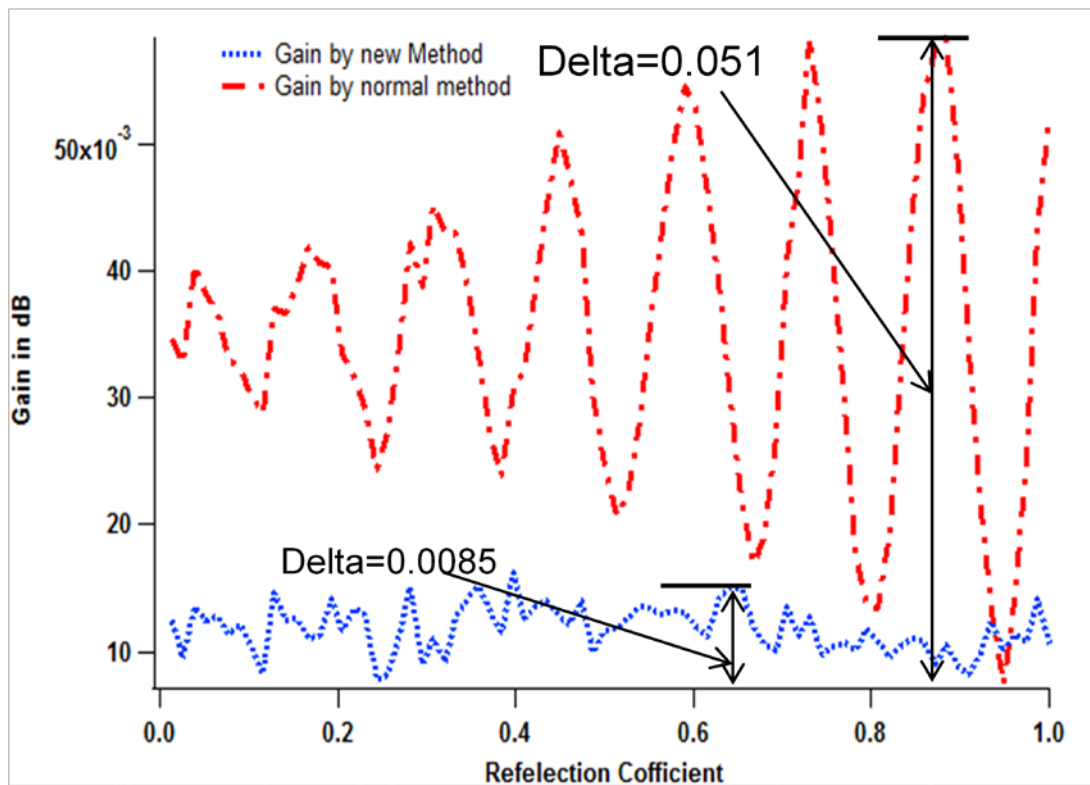
FIGURE 3-35COMPARISON BETWEEN GAIN CALCULATED BY USING NORMAL METHOD AND GAIN CALCULATED BY USING LOAD PULL SYSTEM FOR LINE. (RATIO B2/A1 (IN DB))
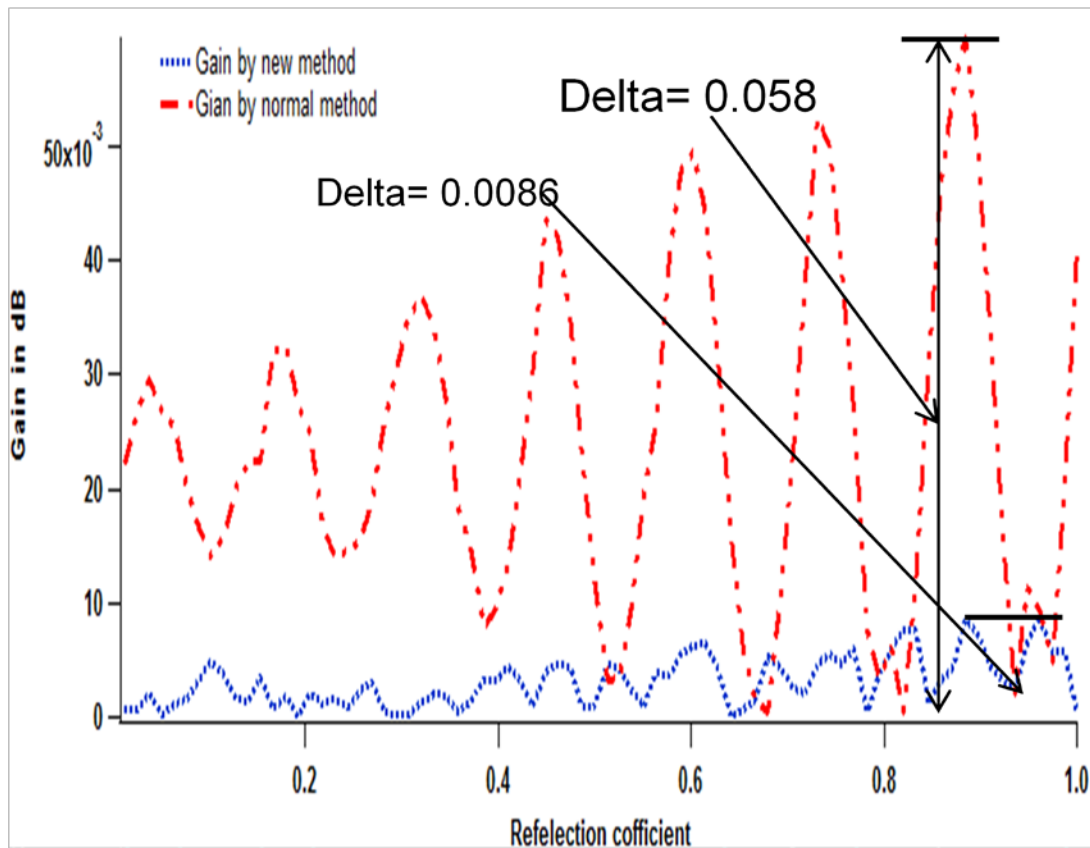
FIGURE 3-36 COMPARISON BETWEEN GAIN CALCULATED BY USING NORMAL METHOD AND GAIN CALCULATED BY USING LOAD PULL SYSTEM FOR THRU. (RATIO B2/A1 (IN DB))

Note:-ratio b2/a1 (in db comparison obtained from measuring Thru by using new and old method.

Figure 3-37 summarises the enhance calibration process. From the initial collection the raw data Thru determine a term of the 7 error coefficients and number for measurement which is used in modelling each standard and total measurement number for obtain error models.

Data Collect

Thru	**Line**	**Reflection**
Forward/Reverse	Forward/Reverse	Forward/Reverse

Data Process

Thru	**Line**	**Reflection**
$[T]_S \longrightarrow [T]_{T\text{-matrix}}$	$[L]_S \longrightarrow [L]_{T\text{-matrix}}$	$[R]_S \longrightarrow [R]_{T\text{-matrix}}$

Number of point 78

Total number of point will be 626

TRL Math

Thru	**Line**	**Reflect**
[T]=312	[L]=312	[R]=2

The result for this step 7 error terms , βι and Γ

Error Model

Error Model

e00, e11, e10e01, e22, e33, e32e23 and e10e32
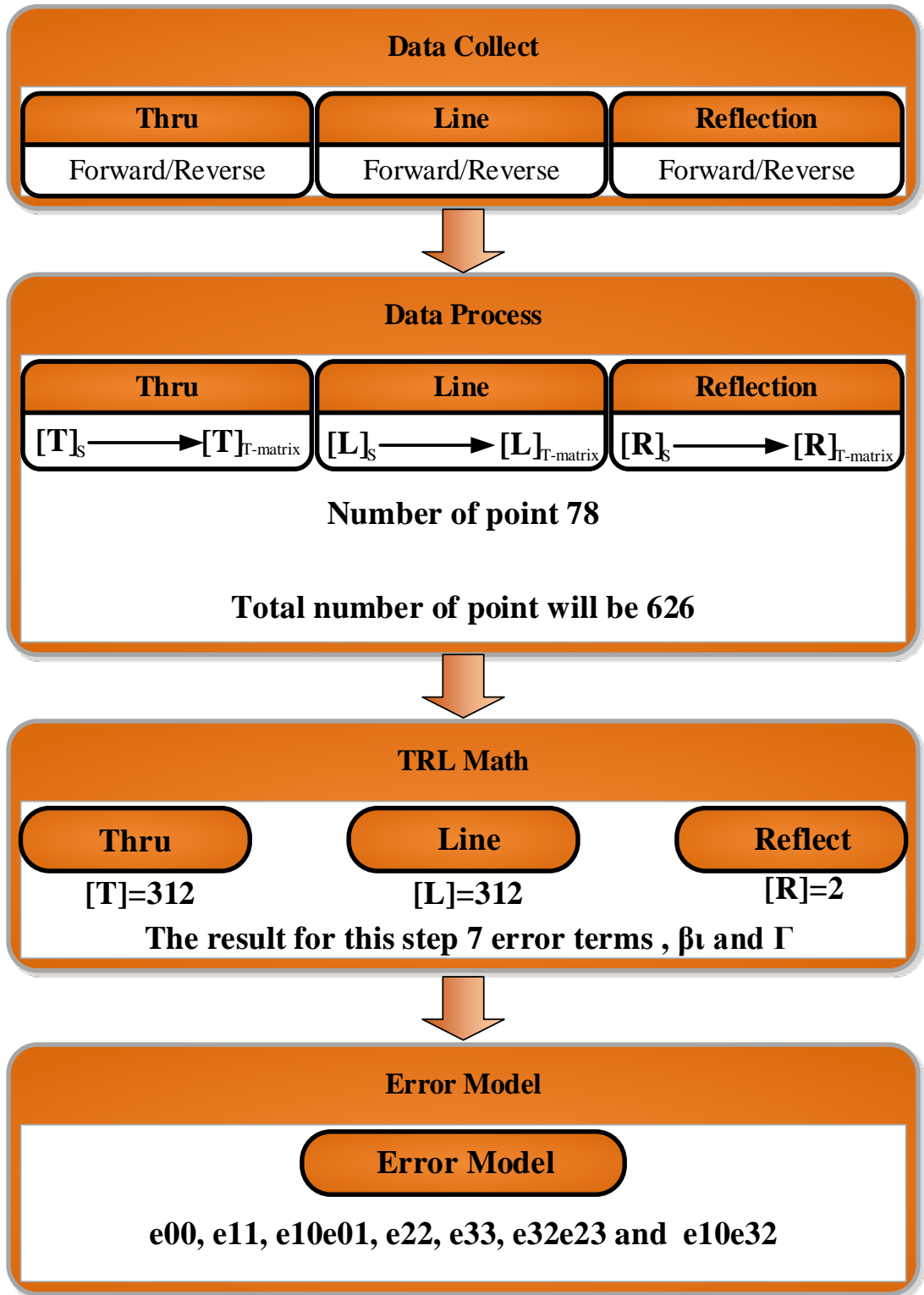
FIGURE 3-37 MATH REPORT ON THE TRL CALIBRATION PROCESS BY ENHANCED VECTOR CALIBRATION.

Improved quality of TRL (or TRM) calibration if load-pull capability is exploited during calibration is achieved by combining multiple forward measurements when the load is varied around the Smith Chart. This method is able to combine all measurements around Smith Chart in one matrix for Thru or Line, which minimises the errors and increases the accuracy of the system with no change in the type or number of calibration standards. Accuracy is maximised by ensuring full coverage of the Smith Chart.

2.3 QUALITY OF RAW DATA EFFECTS ON CALIBRATION ACCURACY

As mentioned before, the effect of raw data quality on accuracy of error terms will obtain in the calibration process. Equation 3-17 can check the quality of raw data for both cases. In the first case (traditional calibration) the *un-corrected S-parameter data* is obtained from the forward/reverse measure $\Delta(X) = 1.00227+0.02143i$ while for the second case the *un-corrected S-parameter data* is obtained from the multiple load-pull measurements $\Delta(X) = 1.00014-0.00405i$. By comparing the results of both cases, Can be notified $\Delta(X)$ in the second case is closer to 1than the first case. The calibration validity is improved because we are now using higher quality raw data.

2.4 RELATION BETWEEN Γ_{load} AND ACCURACY

This experiment attempted to discover the effect (relation between) of load impedance on accuracy of the error coefficient which is obtained during the calibration process. These error coefficients are produced by changing the reflection coefficient for load and using this to correct data obtained when measuring the Thru and Line standards with calculation of the gain for each state (each refection coefficient).

This test was conducted using a load pull system to change the reflection coefficient with each circle and a fixed number of measurement points for each circle (which is 11 points for each circle) as shown in Table 3-2:

Refection	In centre of Smith chart	Circle1 $\Gamma=0.15$	Circle2 $\Gamma=0.3$	Circle3 $\Gamma=0.45$	Circle 4 $\Gamma=0.6$	Circle 5 $\Gamma=0.75$	Circle 6 $\Gamma=0.9$	Circle 7 $\Gamma=1.0$	Total	
										Less Than1
$Gain = 20\ \log\dfrac{b_2}{a_1}$	1.376584	0.385329	0.284703	0.324481	0.334004	0.332863	0.357176	0.336752	0.317035	
										0.316458
Number of points	1 point	11 points	11 points	11 points	11 points	11 points	11 points	11 points	all points78	
										44Points

TABLE 3-2 EFFECT OF THE REFLECTION COFFICIENT ON ACCOURCY OF CALIBRATION.

The table shows how the reflection coefficient of load effects the accuracy of errors coefficient which is obtained from the calibration process. This result leads to the reflection coefficient of load effect on the accuracy of the calibration process, which is lead in accuracy of measurement system. The gain in this table is calculated using Equation 3-21.

The ideal value of the gain is zero, as mentioned previously. The first value is obtained after calibration of the measurement system using the conventional method (load at 50 ohm and 1 measurement for each standard), and gain is calculated by measuring *a* and *b* (should mentioned the Thru standard connect between two ports). The gain was 1.37 dB. The 2nd value was obtained using the load pull system and fixing the refection coefficient at 0.15 and taken 11 points around the original point in Smith Chart and produce new error terms to calibrate the measurement system, the gain obtained in this case was 0.38 dB. By changing the reflection coefficient to 0.3 and repeating the same scenario in the 2nd case, the gain in the 3rd case was 0.28dB.The same scenario was implemented in other cases until the refection coefficient has arrived to unite. In the last stage, 78 points used (first point in centre Smith Chart and 77 points collect from around the centre point in Smith Chart with various the reflection coefficient, as shown in table) .

The accuracy improved when increasing the reflection coefficient during the calibration process. This is due to the VNA having a greater ability to accurately achieve the position of points with a high reflection coefficient than points with a small reflection coefficient.

The distance between two points in the Smith Chart which have the same reflection coefficient will increase with a higher reflection coefficient. This in turn gives the VNA the ability to achieve the point's position which has high reflection more accurately than small reflection coefficient. All these elements work to increase the accuracy of VNA calibration around the Smith Chart rather than just at the centre of the Smith Chart. This is due to the signal near Smith Chart edge having an increased amplitude, hence a reduction in uncertainty as this signal is far from the instrument noise floor.

Figure 3-38 shows comparison of data corrected using error coefficients obtained through both conventional and new methods. It also, presents a comparison with data

corrected by the new method a with different reflection coefficient magnitude. Figure 3-38 clearly shows a reduction in (gain from Thru measure) errors with an increased reflection coefficient magnitude.
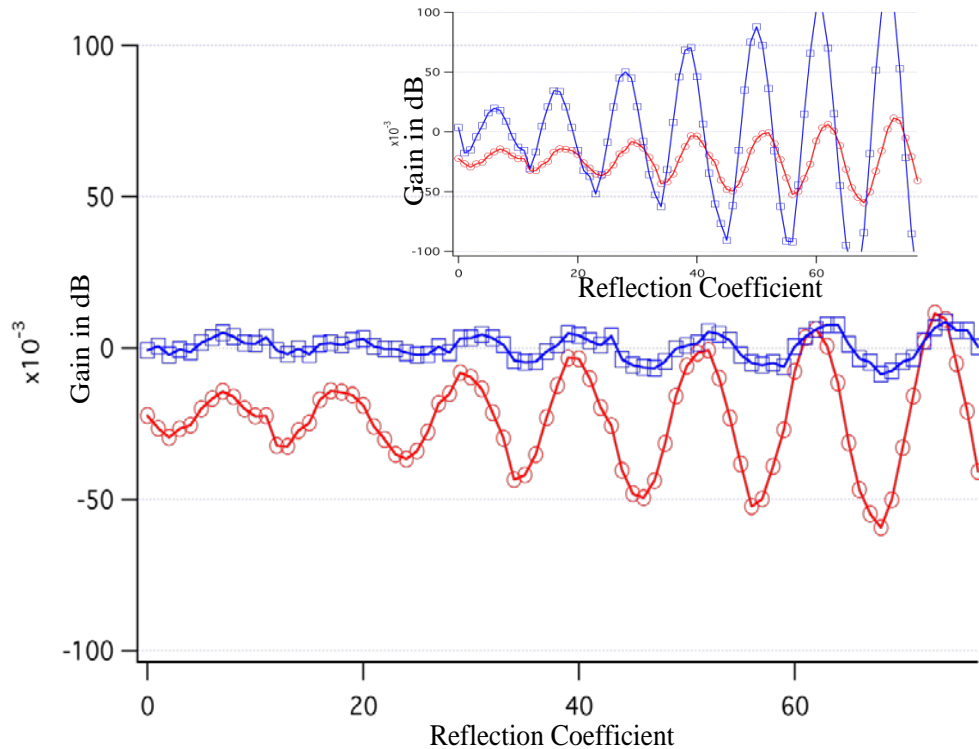
FIGURE 3-38 COMPARISON BETWEEN TWO REFLECTION COEFFICIENTS AND HOW EFFECT ON ACCURACY OF CALIBRATION.

As mentioned previously in this chapter the quality of raw data affects the accuracy of error coefficient during the calibration process. The quality of the raw data improves the accuracy of the error coefficients hence error corrected measurements.

The quality of raw data improves when the reflection coefficient magnitude is closer to 1 as shown Figure 3-39 and Figure 3-40.

This circle represents the ability of the VNA to achieve points around Smith Chart. The increase in reflection coefficient leads to an increase in accuracy of error terms, which reduces measurement error in measurement data during measurement process. Figure 3-39 and Figure 3-40 show the improved ability to achieve the position of points more accurately with an increase of the reflection coefficient (around the edge of the Smith Chart). This is due to the signal generated at the edge of the Smith Chart being

larger than the signal at the centre point (the amplitude of signal) and the arc (distance) between two fallow points in same circle increased with increased the reflection coefficient as shown in Figure 3-41. All these reasons give more space for VNA (signal generator in side VNA) to achieve its aim more accurately, and leads to better calibration and measurement results.
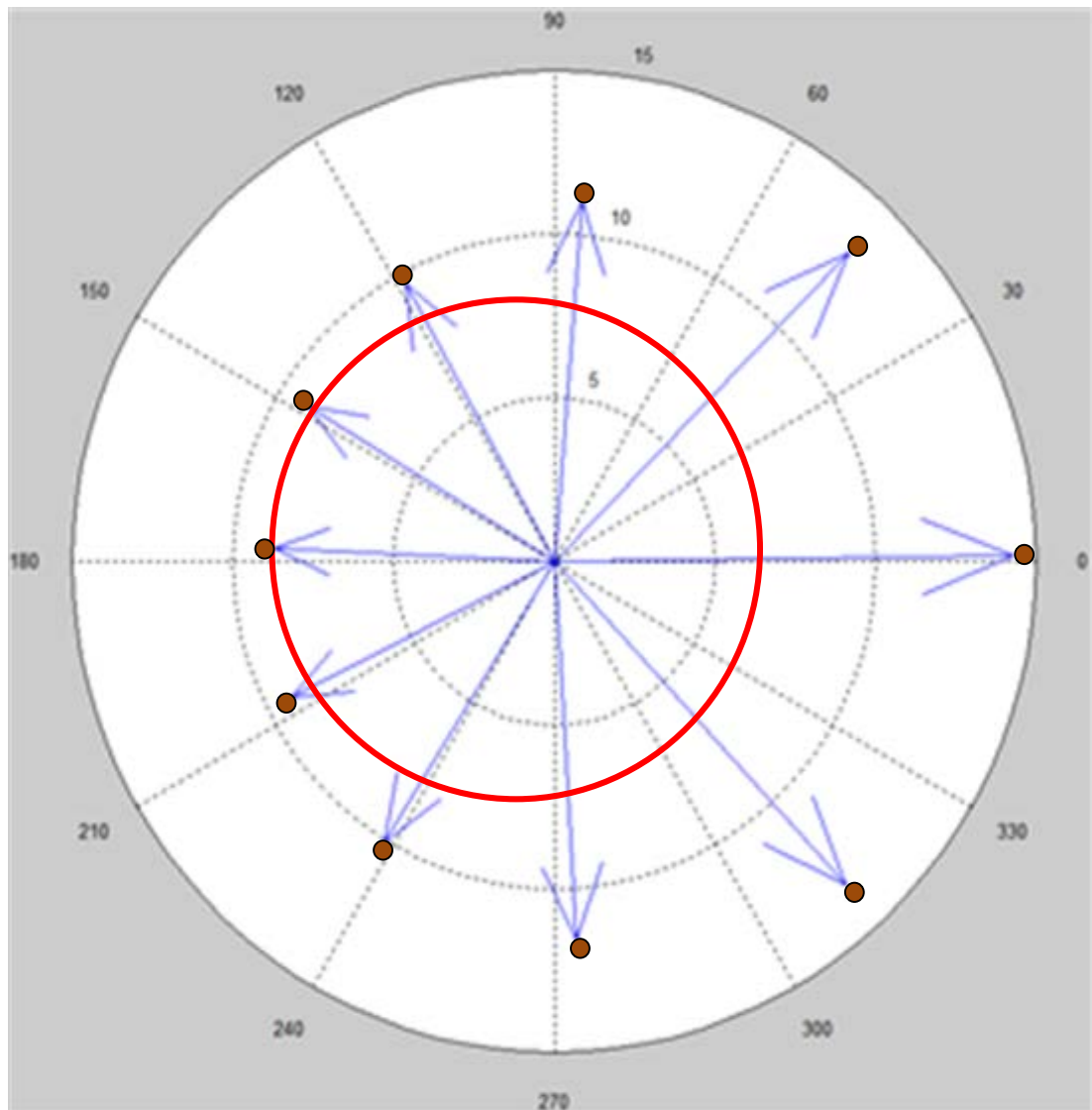
FIGURE 3-39 S22 OBTAINED FROM CORRECTION DATA FOR 0.15 REFLECTION COEFFICIENT.

First circle S22 after correction using the new method.
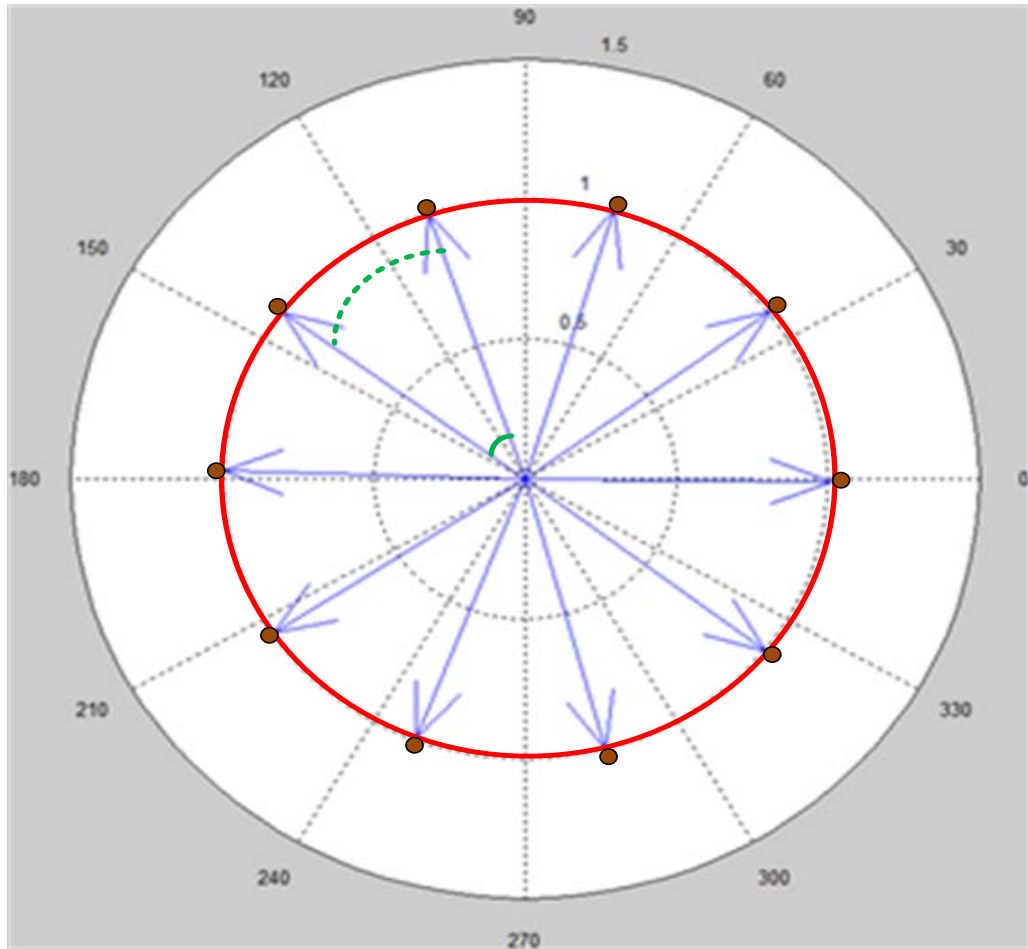
FIGURE 3-40 S22 OBTAINED FROM CORRECTION DATA FOR 1 REFELCTION COEFFICIENT.
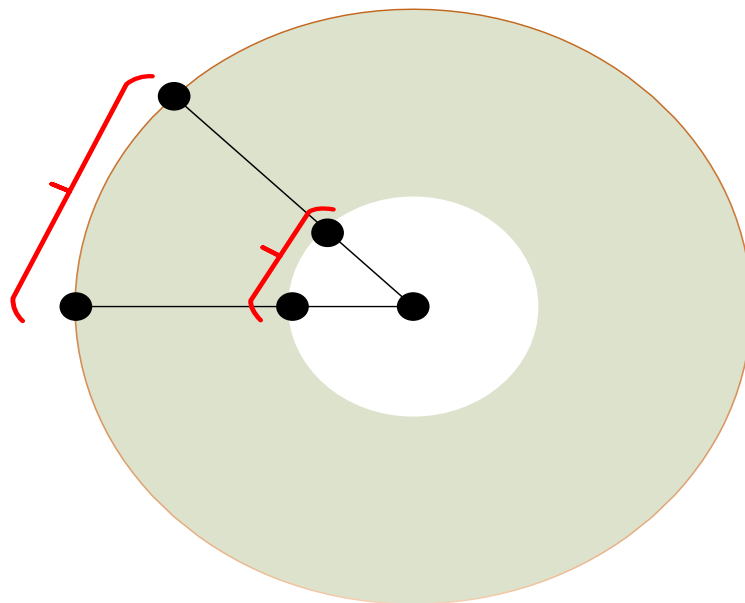
FIGURE 3-41 COMPARISON BETWEEN THE DISTANCE BETWEEN TWO POINTS WITH DIFFERENT REFLECTION COEFFICIENT.

7th circle S22 after correction using the new method. A accuracy will also increase outside the Smith Chart due to an increase in reflection coefficient as shown in Figure 3-41and Figure 3-42.
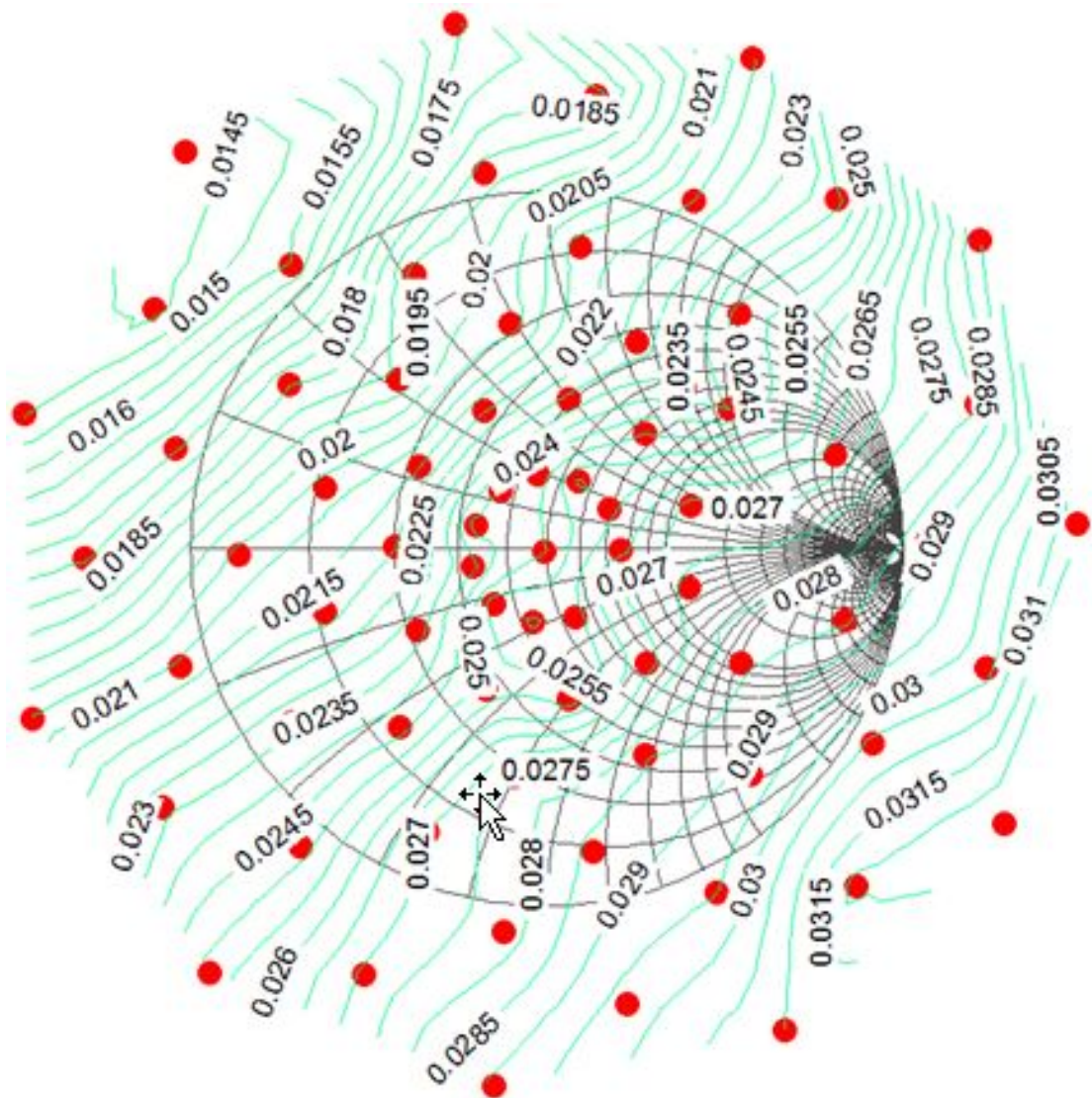
FIGURE 3-42 GAIN OBTAINED FROM MEASURING THRU USING THE LOAD PULL SYSTEM AFTER CALIBRATION USING THE NORMAL METHOD.
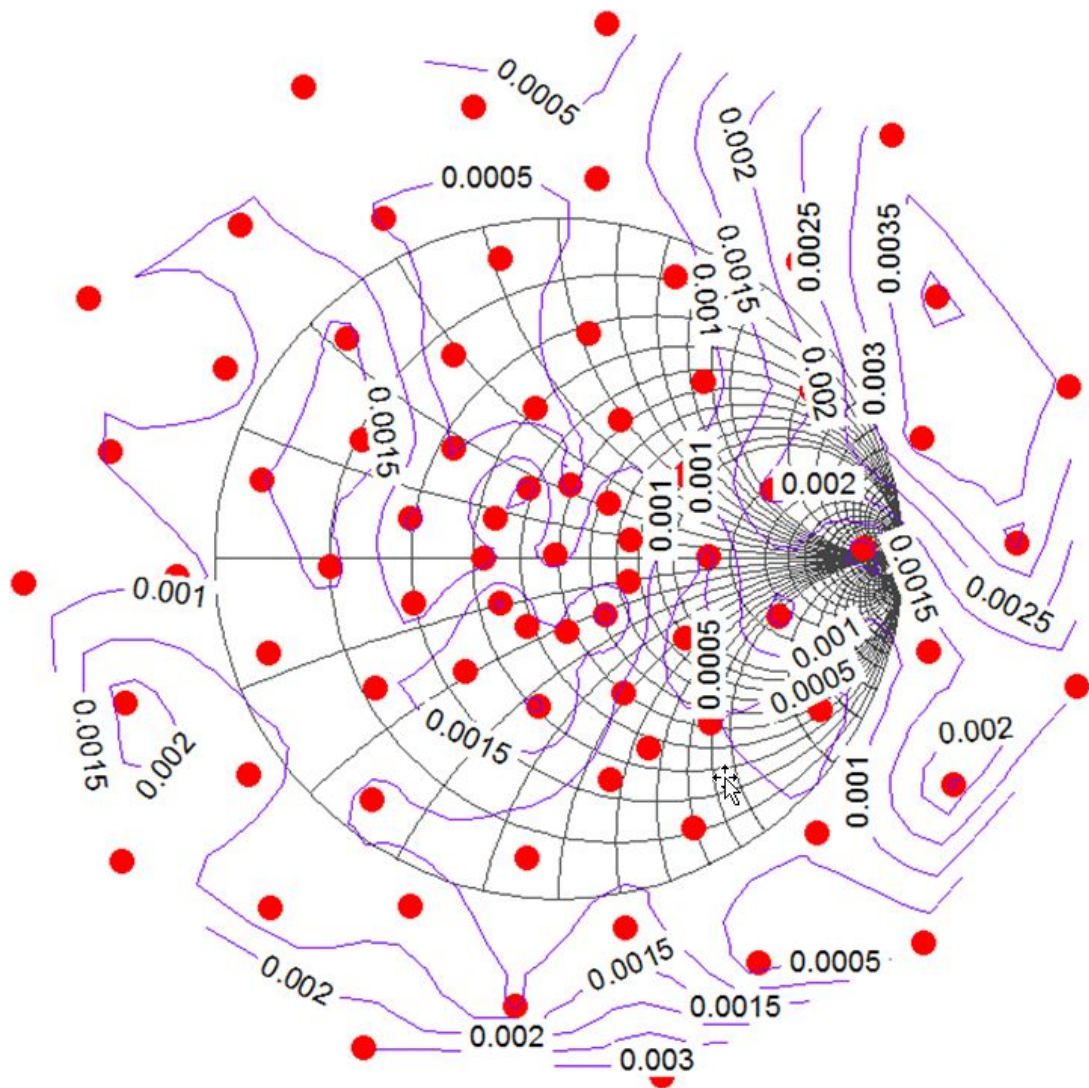
FIGURE 3-43 GAIN OBTAINED FROM MEASURING THRU BY USING THE LOAD PULL SYSTEM AFTER CALIBRATION USING THE NEW METHOD.

In summary, the quality of raw data collected for the calibration process affects the accuracy of the computed magnitude error coefficient. The quality of raw data is improved by using a load-pull with an increased reflection coefficient (around the edge of the Smith Chart). This is due to the signal near the Smith Chart edge having an increased amplitude hence being far from the instrument noise floor father up the distance between two fallow points in same circle increased with increased the reflection.

2.5 SUMMARY

An alternative, systematic, approach for enhancing the calibration accuracy of LSNA (and VNA) systems exploiting load-pull has been developed and demonstrated. Since this approach is based on the pre-processing of multiple measurements it does not require any modification of the LRM/TRM calibration algorithm. A key feature of this approach is that calibration of the measurement system is achieved by using a load pull system to increase the number of measurements points without the need to increase the number of physical connections.

An order of magnitude improvement in the quality of the corrected S-parameters was demonstrated as shown in Figure 3-35 and Figure 3-36. This improvement can be quantified directly during calibration using a derived figure of merit which measures the consistency of the measured raw, *un-corrected S-parameter data* of the Thru and Line standards to satisfy a mathematical constraint implicit in the LRL/TRL algorithm.

2.6 REFERENCE

1- Carrubba, V., Novel Highly Efficient Broadband Continuous Power Amplifier Modes. 2012.

2- Benedikt, J., et al., High-power time-domain measurement system with active harmonic load-pull for high-efficiency base-station amplifier design. Microwave Theory and Techniques, IEEE Transactions on, 2000. 48(12): p. 2617-2624.

3- Tasker, P.J., Practical waveform engineering. Microwave Magazine, IEEE, 2009. 10(7): p. 65-76.

4- Verspecht, J., Calibration of a Measurement System for High Frequency Nonlinear Devices. 1995, Vrije Universiteit Brussel.

5- Benedikt, J., Novel high frequency power amplifier design system, in High Frequency Center. 2002, Cardiff University: Cardiff,UK.

6- Verspecht, J., Large-signal network analysis. Microwave Magazine, IEEE, 2005. 6(4): p. 82-92.

7- Teppati, V., A. Ferrero, and M. Sayed, Modern RF and Microwave Measurement Techniques. 2013: Cambridge University Press.

8- Pozar, D.M., Microwave Engineering, 4th Edition. 2011: Wiley Global Education.

9- Huebschman, B.D., Calibration and Verification Procedures at ARL for the Focus Microwaves Load Pull System. ARL-TR-3985, 2006. ARL-TR-3985(Army Reserch Laboratory).

10- Bonino, S., V. Teppati, and A. Ferrero, Further Improvements in Real-Time Load-Pull Measurement Accuracy. IEEE Microwave and Wireless Components Letters, 2010. 20(2): p. 121-123.

11- Teppati, V., et al., Accuracy Improvement of Real-Time Load-Pull Measurements. IEEE Transactions on Instrumentation and Measurement, 2007. 56(2): p. 610-613.

12- Teppati, V., et al. An unconventional VNA-based time-domain waveform load-pull test bench. in Microwave Conference Proceedings (APMC), 2010 Asia-Pacific. 2010.

13- Golio, M. and J. Golio, RF and Microwave Circuits, Measurements, and Modeling. 2007: Taylor & Francis.

14- Bevilacqua, A., D. Bollini, and R. Campanini, A New Approach to Image Reconstruction in Positron Emission Tomography Using Artificial Neural Networks.

4. CHAPTER 4

NON-LINEAR (ABSOLUTE) CALIBRATION

3.1 INTRODUCTION

Waveform measurement can be defined as "the ability to observe and quantify the time varying voltage $V_n(t)$ and current $I_n(t)$ present at all terminals of the device under test (DUT) and thus involves all frequencies including DC, IF , RF [1].
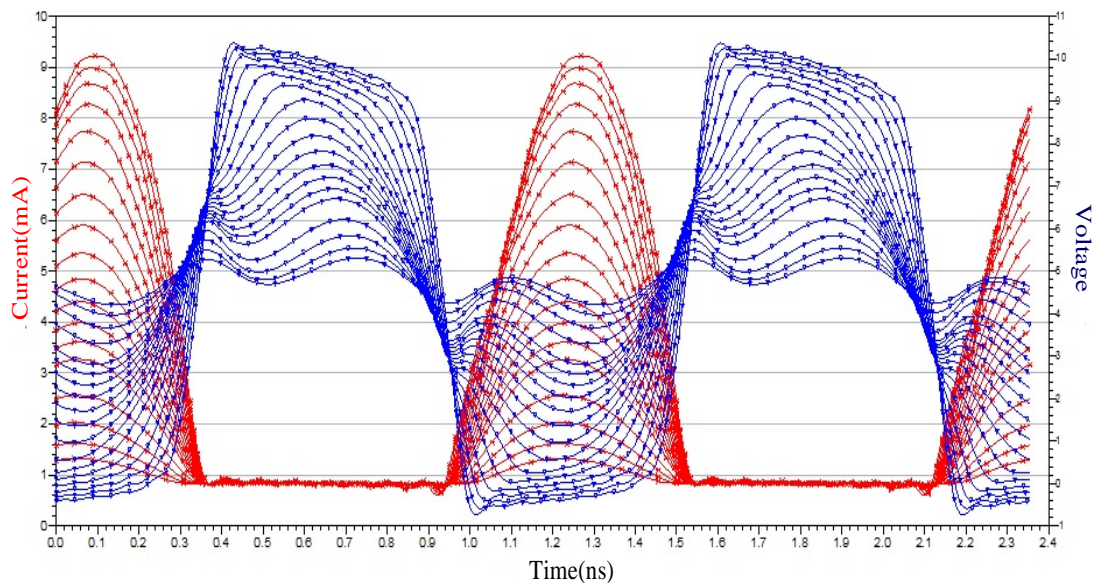
FIGURE 4-1 INGENERAL WAVEFORM ENGINEERING VARYING WITH TIME CLASS F (SMUILATED BY ADS).

The purpose of the wavemeter or LSNA technology is to build an instrument that allows capturing the whole wave spectrum in a single take. This tool has the capability to measure the absolute magnitude of the waves and the absolute phase relations between the harmonics as well as the ability to measure the impedance at all steps in the frequency grid. In other words, the LSNA measures the impedance at the fundamental and all harmonics frequencies. LSNA from a mathematical viewpoint can be

represented as an absolute fast Fourier transform (FFT) analyzer for microwaves. LSNA technology is a result from first recognizing a real situation faced by microwave designers and then designing a suitable solution for it. The real problem is the gap between results obtained from those that can be measured with current microwave instrumentation and those that can be generated via computer-aided design (CAD) tools [2, 3].
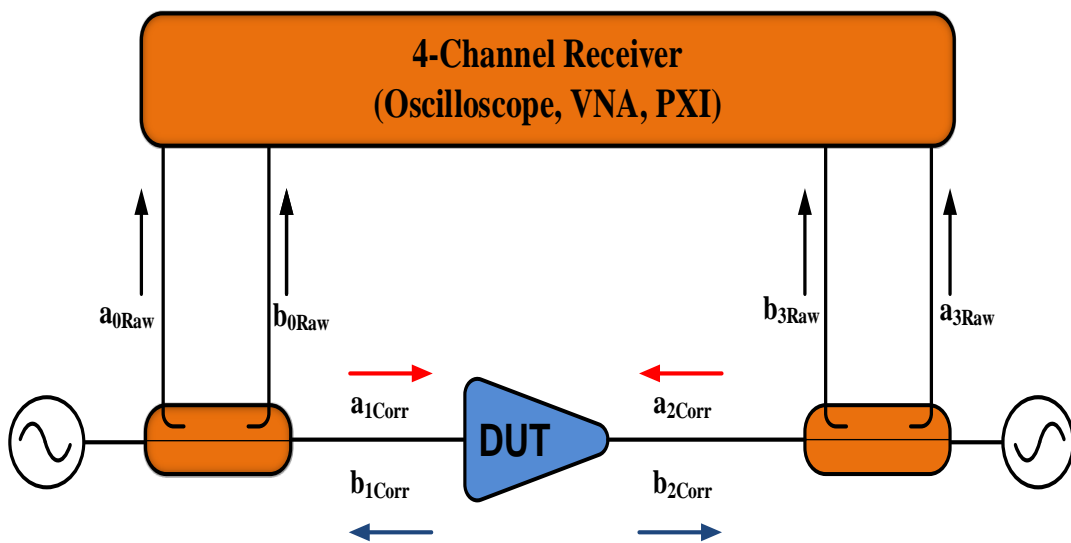
FIGURE 4-2 WAVEFORM METER.

3.2 NONLINEAR MEASUREMENT SYSTEM

LSNA technology allows the combination of two mathematical transformations. The first mathematical operation is to transfer between the frequency domain and the time domain. The second one is the transformation between a voltage-current representation and travelling voltage wave formalism. Technology is not capable combining of both transformations in one box [3-5].

LSNA technology offered two solutions for characterization of the devices: the first technology which is called LSNA (Oscilloscopes and MTA) uses a time-domain solution which measures the terminal voltage and current waveforms directly in terminals of DUT; the second technology which is called NVNA(Non-linear Vector

Network Analyzer) uses a frequency-domain solution which measure their vector spectral components [6, 7].

The LSNA gives the capability for designers to study the device in frequency domain and time domain. LSNA has the capability to capture the spectral components of the A and B waves, the incident and reflection waves contain harmonics and inter-modulation distortion (IMD) products plus fundamental frequency. However, if the only amplitude of all spectral components and the cross-frequency phase relationship between the spectral components are measured, the LSNA is able to perform transformation between the time and the frequency domain. This means that LSNA needs phase relationship between the all spectral components like the phase relation between fundamental (f_0) and harmonics ($2f_0, 3f_{0,........}Nf_0$) [8-12].

The LSNA gives more ability for designers because the LSNA has the capability to offer information about the measurement of time domain waveforms at the same time as the resulting characterisation; The RFPA designers are not capable of determining the class of operation of a PA in the absence of waveforms, such as the class E power amplifier . There are six different names that have been given to this new measurement technology: Large-Signal Network Analyzer (LSNA), Nonlinear Network Measurement System (NNMS), Nonlinear Network Analyzer (NLNA), Vector Nonlinear Network Analyzer (VNLNA), Nonlinear Vector Network Analyzer (NVNA) and Nonlinear Network Analyzer System (NNAS) [1,13].

To generate accurate time domain waveforms all nonlinear measurement systems needs for calibration, in the general calibration nonlinear system consists of :-

1- Vector measurement calibration: *Relative Magnitude & Phase*(*S-parameters)* at each individual frequency.
2- Absolute Magnitude Measurement calibration: Magnitude (*Power*) at each individual frequency.
3- Relative Time "measurement" calibration: (*Relative Phase*) between frequencies [5, 6].

3.2.1 TYPES OF LSNA

In general, LSNA has been classified into three groups depending on the type of test used in the measurement process:-

- Sampling-based,
- Sub-sampling-based,
- Mixer-based systems [3, 5, 6].

4.2.1.1 SAMPLING-BASED (OSCILLOSCOPES)

The prototype for the oscilloscopes-based LSNA is shown in Figure 4-3. The oscilloscopes can either be sampling (equivalent-time) or real time oscilloscopes [1, 4, 12-15].
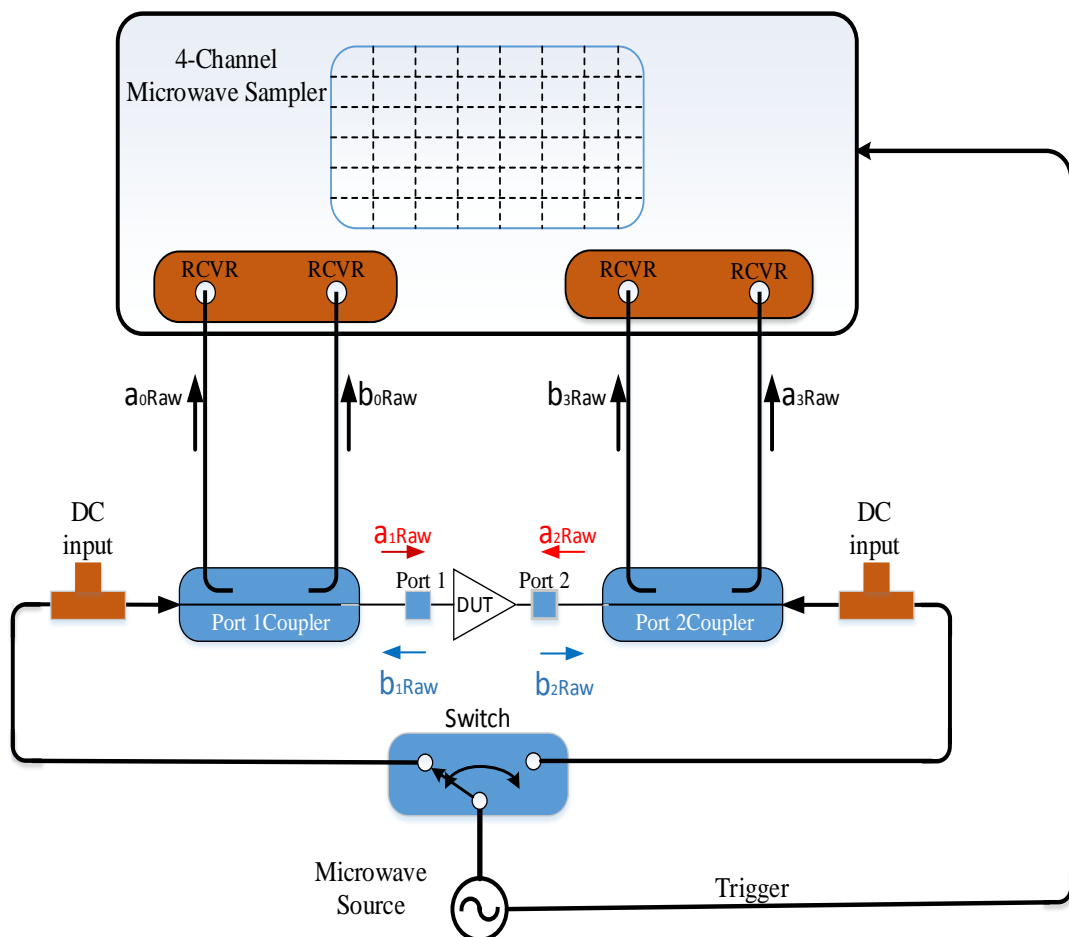
FIGURE 4-3 BASIC SCHEMATIC OF A SINGLE-TONE CONTINUOUS WAVE TIME-DOMAIN-BASED RF I-V WAVEFORM MEASUREMENT SYSTEM.

Real-time oscilloscopes work on the basis of repeated sample of the waveform under a high rate, stoting the measurements in a circular memory buffer. The user sets the trigger events to determine which section of the waveform to view. The main aim of real-time oscilloscopes is to measure voltages inside operating electrical circuits in real time because it has high input impedance. These types of oscilloscopes have limitations in bandwidth to about 500 MHz due to parasites in the input circuitry for oscilloscopes [1, 12-15].

Real-time oscilloscopes capture an entire waveform on each trigger event by using an interleaved analogue-to digital converter which should be significantly faster than the frequency of the incoming waveform. The present system is able to achieve sampling rates as high as 80 Gsamples/s and bandwidths currently extend to 63 GHz. These types of oscilloscopes are capable of acquiring hundreds of millions of samples to analyse the waveform and inform users about information of various properties of the signal which were captured, such as microwave modulation and jitter [15, 16].

Sampling oscilloscopes, which will be the focus of the remainder of this thesis, are designed to measure the instantaneous amplitude of the waveform at a sampling instant. To achieve useful bandwidths as high as 100 GHz the sampling oscilloscope need to use an equivalent-time sampling strategy to give it the ability for greater accuracy than is possible in real-time oscilloscopes. These oscilloscopes have excellent dynamic ranges, normally having 50 ohm input impedance, a large number of samplers and the ability to measure repetitive input signals. To measure the voltage at the input of the oscilloscope, a clean the trigger source is required in order to operate sampling oscilloscope and both trigger source and signal source need to be synchronous in order to obtain correct results or the oscilloscope can obtain trigger from an external clock source [17].

4.2.1.1.1   CALIBRATION (OSCILLOSCOPES)

Full vector calibration is necessary to obtain a fully functional I-V waveform measurement system and providing the user data-corrected time-varying voltage and current waveforms present a reference plane. The aim of calibration now is to determine all 8 error terms of the error model defined. To calculate the incident and reflection waveform at a reference plane requires use of the equations 4-1, 4-2.4-3 and 4-4 [1, 2, 18].

$$b_1 = (b_0 - \varepsilon_{00}.a_0)/\varepsilon_{01}$$

EQUATION 4-1

$$a_1 = \frac{(\varepsilon_{01}.\varepsilon_{10} - \varepsilon_{00}.\varepsilon_{11}).a_0 + \varepsilon_{11}.b_0}{\varepsilon_{01}}$$

EQUATION 4-2

$$b_2 = (b_3 - \varepsilon_{33}.a_3)/\varepsilon_{32}$$

EQUATION 4-3

$$a_2 = \frac{(\varepsilon_{32}.\varepsilon_{23} - \varepsilon_{33}.\varepsilon_{22}).a_3 + \varepsilon_{22}.b_3}{\varepsilon_{32}}$$

EQUATION 4-4

Calibration of the measurement system consists of two main parts. The first part is called relative calibration (small signal calibration) as previously discussed, duration this type of calibration 7 error terms of the 8 determine the last one being set to unity. This calibration step provided the following individual error term values e_{00}, e_{11}, e_{22} and e_{33}. The other error terms are determined as products $e_{01}e_{23}$, $e_{01}e_{10}, e_{23}e_{32}$ and $e_{10}e_{32}$. This is because to correct raw ratio data obtained from measurement system, all the error terms do not necessarily have to be individually determined [1, 2, 18].

The second part, called absolute calibration, will now be addressed; this step involves the determination of magnitude and phase of e_{10} if Port1 is the reference Port or a e_{32} if Port2 is reference Port. The e_{10} magnitude can be determined by attaching a power meter to Port1 and performing a comparison measurement with a calibrated power meter to Port1. The e_{10} phase is determined by attaching a phase meter to or a calibrated the phase source. In this thesis the phase meter approach is used and developed. The phase of e_{10} is measured by attaching an oscilloscope by Port1 directly [1, 2, 18, 19].

The pros for this type of measurement approach, are that all spectra of the incident (a_n) and reflected (b_n) waves are measured at once, thereby the phase coherent measurements are achieved and the phase synchronization problems between the spectral components do not exist. The cons of this system are that this system is not optimal for small-signal characterization but designed large-signal characterization, and have a low dynamic range, the signal-to-noise ratio (SNR) of the NVNA being 100 db which is bigger than LSNA (60 db) [6].

4.2.1.2 SUB-SAMPLING-BASED

Oscilloscopes suffer from problems in the presence of the timebase errors. The problems of the timebase are twofold: absence of coherence between the signal source

and the timebase risk the measurement quality and stability of the trigger source. To evade these, it is better to use a sampling clock instead of a timebase [20, 21].

The sampling-clock-generator offers an instrument that generates a similarly separated sampling grid that is phase coherent with the signal source by construction. By replacing a timebase with a sampling clock, it offers the RF engineer an effective instrument that enables them to measure more quickly and more accurately by reduction of the A\D conversion speed, thereby this affecting the digital signal processing which reduces the leakage problems. Reduced leakage problems lead to increased measurement resolution and a reduction in digitization time (discrete time) signal to zero, Figure 4-4 shows a generic block diagram for a simple LSNA based on sampling down-converters [3, 6, 20, 21].
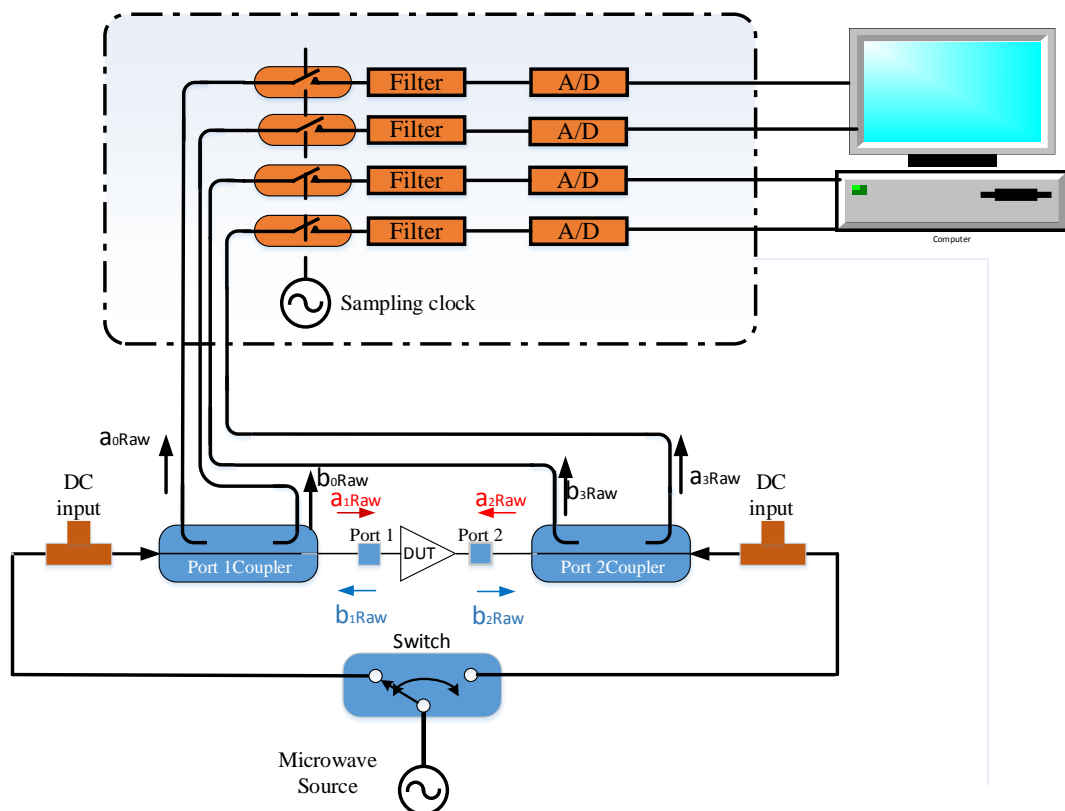
FIGURE 4-4 BLOCK DIAGRAM OF A GENERIC SAMPLING DOWN-CONVERTER BASED LSNA.

The sub-sampling technique works in both frequency and time domains. The down-conversion process is the core operation for instruments that uses as sub-sampling

technique. The instruments use down-conversion to digitise the high frequency periodic signals through the transfer of the RF signal to an IF frequency [3, 6, 20- 21].

4.2.1.2.1 MICROWAVE TRANSITION ANALYSER (MTA)

The microwave Transition Analyser (MTA 70820A) is good example of the sub-sample system. MTA has a dual channel sampling scope, which gives the ability to measure both parts for the waveform signal (the magnitude and phase of signals) for a range between DC and 40 GHz. The significant preference of MTA over customary oscilloscope instruments is that its sampling rate is synthesized from a typical clock-generator, which permits this dual channel two mode MTA to perform phase relation analysis between Channel A and Channel B.

The time-domain sampling technique is used for digitised signals, where Channel A and Channel B are sampled simultaneously within 10 ps. These features allow for accurate phase measurements between both channels. The RF signals captured by using a down conversion process based on the harmonic mixing principle. Down converted for RF signal to an intermediate frequency (IF) between 10MHz and 20MHz is received in both channels. Figure 4-5 shows the rearranged operation of the MTA.
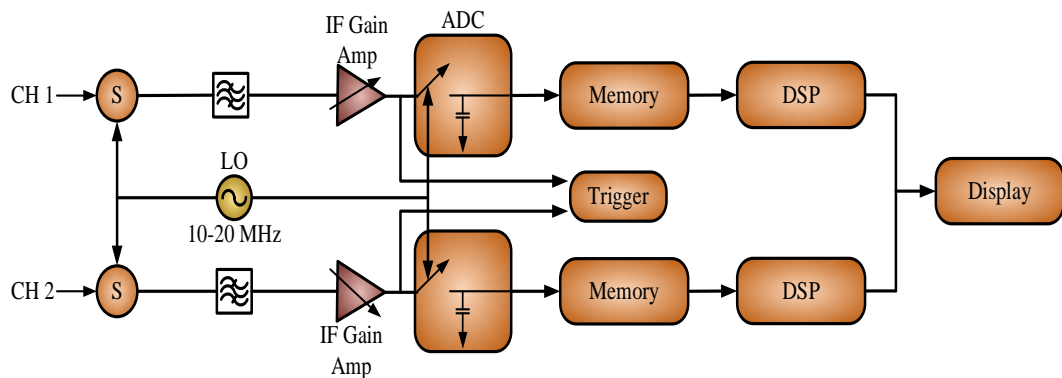
FIGURE 4-5 BLOCK DIGRAM OF MICROWAVE TRANSITION ANALYSER.

MTA down-converts all signals captured between DC and 40GHz, where they are digitised between 10MHz and 20MHz using one of three techniques. MTA has the capability for work in dual mode, which are the time domain (waveform measurement) and frequency domain (S-parameter measurement). This gives MTA the ability to

measure the S-parameter in the frequency domain and is quite useful as it allows the calibration of the measurement system by calculation of the error terms e_{00} , e_{11}, $e_{10}e_{01}$, e_{22}, e_{33} , $e_{23}e_{32}$ and $e_{10}e_{32}$ during the measurement process. To measure the voltage and current waveforms in the time domain at reference plane for DUT, the system does not require the phase reference during the measurement process where the MTA measure in the time domain as mentioned regard to in oscilloscopes [3, 6, 20-21].

4.2.1.2.2 CALIBRATION

Once the error coefficients for the measurement system have been calculated by using the S-parameter model for MTA, an extra calibration procedure is needed to find out $K(f)$which means the absolute power(magnitude of $K(f)$) and phase of the travelling waves(phase of $K(f)$). This is done by scaling the $K(f)$factor for the S-parameters, by directly measuring the travelling waves at the reference port using the oscilloscope for the low frequencies and the MTA for high frequencies [22].

Use the sampling converter technique in MTA leads to free from the time base problems and consecutive spectral leakage problems affecting the oscilloscope time base. This type of system is suitable to measure sine waves and modulated signals (low bandwidth) but in wideband modulation need to determine the origin of the measured spectral lines [22].
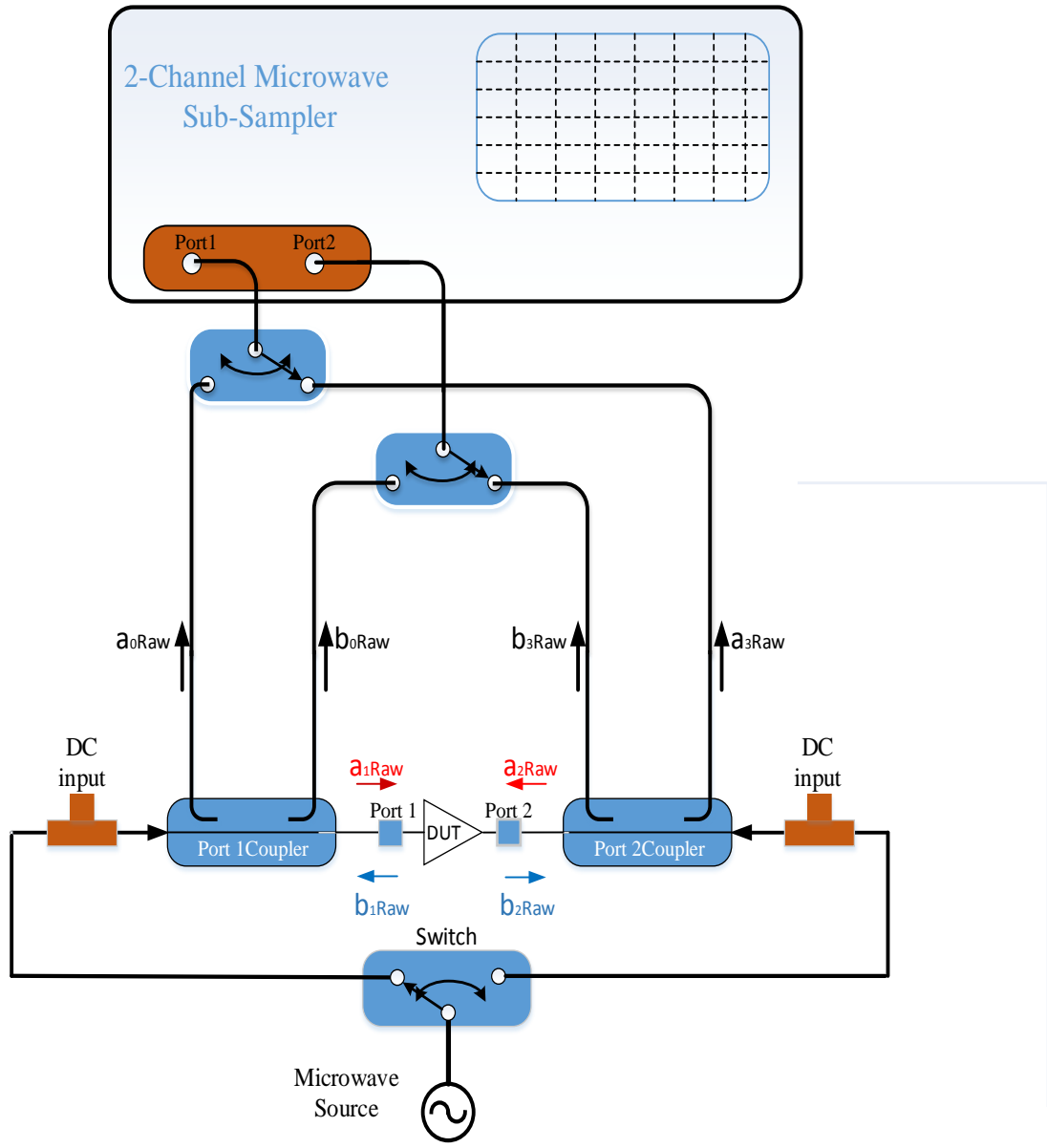
FIGURE 4-6 TIME- DOMAIN WAVEFORM MEASURMENT SYSTEM BASE ON MTA.

4.2.1.3 MIX-MIXER-BASED

Until now, all the previous measurement systems measuring directly in the time domain or the synonymous to time domain, leads us to conclude that the LSNA is able to measure the whole wave spectrum in one single take. The essential advantage of this type of working lies in the fact that the varied lines are synchronized by construction of the measurement. Alternatively, the NVNA can be considered as a frequency-domain acquisition system [11].

The NVNA uses mixers for the down conversion process instead of using samplers to down convert the RF signals to an IF spectrum. The core of the acquisition system for NVNA is based on the mixer concept. This type of acquisition system is able to measures only one frequency component at a time as shown below in Figure 4-7 [6, 11, 12].
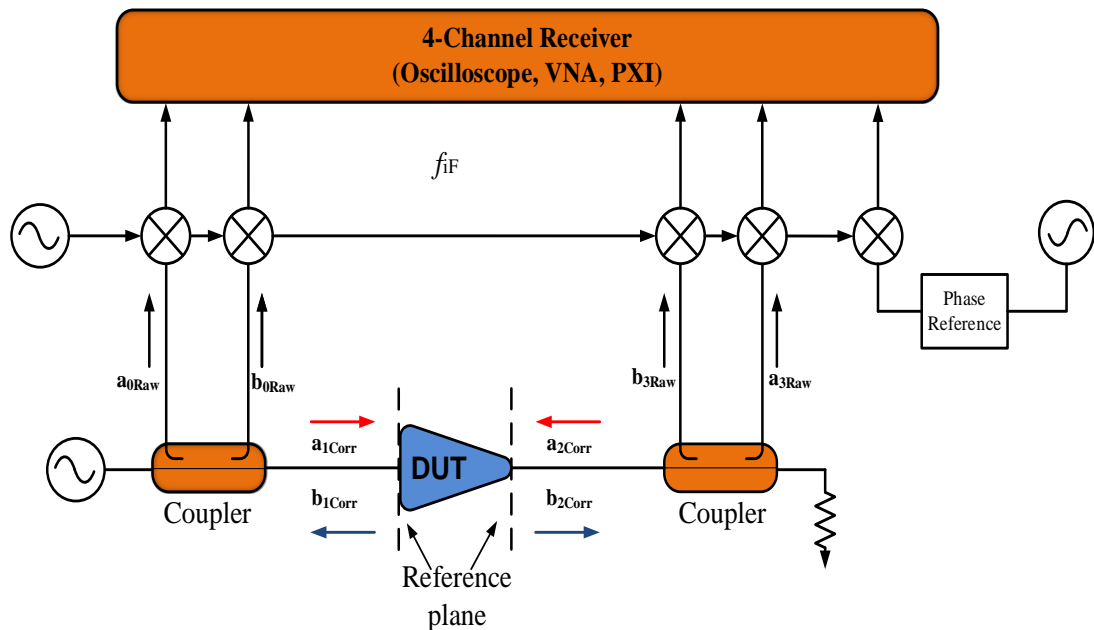
FIGURE 4-7 SIMPLIFIED BLOCK SCHEMATIC OF A TWO-PORT NVNA.

The NVNA is based on VNA which is considered as a frequency-domain acquisition device. The VNA is able to capture four waves incident and reflected (a_0, a_3, b_0, b_3) waves at each port of the two-port device simultaneously. VNA is able to measure one

frequency from the frequency grid at a time, and this conduct leads to the fact that all spectral lines captured by the NVNA must be down converted separately. This is because the VNA is able to measures only one frequency from the frequency grid and, hence, the phase relation among the frequency grid is lost. The signals captured by the NVNA request two stages: the first stage down-convert the signals by using mixers driven by a local oscillator; the second stage finds the phase relation among frequencies in the frequency grid. This is the roll of the harmonic phase reference in the NVNA measurement system. This harmonic phase reference must be measured with of the fifth mixer of the NVNA, this is very important step allowing for the reconstruction the time waveform at the reference plane for the device under test [23- 25].

Since the measurement system depends on the phase reference to find the relative phase between frequency components its ability to measure is restricted to RF signals that must be on the same frequency as the phase reference or one of the harmonic phase reference and on a known the frequency grid. This system has the further requirement that the frequency step inside frequency grid should be one of harmonics phase reference which means that the frequency grid must be harmonics for the fundamental frequency to give the ability for the system to find the relative phase for the reconstruction wave in the time domain. Additional to that the comb generator and signal generator should be frequency locked to each other. For a two port device measurements this operation is achieved via the following mathematical transformation:

$$\begin{bmatrix} \widetilde{a}_{1,COR}(\omega) \\ \widetilde{b}_{1,COR}(\omega) \\ \widetilde{a}_{2,COR}(\omega) \\ \widetilde{b}_{2,COR}(\omega) \end{bmatrix} = k(\omega)[e(\omega)] \begin{bmatrix} \widetilde{a}_{1,RAW}(\omega) \\ \widetilde{b}_{1,RAW}(\omega) \\ \widetilde{a}_{2,RAW}(\omega) \\ \widetilde{b}_{2,RAW}(\omega) \end{bmatrix} \qquad \text{EQUATION 4-5}$$

Where $[e(\omega)]$ are 7 errors terms and $k(\omega)$ represented the magnitude and the phase of error term e_{10}. At every frequency to be measured, the local oscillator is tuned to down-convert over that frequency to an intermediate frequency (IF) and then pass through filtered, digitized, and read into the PC. This type of measurement system can control the magnitude and phase of the local oscillator and can also control the relative

magnitudes and phases of the down-converted signals. Each time the local oscillator is tuned to a new frequency, the magnitude of the local oscillator can be controlled but the phase is randomly changed, thereby each time measuring a new frequency, the phase has a random offset from all prior measurements. Repeating the measurement for the same frequency many times will not change the random phase for each time, which means that the phase changes randomly from measurement to measurement. By using a fifth mixer it can measure a comb generator to get around this. The harmonic phase reference generator is intended to create a full spectrum signal with a component at each of the frequencies to be measured with an exceptionally stable stage phase offset between these different frequencies in the frequency grid. So long as this phase change cannot be controlled, the phases of the incident and reflected (a_1, b_1, a_2 and b_2) waves are referenced to the phase of the harmonic phase reference generator. Therefore a fixed phase relationship between frequencies is accomplished. Using a mixer-based front-end VNA we can exploit a narrowband measurement principle, achieving a higher dynamic range. However, because the VNA can only measure one frequency at each time, this can lead to an increased measurement time and a slower system in general. During a measurement sweep it is very important that the synchronizer, the local oscillator and the mixers remain very stable and phase coherent to correctly reconstruct the time signals at the reference plane of the DUT. The NVNA (mixer-based approach) offers a high dynamic range compared with sampler approach which is considered one of the main advantages of the mixer-based approach, and can be used for small signal (S-parameter) and large signal. Phase calibration is used to find the phase relation between the measured harmonic, thus the NVNA is able to reconstruct the waveforms in time-domain perfectly. The minimum grid space in phase calibration that can be achieved is 625kHz for CW waves and in modulation case minimal tone spacing between calibrated modulation tones is 625 kHz to avoid interpolation algorithms, Compared to the sampler approach the a NVNA has better noise floor, although we should consider the linearity of the NVNA when measuring the nonlinear behaviour of a DUT.

The NVNA has some disadvantages which affect the system by the increased complexity of the system and in the measurement process, to reconstruct phase coherence which should offer for system external phase reference which affects the complexity of the system. The NVNA is able to measure a single frequency per time

that will increase the measurement time which is affected by the IF bandwidth [6, 7, 11, 14, 17, 24, 25].

4.2.1.3.1   CALIBRATION

The first stage in calibrating any measurement system starts by determining the error model for this system. Figure 4-8 shows the NVNA measurement system of which the mathematical description is shown in equation 4-6 [26].
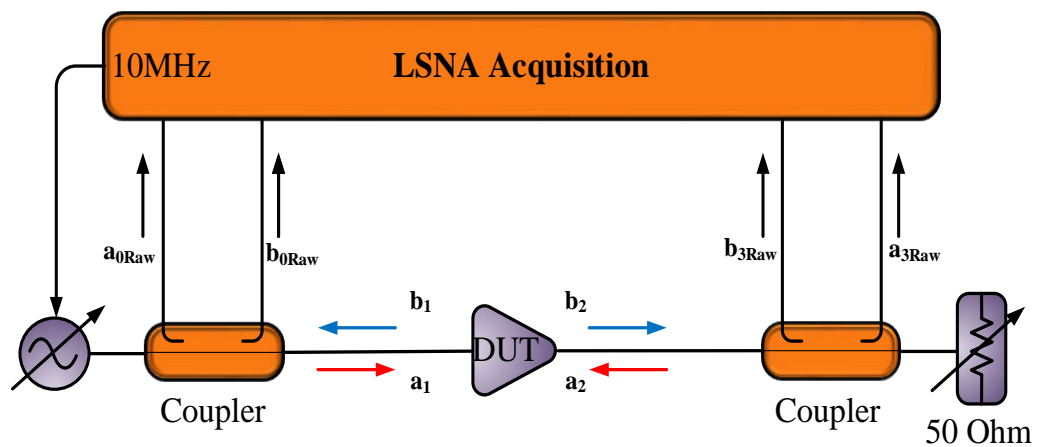
FIGURE 4-8 NVNA ARCHITECTURE.

$$\begin{bmatrix} a_{D1}(f) \\ b_{D1}(f) \\ a_{D2}(f) \\ b_{D2}(f) \end{bmatrix} = K(f) \begin{bmatrix} 1 & \beta_1(f) & 0 & 0 \\ \gamma_1(f) & \delta_1(f) & 0 & 0 \\ 0 & 0 & \alpha_2(f) & \beta_2(f) \\ 0 & 0 & \gamma_2(f) & \delta_2(f) \end{bmatrix} \begin{bmatrix} a_{R1}(f) \\ b_{R1}(f) \\ a_{R2}(f) \\ b_{R2}(f) \end{bmatrix} \qquad \text{EQUATION 4-6}$$

It can be assumed that there is a linear relationship between the raw data measured and correct data at reference planes for each port for DUT, which is described by the equation 4-6 normalizing the spectral line. There are three steps for calibrating the NVNA system [27]:-

1- Vector Measurements: S-parameter calibration

this stage to obtain the 7 error terms(S-parameter) for the system , starts by acquiring the values of(e00,e11,e10e01) for each port by using (Open, Short, and Load) standards as shown in Figure 4-9 and reference all measurements to reference port by using a Thru standard to obtain e10e32 or e01e23 as shown in Figure 4-10. The result of this stage is a 7 error term.
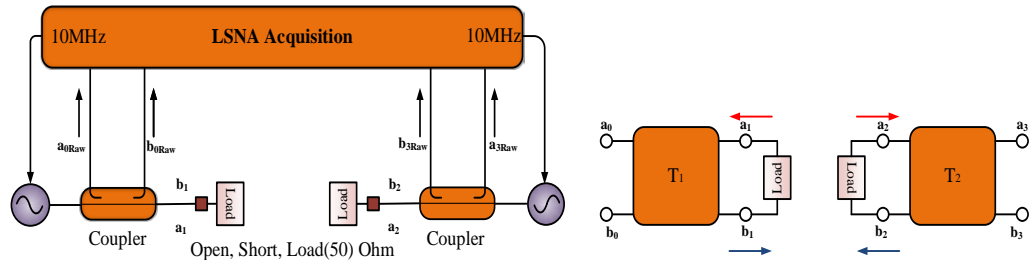
FIGURE 4-9 RELATIVE CALIBRATION (LOAD, OPEN, SHORT).
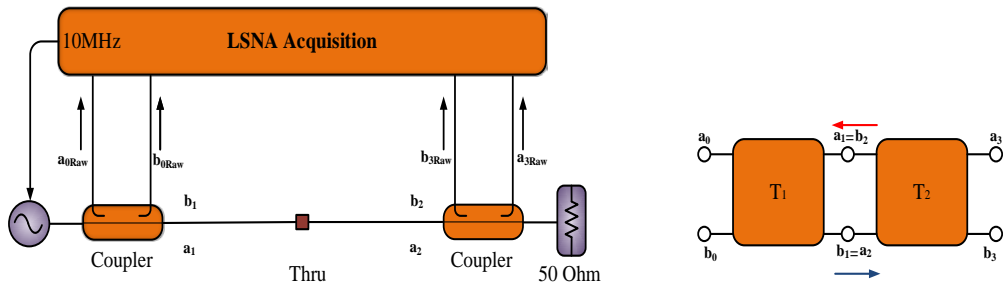
FIGURE 4-10 RELATIVE CALIBRATION (THRU).

2- Absolute Magnitude Measurements: Magnitude (Power)

This stage is to find the absolute value for $|K(f)|$ or ($|e_{10}|$) by connecting the power meter directly to the reference port. In this example Port1 is the reference port, by connecting the power meter to port1 directly and by using the equation 4-7.

$$|k(f)| = \frac{|\tilde{a}_{Power}(f)|}{\left|\left(e_{21}(f)\tilde{a}_{1,RAW}(f)+e_{22}(f)\tilde{b}_{1,RAW}(f)\right)\right|}$$

EQUATION 4-7
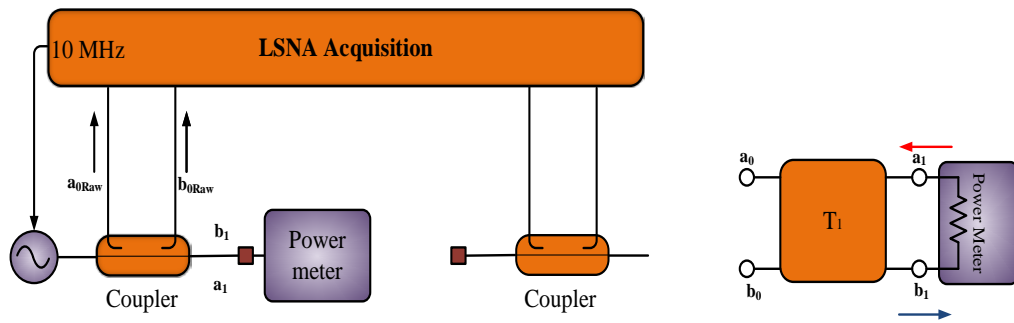
FIGURE 4-11 ABSOLUTE CALIBRATION (POWER).

3- Measurements: Relative Phase.

As mentioned before, VNA is able to measure one spectral line at time and, therefore, the phase reference (phase calibration) required to find the relation between spectral lines is measured by VNA, hence reconstruction allow of waveform in time domain. Phase calibration finds the phase the $< e_{10}$ terms, as shown in Figure 4-12.
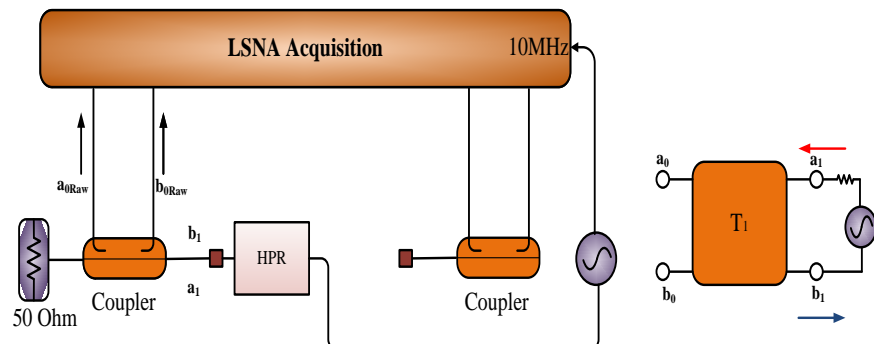
FIGURE 4-12 ABSOLUTE CALIBRATION HARMONIC PHASE CALIBRATIONS.

The system is now fully calibrated and ready to measure the full nonlinear behaviour of microwave devices. The full characterization for large-signal measurement system is done, [6,7, 11, 14, 17, 24-27].

4.3 SUMMERY NONLINEAR

Nonlinear measurement systems are classified into three types which are the sampling base, sub sampling base and mixer-based systems each of which has advantages and disadvantages

1. Sampling base and sub sampling base:- both types are measured in the time domain. There is no need to phase reference (com generator) due to phase coherent measurement by nature but they needed for triggers, these kinds of measurement system being able to capture all spectral components measured in one shot measurements. This has the, ability to over-ranging detection at receiver front-end, and this kind of measurement system achieved good results in linearity of the receivers and medium to high power handling capability but also suffering from spurious signals, low down-converted, low dynamic and not optimal for small-signal characterization [12, 17, 19].

2. Mixer-based system:- this kind of nonlinear measurement system has good dynamic range, the system can be used for small signal plus large signal but the mixer based needs to phase reference which leads to the NVNA has some disadvantages which affect the system by the increased complexity of the system and in the measurement process. Therefore, we need to allow a Vector Network Analyzer to be operated as a Large Signal Network Analyzer without the need for a harmonic phase reference generator, for many reasons, including reducing complexity, offering more port free which be use for other reasons, and reducing cost by reducing the number of instruments used in measurement system [12, 17, 19].

The next chapter will discuss calibration and operation VNA without phase reference which will give us the ability to building a NVNA measurement system which has the capability to calibrate and operate with no phase standard, no bandwidth limitations and no frequency restrictions [12, 17, 19].

4.4 REFERENCE

1- Tasker, P.J., Practical waveform engineering. Microwave Magazine, IEEE, 2009. 10(7): p. 65-76.

2- Tasker, P.J. RF Waveform Measurement and Engineering. in Compound Semiconductor Integrated Circuit Symposium, 2009. CISC 2009. Annual IEEE. 2009.

3- Golio, M. and J. Golio, RF and Microwave Circuits, Measurements, and Modeling. 2007: Taylor & Francis.

4- Sipila, M., K. Lehtinen, and V. Porra, High-frequency periodic time-domain waveform measurement system. Microwave Theory and Techniques, IEEE Transactions on, 1988. 36(10): p. 1397-1405.

5- Teppati, V., A. Ferrero, and M. Sayed, Modern RF and Microwave Measurement Techniques. 2013: Cambridge University Press.

6- Roblin, P., Nonlinear RF Circuits and Nonlinear Vector Network Analyzers: Interactive Measurement and Design Techniques. 2011: Cambridge University Press.

7- Verspecht, J., Large-signal network analysis. Microwave Magazine, IEEE, 2005. 6(4): p. 82-92.

8- Verspecht, J., Calibration of a Measurement System for High Frequency Nonlinear Devices. 1995, Vrije Universiteit Brussel.

9- Ghannouchi, F.M. and M.S. Hashmi, Load-Pull Techniques with Applications to Power Amplifier Design. 2012: Springer.

10- Instirment, N., Introduction to Network Analyzer Measurements Fundamentals and Background. 2013, National Insturments

11- Lott, U., Measurement of magnitude and phase of harmonics generated in nonlinear microwave two-ports. Microwave Theory and Techniques, IEEE Transactions on, 1989. 37(10): p. 1506-1511.

12- Van Moer, W. and Y. Rolain, A large-signal network analyzer: Why is it needed? Microwave Magazine, IEEE, 2006. 7(6): p. 46-62.

13- Remley, K.A. Practical applications of nonlinear measurements. in Microwave Measurement Conference, 2009 73rd ARFTG. 2009.

14- Verbeyst, F. and E. Vandamme. Large-Signal Network Analysis. Overview of the measurement capabilities of a Large-Signal Network Analyzer. in ARFTG Conference Digest-Fall, 58th. 2001.

15- Williams, D., P. Hale, and K.A. Remley, The Sampling Oscilloscope as a Microwave Instrument. Microwave Magazine, IEEE, 2007. 8(4): p. 59-68.

16- Williams, D.F. and K.A. Remley, Analytic sampling-circuit model. Microwave Theory and Techniques, IEEE Transactions on, 2001. 49(6): p. 1013-1019.

17- Pailloncy, G., et al., Large-Signal Network Analysis Including the Baseband. Microwave Magazine, IEEE, 2011. 12(2): p. 77-86.

18- Benedikt, J., et al., High-power time-domain measurement system with active harmonic load-pull for high-efficiency base-station amplifier design. Microwave Theory and Techniques, IEEE Transactions on, 2000. 48(12): p. 2617-2624.

19- Van Moer, W. and L. Gomme, NVNA versus LSNA: enemies or friends? Microwave Magazine, IEEE, 2010. 11(1): p. 97-103.

20- Williams, T.V., A Large-Signal Multi-tone Time Domain Waveform Measurement System with Broadband Active Load Impedance Control, in School of Engineering 2007, Cardiff University Cardiff.

21- Gaddi, R., On the characterisation and Modelling of Silicon RF LDMOS Transistors, in School of Engineering. 2002, Cardiff University.

22- Williams, D.J., Non-Linear Measurement System and Techniques for RF Power Amplifier Design, in Division of Electrical and Electronic Engineering. 2003, Cardiff University,UK: Cardiff University.

23- Lott, U. A method for measuring magnitude and phase of harmonics generated in nonlinear microwave two-ports. in Microwave Symposium Digest, 1988., IEEE MTT-S International. 1988.

24- Barataud, D., et al., Measurements of time-domain voltage/current waveforms at RF and microwave frequencies based on the use of a vector network analyzer for the characterization of nonlinear devices-application to high-efficiency power amplifiers and frequency-multipliers optimization. Instrumentation and Measurement, IEEE Transactions on, 1998. 47(5): p. 1259-1264.

25- Blockley, P., D. Gunyan, and J.B. Scott. Mixer-based, vector-corrected, vector signal/network analyzer offering 300kHz-20GHz bandwidth and traceable phase response. in Microwave Symposium Digest, 2005 IEEE MTT-S International. 2005.

26- Vandenplas, S., et al. Calibration issues for the large signal network analyzer (LSNA). in ARFTG Conference Digest, Fall 2002. 60th. 2002.

27- Verspecht, J., et al. Accurate on wafer measurement of phase and amplitude of the spectral components of incident and scattered voltage waves at the signal ports of a nonlinear microwave device. in Microwave Symposium Digest, 1995., IEEE MTT-S International. 1995.

5   CHAPTER 5

OPERATION AND CALIBRATION NONLINEAR MEASUREMENT SYSTEM WITHOUT PHASE REFERENCE

Large Signal Network Analyzer system is wave meter tools designed to detect and specify the time varying current $I_n(t)$ and voltage $V_n(t)$ present at all terminals of the transistor or circuit, are primary for investigating the operation of DUT under large signal operating conditions and so go beyond linear S-parameters. In order to give the user the ability to analysis efficiently and accurately dot behaviour under realistic operating conditions [1].

Microwave engineer by employing LSNA will able to perform precise characterization of active devices in nonlinear mode of operation such waveform measurements also can be amassed utilizing a frequency-domain based receiver such as a vector network analyser (VNA) or a time-domain based receiver such as sampling a oscilloscope, which is offers robust insight into the nonlinear behaviour of your (DUT) under real operation and large signal operating conditions [1-4].

4.1   INTRODUCTION

As mentioned in last chapter there are various architectures for large signal measurement systems. Targeting for good dynamic range with rapid measurement time the NVNA (Mixer-Base) would be the system of choice. But typically suffer from random phase changes when the Local Oscillator (LO) is tuned to a new frequency. This leads to a loss of knowledge of the relative phase between harmonics, therefore a

loss of the ability to reconstruction the waveform in time domain. This problem has typically been addressed by using a harmonic phase reference (comb generator) [4].

So to use a vector network analysers (VNA) for waveform measurement harmonic phase reference (HPR) devices are need for both triggering and relative phase (to set an absolute phase reference) calibration. This solution (harmonic phase reference) however has restrictions, 1) the measurement frequency grid of is set by the harmonic phase reference generator which rather than the NVNA often limited performance and 2) leads to increased system cost and complexity because of the needs for an extra receiver. For example, the large signal measurement system able to measure all harmonics within the frequency grid and the frequency grid must be equal to the output of the RF the harmonic phase reference or might force limitations on harmonic spacing in multi-harmonics measurements for NVNA based on a 4-ports VNA and using harmonic phase reference in NVNA to characterising memory behaviour for RF nonlinear circuits lead to severe limitation during characterization process, the harmonic phase reference solution can make certain measurements e.g. modulated measurements exceedingly challenging for that can recap using HPR is difficult and complicated process. Therefore in this chapter alternative approach will be presented using the unique properties of ZVA-67 based LSNA, that does not required HPR will be investigated in this chapter. Thus removing the increased complexity during large signal measurements and eliminate the restriction that resulted from the use of RF the harmonic phase reference solution [3-6].

4.2 MOTIVATION

In this chapter an approached that is allows a Vector Network Analyzer to be operated as a Non-linear Network Analyzer without the use for a harmonic phase reference when measuring the voltage and current in terminal of DUT in time domain is presented. The mode of operation developed exploits the architecture of a Rohde and Schwarz ZVA67, which including local oscillator sources and internal signal sources based on direct digital synthesis. Thus it has a unique capability to provide for a Vector Network Analyzer based Large Signal Network Analyzer configuration that has time coherent receivers and sources [7, 8].

This advantage in ZVA-67 signal acquisition has allow of for a modified calibration procedure to be developed. By using its internal signal sources and an external phase meter (oscilloscope DSA8200) eliminating any requirement of a HPR. This achievement leads to reduced system cost and simplifies architecture, including removing the requirement for an additional receiver. In addition, further hardware development of the phase reference generators is not required each time the bandwidth of the VNA is advanced [7-9].

4.3 PHASE COHERENCE

Phase coherence is defined as when two or more RF signals have fixed relative phase to each other (stable phase relationship) ,over given time as shown in Figure 5-1 for two waves with same frequency or Figure 5-2 for two waves with a different frequency [10-12] .
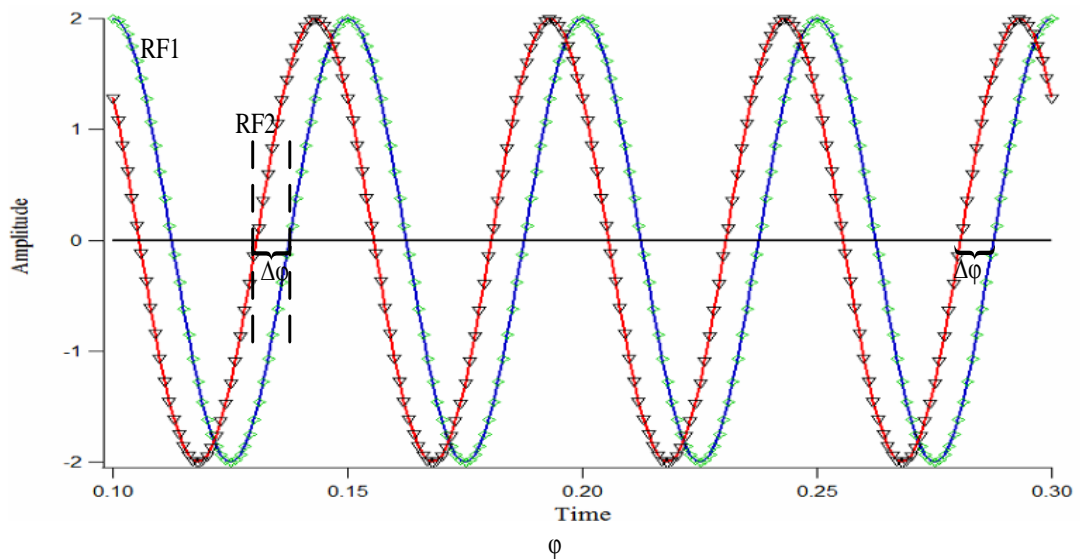
FIGURE 5-1 TWO SIGNALS WITH CONSTANT PHASE DIFFERENT.

Could be used same interpreted for waves of different frequencies as shown in Figure 5-2 .
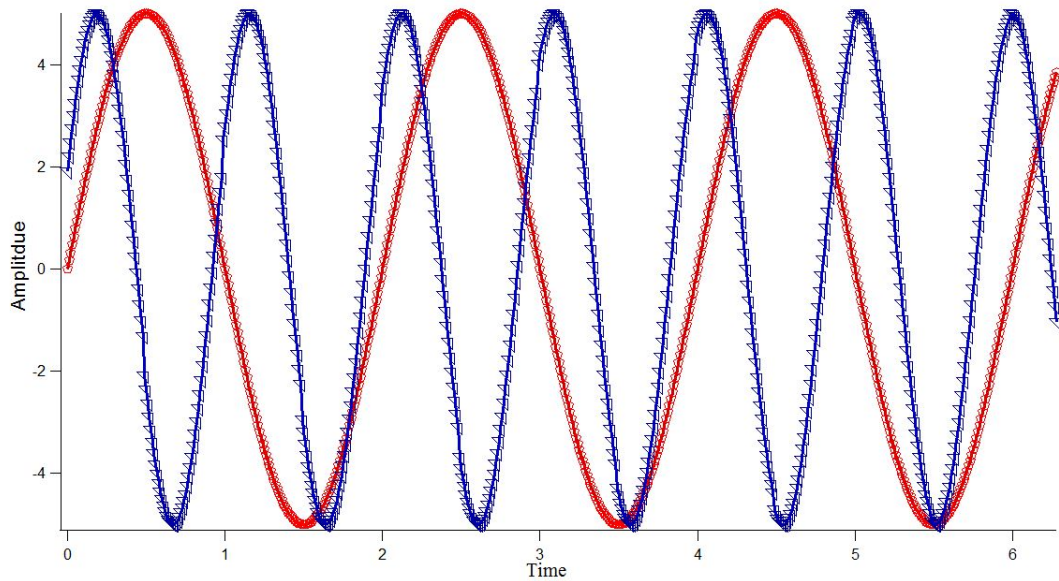
FIGURE 5-2 WO SIGNALS WITH RANDOM PHASE DIFFERENT.

Figure 5-2 Signals are at a specified phase relationship every N cycles.

4.4 DIRECT DIGITAL SYNTHESIS

Direct digital synthesis (DDS) technology is used in signal generators to generate precise frequencies through a unique clocking mechanism and memory access as shown Figure 5-3 [10-12].
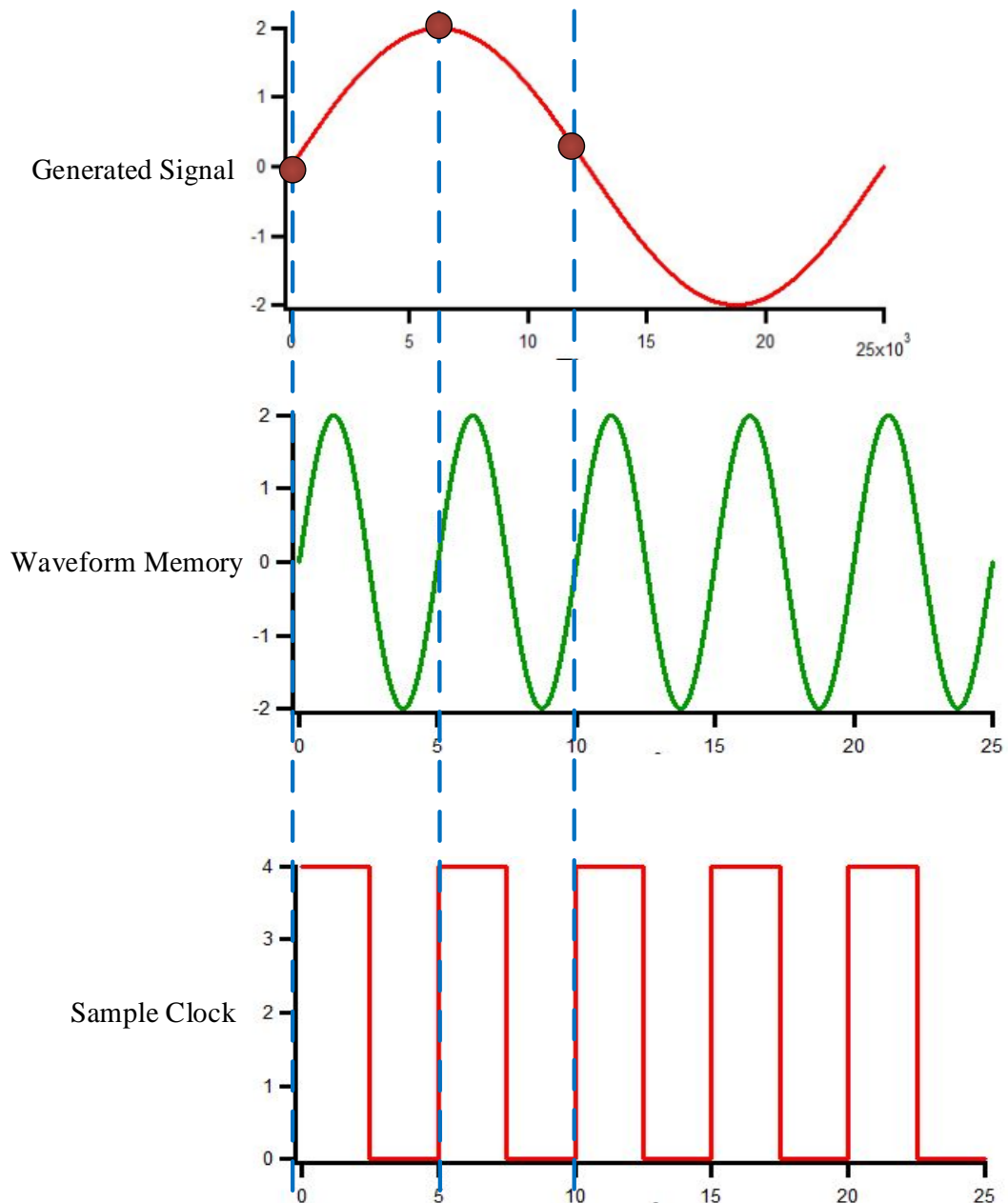
FIGURE 5-3 INSIGHT ABOUT IN DDS CAPABLE HARDWARE.

To implement technology of DDS requires three essential hardware building blocks

- Phase accumulator,
- Sample clock,
- Lookup table.

Which is executed of in a programmable ROM [10-12]. By using the DDS technology in the architecture of a Rohde and Schwarz ZVA-67 provide a VNA with both time (phase) coherent sources and receivers. Therefore, eliminating the

need for using HPR generator trigger to allow the VNA to measure waveform in time domain. Also, allowing the use relative phase meter to be perform relative phase calibration such as a broadband sampling oscilloscope. Thus, avoiding, the requirement for a HPR generator completely. The operation and relative phase calibration, of a ZVA-67 based LSNA is investigated, in this chapter the following issues can addressed [10-12]:-

- Validating the ZVA-67 can provide the necessary time coherent receiver functionality will be verified during this chapter.
- Demonstrate the calibrate the ZVA67 (VNA) using only its internal signal sources and an external relative phase meter (oscilloscope).
- Verifying the operation of the ZVA-67 as a fully functional LSNA, without a HPR generator.

4.5 OPERATION VNA WITHOUT PHASE REFERENCE

Figure 5-4 reviews shows a generic block diagram for NVNA. The dual directional couplers are employed to separate the time varying signals incident wave $A_n(t)$ and reflect wave $B_n(t)$, and direct $A_n(t)$ and $B_n(t)$ to pairs of receivers. An NVNA is designed to measure $A_n(t)$ and $B_n(t)$ present at each port of the DUT in either the frequency domain or time domain [6, 13].
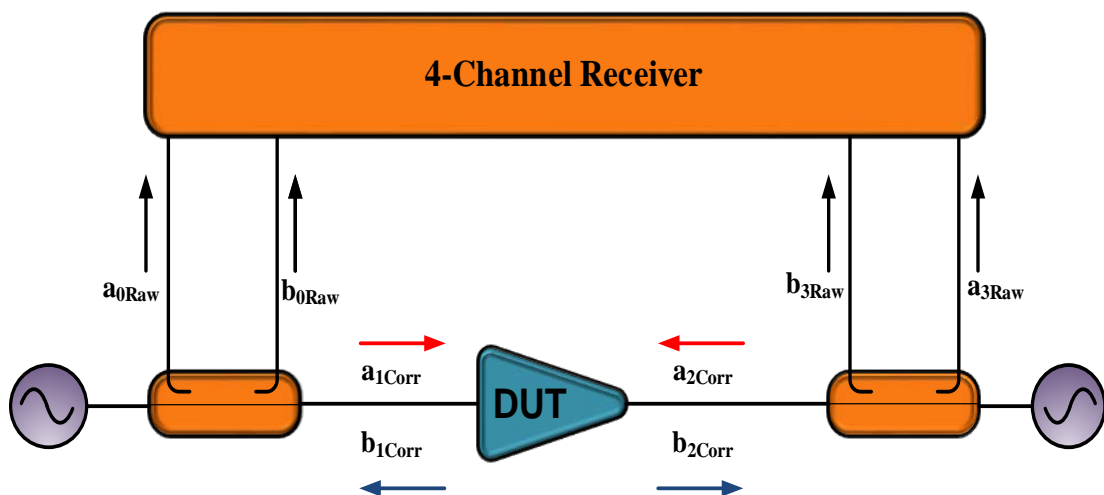
FIGURE 5-4 TWO SIGNALS WITH RANDOM PHASE DIFFERENT 2 PORTS.

The incident and reflect signals are directly time sampled. If the receivers operate in the time domain this is due to these measurement system is thus able to captures all spectral components at the same time, of course with reference to a common time trigger as shown in Figure 5-5 shown signal measured in time domain as example about captures all spectral components at the same time [13-15].
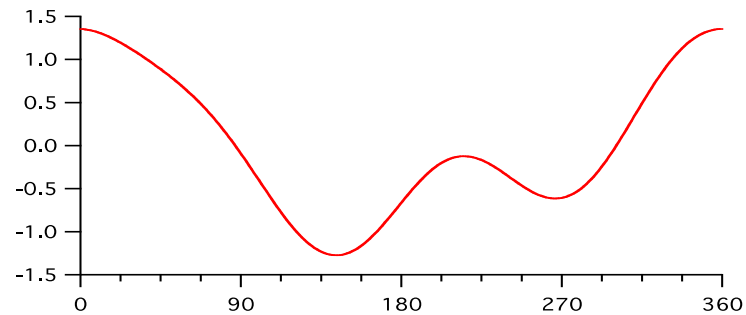
FIGURE 5-5 WAVEFORM OBTAINED FROM COMPAINED THREE TONES WITH COMMAN TRIGGER.

Alternatively, VNA measures the Fourier coefficients A(ω) and $B(\omega)$ of a two-port device simultaneously, but a one frequency at a time. These measurements, that are happened at different harmonics, are may not know affixed time trigger. This lead to the relative phase of the waveforms frequency being unknown. Hence simple addition of each component does not generate the correct time domain waveform, as shown in Figure 5-6 [2, 13-15].
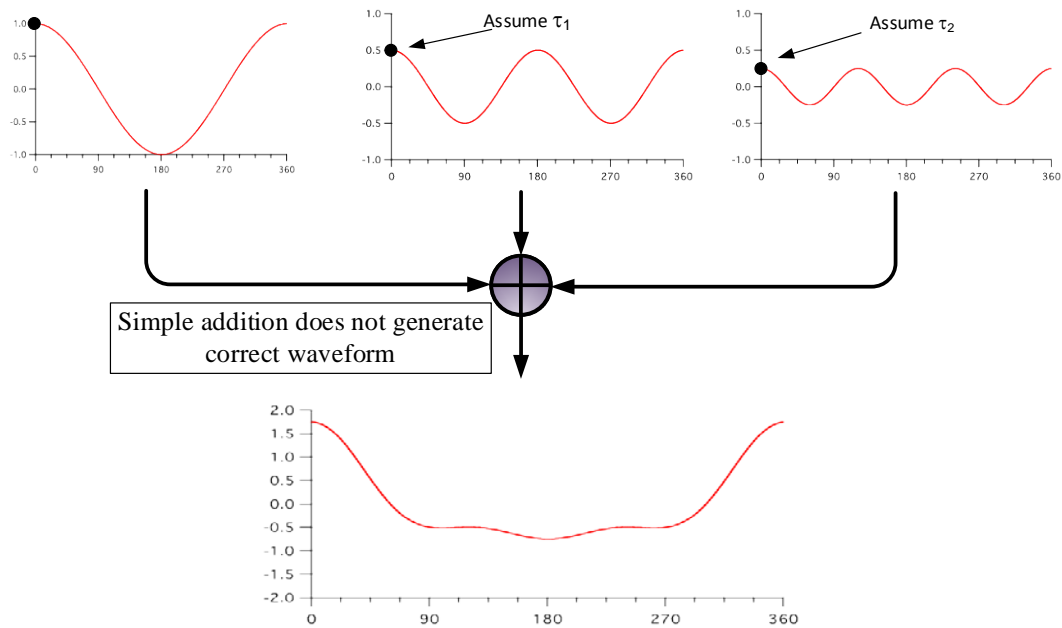
FIGURE 5-6 SIMPLE ADDITION DOES NOT GENERATE CORRECT WAVEFORM.

Almost the theory of design RFPA works in time domain waveform therefore transformation of these Fourier coefficients a(ω) and b(ω) which is obtained from VNA back into the time domain, this aim achieved by using common time reference during the swept frequency VNA measurements. The Figure 5-7 shows that to determine the correct waveforms the correct time alignment (phase adjust) is required. Traditionally the was the roll of measuring a known signal HPR, with an additional receiver. The harmonic waveforms are the correct waveform will be determined corrected time align (Phase adjust) [2, 12-15].
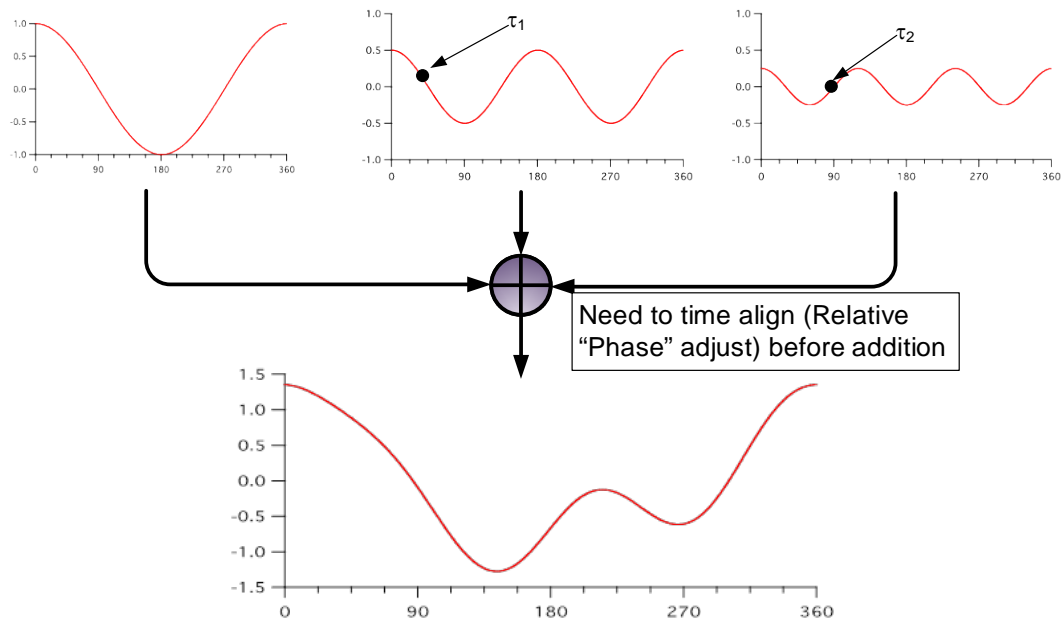
FIGURE 5-7 NEED TO TIME ALIGN PHASE ADJUST BEFORE ADDITION.

Since time a VNA performs a frequency sweep the relative phase between harmonics various. The VNA uses mixers with one internal local oscillator (LO) to down converted all four waves ensuring phase stability at each frequency, however the phase of the LO signal is unknown and can vary, this mean each sweeping of frequency will lead to a different waveform [13].

As long as the phase of LO is not controlled, it is not possible directly measure and/or calibrate the relative phase between the different frequency components. To overcome this issue involved incorporating a HPR generator measurement. By attaching the HPR generator to an additional receiver provides the measurement system a calibration using another HPR can then be performed common time trigger to freeze alignment the phase for harmonics [13-16].

By using HPR generator in measurement system (the VNA with HPR generator to construction VNA) gives ability for measurement system to reconstruction the signal in time domain but will increases both the cost and complexity with respect to the time sampling alternative. In addition, the operational functionality of the measurement system is completely dependent of the availability and quality of an appropriate HPR

generator. Even with these limitation, the VNA based NVNA systems are becoming, the best solution, this is due to their significantly improved dynamic range [13-16].

4.5.1 PHASE COHERENCE OF VNA (ZVA-67)

This part of thesis focus on functionality of measurement system especially on the limitation of VNA based systems is that they need harmonic phase reference (HPR) generators for both triggering and relative phase calibration to reducing the complexity by modified the phase calibration process. This part presents a solution that allows a VNA to operate as a LSNA without requiring a HPR generator, either for triggering or calibration. this approach to operation and relative phase calibration, using a ZVA-67 based LSNA that is investigated in this chapter. At first the ability of the ZVA-67 to provide the necessary time coherent receiver functionality will be verified. Following this, a calibration procedure using only the internal signal sources and an external relative phase meter will be presented and demonstrated. Finally measurements verifying the operation of the ZVA-67 as a fully functional LSNA, without a HPR generator will be shown.

5.5.1.1 PHASE REFERENCE TRIGGER

As mentioned before, in order to enable the VNA to measure the signal in frequency domain and reconstruction the signal correctly in time domain, Should be calibrating the phase of measurement system by setting the system as shown in Figure 5-8.
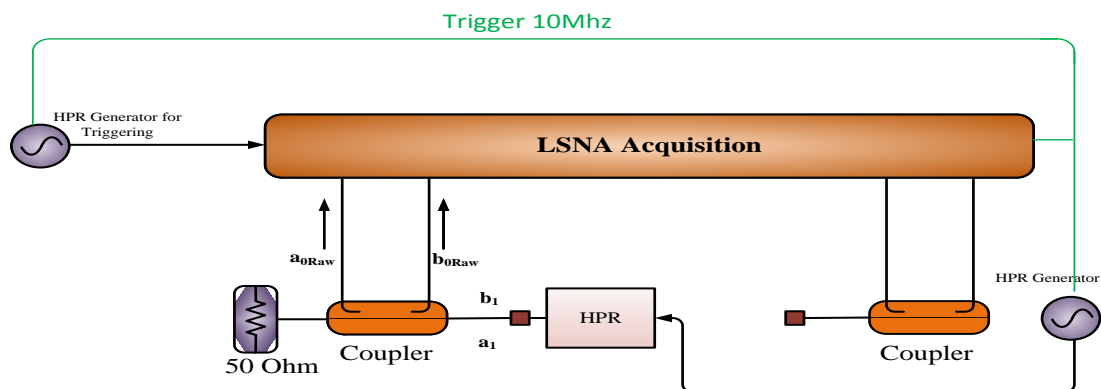
FIGURE 5-8 PHASE CALIBRATION FOR LSNA.

Figure 5-8 is shown VNA is triggered by the harmonic phase reference (HPR) generators trigger which is necessary for given the VNA an ability to capture the correct phase of the phase reference during the calibration which is used to correct the raw data obtain during measurement process. Correct operation is achieved by:-

[1]-A HPR is connected to a port on the VNA that is not in use (an additional receiver) to take measurements. The HPR has been previously characterised and so is generating a known waveform. This can then be used as a reference to correct future measurements. It relative phase is fixed so a time invariant waveform is know measured.

[2]-T The additional HPR is connected to the measurement port that is being calibrated. The signal measured on this port is then compared to the measurement on the unused port to generate error coefficients.

The following investigations were then undertaken firstly to investigate the time coherent (also known stability) of the sources in ZVA-67. This was a one by combining two signals from two internal sources of ZVA-67 and using DSA8200 sampling oscilloscope to capture the signal. DSA8200 oscilloscope is triggered at the common fundamental frequency for sources 1 and 2, using other source of the ZVA67, as shown in Figure 5-9.
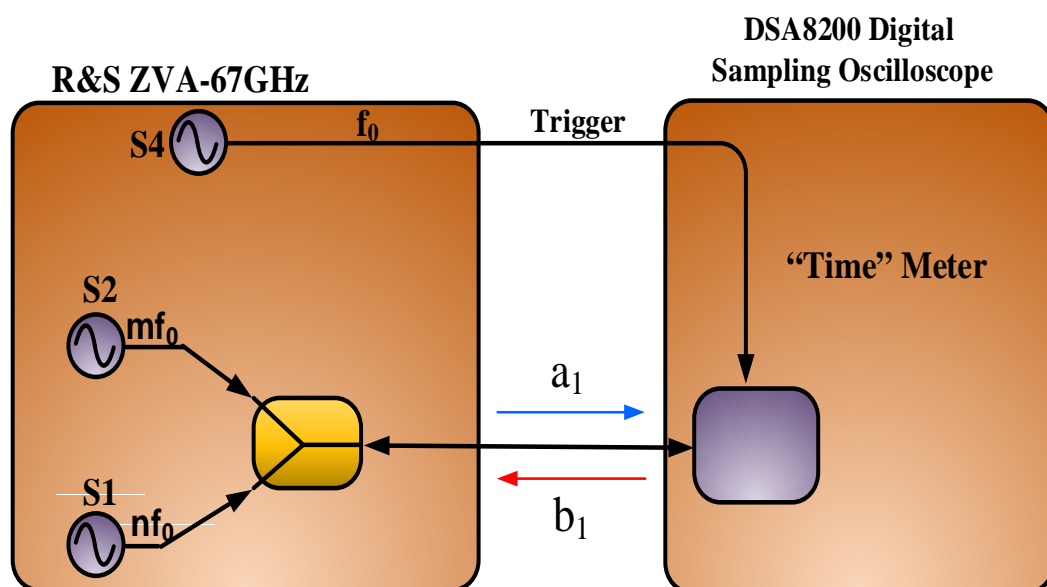
FIGURE 5-9 ZVA RF SOURCES UTILIZE DIGITAL SYNTHESISERS.

In this experiment, The first source in ZVA-67 set to 1 GHz, second source in ZVA-67 set for 2GHz and third source set to common fundamental frequency which is 1 GHz in these case and the used as for trigger for the DSA8200 sampling oscilloscope. The waveform was observed over a 48hrs period. Initial waveform, waveform after 24 hrs and then after 48hrs are shown in Figure 5-10.
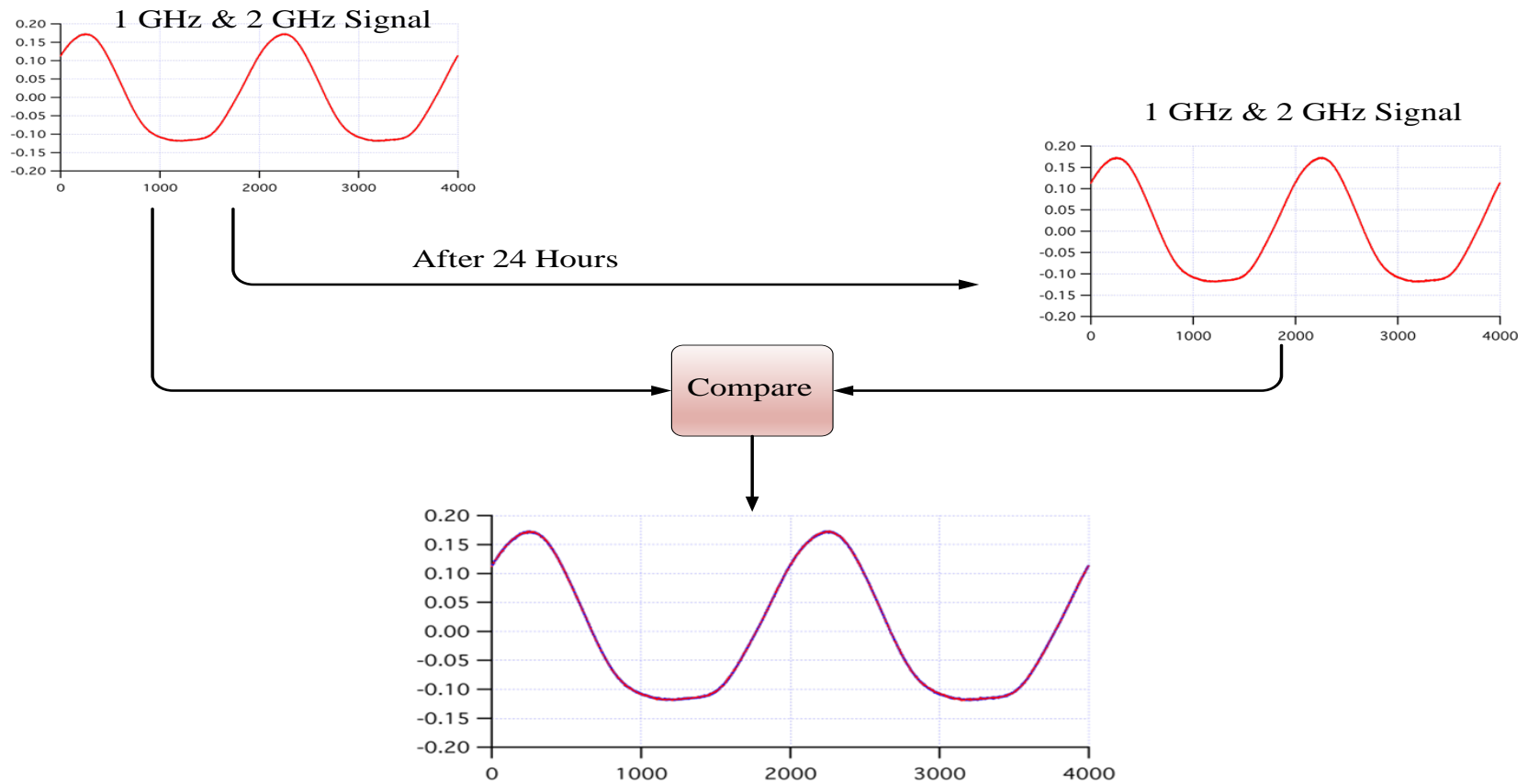
FIGURE 5-10 COMPARISON BETWEEN SAME SIGNAL AFTER 48 HOURS.

No observable change in the shape of the waveforms is clearly observed. The use of DDS LO should also provide a VNA with time coherent receivers, hence a constant relative phase response, which is lead to eliminating the need for a HPR generator for triggering. In addition, while open the door to ability to calibration and operation just with HPR generator as shown in Figure 5-11 or relative phase (time) calibration can be performed by simply using a relative phase (time) meter, such as a broadband sampling oscilloscope, thus avoiding, if desired, the need for a HPR generator altogether as shown Figure 5-12.
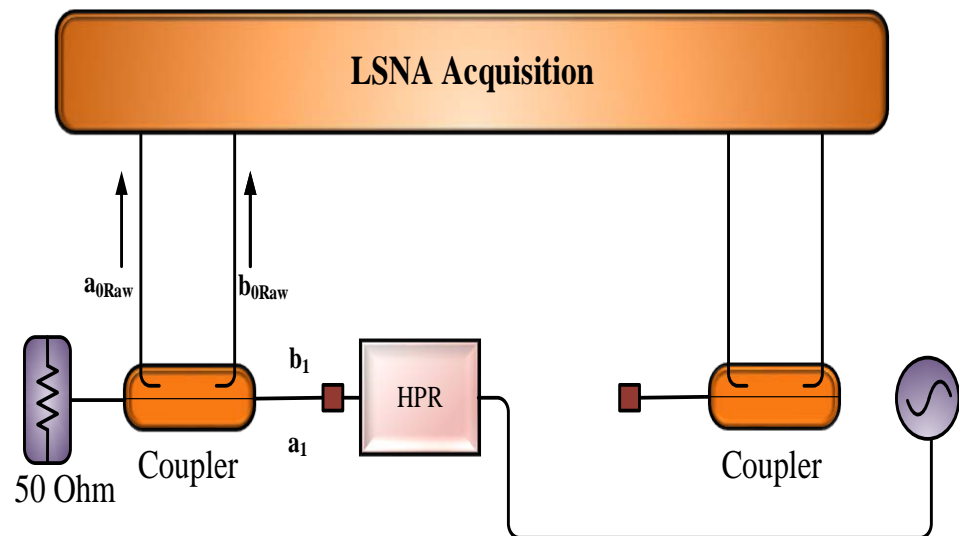
FIGURE 5-11 CALIBRATION AND OPERATION JUST WITH HPR GENERATOR FOR TRIGGERING.
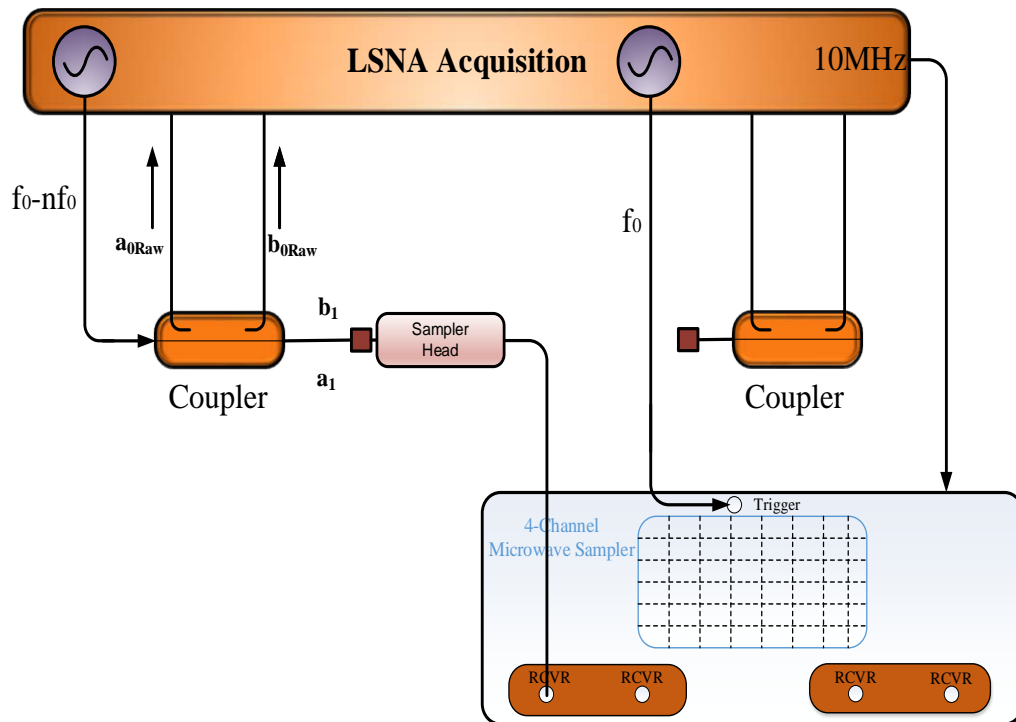
FIGURE 5-12 CALIBRATION AND OPERATION WITH PHASE METER.

5.5.1.2 RECEIVER

Consider now a VNA based LSNA system using the Rohde and Schwarz ZVA-67, in this case the phase of the LO while not known, when sweeping the frequency, should no longer vary and be repeatable between measurements. This should happen since the ZVA-67 integrates multiple internal DDS signal sources, for both the local oscillator and the device excitation as result all the internal sources should be time coherence, hence also any IF down converted signal.

In this case the VNA (ZVA-67) should has ability to following a relative phase calibration therefore, the VNA (ZVA-67) will able to do directly measure the Fourier coefficients $\tilde{A}_n(\omega)$ and $\tilde{B}_n(\omega)$ with respect to a common time trigger as well as ability to do accurately measure $A_n(t)$ and $B_n(t)$ without the requirement of attaching a HPR generator to an additional receiver. this advantage give an ability to correct the phase during measurement by two ways, the first method by using HPR generator or relative phase meter a broadband sampling oscilloscope. This stage consist of practical investigating for the possibility of utilized the "time coherence" of the ZVA in mode of the measurement operation.
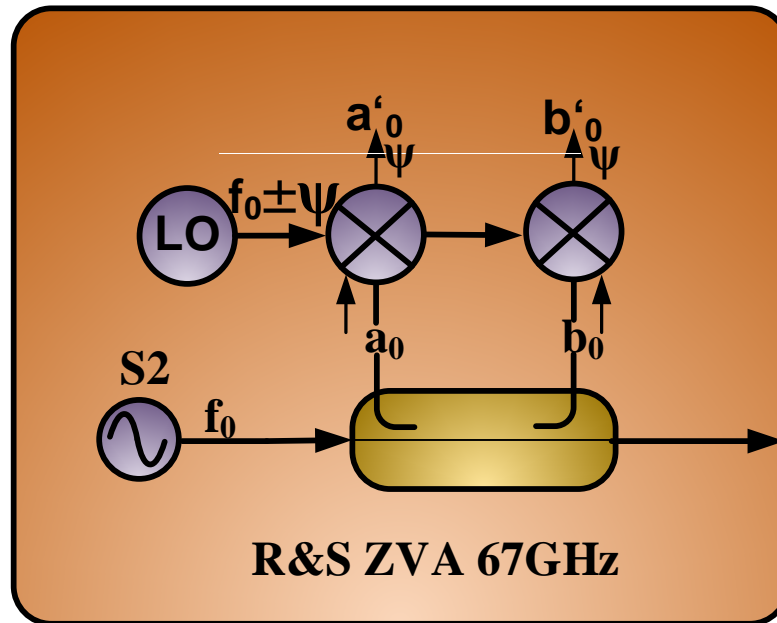
FIGURE 5-13 ZVA LO SOURCES UTILIZE DIGITAL SYNTHESISERS.

The next investigation involves testing the time coherence of the receivers in the VNA (ZVA-67). These involve measuring the phase jitter which is observed over time. It can be described as a variation in phase with time for $\tilde{a}_{1,RAW}(\omega)$ and $\tilde{b}_{1,RAW}(\omega)$ as a function of frequency. Figure 5-13 shows the hardware configuration of ZVA, the ZVA67 was configured to perform swept frequency measurements on a 1 GHz grid from 1 GHz to 50 GHz. A subroutine was written to collect a dataset sequence; the raw ZVA data from port 1, the measured frequency response $\tilde{a}_{1,RAW}(\omega)$ and $\tilde{b}_{1,RAW}(\omega)$, for each one minute interval during the first hour followed by 30 minutes intervals for the next 24 hrs.
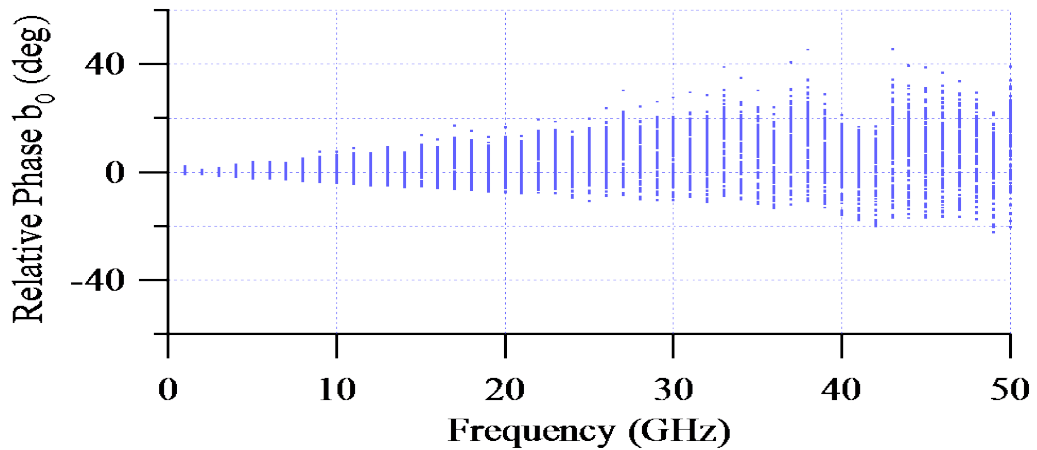
FIGURE 5-14 14MEASURED PHASE JITTER OBSERVED OVER A 24 HR PERIOD FOR $b_{\widetilde{raw}}$ AS FUNCTION OF FREQUENCY.
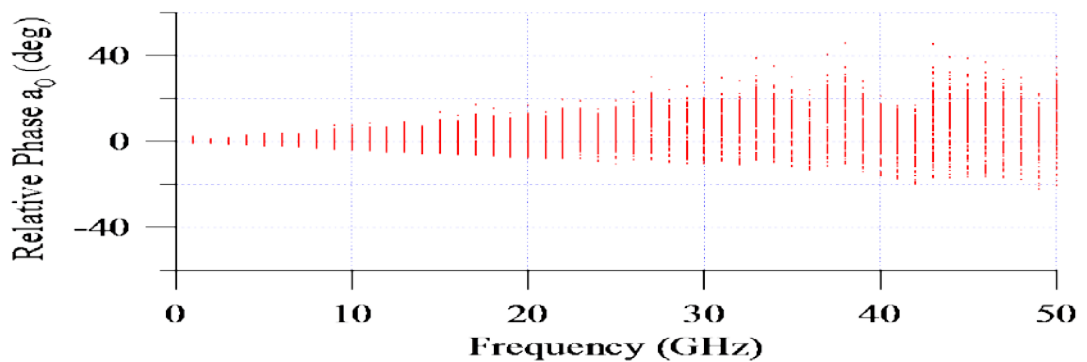
FIGURE 5-15 MEASURED PHASE JITTER OBSERVED OVER A 24 HR PERIOD FOR $a_{\widetilde{raw}}$AS FUNCTION OF FREQUENCY.

The Figure 5-14 and Figure 5-15 show (b_{0Raw} and a_{0Raw}) which is obtained as results for measuring relative phase for 24 hours. The plots show the relative phase variation over this period as a dot for each frequency at each sample time, these dots then show the total variation for each frequency over this time. It is seen that while the measured phase of each signal is not constant and varies randomly, the two receivers are tracking each other. This indicates that the source of the variation is not in the receivers but the source (LO), which is common to both receivers. This means for each frequency the phase of the LO changes by a constant amount, and so can be calibrated out. As conclusion: the measured relative phase is not randomized anymore, this means for each sweeping of frequency to change the phase for LO by an known amount. Since these travelling wave signals have common internal excitation and LO sources.

Of critical interest is the variation in the measured relative phase response $\Delta\phi$ over time of the multiple sources, $\Delta\phi$ consist of (Δt_P) due to the variation in source and (Δt_{LO}) due to variation in local oscillator, time, normalized to first measurement dataset. The measured dataset at the ith time interval is thus given by;

$$\tilde{a}^i_{1,RAW}(\omega) = \tilde{a}^0_{1,RAW}(\omega)e^{j\Delta\phi} = \tilde{a}^0_{1,RAW}(\omega)e^{j\omega(\Delta t_P+\Delta t_{LO})}$$ EQUATION 5-1

$$\tilde{b}^i_{1,RAW}(\omega) = \tilde{b}^0_{1,RAW}(\omega)e^{j\Delta\phi} = \tilde{b}^0_{1,RAW}(\omega)e^{j\omega(\Delta t_P+\Delta t_{LO})}$$ EQUATION 5-2

Figure 5-16and Figure 5-17 shown the normalization $a_0 Raw$ and $b_0 Raw$ normalized to first measurement in dataset, which is obtained during 24 hours to fundamental frequency as function for frequency. These figures shown there is a considerable scatter observed for $a_0 Raw$ and $b_0 Raw$ and difference in relative phase between fundamental and each harmonics. However, ratio measurement found the phase drift 0.01 deg and maximum phase uncertainty +/-0.16 deg.
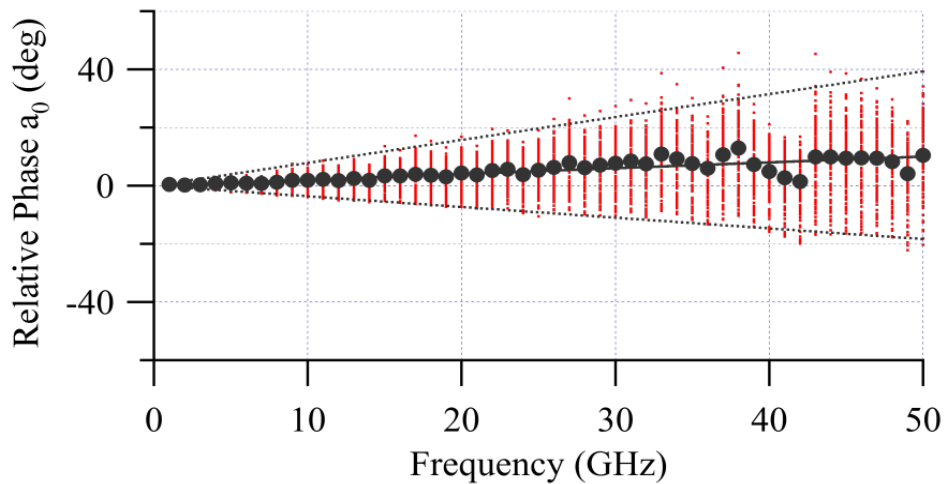
FIGURE 5-16 MEASURED PHASE JITTER OBSERVED OVER A 24 HR PERIOD FOR RAW a_0, AS A FUNCTION OF FREQUENCY. AVERAGE VALUES IS ALSO IDENTIFIED WITH DOT.
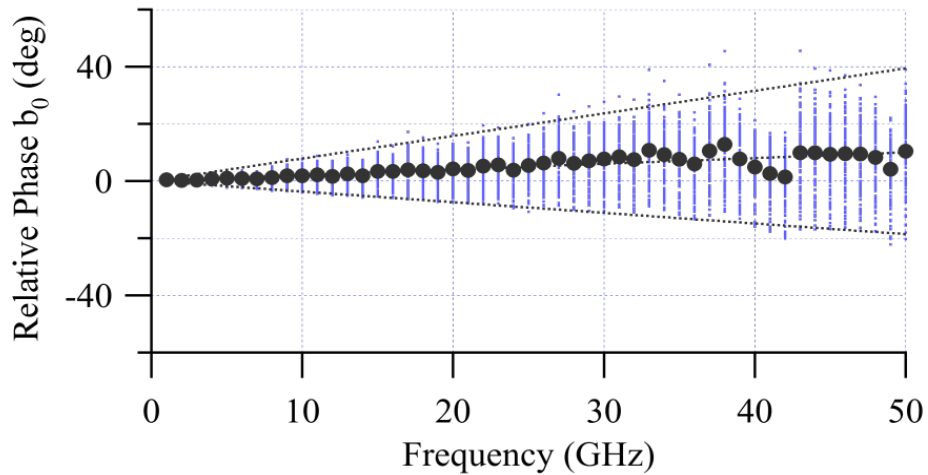
FIGURE 5-17 MEASURED PHASE JITTER OBSERVED OVER A 24HR PERIOD FOR RAW b_0, AS A FUNCTION OF FREQUENCY. AVERAGE VALUES IS ALSO IDENTIFIED WITH DOT.

From Figure 5-16 and Figure 5-17 can observe the $a_0 Raw$ and $b_0 Raw$ have same (same scatter is just because coherence a common LO which is lead to the pattern of LO and source phase) distribution scattering as function for frequency during period 24 hours this due to DDS technology used in sources and receivers of ZVA-67 as shown in equation 5-3 and 5-4.

$$a_0'^i = a_0 e^{j\omega_{\Delta f}(t-(\tau_s-\tau_{LO}))} \qquad \text{EQUATION 5-3}$$

$$b_0'^i = b_0 e^{j\omega_{\Delta f}(t-(\tau_s-\tau_{LO}))} \qquad \text{EQUATION 5-4}$$

For that the scatter should not be observed in the ratio $\dfrac{\tilde{b}_{1,RAW}^i(\omega)}{\tilde{a}_{1,RAW}^i(\omega)}$ S_{11Raw} as shown in Figure 5-18, this due to these travelling wave signals have common LO sources and internal excitation as mentioned before.
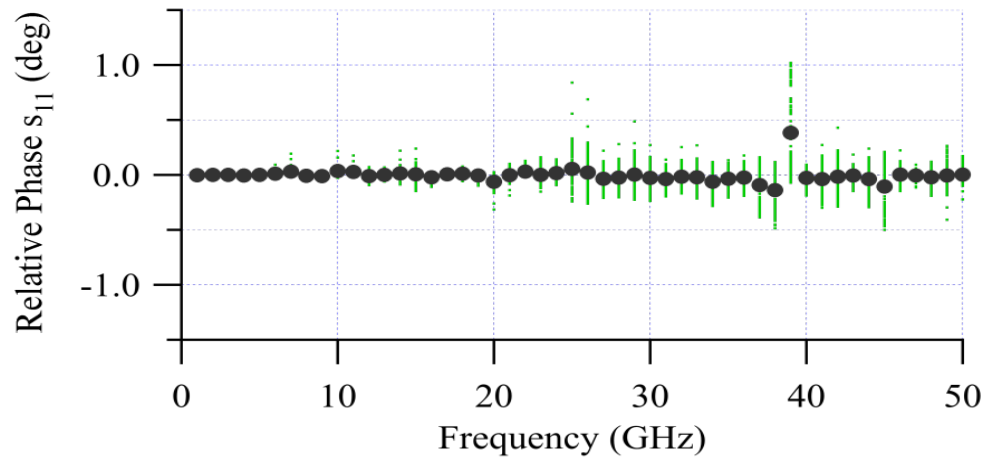
FIGURE 5-18 MEASURED PHASE JITTER OBSERVED OVER A 24HR PERIOD FOR RAW S11, AS A FUNCTION OF FREQUENCY. AVERAGE VALUES IS ALSO IDENTIFIED WITH DOT.

By observing the time jitter as function of frequency for over a 24 hours period for $\grave{b}_{1,RAW}(\omega)$ and $\grave{a}_{1,RAW}(\omega)$ they are identical, this is shown in Figures 5-19 and 5-20. This verifies the results shown by the previous measurements in Figures 5-14 and 5-15, that the apparent increase of this relative phase scatters with frequency is consistent with the source being related to frequency independent timing jitter. This effect has now been shown in both the time in Figures 5-19 and 5-20, in the DDS internal signal generators; the LO signal generator and/or phase jitter ωt_{LO}, port signal generator, phase jitter $\omega \Delta t_{LO}$. By focusing across frequency see that thus phase drift is simply an associated to as common time jitter for all frequencies.
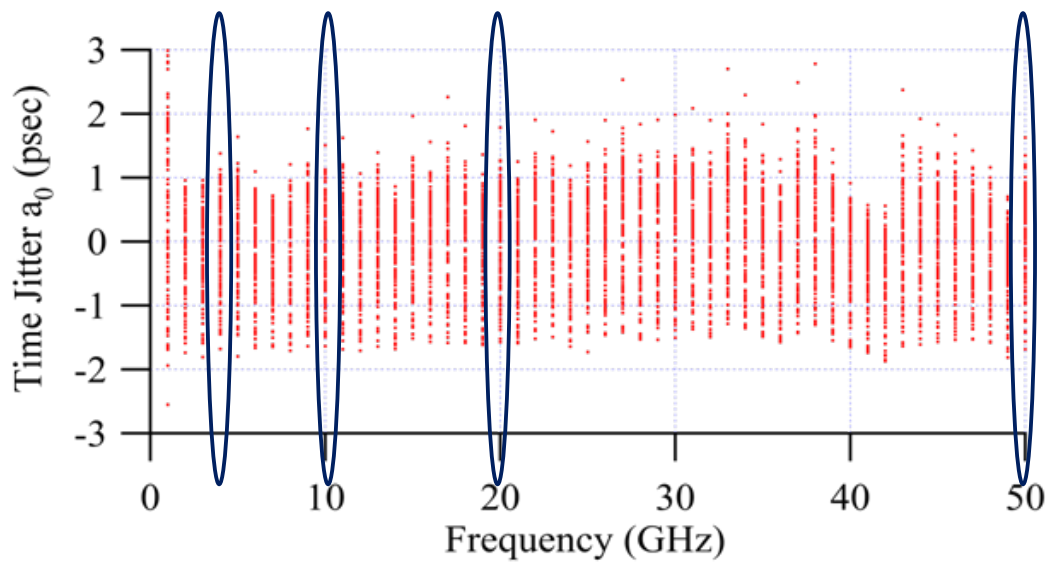
FIGURE 5-19 MEASURED TIME JITTER OBSERVED OVER A 24HR PERIOD FOR $\widetilde{a_{0,RAW}}(\omega)$ (Ω) AS A FUNCTION OF FREQUENCY.
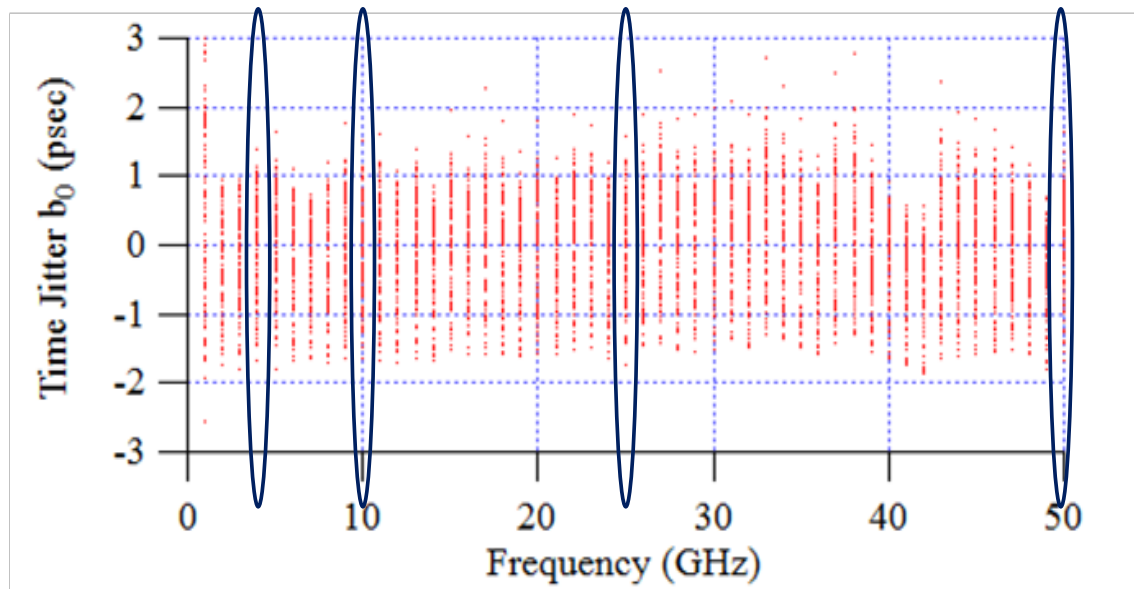
FIGURE 5-20 MEASURED TIME JITTER OBSERVED OVER A 24HR PERIOD FOR $\widetilde{b_{0,RAW}}(\omega)$ AS A FUNCTION OF FREQUENCY.

In any case, A closer inspection for result obtained from measured the time jitter for a_{0Raw} and b_{0Raw} that not all this time jitter, +/- 1.6 spec, is random and that a major component is in reality a time drift term that is identical (coherent) across the measured 50 GHz bandwidth, as clearly shown in Figure 5-21 A and 24 hours as shown in Figure 5-21B for a_{0Raw} as a function of observation time at selected frequencies as well as Figure 5-22 A and Figure 5-22 B obtained as result for measured time jitter observed over for 1 hour and 24 hours for b_{0Raw} as a function of observation time at selected

frequencies, So the time drift elements can be removed, which is mean at each moment in time each frequency has the same common, time drift.
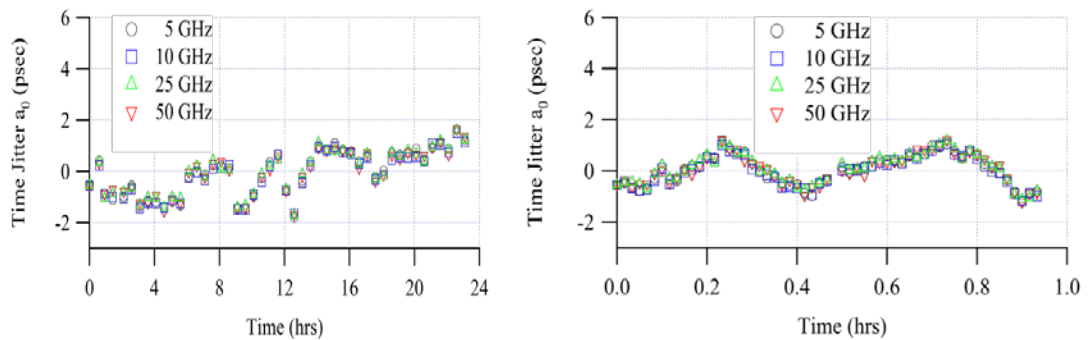
FIGURE 5-21 MEASURED TIME DRIFT OBSERVED OVER (A) 1HR PERIOD AND (B) 24HR PERIOD FOR $a_{1,Raw}^{\sim}$, , AS A FUNCTION OF OBSERVATION TIME AT SELECTED FREQUENCIES.
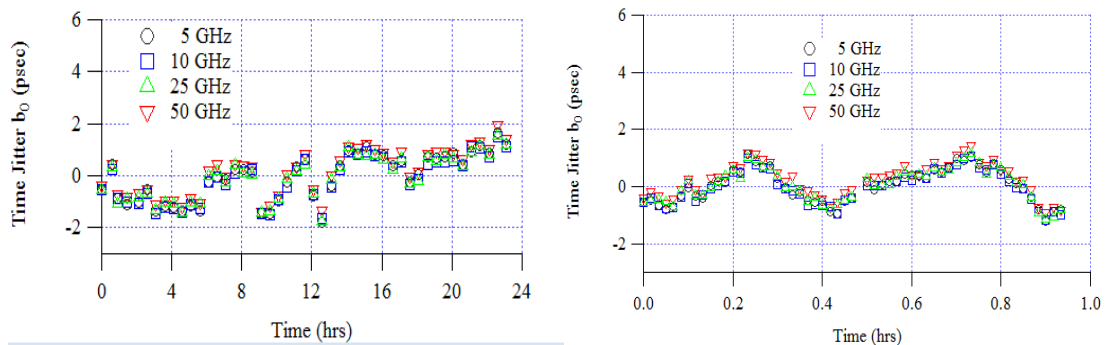
FIGURE 5-22 MEASURED TIME DRIFT OBSERVED OVER (A) 1HR PERIOD AND (B) 24HR PERIOD FOR $b_{1,Raw}^{\sim}$, AS A FUNCTION OF OBSERVATION TIME AT SELECTED FREQUENCIES.

In order to more focusing on time jitter,5GHz chosen arbitrary from frequency grid, Figure 5-23 and Figure 5-24 shown identical result obtained from measuring time jitter observed over a 24hours period for $b_{1,RAW}^{\grave{}}(\omega)$ and $a_{1,RAW}^{\grave{}}(\omega)$ at certain frequency which is 5 GHz. Using DDS in the ZVA architecture distinctly led to the same time drift at all frequency. Hence this common drift can be eliminated by normalizing to single frequency point.
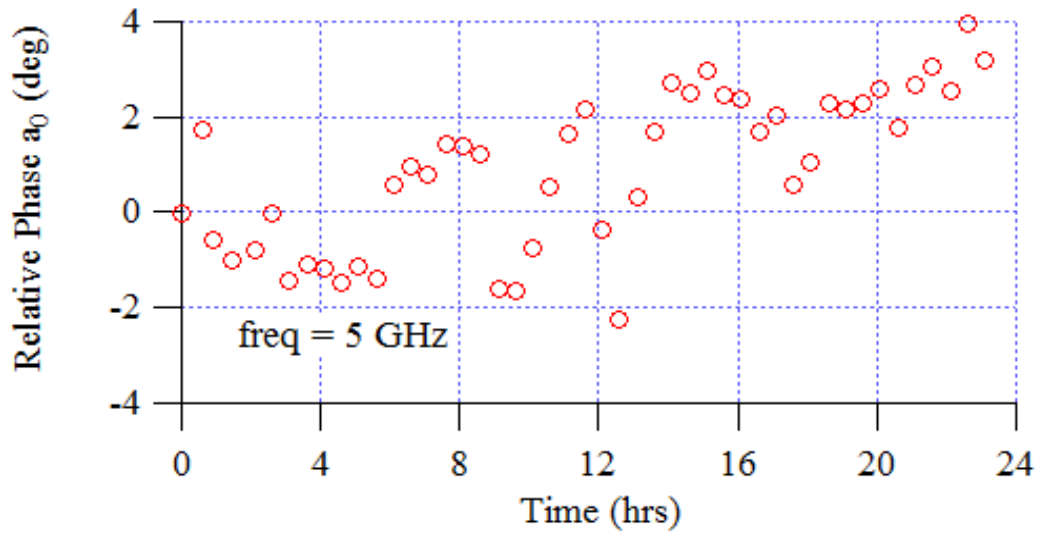
FIGURE 5-23 MEASURED TIME JITTER OBSERVED OVER A 24HR PERIOD FOR $a\tilde{_{1,Raw}}$ **AT A 5 GHZ.**
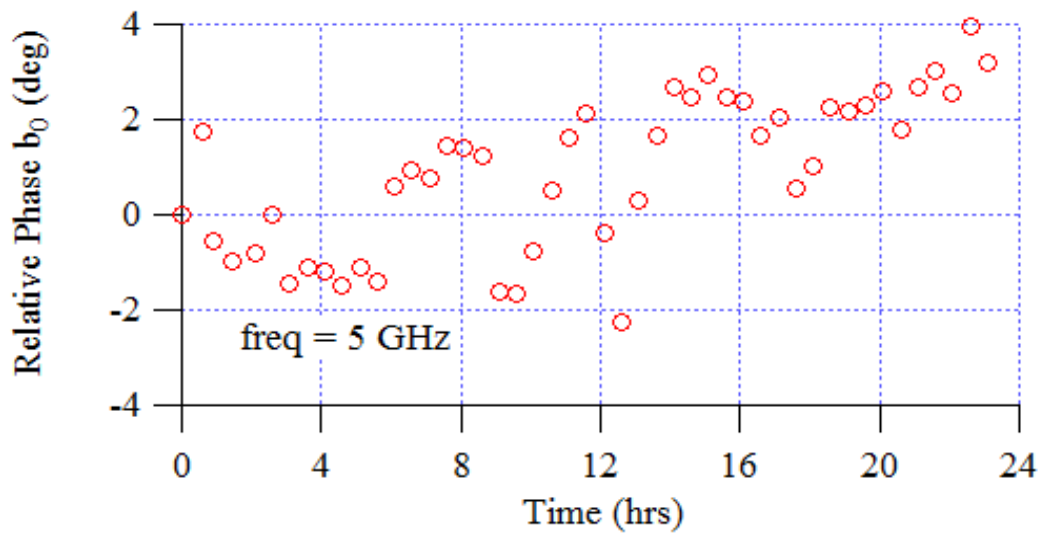
FIGURE 5-24 MEASURED TIME JITTER OBSERVED OVER A 24HR PERIOD FOR $b\tilde{_{1,Raw}}$**AT A 5 GHZ.**

Critically, can understand from above the process of determine time varying signals $a_n(t)$ & $b_n(t)$ which is obtained from compute the measured Fourier coefficients $a\tilde{_n}(w)$ and $b\tilde{_n}(w)$ will not effect by the coherent time drift or could say the coherent time drift has no influence on the determined time varying signals $a_n(t)$& $b_n(t)$this

happen when time aligning the individually computed spectral components since it is common for all.

As shown in Figure 5-25 the ZVA-67 has residual measured LO time (phase) jitter after disarmament of the coherent drift component is observed to be below +/- 0.3 psec. The above investigations prove that the ZVA-67 is a "time coherent" system, which, after relative phase (time) calibration should be able to perform accurate measurement of time varying signals $a_n(t)$ & $b_n(t)$ without requiring a HPR generator connected to an occupying an additional channel.
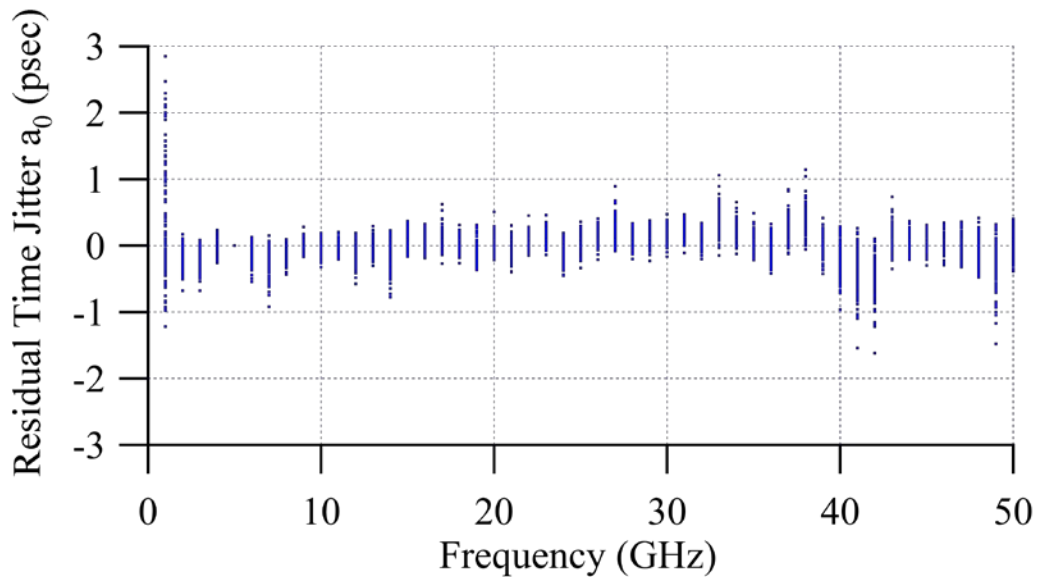
FIGURE 5-25 MEASURED RESIDUAL TIME JITTER OBSERVED OVER A 24HR PERIOD FOR $a_{\widetilde{1,Raw}}$, AS A FUNCTION OF FREQUENCY AFTER REMOVAL OF THE COHERENT DRIFT COMPONENT (DETERMINED IN THIS CASE AT 5 GHZ). AN IDENTICAL RESULT IS ACHIEVED FOR $b_{\widetilde{1,Raw}}$.

5.5.1.4 PHASE CALIBRATION

The ZVA-67 is a "time coherent" system able to perform accurate measurement of time varying signals $a_n(t)$ & $b_n(t)$ with or without requiring a HPR generator .This led to ability correct the phase by traditional method (using HPR generator) or without by using phase meter determine the phase of $a_n(t)$ & $b_n(t)$ as shown in Figure 5-26 and Figure 5-27.
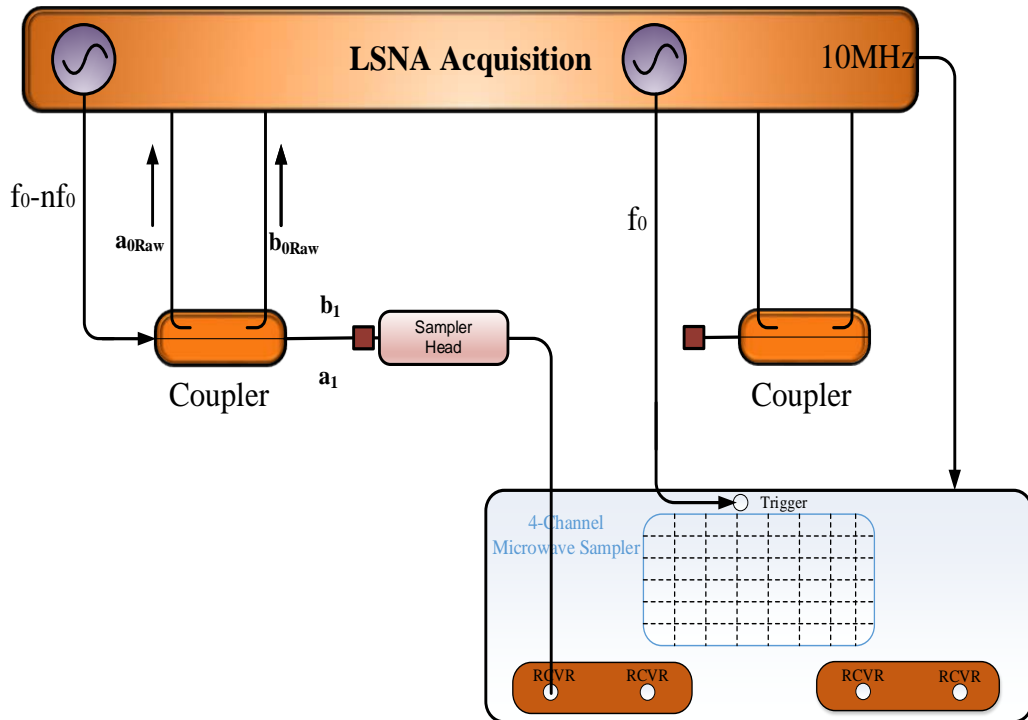
FIGURE 5-26 GENERIC LSNA CONFIGURATION FOR ZVA RELATIVE PHASE CALIBRATION.
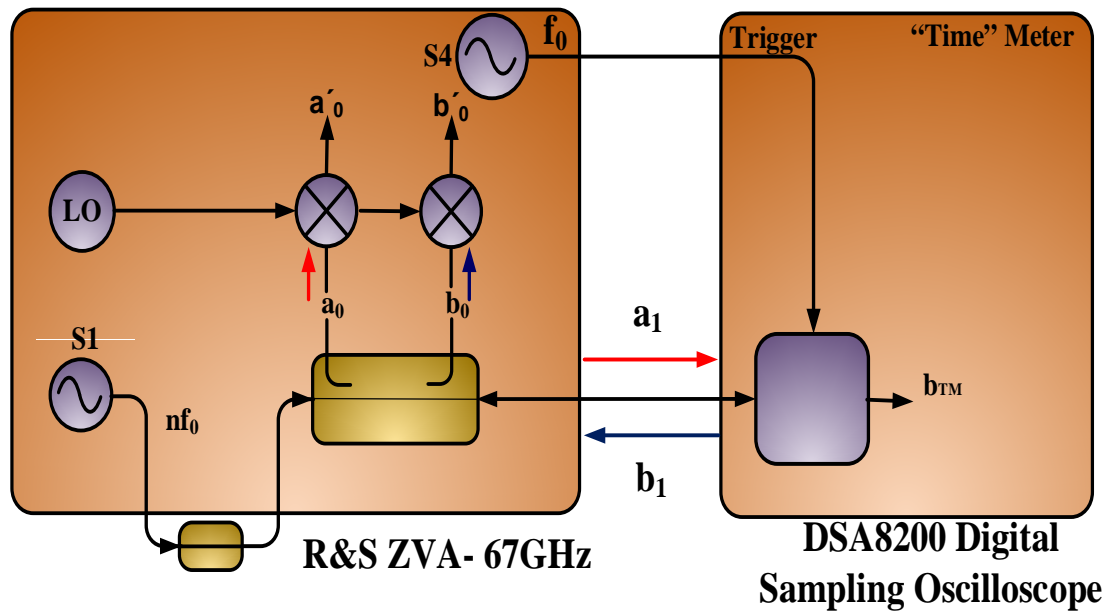
**FIGURE 5-27 HARDWARE CONFIGURATION FOR ZVA RELATIVE PHASE
CALIBRATION.**

4.5.2 Calibration

No measurement system is perfect, therefore the LSNA performs un-calibrated or 'raw'
measurements by other words the LSNA measurements contain errors resulting from
systematic, random and drift components as mentioned in pervious chapter, therefore
full calibration is necessary to minimized systematic errors [1-4].

This section deal with full calibration for NVNA (ZVA-67GHz) after approved ZVA-67
phase coherent, calibration is technical process used to characterizing the measurement
system so that systematic errors can be minimized from the measurement result and
transfer the reference planes for measurement system from ports reference planes to
desired DUT reference planes by calculate the 8 coefficients of the error model defined
in frequency domain [6-8, 13-16].

Before proceeding with the calibration aspects, it is valuable to consider the equipment
schematic of a NVNA's this is due to the fact that there are three types of (LSNA)
systems and ZVA 67-GHz considered is Mixer-based vector (NVNAs). The outline of
the calibration measurement consists of three stages which should be performed for
every single measured frequency:-

1. Relative calibration(Small Signal calibration),

2. Phase calibration,

3. Power calibration.

The Figure 5-28 shown three stages of full calibration for NVNA.
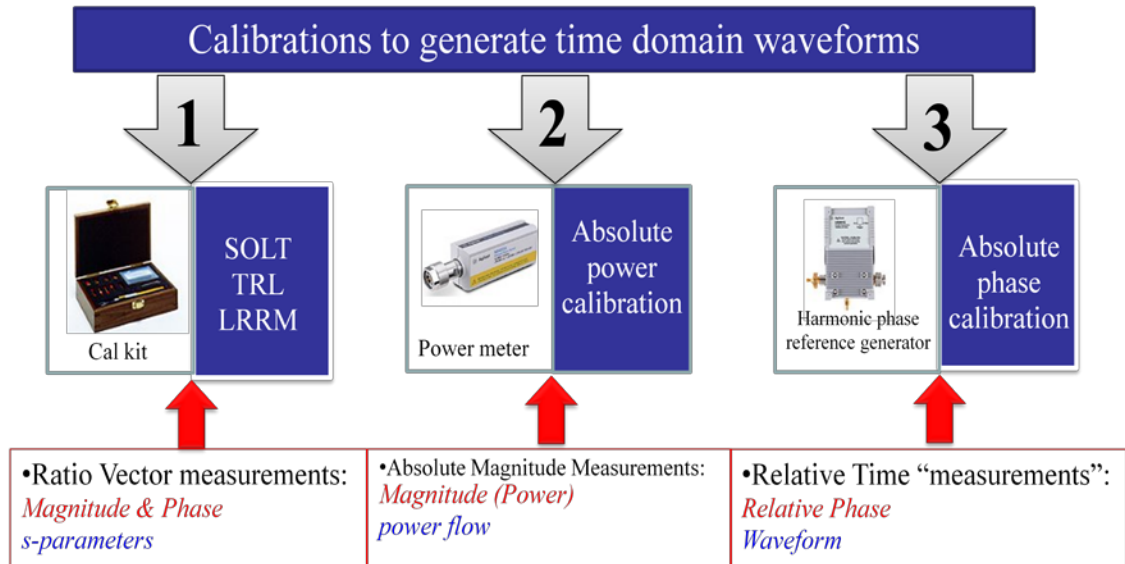
FIGURE 5-28 STEPS NECESSARY FOR CALIBRATION NVNA.

For a two-port device measurements this operation is achieved via the following mathematical transformation;

$$\begin{bmatrix} \tilde{a}_{1,COR}(\omega) \\ \tilde{b}_{1,COR}(\omega) \\ \tilde{a}_{2,COR}(\omega) \\ \tilde{b}_{2,COR}(\omega) \end{bmatrix} = k(\omega)[e(\omega)]\begin{bmatrix} \tilde{a}_{1,RAW}(\omega) \\ \tilde{b}_{1,RAW}(\omega) \\ \tilde{a}_{2,RAW}(\omega) \\ \tilde{b}_{2,RAW}(\omega) \end{bmatrix}$$
EQUATION 5-5

Where

$$[e(\omega)] = \begin{bmatrix} 1 & e_{12}(\omega) & 0 & 0 \\ e_{21}(\omega) & e_{22}(\omega) & 0 & 0 \\ 0 & 0 & e_{33}(\omega) & e_{34}(\omega) \\ 0 & 0 & e_{43}(\omega) & e_{44}(\omega) \end{bmatrix}$$
EQUATION 5-6

The error model $[e\langle w\rangle]$ generated by calibration process, is used to describes the raw data and reference plane data.

The linear calibration (small signal calibration or relative calibration) in reality is exactly the same as for a VNA calibration and is performed by using a classical VNA calibration on a selected frequency grid, the calibration procedures executed for instance be obtained by a Short-Open-Load-Thru (SOLT), Thru-Reflect-Load (TRL), Load-Reflect-Match (LRM), or other calibration standards. The relative calibration provides the following individual error coefficient values: for port 1 e_{00} , e_{11} and $e_{10}e_{01}$ and for port 2 e_{22}, e_{33} and $e_{32}e_{23}$, the other products: $e_{10}e_{32}$ and $e_{01}e_{23}$ obtained from connected Thru standard between port 1 and port 2. The error matrix $[e(\omega)]$ represents all error terms obtained during small signal calibration, should be mentioned S-parameters are a ratio measure [13-20].

At the end of this stage the relative calibration ended, the ZVA-67 GHz can be used as a normal VNA to measure S-parameter for DUT but S-parameter do not have ability to characterize nonlinear system, therefore the determination of the additional vector error term $k(\omega)$ is considered necessary step for LSNA calibration and operation. This usually includes a two-step process where the magnitude and relative period of $k(\omega)$ are determined independent [13-20].

The aim from power calibration is to determine the magnitude of $k(w)$ which is mean absolute power. During this stage a power meter is connected to the reference port directly, in this case it is connected to port 1 in order to enable the power meter from reading the absolute value of flowing power into the DUT which, in this case, is the magnitude of $|\tilde{a}_{1,COR}(\omega)|$. It is equal $to\ |\tilde{a_{Power}}(\omega)|$ the magnitude of $|k(\omega)|$ is computed as follows;

$$|\boldsymbol{k(\omega)}| = \frac{|\tilde{a}_{Power}(\omega)|}{\left|\left(e_{21}(\omega)\tilde{a}_{1,RAW}(\omega)+e_{22}(\omega)\tilde{b}_{1,RAW}(\omega)\right)\right|} \qquad \text{EQUATION 5-7}$$

It is worth to mention, if a CW frequency stimulus signal is applied and can be stepped-thru the calibrated frequency grid [13-20].

The final step was determines the relative phase which is achieved by connecting a HPR generator a known harmonically rich stimulus, in this case port 1. Calibration NVNA

can only be achieved if the HPR generator is able to generate a stimulus that has frequency components covering the desired frequency grid. As the requirement for a triggering HPR generator standard during the measurement step has been removed, its complete elimination from the phase calibration step would further simplify the system architecture.

Consider instead an alternative approach to relative phase calibration: To determine the relative phase, a phase meter is connected to the reference port which is in this case port 1. In this demonstration, a Tektronix DSA 8200 sampling scope with high frequency (67GHz) sampling head is used as the relative phase meter. To ensure a common time reference for the relative phase measurements, the Tektronix sampling scope is triggered using one of the spare internal ZVA-67 DDS signal sources, as shown in Figure 5-29, which in this case is set to an appropriate reference frequency of 1 GHz.
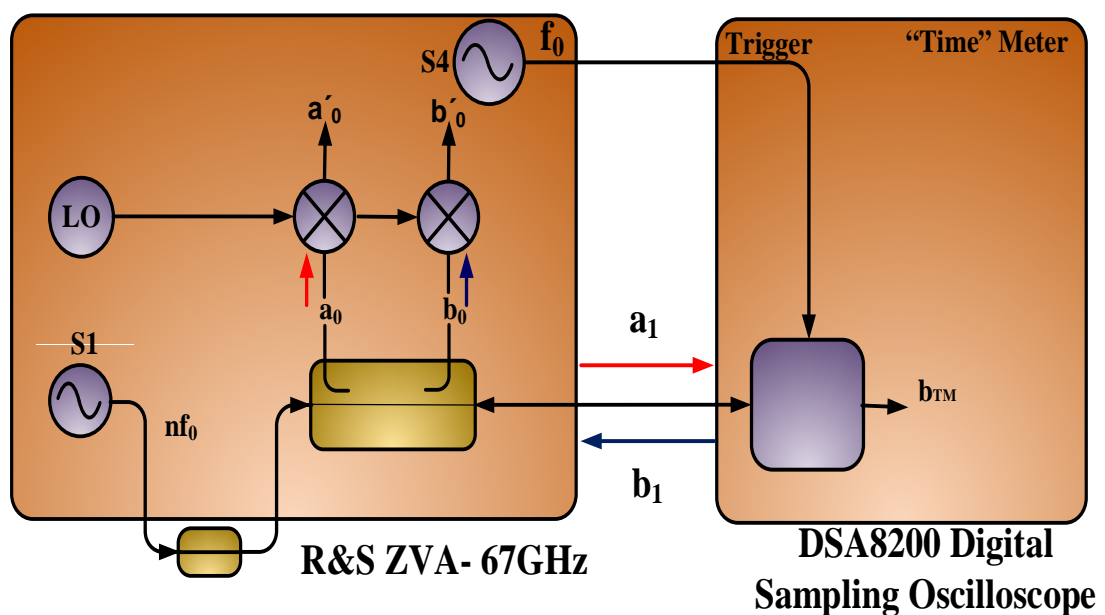
FIGURE 5-29 HARDWARE CONFIGURATION FOR ZVA RELATIVE PHASE CALIBRATION USING A PHASE METER.

A stepped frequency CW stimulus signal is then applied to the reference port (Perform a sequence of simultaneous ZVA-67 and scope measurements $f_o, 2f_o, 3f_o \dots nf_o$), and since the angle $\angle \tilde{a}_{1,COR}(\omega)$ is now directly measured, it is equal to $\angle \tilde{a}_{Phase}(\omega)$ (the phase component of the Fourier transformed sampling scope measured waveform), the relative phase $\angle k(\omega)$ is computed as follows;

$$\angle k(\omega) = \angle \tilde{a}_{Phase}(\omega) - \angle \left(e_{21}(\omega)\tilde{a}_{1,RAW}(\omega) + e_{22}(\omega)\tilde{b}_{1,RAW}(\omega) \right) \quad \text{EQUATION 5-8}$$

In this case, a simple, easily generated, single frequency signal of appropriate power level is all that is required for phase calibration.

Using the internal ZVA-67 sources ensures that LSNA operation can be achieved over its full bandwidth of 67GHz. At this point, the ZVA-67 LSNA system is fully calibrated and ready to perform coherent measurements of time varying signals $A_n(t)$ and $B_n(t)$ at all four ports. This is now possible as the fourth port is no longer required as a reference receiver to measure the HPR.

The LSNA system is now fully calibrated, at the verification can be performed by comparing the ZVA-67 and scope to measure a waveform at the reference port, which in this case port1. Both instruments should have same result as shown in Figure 5-30.
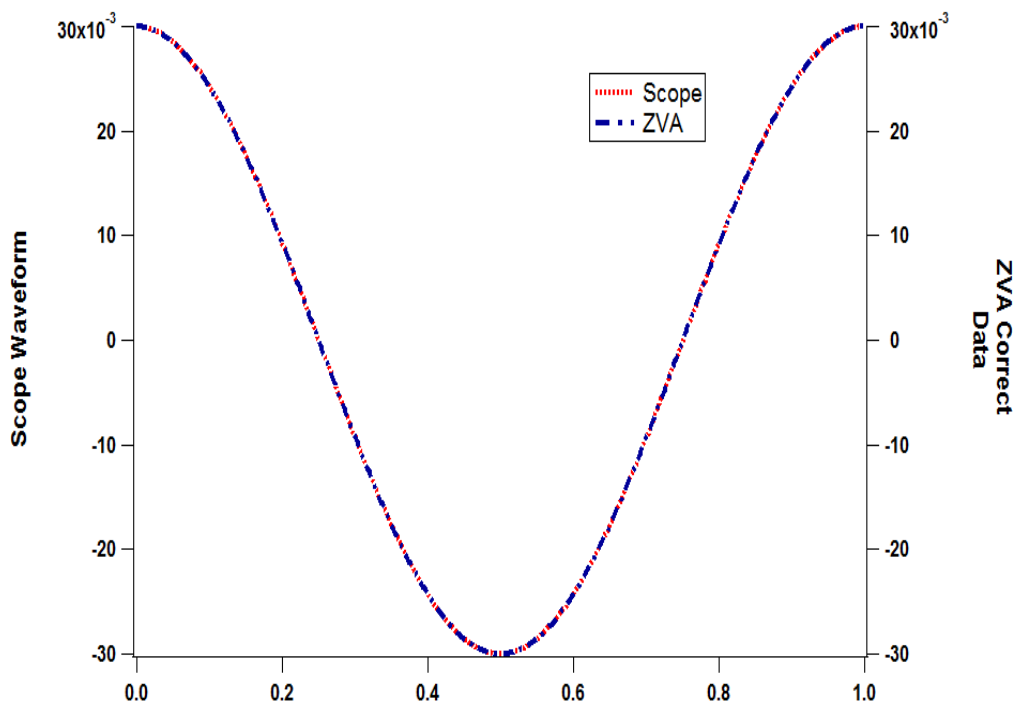
FIGURE 5-30 SYNTHESIZED POWER AMPLIFIER TYPE TIME VARYING SIGNAL AT 1 GHZ.

Typical results achieved are shown in Figure 5-30, both ZVA -67 and scope measure the same waveform.

4.5.3 CALIBRATION VALIDATION

This section is to verify the functionality of the calibrated ZVA-67 based on LSNA system. To achieve this measurement were performed using the experimental setup shown in Figure 5-31.
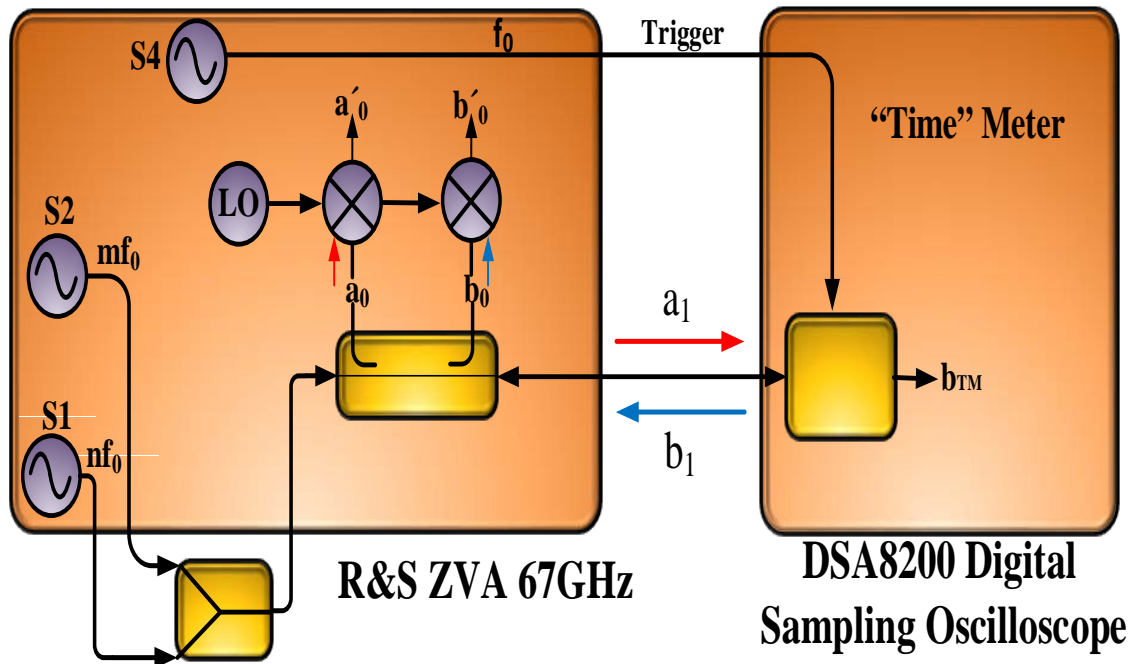
FIGURE 5-31 EXPERIMENTAL SETUP USED FOR ZVA WAVEFORM MEASUREMENT VERIFICATION.

Figure 5-31 shown two of the ZVA's internal DDS sources set to different frequencies, power levels and phases, are combined in order to synthesize complex time varying signals at one of the calibrated port (in this case port 1). Both the ZVA-67 and the Tektronix sampling scope measure these signals simultaneously.

Figure 5-32 shown waveform measured by using Scope and ZVA-67 before phase correction and Figure 5-33 shown waveform measured by Scope and ZVA-67 after phase correction by phase meter. In this case the internal source for ZVA-67 S1 set in this case to 1 GHz and S2 to 2 GHz and Scope trigger S4 to 1GHz (fundamental frequency).
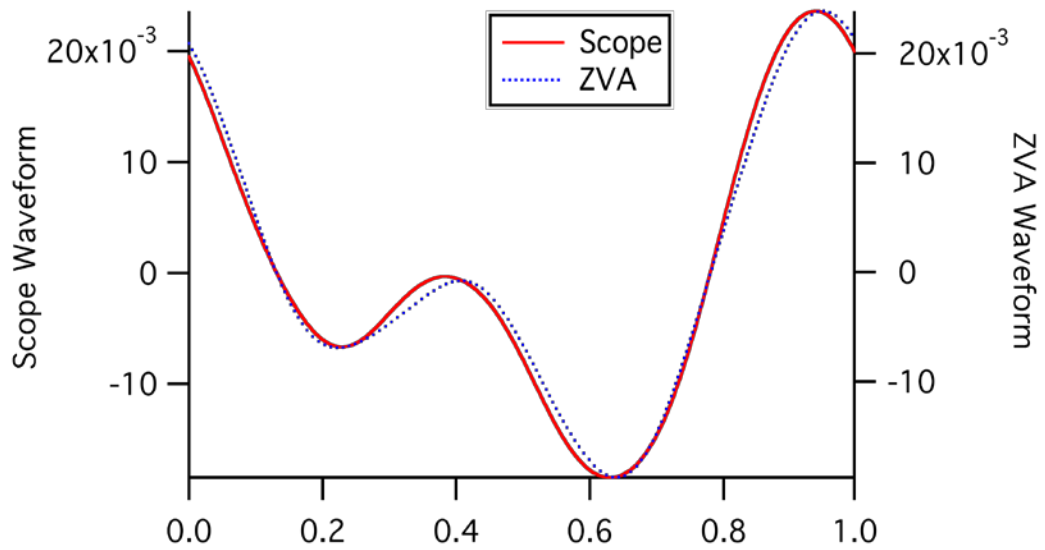
FIGURE 5-32 RF WAVEFORM MEASURED BY ZVA AND SCOPE BEFORE CORRECT THE PHASE BY PHASE METER. (AT 1GHZ AND 2GHZ)
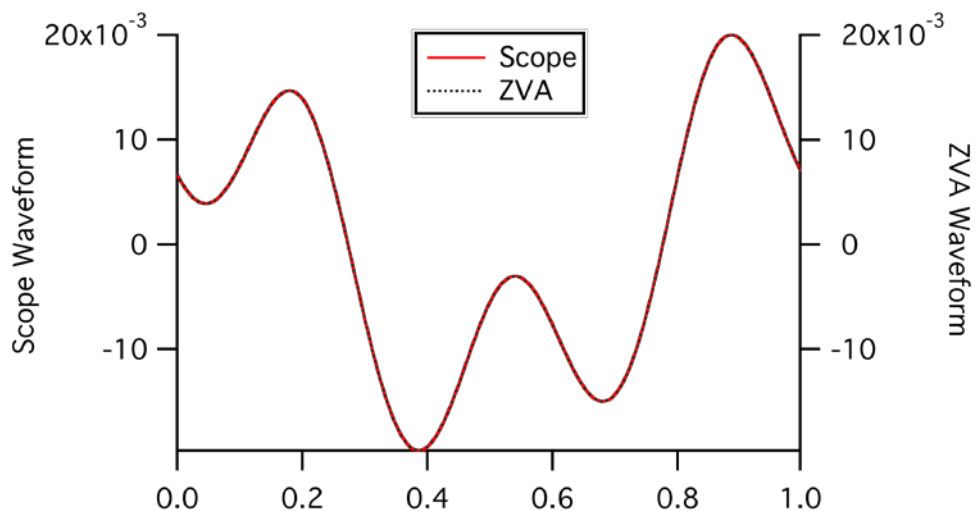
FIGURE 5-33 RF WAVEFORM MEASURED BY ZVA AND SCOPE AFTER CORRECT THE PHASE BY PHASE METER. (AT 1 GHZ AND 2GHZ)

Figure 5-34 shown and their example for waveform measured by using Scope and ZVA-67 before phase correction and Figure 5-35 shown waveform measured by Scope and ZVA-67 after phase correction by phase meter.

In this case the internal source for ZVA-67 S1 set in this case to 1 GHz and S2 to 3 GHz and scope trigger S4 at 1GHz (fundamental frequency).
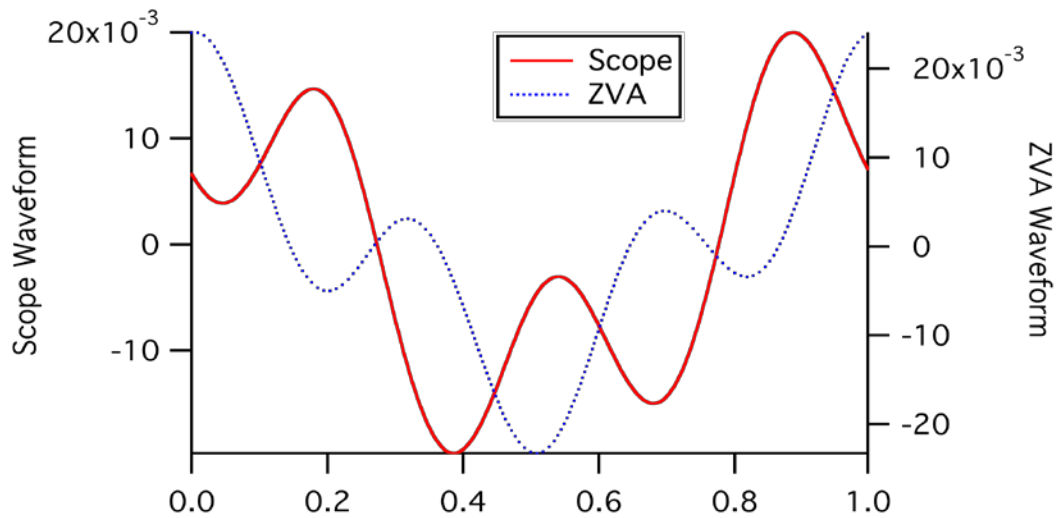
FIGURE 5-34 RF WAVEFORM MEASURED BY ZVA AND SCOPE UNCORRECTED THE PHASE BY PHASE METER.(AT 1 GHZ AND 3 GHZ)
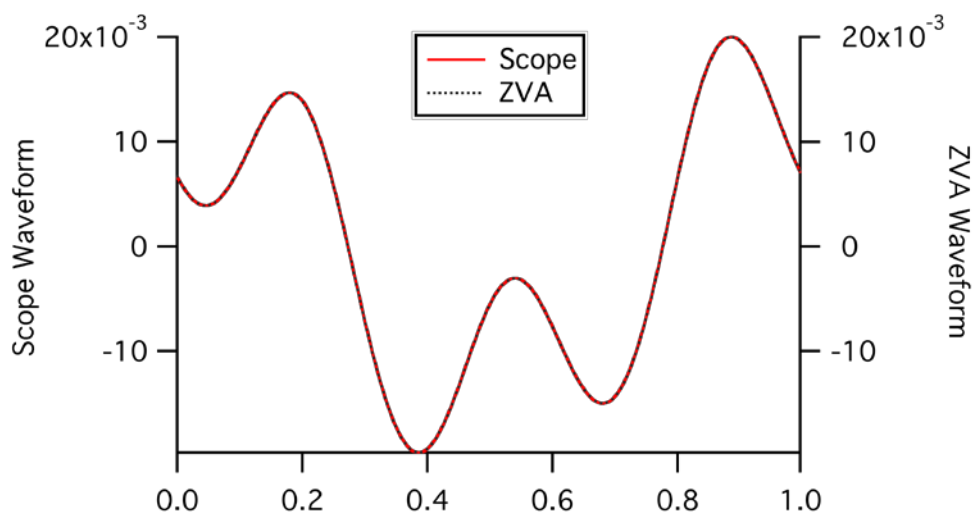
FIGURE 5-35 RF WAVEFORM MEASURED BY ZVA AND SCOPE AFTER CORRECTED THE PHASE BY PHASE METER.(AT 1 GHZ AND 3 GHZ)

Figure 5-36 shown another example for waveform measured by using Scope and ZVA-67 before phase correction and Figure 5-37 shown waveform measured by Scope and ZVA-67 after phase correction by phase meter. In this case the internal source for ZVA-67 S1 set in this case to 1 GHz and S2 to 4 GHz and Scope trigger by S4 at 1GHz (fundamental frequency).
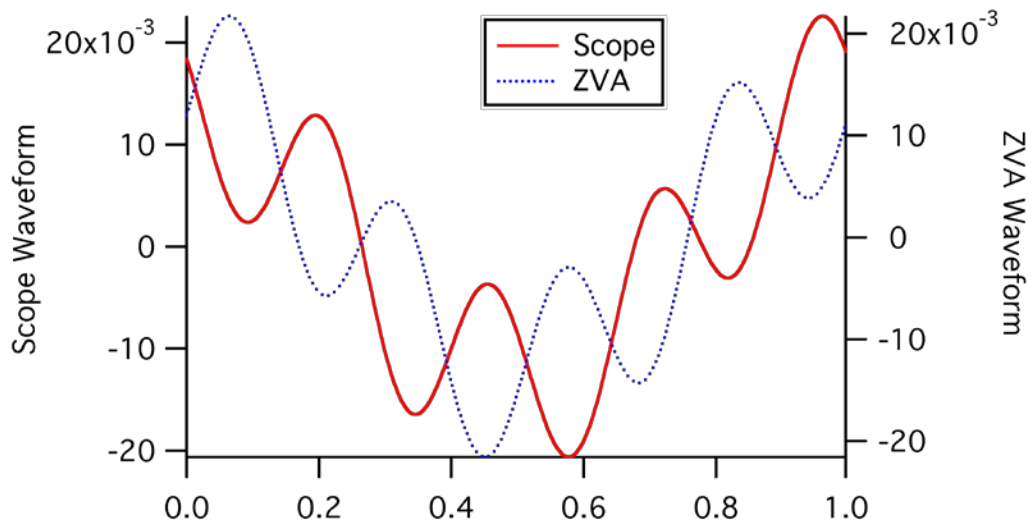
FIGURE 5-36 RF WAVEFORM MEASURED BY ZVA AND SCOPE BEFORE UNCORRECTED THE PHASE BY PHASE METER.(AT 1 GHZ AND 4 GHZ)
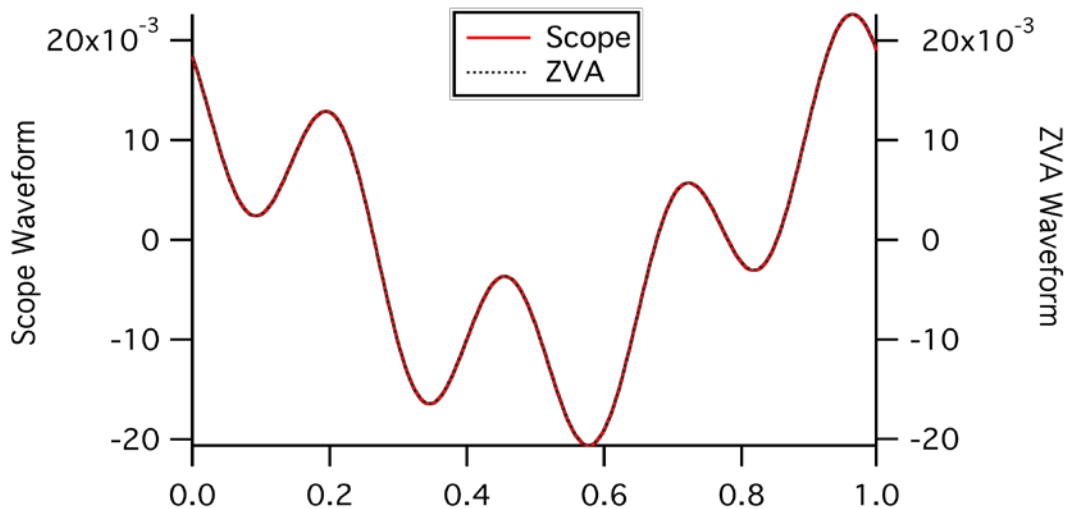
FIGURE 5-37 RF WAVEFORM MEASURED BY ZVA AND SCOPE BEFORE CORRECTED THE PHASE BY PHASE METER. (AT 1 GHZ AND 4 GHZ).

The Figure 5-38 shown other example for waveform measured by using Scope and ZVA-67 before phase correction and Figure 5-39 shown waveform measured by Scope and ZVA-67 after phase correction by phase meter, which is match the result in both system. It is useful to mention the internal source for ZVA-67 S1 set in this case to 2 GHz and S2 to 5 GHz and trigger the Scope by S4 at 1GHz (frequency).
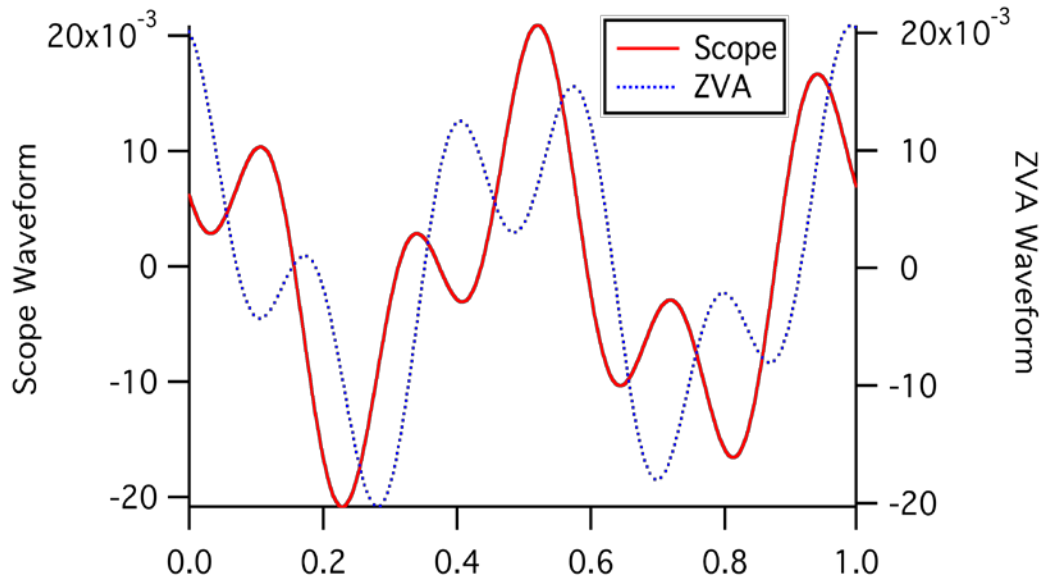
FIGURE 5-38 RF WAVEFORM MEASURED BY ZVA AND SCOPE BEFORE UNCORRECTED THE PHASE BY PHASE METER. (AT 2GHZ AND 5 GHZ)
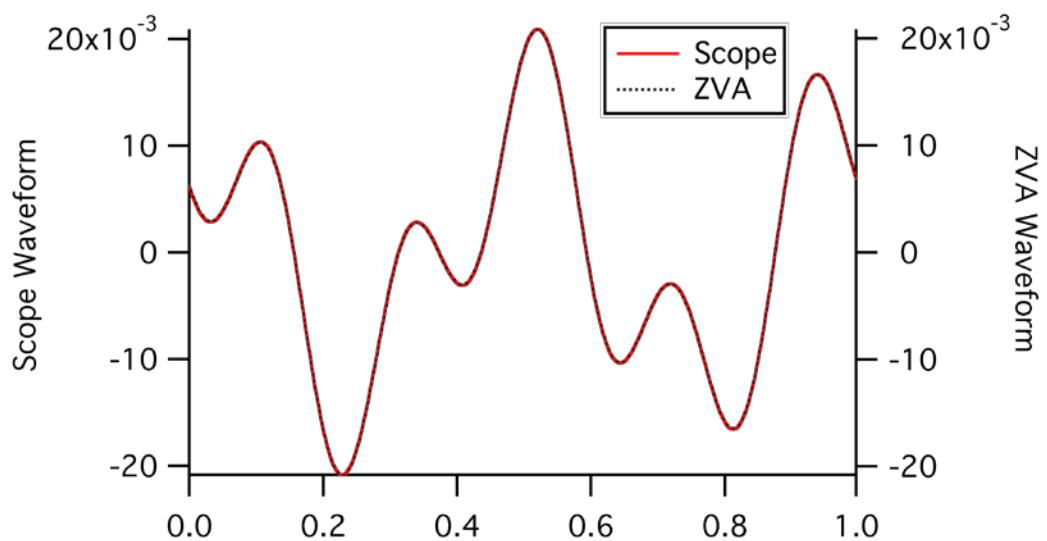
FIGURE 5-39 RF WAVEFORM MEASURED BY ZVA AND SCOPE AFTER CORRECTED THE PHASE BY PHASE METER. (AT 2GHZ AND 5 GHZ)

More tests lead to typical results achieved are shown in Figure 5-40, Figure5-41,Figure5-42 and, indicating that the displayed ZVA DDS waveforms$A_{1,CORR}(t)$, computed from vector error correct measurements performed in the frequency domain, $\tilde{A}_{1,COR}(\omega)$ and $\tilde{B}_{2,COR}(\omega)$, are identical to those measured directly in the time domain with the Tektronix Sampling Scope $A_{scope}(t)$. The results

confirm that the calibrated ZVA LSNA system is fully functional and can perform waveform measurements over its full bandwidth. The relative phase uncertainty observed in these measurements is again consistent with the previously observed value of +/- 0.3 psec.
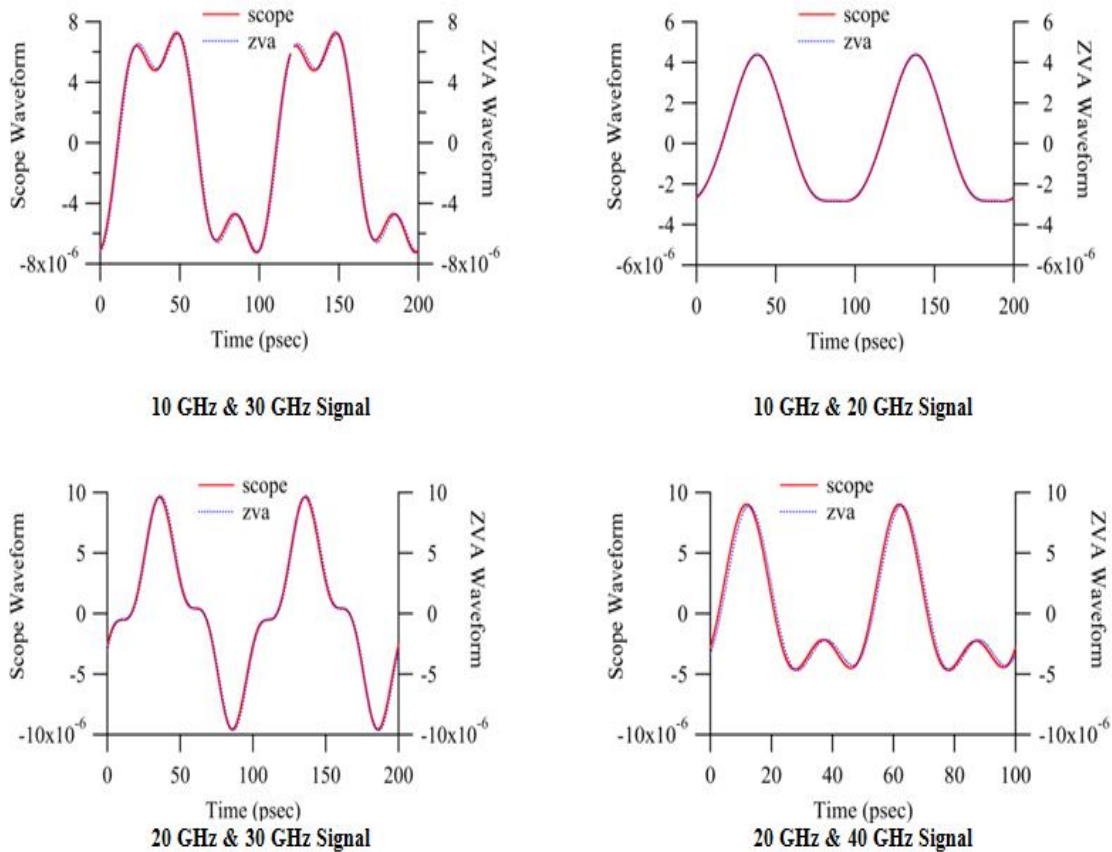
FIGURE 5-40 SYNTHESIZED POWER AMPLIFIER TYPE TIME VARYING SIGNAL CONTAINING FREQUENCY COMPONENTS AT 10 (FUNDAMENTAL FREQUENCY) GHZ AND 20,30 AND 40 GHZ HARMONICS.
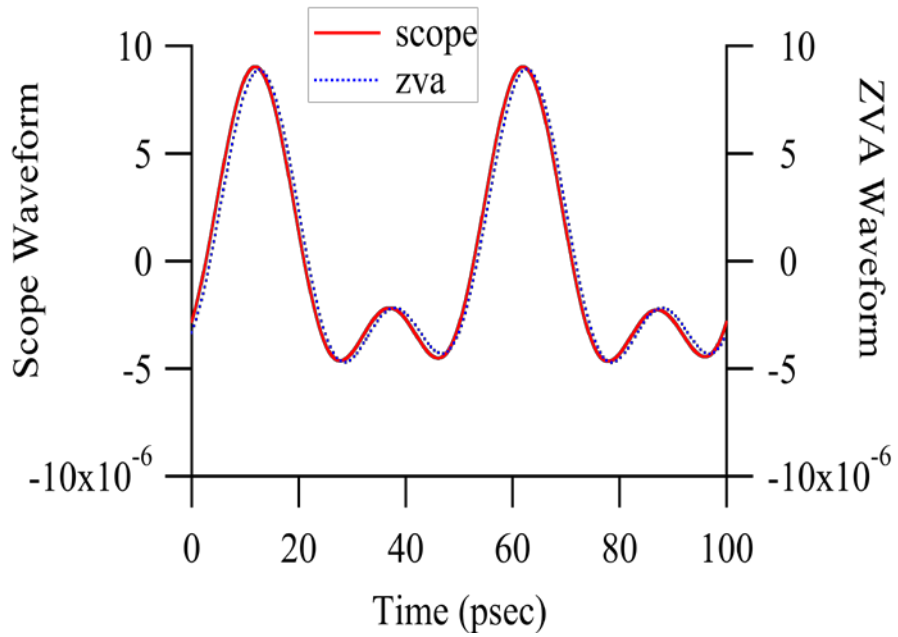
FIGURE 5-41 SYNTHESIZED POWER AMPLIFIER TYPE TIME VARYING SIGNAL CONTAINING FREQUENCY COMPONENTS AT 20 GHZ AND 40 GHZ.
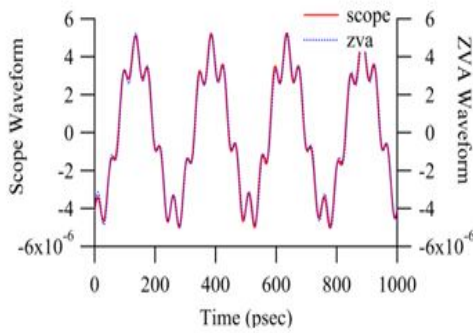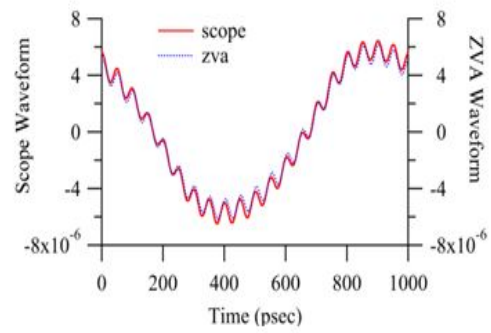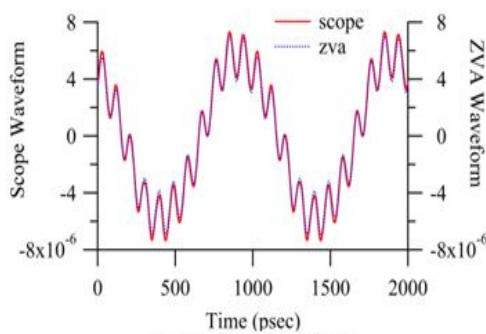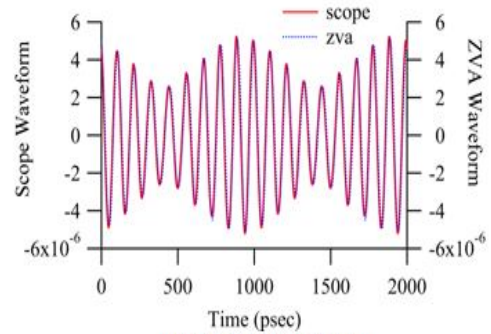
FIGURE 5-42 SYNTHESIZED MIXER TYPE SIGNALS CONTAINING FREQUENCY COMPONENTS AT DIFFERENT FREQUENCIES.
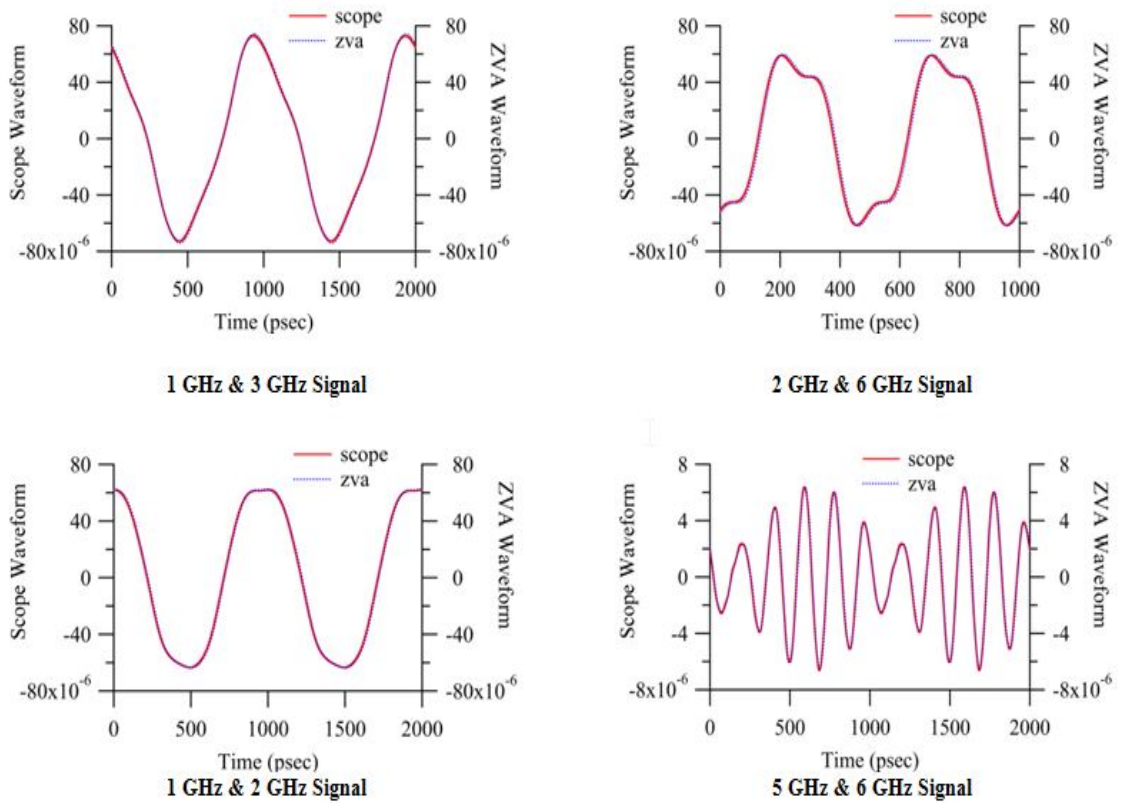
FIGURE 5-43 SYNTHESIZED MIXER TYPE SIGNALS CONTAINING FREQUENCY COMPONENTS AT DIFFERENT FREQUENCIES.

Calibration is done using internal sources and a phase meter. No phase standard required, no bandwidth limitations and no frequency restrictions. VNA systems with digital sources, both RF stimulus and LO, can after calibration provide for RF I-V waveform measurements.

4.6 SUMMARY

A new approach for operating and calibrating emerging VNA systems use in LSNA measurement systems has been developed, implemented and verified. A key feature of this approach is that both the operation and calibration of the VNA based LSNA system is achieved without the requirement of a harmonic phase reference HPR generator.

The implementation exploits the fact that emerging VNA architectures, e.g. the Rohde and Schwarz ZVA-67 incorporate internal signal and local oscillator (LO) sources based on Direct Digital Synthesis. The use of such DDS components provides a VNA receiver that is both repeatable and coherent in terms of relative phase over its full frequency bandwidth, in this case to within +/- 0.3 psec. DDS based sources remove the need for a phase reference during measurement, frees up one of the sources allowing 1-in-3 out operation with no additional sources. Also opens potential for full 4 port measurements with time domain information. No phase drift between drive signal and load-pull signals means convergence is faster, and makes very high frequency load-pull possible. Can also revisit past known impedance states (could be very useful for production testing)

The calibration approach developed uses a relative phase (time) meter, i.e. a sampling oscilloscope to perform the relative phase (time) calibration. Since calibration in this case is carried out using the VNA internal sources and a broadband sampling scope, there are reduced restrictions on the frequency grid and bandwidth. Importantly, as no dedicated channel is required for triggering during waveform measurements, all four VNA ports are available for DUT characterization, eliminating the need for multiplexing measurement signals, and allowing a simple and rapid measurement approach.

4.7 REFERENCE

1- Tasker, P.J., Practical waveform engineering. Microwave Magazine, IEEE, 2009. 10(7): p. 65-76.

2- Golio, M. and J. Golio, RF and Microwave Circuits, Measurements, and Modeling. 2007: Taylor & Francis.

3- Pailloncy, G., et al., Large-Signal Network Analysis Including the Baseband. Microwave Magazine, IEEE, 2011. 12(2): p. 77-86.

4- Benedikt, J., et al., High-power time-domain measurement system with active harmonic load-pull for high-efficiency base-station amplifier design. Microwave Theory and Techniques, IEEE Transactions on, 2000. 48(12): p. 2617-2624.

5- Blockley, P., D. Gunyan, and J.B. Scott. Mixer-based, vector-corrected, vector signal/network analyzer offering 300kHz-20GHz bandwidth and traceable phase response. in Microwave Symposium Digest, 2005 IEEE MTT-S International. 2005.

6- Verspecht, J., Large-signal network analysis. Microwave Magazine, IEEE, 2005. 6(4): p. 82-92.

7- Rohde & Schwarz USA, I., R&S ® ZVA Vector Network Analyzer High performance up to 110GHz with up to four test ports.

8- Broeck, T.V.d. and J. Verspecht. Calibrated vectorial nonlinear-network analyzers. in Microwave Symposium Digest, 1994., IEEE MTT-S International. 1994.

9- Williams, D., P. Hale, and K.A. Remley, The Sampling Oscilloscope as a Microwave Instrument. Microwave Magazine, IEEE, 2007. 8(4): p. 59-68.

10- NI. Understanding Direct Digital Synthesis (DDS). [cited 2015 Oct 10, 2015]; Available from: www.ni.com.

11- Agilent, Agilent U9391C/F/G Comb Generators.

12- Systems, S.R. Direct Digital Synthesis Application Note #5. Available from: www.thinkSRS.com.

13- Roblin, P., Nonlinear RF Circuits and Nonlinear Vector Network Analyzers: Interactive Measurement and Design Techniques. 2011: Cambridge University Press.

14- Van Moer, W. and Y. Rolain. An improved broadband conversion scheme for the large signal network analyzer. in Microwave Symposium Digest, 2005 IEEE MTT-S International. 2005.

15- Van Moer, W. and L. Gomme, NVNA versus LSNA: enemies or friends? Microwave Magazine, IEEE, 2010. 11(1): p. 97-103.

16- Verspecht, J., Calibration of a Measurement System for High Frequency Nonlinear Devices. 1995, Vrije Universiteit Brussel.

17- Jarndal, A. and G. Kompa, Large-Signal Model for AlGaN/GaN HEMTs Accurately Predicts Trapping- and Self-Heating-Induced Dispersion and Intermodulation Distortion. Electron Devices, IEEE Transactions on, 2007. 54(11): p. 2830-2836.

18- Agilent, High Power Amplifier Measurements Using Agilent's Nonlinear Vector Network Analyzer Application Note 1408-19. 2010.

19- Scott, J.B., P.S. Blockley, and A.E. Parker. A new instrument architecture for millimetre-wave time-domain signal analysis. in ARFTG Conference Digest Spring, 2004. 63rd. 2004.

20- Verspecht, J., F. Verbeyst, and M. Vanden Bossche. Network Analysis Beyond S-parameters: Characterizing and Modeling Component Behaviour under Modulated Large-Signal Operating Conditions. in ARFTG Conference Digest-Fall, 56th. 2000.

6 CHAPTER 6

CONCLUSIONS AND FUTURE WORK

The objective of this research was to improve the calibration and functionality of waveform measurement systems. The focus of this research has been split into two main sections:-

1) Enhancement vector calibration of any VNA measurement system to increase the S-parameter calibrated accuracy, especially at the edge of the Smith Chart and 2) operation and calibration of VNA based on large signal network analyzer systems without using phase reference. This thesis discussed the development of error models for measurement system, calibration algorithms, calibration kits, architecture of nonlinear measurement systems, and calibration of each type of non-linear measurement system.

The common focus in both of these areas has been utilising the RF IV waveform measurement system reading to increase the accuracy of error terms which in turn increased the accuracy of the measurement system and calibration and operation VNA base on LSNA without required to phase standard to obtain system not suffering from bandwidth limitations and frequency restrictions with high accuracy.

5.1 CONCLUSIONS

Two main concepts are investigated in this thesis. The first concept emerged in Chapter 2 with a literature review for a theoretical analysis of S-parameter starting by error model for 1 Port networks, 2 Ports networks, calibration algorithm for SLOT and TRL, calibration tools kits and small overview about uncertainty in small signal calibration.

Chapter 3 introduce the new approach to improving vector measurement accuracy developed in this work, especially near the edge of the Smith Chart, very important in load-pull measurement systems. Improved measurement accuracy after vector calibration, is achieved by exploiting the load-pull capability during calibration to minimise the impact of measurement errors on the raw calibration standards data before it is utilised in the traditionally implemented LRL/TRL calibration algorithm. This new approach eliminates the need to utilise complex optimisation algorithms post calibration. The proposed method has been tested and applied to actual measurement data, as well as in investigating the relationship between reflection coefficient and quality of raw data obtained during calibration using a load pull system.

The second part of this thesis addresses augmentations about wave meter and it's aimed to more develop in the non-linear measurement efficiency of the large signal network analyzer systems, which lead to the development of its applicability for use in helping design RFPA. Chapter 4 extended the review and insight about existing large signal network analyser measurement systems and briefly discussed the architecture and advantages and disadvantages of each type. A new approach to calibration is introduction in Chapter 5. The present LSNA measurement systems provide measurement capabilities to perform full error correction in frequency domain and present the result in voltage and current waveform in time domain measurements using a harmonic phase reference generator which limits bandwidth and frequency restrictions during measurement. Therefore a new approach is presented in Chapter 5 that allows a Vector Network Analyzer to be operated as a Large Signal Network Analyzer without the need for a harmonic phase reference generator. This mode of operation exploits the architecture of the Rohde and Schwarz ZVA-67, which incorporates internal signal and local oscillator sources based on direct digital synthesis. This unique capability leads to a Vector Network Analyzer based Large Signal Network Analyzer configuration that incorporates time coherent sources and receivers. This feature combined with a modified calibration procedure, allows the instrument, to provide error corrected RF current and voltage waveform measurements, requiring only internal signal sources and an external phase meter. This approach simplifies the Large Signal Network Analyzer architecture and removes the complexities and bandwidth limitations introduced when employing a harmonic phase reference generator. Further development of the LSNA was achieved to improve the measurement system, particularly this technical make all

four VNA ports are available for DUT characterization, eliminating the need for multiplexing measurement signals, and allowing a simple and rapid measurement approach. This method can provide a full calibration for N ports VNAs and be used in LSNA allowing capable systems to provide mixer and antenna measurements.

5.2 FUTURE WORK

The main development of the measurement throughout this work has certainly been achieved with respect to improving the vector measurement accuracy and the functionality of large signal network analyzer-systems. However, there is still a lot that can be done to support previous efforts as well as the developments contained in this thesis. The LSNA has been developed to the stage where architecture has been implemented to measure waveform without using a harmonic phase reference standard for continuous signals and modulation signals. A drawback of this approach is that coherent phase will be lost after harmonic 15 due to a +/- 1.6 time jitter of the oscilloscope used to collect the phase of the calibration wave signal. This problem can be overcome the problem by using new technique for phase alignment and real time oscilloscope.

Accurate predictions of the vector measurement, especially near the edge of the Smith Chart, of load-pull measurement systems, have been shown to improved when using the load-pull capability during calibration to minimise the impact of measurement errors on the raw data of the calibration standards before it is utilised in the traditionally implemented LRL/TRL calibration algorithm. This method implemented for 2 ports DUT which can be extended for calibration n ports but need modified the algorithm for TRL.

5.3 REFERENCE

1- Tasker, P.J., Practical waveform engineering. Microwave Magazine, IEEE, 2009. 10(7): p. 65-76.

2- Tasker, P.J. RF Waveform Measurement and Engineering. in Compound Semiconductor Integrated Circuit Symposium, 2009. CISC 2009. Annual IEEE. 2009.

3- Golio, M. and J. Golio, RF and Microwave Circuits, Measurements, and Modeling. 2007: Taylor & Francis.